Towards Passive Fluidic Control: Optimisation of Non-Uniform Suction of Separated Flows

James Robert Ramsay

A thesis presented for the degree of
Doctor of Philosophy
in
Mechanical Engineering
at the
University of Canterbury,
Christchurch, New Zealand.

15 June 2021

ABSTRACT

Separated flows – such as those around bluff bodies – can be greatly improved by removing some of the fluid through bounding surfaces. This 'suction flow control' reinvigorates the boundary layer, delaying separation and altering the pressure field of the flow. In this research, suction and blowing control was optimised for two representative separated flows: the flow around the circular cylinder (external flow), and the flow through a conical diffuser (internal flow). The aim was to progressively develop from broadly-applied uniform suction to refined and passively generated (autogenous) non-uniform suction and blowing. These flows were investigated using numerical simulations employing the Finite Element Method.

It was found that non-uniform suction of the boundary layer was always more efficient, and usually more effective, than uniform suction in the representative flow-cases. Separation could be entirely eliminated around the cylinder when sufficient suction control is applied, and there is a compelling relationship between the optimal control parameters and the uncontrolled separation values. Drag on the cylinder could be reduced by over 30% and performance of the diffuser could be increased by over 50% in the investigated Reynolds number ranges. Combining suction with blowing control produced even better performance in most circumstances, especially if a non-zero mass flux was permitted.

Constraining the control so that the flow-rates were balanced (Q-balanced) and that a positive pressure gradient from suction-to-blowing loci is present (P-Q-balanced) allowed for the design and testing of potentially autogenous suction control. For the 5° diffuser, this control arrangement was unable to improve performance due to the monotonically increasing pressure profile. For the cylinder at $Re = 40$ and $Re = 120$, however, it was capable of reducing the drag compared to the uncontrolled case (reduced by $\sim 5\%$. In unsteady simulations (at $Re = 120$) this also reduced fluctuations in the flow.

When considering a practical implementation, with ducting and porous materials to produce the connection between suction/blowing loci, additional losses are present that are not accounted for by assuming that $dP > 0$ is sufficient for autogenous control. Numerical tests of promising dual-loci control were performed with geometric design concepts applied to the cylinder. At $Re = 40$ the drag was reduced with these designs, but not at $Re = 120$ because the desired suction profile was not appropriately produced. Suggestions for overcoming this issue are detailed.

Overall, autogenous suction control has been proven to be a feasible method for reducing drag on bluff body flows, and can offer a modern tool for improving the efficiency of vehicles for a future "net-zero" world.

CONTENTS

ACKNOWLEDGEMENTS

First of all, I would like to thank my PhD supervisors Mathieu Sellier and Wei Hua Ho. Thank you, Mathieu, for your patient helping-hand, your eye for accuracy, and your heart for fluid dynamics. More times than you know, you have kept me motivated and interested when otherwise I would have faltered. Support and enthusiasm are so part of your nature, you probably didn't even notice.
Thank you Wei, for your diligent support and timely feedback. It is amazing to think that you have been such an important influence in this work, and yet we have not had the chance to meet face-to-face.

I am grateful to the University of Canterbury for sponsoring this work through a UC Doctoral Scholarship which paid enrolment fees so I could work and a stipend so I could live. I am also grateful to the Royal Aeronautical Society for the Mercer Memorial Scholarship, as well as to the Canterbury branch of the Royal Society and the American Physical Society which helped fund travel to the U.S. so I could speak a little and listen a lot.

One week after beginning my PhD research, I broke my back. Without the help, kindness and expertise of many generous individuals I would not have been able to continue. They are so numerous, I can not name them all, but I think of them as I write this.

Thank you to Rob F. for helping me in recovery and so much more.

Thank you to my friends and flatmates who put up with my variable schedule and emotions. I appreciate you getting my spirits up when they were down.

Thank you to my siblings who always asked *how* things were going, even though I could never rightly explain *what* I was doing.

Most of all, though, I must acknowledge the love, support and encouragement of my parents. As long as I can remember Mum has always said that 'education is the ticket out of poverty', and at each step of my life Mum and Dad have made every sacrifice so that my education could thrive – both in and out of school. Thank you for giving me the freedom to follow my own path, even at those times you could see me heading to a dead-end. This work was not possible without your patience and example.

It has been a privilege to conduct this post-graduate research, and I recognise that it has required a significant investment of time and money from many individuals, groups and Aotearoa as a whole. I hope to be able to return that with interest over the course of my life.

PREFACE

This journey did not run straight and smooth.
But, then again,
None of the interesting flows do...

J.R.R.

Nomenclature

Acronyms

2D	Two-Dimensional
3D	Three-Dimensional
ANN	Artificial Neural Network
AOS	Angle of Separation
APG	Adverse Pressure Gradient
BC	Boundary Condition
BL	Boundary Layer
BLS	Boundary Layer Separation
BR	Blockage Ratio
CFD	Computational Fluid Dynamics
FEM	Finite Element Method
FPG	Favourable Pressure Gradient
GHG	Greenhouse Gas Emissions
IJAE	International Journal of Aerospace Engineering
IJHFF	International Journal of Heat and Fluid Flow
IV	Initial Values
J-H	Jeffery-Hamel
JRSNZ	Journal of the Royal Society of New Zealand
LE	Leading Edge
N-M	Nelder-Mead optimisation method

N-S Navier-Stokes

PDE Partial Differential Equation

POS Point of Separation

SEF Sudden Expansion Flow (diffuser case where $2\alpha = 180°$

SNOPT Sparse Non-linear OPTimiser

SS Steady-State (simulation)

TD Time-Dependent (simulation)

TE Trailing Edge

VIV Vortex-Induced Vibrations

Flow Around Cylinder Symbols

γ_q Spread of control

λ_q Control directional bias

θ Angle measured from trailing edge

θ_q Centre of control

θ_s Separation angle

θ_{s_0} Separation angle of uncontrolled flow

C_q Net control coefficient – sometimes C_Q

c_q Local control coefficient

$c_{q_{max}}$ Peak strength of control

D Cylinder diameter

Da Darcy number, $Da = \frac{\kappa}{D^2}$

f Frequency of vortex shedding period

St Strouhal number, $St = \frac{fD}{U}$

T Period of vortex shedding period

t^* Dimensionless time, $t^* = \frac{tU}{D}$ (sometimes $t^* = \frac{tU}{x_0}$)

x_0 Distance from inlet to centre of cylinder

Diffuser Flow Symbols

2α Divergence angle

α Semi-divergence angle

β Expansion ratio, $\beta = D/d$

$\eta_{Ackeret}$ Performance of diffuser with suction as devised by Ackeret [1926], $\eta_{Ackeret} = \frac{P_2 - P_1}{\left[1-\left(\frac{1}{AR}\right)^2\right]h_0 + \frac{C_q P_w}{\eta_{pump}}}$

η_{out} Performance of diffuser with suction/blowing control, $\eta_{out} = \frac{Q_2 P_2}{Q_1(P_1+h_1)+Q_w(P_w+h_w)}$

η_{pr} Performance of ideal diffuser $\eta_{pr} = \frac{P_2 - P_1}{\left(1-\frac{1}{AR^2}\right)0.5\rho U_1^2}$

ϕ Azimuthal direction of diffuser

AR Area ratio, $AR = \frac{D^2}{d^2}$

C_q Suction coefficient

$C_{pr_{theor}}$ Performance of diffuser with zero velocity at exit $C_{pr_{theor}} = \frac{P_2 - P_1}{0.5\rho U_1^2}$

D Diameter at exit of diffuser

d Diameter at entry to diffuser

L Length of diffuser along z-axis (from entry to exit)

L_{sep} Length of recirculation region (separation bubble) measured along z-axis

L_{tail} Distance from diffuser exit to outlet of domain

l_{up} Distance from domain inlet to entry of diffuser

n 'Flatness' parameter for inlet profile, $u(\lambda) = (1 + \frac{2}{n})U(1 - \lambda^n) \quad \text{for} \quad 0 \leq \lambda \leq 1$

r Radial direction of diffuser

r_w Area ratio of diffuser wall to diffuser entry, $r_w = \frac{3L}{r\tan(\alpha)}$

z Axial direction of diffuser

z_q Centre of control

z_r Reattachment point (measured along z-axis)

z_s Separation point (measured along z-axis)

z_{s_L} Separation point non-dimensionalised by diffuser length rather than entry diameter

Free-stream vs. Local Parameters

C_q Net/Global value – upper-case

c_q Local value – lower-case

P Free-stream variable or spatially-averaged variable – upper-case

p Local variable – lower-case

Subscripts

0 Uncontrolled flow parameter

b Blowing control parameter

n Direction normal to wall

q Control parameter – suction by default unless specified otherwise

s Suction control parameter

t Direction tangential to wall

Universal Symbols

ϵ Porosity

κ Permeability

μ Dynamic viscosity

ν Kinematic viscosity, $\nu = \mu/\rho$

ρ Fluid density

C_{d_f} Skin friction drag coefficient

C_{d_p} Pressure drag coefficient

C_{d_t} Total drag coefficient

$C_{d_{t_u}}$ Total drag coefficient, evaluated using momentum integral approach

dP Average pressure difference from suction locus to blowing locus

F_d Total drag force

F_{d_f} Skin friction drag force

F_{d_p} Pressure drag force

h_0	Dynamic pressure, $h_0 = 1/2\rho U^2$
J	Objective functional
lb	Lower bound of control
Q	Volumetric flow rate, $Q = \int_C \mathbf{u} \cdot \vec{n} ds$
Re	Reynolds number, $Re = \frac{\rho U D}{\mu}$ (cylinder) or $= \frac{\rho U d}{\mu}$ (diffuser)
U	Mean free-stream velocity
u_n	Velocity normal to wall
u_t	Velocity tangential to wall
ub	Upper bound of control
v_w	Local suction velocity (velocity at wall)

Vector Notation

k	Scalar – lower-case
$\vec{k}$	Unit Vector – lower-case and over-arrow
$\mathbf{k}$	Vector – lower-case and bold
K	Matrix – upper-case

Chapter 1

INTRODUCTION & MOTIVATION

1.1 BACKGROUND/MOTIVATION

1.1.1 Greenhouse Gas Emissions from Transport

Approximately 9% of New Zealand's greenhouse gas emissions arise from the energy consumed to overcome drag in road transportation. This estimate comes from New Zealand's emissions data and estimates of the energy use in transport by other authors, particularly the work by Wood [Ministry for the Environment 2016, Ministry of Transport 2017, Wood 2004]. Figure 1.1 shows how national emissions have increased over time, while and Figure 1.2 breaks down the 2014 carbon emissions by sector. In 2014, 40% of the country's total greenhouse gas emissions were attributable to the Energy sector, of which 39.5% is from road transport. Wood [2004] estimates that the ratio of drag energy to total energy used by road vehicles is 59% for heavy ground vehicles like trucks, and 45% for light vehicles (regular cars). Applying this methodology to the New Zealand data, a rough approximation of 9% of emissions arise from the drag component. It should also be noted that this excludes the energy used in marine and aircraft transportation, of which almost the entirety of the energy is used to overcome drag.

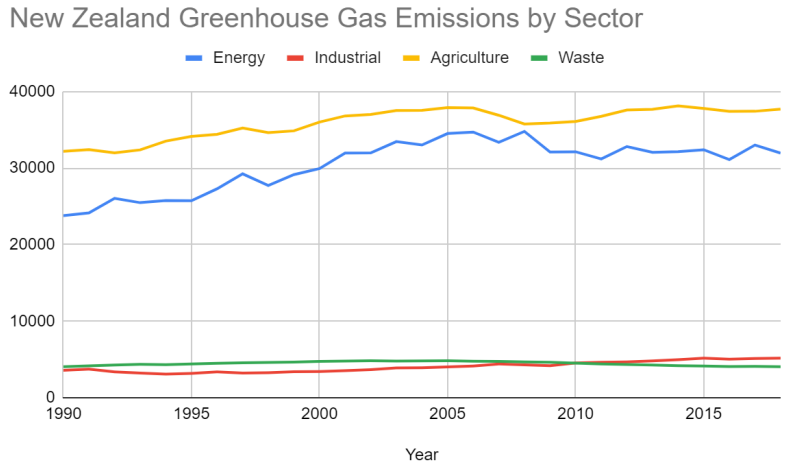

Figure 1.1 New Zealand greenhouse gas emissions in CO2e over time [Ministry of Transport 2017]

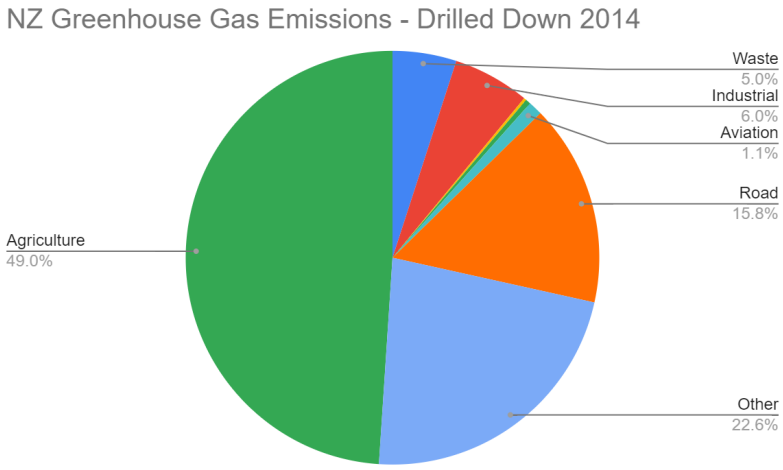

Figure 1.2 New Zealand greenhouse gas emissions by sector in 2014 [Ministry of Transport 2017]

Given the acceleration of climate change and the global commitment to decrease greenhouse gas (GHG) emissions, there is a strong motivation to increase the efficiency of vehicles. In the Paris Climate Agreement, signed by nearly every country in the world, all parties committed to reducing CO2e emissions to leves that woud restrict global average temperature gain to below 2°C [UNFCCC 2015]. On a national scale, New Zealand has committed itself to become 'net zero' by 2050 [New Zealand Parliament 2019]. In late 2020, the New Zealand government even announced a climate emergency [New Zealand Parliament 2020]. Some local councils – including Christchurch, where over 60% of its emissions arise from transportation – have committed to even tighter deadlines (2045) [Christchurch City Council 2019]. To achieve this, either a significant reduction in transport will have to occur, or the efficiency and sustainability of vehicles will have to improve. Therefore, reducing the drag experienced by vehicles, and thereby reducing their energy consumption, is a key priority for transitioning to net-zero.

1.1.2 Losses in Internal Flows

Although making up a much smaller portion of the GHG emissions, the energy used in industry is also significant – 6.5% of NZ's emissions in 2018 [Ministry of Transport 2017]. Some of this comes from inefficiencies in the movement of fluids in industrial infrastructure, for example: pipes, ducts, and open channels. It is well known that significant losses occur in pipe systems with bends, obstacles, or changes in diameter [White 2017, sec. 6.9]. This is because the free-stream flow is disturbed by these changes often resulting in secondary, recirculating flows. The physical phenomena that cause these losses are very similar to those that produce drag in external flows, particularly boundary layer separation (more on this in Chapter 2). While the environmental incentive to improve the efficiency of fluid transport in internal flows is not as

strong as for transportation at this point in time, there is still the potential for large improvements in efficiency which would be environmentally advantageous on the global scale and economically beneficial on the local scale. If the losses in pipe systems can be substantially reduced by efficient control of the flow so as to prevent it from separating and recirculating, then weaker pumps (which consume less power) can be used to drive the flows, reducing energy usage and thereby reducing expenditure and emissions.

1.1.3 Beyond Losses

Controlling fluid flows where separation occurs and produces large drag or energy losses is obviously beneficial, but there are other reasons to desire effective flow control. The formation of wakes behind moving bodies in fluids – from frigates to tennis balls – can also result in undesirable vibrations, markers of their motion, and increased thermal transfer between the body and fluid. It is beneficial to minimise all of these consequences in certain scenarios. For example, in naval warfare the wake of a ship inadvertently communicates to the enemy where and how fast the ship is moving [Alton 1997, Stewart and Miner 1987, Trevorrow et al. 1994]. Overhead electrical cables and structural cables for bridges often experience strong aerodynamic forces as wind blowing past them induces strong vortex-induced vibrations (VIV) that can reduce their lifespan and threaten failure if not appropriately considered by the designer [Schumm et al. 1994, Zuo et al. 2008]. In some circumstances the enhanced mixing resulting from turbulent and recirculating wakes may often be desirable – such as in a heat exchanger – but in others may be undesirable. In all these cases, it is the separation of the fluid from the body wall that produces the undesirable effects. Having more effective measures for controlling and delaying the separation of flow is desirable.

1.1.4 Flow Control

Historically, the first method to improve separated flows has been to control the shape and geometry of the interacting bodies. For an external flow, this means streamlining the body (usually making it smooth and thin) while for internal flows, this means minimising the twists and turns and making any changes in shape very gradual. These are extremely effective measures. The drag force experienced by a body is proportional to its frontal area (projected area perpendicular to the flow), so reducing this has a strong impact. What is more, a streamlined body will deter separation by allowing the flow to move smoothly around its shape without generating strong adverse pressure gradients. The downside of this approach, though, is that the shape has changed. In some circumstances this is undesirable or not possible. For example, in the case of heavy road vehicles, the rectangular shape of trucks enables efficient packing of cargo. Smooth curved containers would either be very difficult to pack efficiently, or would have wasted

space. So, in some cases it is not feasible to change the shape of the body – however, we still want to reduce drag if possible. The alternative approach is flow control.

Flow control is the overarching term describing all methods of manipulating and controlling the flow of a fluid to achieve some objective. As such, it does include streamlining, however the are of most interest is *fluidic* flow control. This is where the flow is influenced directly, for example by suction of part the flow through the bounding surface, or by installing plasma jets which create small vortices to re-stimulate the boundary layer [Cattafesta and Sheplak 2011, Hurley and Thwaites 1951]. There are many vastly different potential flow control devices, and many of the technologies are modern – being proposed only in the last half century. These methods and their histories will be discussed in depth in Chapter 2.

Real attempts at flow control only really arose in the early 20^{th} Century, and interest in the field ballooned with the invention of powered flight by the Wright brothers in 1903 and the nascence of aerodynamics. Ludwig Prandtl, famed engineer and fluid dynamicist, tested his boundary layer theory in 1904 by implementing flow control on the flow around a circular cylinder. By sucking a small amount of fluid through a slot in the surface of a cylinder placed in a water tunnel, he found the wake was greatly reduced [Prandtl 1904]. Similarly, by rotating the cylinder, the wake was again improved – although now with a downwash due to the directional rotation. These tests verified his theory that even in fast flows where viscous effects are very small, the fluid particles near the wall of the bounding body (the 'boundary layer') are near-stationary and as such the viscous effects have a strong effect. When the flow experiences an adverse pressure gradient (APG) – a pressure gradient opposing the direction of the fluid and which is experienced on the rear of all uncontrolled bodies in fluids – the low momentum particles in the boundary layer are forced to stagnate and then reverse direction. This is the mechanism by which a wake forms, and causes the pressure in the flow to never recover on the rear of the body. Suction (and removal) of the slow fluid near the wall causes the boundary layer to be re-stimulated as these removed particles are replaced by the high-momentum particles in the free-stream. By such means, fluid flows can be directly influenced, instead of by the indirect method of altering the geometry of the body.

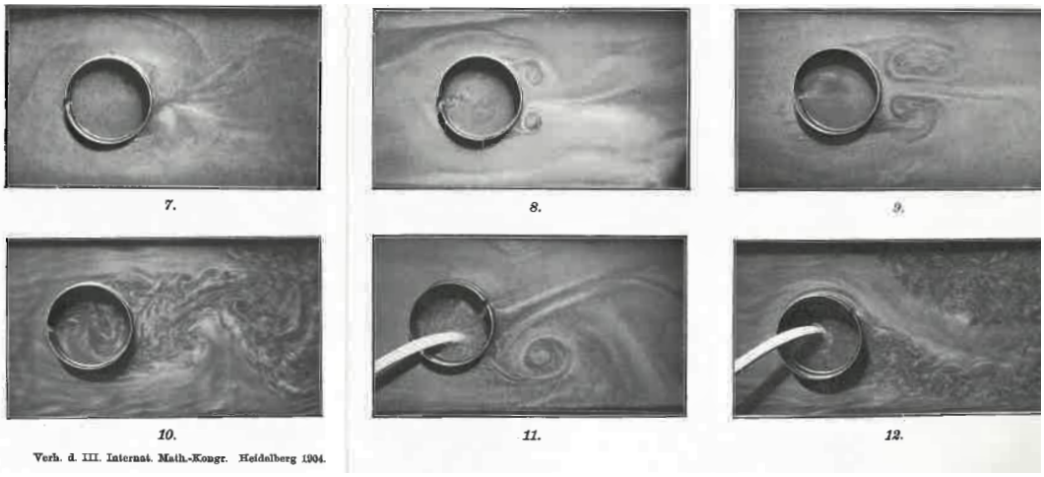

Figure 1.3 Images included in the breakthrough paper by Prandtl [1904] demonstrating the effect of boundary layer suction (those labelled 11 and 12).

1.1.5 Autogenous Flow Control

There is a major issue which makes the use of direct flow control less desirable. Whereas a geometric change is permanent and passive (requires no energy to operate), most direct flow control methods do. To drive a suction through the wall of a body, a low pressure sink must be produced to pull the fluid from the flow through the wall. This is typically achieved using a pump. Pumps require energy to run, and – in the case of vehicles – also adds weight which adds to the energy requirements for motion. Another example is the plasma jet actuator. While these are often micro-devices that relatively small electric potentials, they still require energy to be run and further infrastructure to enable their use. If the energy required to operate the flow control exceeds the energy it saves by reducing drag or improving performance, the system as a whole is not efficient. This has typically been the reason that flow control technologies have not been widely adopted, alongside the more technical designs necessary [Lachmann 1961]. Table 1.1 outlines some of the advantages and disadvantages of flow control compared to geometric changes.

Table 1.1 Pros and cons of direct flow control in contrast to geometric design (streamlining).

Advantages	**Disadvantages**
Direct influence on flow	More complicated design
No need to change shape	Auxiliary equipment needed
Varying control (time and space)	Require additional energy
Versatile objectives	
Out-sized impact	

However, flow control using suction and blowing does not necessarily need energy

input. Since a pressure difference is what drives the control flow through the bounding surface (whether for suction or blowing), then the pressure gradients already existing in separated flows might be used to drive them. For such an arrangement, the suction must be accompanied by an equivalent blowing somewhere else in the flow (and lower pressure). This type of flow control has been termed 'autogenous suction' by researchers Atik and van Dommelen [2008] in their paper *'Autogenous suction to prevent laminar boundary-layer separation'* – autogenous meaning self-generating ('auto' – self and 'genous' to generate). The researchers performed numerical investigations into the possibility of generating autogenous suction on an airfoil at various angles of attack, and found that it was theoretically possible to prevent laminar boundary-layer separation. However, the authors made several simplifying assumptions about the conditions needed for autogenous control. Their research was inspired by earlier studies to generate suction behind shock-wavess, and the idea has been credited to Bushnell and Whitcomb in 1979 [Nagamatsu et al. 1987]. However, Atik and van Dommelen [2008] were the first to investigate the possibility of using this type of control at lower, sub-sonic velocities.

The key to autogenous suction control comes from its particular application in separated flows. Separation occurs when three conditions are met:

1. No-slip condition between fluid and bounding wall
2. Adverse pressure gradient (APG) – increasing pressure in the direction of the flow
3. Insufficient momentum in the flow and boundary layer

Since there will always be an APG where separation occurs, the pressure differential can be used to drive the controlling flow. Blowing can be situated at the minimum pressure point before the commencement of the APG, and suction can be applied within it. It is well known that suction of the boundary layer delays its separation, so this arrangement can naturally drive the flow. The major issues arise from the following concerns:

- Will the blowing upstream promote separation, despite the suction now present downstream?
- The application of the control changes the pressure profile, can a suitable equilibrium be reached?
- Will the system result in the flow characteristics being improved as desired?

These questions are key subjects of this thesis.

Atik and van Dommelen [2008] only investigated the arrangement where the fluid removed by suction is exhausted upstream of the suction control. However, it is possible to conceive of other arrangements where the flow can run downstream. In other words, where suction is located upstream and blowing downstream. In many cases this would require the suction to be in a region of lower pressure than the blowing, so methods for

inducing a control flow with such an arrangement are needed. If this type of autogenous control were possible, it would have the advantage of not disturbing the upstream flow while still gaining the benefit of the suction control. Since the work of Atik and van Dommelen [2008], there has been little published research on autogenous suction control, however their study demonstrated its potential. Autogenous suction control is more complicated to design than other flow control methods, and recently optimisation of suction-only control and other flow control methods have been showing more promise in terms of efficiency [Li et al. 2003]. However, autogenous suction control has the benefit of requiring no power to run, no additional weight from pumps or other mechanisms, and requires no change to the external shape. As a result, cargo trucks can remain rectangular.

1.1.6 Circular Cylinders and Conical Diffusers

Upwind autogenous suction control should theoretically be possible in any separated flow. Whether it will improve the flow is uncertain. In undertaking this research it was decided to focus on two representative geometries: one for external flows, one for internal. These were the circular cylinder (external flow) and the conical diffuser (internal flow), respectively. While Atik and van Dommelen [2008] decided to focus on the case of an airfoil and the benefits for aircraft fuel economy, the need for effective flow control in more general flows has been amply demonstrated. If autogenous suction control can be effective for an highly non-aerodynamic (bluff) body like the circular cylinder and the resulting unsteady flow, it would firmly demonstrate its potential. Most flows exhibit similar phenomena to the cylinder, such as vortex shedding and various flow regimes at different Reynolds numbers. Importantly, there is also a great deal of experimental data on the uncontrolled flows around circular cylinders which is useful for validating computational models – so much so, that Zdravkovich has dedicated a two-volume textbook to the topic [Zdravkovich 1997]. On the other hand, the pressure profile over a cylinder is complex – even the ideal case is sinusoidal. This adds to the difficulty of arranging a control system that can use the pressure gradients already present in the flow. So as a stepping stone in the development of autogenous control theory, the conical diffuser was chosen as a second geometry. Its pressure profile is monotonically increasing, and so offered a simpler example to test the principles of autogenous control. Like the cylinder, it was an early subject of boundary layer suction tests [Ackeret 1926]. However, unlike the cylinder its control by fluidic-means received much less interest over the following years, making it a good subject for novel research on this topic.

1.2 RESEARCH QUESTIONS

Listed below are the research questions that this thesis sets out to answer:

1. If any **suction/blowing control** can be applied to the flow around a circular cylinder or through a conical diffuser, what is their **optimal application** to a) prevent separation, and b) reduce drag?
2. What **relationships** can be found between the optimal control and the characteristics of the uncontrolled flows?
3. **Is autogenous suction control possible** for these flows? And in what arrangement?
4. What is the **optimal autogenous suction control** for one of these flows, and how much does it improve upon the uncontrolled case?
5. What would a **practical implementation** of this control look like? Can we design a physical system to achieve autogenous suction control that improves drag for the circular cylinder?

The approach to exploring these questions is described in depth in Chapter 3, but the overall process will be briefly stated here. The research was performed primarily using computational fluid dynamics (CFD) software coupled with optimisation methods – such as the adjoint and derivative-free approaches. The numerical models were validated against experimental data available in the literature for the uncontrolled flows. While many studies have demonstrated the effectiveness of suction control [Fransson et al. 2004, Sohankar et al. 2015], and some have performed optimisation of its implementation [Chen et al. 2013, Li et al. 2003, Min and Choi 1999], we were particularly interested in the objective of eliminating separation, and whether there are any useful relationships between the separation characteristics of the flow and optimal control to eliminate separation or minimise drag. This interest comes from the natural of autogenous suction control which depends on the same flow features that lead to separation. Determining these relationships might reveal whether autogenous control can be effective for a given flow, without performing further simulations.

As for the design of autogenous suction control, Atik and van Dommelen [2008] had provided a basic proof-of-concept for 'upwind' autogenous control, however their application had several advantages that are not present in the bluff body flows we chose to investigate. For one, the flow around bluff bodies like the circular cylinder is almost always unsteady, as vortex shedding occurs in the wake from very low Reynolds numbers. Secondly, the pressure profiles around an airfoil are already carefully designed to be favourable, and the geometry allows plenty of room for the flow to develop and respond to a control stimulus. This is not the case for a geometry like the circular cylinder – which represents an extreme challenge for developing autogenous control. We believe that if autogenous control can be effective for this flow, it can be for all other

smooth/continuous bluff bodies. To investigate this, we took the following approach to methodically approach optimal autogenous control design:

1. The autogenous control can be modelled by using velocity inlet/outlet boundary conditions on the bounding wall
    (a) By matching the flow rates the system satisfies continuity
    (b) However, the pressures of the suction and blowing regions must be matched to replicate a real system where losses occur in the porous wall and connecting ducts
        i. The pressure profile changes whenever we apply or adjust the control, therefore the solution to a dynamic system is needed.
        ii. This can be achieved by again utilising optimisation methods. Here, the objective is to minimise the absolute difference in the control pressure differential between the real differential and the desired one (that which will match the expected losses). Or to achieve the major objective (e.g. minimise drag) while enforcing a constraint that the pressure differential must be greater than some value.
2. The optimisation can be performed of this entire system to determine the most effective autogenous control for a given objective, e.g. to minimise drag
3. This system which was imposed by boundary conditions can be translated to a real system by designing an appropriate geometry

The usefulness of this approach, its benefits, flaws and achievements, makes up a large part of the research findings.

1.3 KEY CONTRIBUTIONS AND THESIS OUTLINE

Our main contribution is the development of a robust method to model and optimise effective autogenous control by imposed-boundary condition simulations. On the path to this objective, however, we made several other novel contributions.

First, the control of separated internal flows was demonstrated by parametric and optimisation studies of suction control of the conical diffuser, described in Chapter 4. Suction control of diffusers had previously been disregarded by most engineers as too inefficient to be worthwhile [Sparrow et al. 2009], but we found this was not the case. Our wide-ranging simulations of suction control over a wide-range of parameters (divergence angle, Reynolds numbers, and control parameters) was entirely novel. This uncovered several interesting results including the development of hysteresis in the controlled flows, and optimised non-uniform suction profile. Some of this work was also published in the Journal of the Royal Society New Zealand [Ramsay et al. 2020b].

In Chapter 5 CFD simulations were coupled with neural networks in order to train a system which can design geometries that induce arbitrary non-uniform suction profiles in an adjacent flow. While tools like the Venturi tube have long been used to induce suction, we believe this is the first time geometries have been designed to develop non-uniform suction profiles, and the approach using neural networks to develop a versatile designing system is novel. This work was presented at the Australasian Fluid Mechanics Conference and published in its peer-reviewed proceedings [Ramsay et al. 2020a]. This investigation was a stepping-stone towards autogenous suction control where the control ducting may need to be designed to generate more complex and effective suction profiles.

The circular cylinder was our primary geometry to investigate the potential of autogenous suction control. To begin the investigation, extensive parametric and optimisation studies were performed on the suction control of the cylinder at low Reynolds Numbers ($Re \leq 180$) where the flow is entirely two-dimensional and laminar. This is described in Chapter 6, and in the papers [Ramsay et al. 2020c, d]. The investigation comprehensively compared uniform and non-uniform suction. The relationships uncovered between the optimal control parameters and the characteristics of the uncontrolled flow were also novel. Significant improvements in drag were achieved with optimised non-uniform suction control, particularly once the uncontrolled flow had become dynamic ($Re \geq 48$). An interesting finding was that in this Re range, the optimal location for control was not at the point of separation, and that it moved in opposition to the separation point as the Reynolds number was increased.

Atik and van Dommelen [2008] had shown that autogenous control could improve the flow around an inclined airfoil, however it was not known whether autogenous control could be effectively implemented for a bluff body, particularly one with a highly dynamic wake. In Chapter 7 we perform the first investigation into such a situation. The development of a model which can accurately represent the controlling flows and be used to optimise its arrangement was entirely new. This work was performed in laminar conditions and with both steady and unsteady assumptions to develop an understanding of the conditions that need to be considered in such future design work. Flow-rate suction/blowing control was implemented and optimised to minimise drag while maintaining a positive pressure gradient from suction to blowing (P-Q-balanced Dual-Loci control)

Finally, the development of a practical implementation is described in Chapter 8. Physical design concepts were developed to produce the optimised autogenous control profiles found in Chapter 7 and the resulting flows were simulated. This approach for designing drag-reducing geometries is unique.

A detailed discussion of the background of this field and the state of the art is presented in Chapter 2 - Literature Review. Then the methodology used in this work

is described in-depth in Chapter 3, particularly the development and validation of the simulations and optimisation procedures. The thesis concludes with a chapter summarising the key findings, and discussing some of the potential future work that could beneficially follow-on from this research (Chapter 9).

Chapter 2

LITERATURE REVIEW

2.1 BACKGROUND & MOTIVATION

2.1.1 Drag and its Impact

In practically every fluid-body interaction, drag is induced on the body by the relative flow of fluid around it. Drag acts as a force in opposition to the motion of the body, thus decelerating it or else inducing stresses in the structure. The influence of drag-loading can be seen throughout engineering design. For example, in civil engineering, buildings must be built to withstand the drag loads from wind; in mechanical and aeronautical engineering, vehicles are streamlined to minimise drag and their engines are designed to provide enough power to overcome these loads; even in process engineering, the flow rate in pipe-systems is greatly reduced by skin friction drag with the walls or separation of the fluid around bends. As Frank White put it in his textbook on fluid mechanics: *"Since the Earth is 75 percent covered with water and 100 percent covered with air, the scope of fluid mechanics is vast and touches nearly every human endeavour"* [White 2017]; with viscous fluid dynamics, inevitably comes drag.

The cost of drag worldwide is huge, both financially and environmentally. A 2004 paper by Wood, found that approximately 16% of the total energy consumed in the United States is used to overcome aerodynamic drag in transportation systems [Wood 2004]. A more specific example is given in a review on turbulent boundary layer control by Kornilov [2015], which estimated that a 1% reduction in drag load for an aircraft like the A340-300 could save 400,000 L of fuel per year per plane. One example outside of the transportation sector, is the decrease in life-span of suspension bridge cables due to periodic drag loading [Zuo et al. 2008]. Efforts to minimise drag have been an area of research for over a century now, with informed investigation possible following the advent of boundary layer theory in 1904 [Prandtl 1904]. The rising concerns of climate change, and the commitment of most nations to the Paris Accords, means that there is a stronger impetus now, more than ever, to make transportation more efficient and develop better drag-reduction methods.

2.1.2 Causes of Drag

The total drag on a body can be broken down into two contributing forces, each arising due to a different phenomenon of the fluid-body interaction. Firstly, *skin friction drag* (also referred to as *viscous drag*) which is equal to the integral of the shear stresses on the body surface. These shear stresses arise due to the viscosity of the fluid (its internal friction from cohesive forces) and the fluid's deceleration from the free-stream because of adhesive forces at the fluid-body interface. Secondly, *pressure drag* (sometimes called form drag) arises due to the presence of a lower pressure region behind the body than in front of it – a result of separation of the boundary layer, and recirculation. Pressure drag is evaluated as the integral of normal forces acting on the body.

Depending on the body shape and the fluid flow, the relative contributions of these two components to the total drag force may differ. For example, a streamlined body like an airfoil will have a very low pressure drag, thus the total drag is dominated by skin friction drag. On the other hand, a bluff body like a cylindrical or rectangular body will have their total drag dominated by the pressure drag component. Figure 2.1 below, taken from the popular textbook by White [2017], shows the contributions of each drag component for a streamlined cylinder with varying thickness-chord ratio, further illustrating how these components relate strongly to the body shape. According to Wood [2004], the relative contribution of pressure drag for ground vehicles is upwards of 75%, and about 50% for subsonic aircraft and surface water vehicles. The contributions of each drag component to the total are also dependent on the Reynolds number of the flow, Re, as well as the shape. Generally, at low Re the skin friction drag is more important, whereas at high Re ($Re > 10^5$) the pressure drag is much larger and the primary concern (though for streamlined bodies the skin friction drag is more significant at high Re).

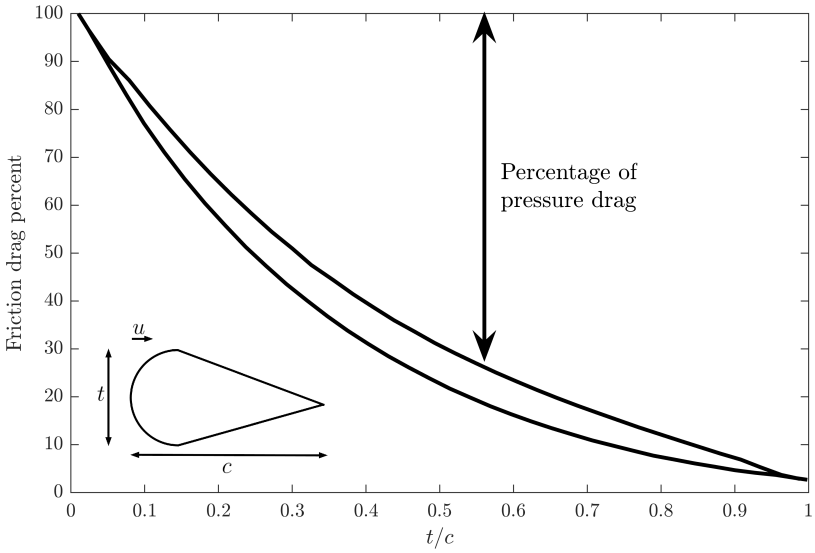

Figure 2.1 Contribution of skin friction drag to total drag for a streamlined cylinder with varying thickness-chord ratio. Data taken from White [2017, p. 485]

Skin friction drag cannot be eliminated in any practical way. There will always be strong adhesive forces between a wetted-body and the fluid. The skin friction drag can be minimised, however, by extending the regime of laminar flow or by decreasing the wetted area [Lachmann 1961]. An example of the minimisation of friction drag can be seen in the study by Klyuev et al. [2017], where a liquid film covering a flat plate greatly reduced the frictional resistance in air. This is effective as it produces a slip-boundary rather than a no-slip one, reducing the adhesive forces on the fluid. Pressure drag, on the other hand, can theoretically be eliminated. Zdravkovich claims that potential flow (fluid flow that ignores viscous effects) can be simulated in a real flow by removing the boundary layer with surface suction [Zdravkovich 1997, p. 945]. Early experiments by Thwaites found that with suction on a porous cylinder, combined with a small stabilising flap at the rear of the cylinder, the pressure distribution of potential flow was almost achieved, but with slightly lower minimum pressure coefficient [Pankhurst et al. 1953]. One of the most important flow features that must be altered to achieve such a pressure distribution is boundary layer separation, since after separation the pressure does not fully recover, as shown in Figure 2.2.

Altering the flow to reduce pressure drag can result in considerable changes to the magnitude of the skin friction drag, so care must be taken to not increase the net drag accidentally. Because of the complex relationships between the two drag components and the methods of flow control, it is difficult to know what the lowest possible drag for a body in real flow is. It seems reasonable that a body which, through the use of flow control, achieves the pressure distribution given by ideal potential flow would have the minimum drag, however Choi et al. [2008] in their review have identified that this has not been definitively proven and identified the issue as important for further

investigation.

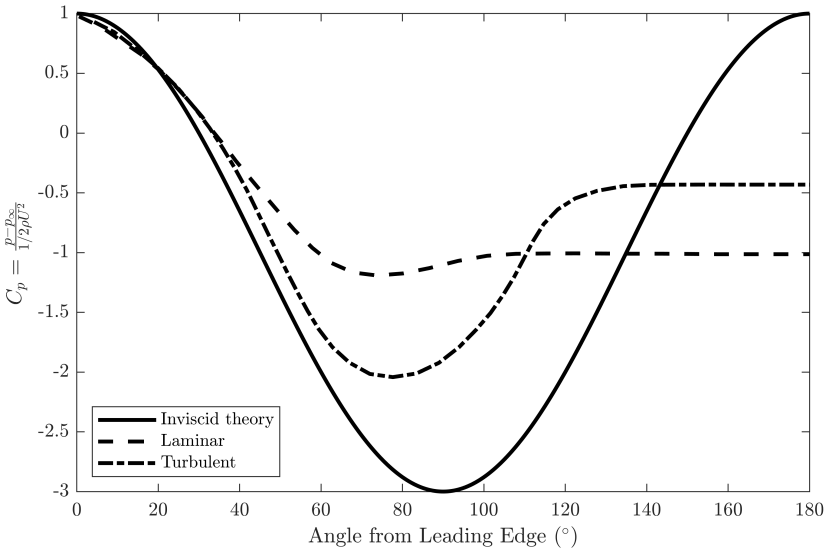

Figure 2.2 Pressure coefficient along one half of a circular cylinder for laminar, turbulent, and potential flow. Note that the pressure is never fully recovered in either of the real flow examples resulting in a deficit and net force on the body. Data from White [2017, p. 486].

2.1.3 Boundary Layer Separation

Preventing boundary layer separation can greatly improve the pressure profiles around bluff bodies. In order to properly control boundary layer separation, it is vital to understand what it is. In particular: how it arises, its effect on a flow, and how it can be precisely identified. The "boundary layer" (BL) is a concept introduced by Ludwig Prandtl at the beginning of the 20th Century. At a 1904 conference Prandtl [1904] proposed that the viscosity of a fluid need only be considered in the region very near to a body surface. This is because it plays an important role in this area due to the slower velocities as the no-slip condition (from the adhesive solid-fluid forces) decelerates the flow at the wall. Outside of this boundary layer, the viscous effects are negligible and the free-stream of the fluid can be fully described by Bernoulli's or Euler's equations. The concept of the boundary layer makes it possible to explain how pressure drag arises on a body. It can be explained by the separation of the boundary layer from the body surface - where the fluid begins to recirculate. Downstream of the separation, the pressure never recovers as the energy in the flow remains in the form of kinetic energy dispersed in the vortices that form in the wake. It is important, therefore, to understand why boundary layer (boundary layer) separation occurs. In order for a boundary layer to separate, three conditions need to be satisfied:

1. **No-slip condition** at the body-fluid interface.
2. Presence of an **adverse pressure gradient (APG)**.
3. **Insufficient momentum** in the fluid volume.

The fluid-body interaction takes energy from the free-stream flow, and so the BL grows in thickness along the bounding wall of the body. More momentum has to be supplied by the free-stream to account for the accumulative interfacial surface. This alone is not sufficient to cause separation, however, as seen by the lack of separation on a flat plate with zero-incidence to a crossflow Schlichting [1987, p. 35]. In order for separation to occur, an adverse pressure gradient (APG) is necessary. This is one where the pressure increases in the streamwise direction. The APG enacts an additional opposing force on the fluid. The already decelerated particles in the boundary layer, particularly those nearest the wall, are thus susceptible to having their flow reversed. Here, the third condition comes into effect. Even if the first two criteria are satisfied, separation is not necessarily guaranteed. A flow with sufficient momentum can overcome the opposing forces from the no-slip condition and the adverse pressure gradient, while one with insufficient momentum will separate. This partly explains why turbulent flow has a further-delayed separation point than laminar flow – turbulent flow has better momentum mixing properties, thus the boundary layer is stimulated by the free-stream more effectively.

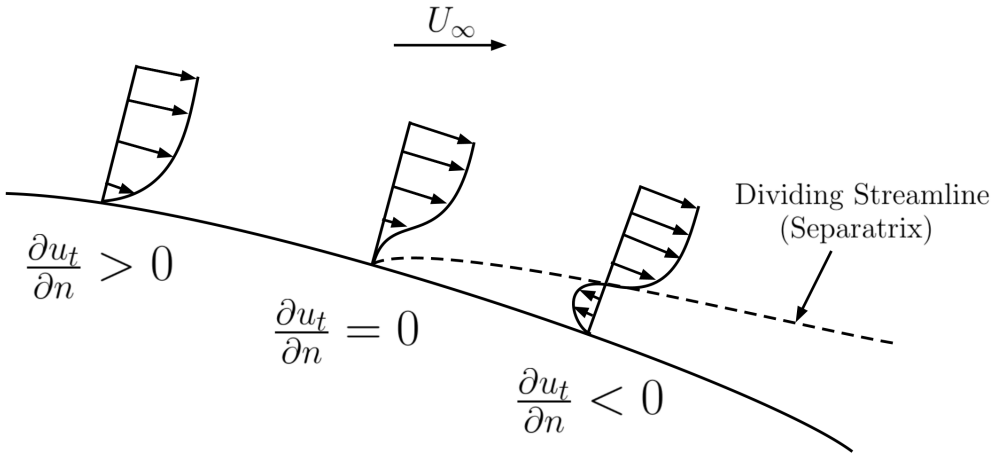

Figure 2.3 Schematic of boundary layer separation. Flow moves from left-to-right over a curved surface, into an APG. The flow nearest the wall slows, stalls, and reverses.

Knowing these criteria for separation, it is now possible to see what scenarios are at risk of undergoing boundary layer separation. Obviously, there is the problem of a bluff body exposed to a flow, like vehicles and cylinders, as discussed earlier, but these conditions can also be satisfied in internal flow. In a diverging channel, an APG is imposed on the flow, thus the divergence angle must be small in order to avoid separation [Sparrow et al. 2009]. The problem arises in pipe-bends also, and can severely inhibit the net flow-rate of the fluid [Fried and Idelchik 1989]. Ultimately, in almost any fluid flow problem, boundary layer separation is likely to be a concern as any practical use of fluid requires some solid body boundaries or interactions, and the pressure contours in any non-trivial scenario can be complex.

2.1.4 Effects of Boundary Layer Separation

Boundary layer separation has a drastic effect on a flow. The obvious effect is reversed flow after the point of separation. In external flows this usually results in a recirculatory wake behind the body; for internal flows, eddies may be produced. Consequently, the properties of a flow regime with separation deviate greatly from that predicted by potential flow theory. The loss of momentum in the boundary layer produces a pressure field along the surface of the body that does not agree with the potential flow, and after the boundary layer has separated the pressure is never fully recovered, as can be seen in Figure 2.2 [Schlichting 1987, p. 35]. The net pressure deficit on the leeward side of the body results in the pressure drag as described earlier.

The formation of a wake after separation might be considered as a rapid growth of the boundary layer so that it is very thick. The assumptions underlying the boundary layer equations breakdown, and the flow cannot be resolved analytically. Physical experiments or numerically resolving the full Navier-Stokes (N-S) equations becomes necessary to determine the pressure distribution impressed on the boundary layer. This breakdown of the boundary layer equations is called the Goldstein singularity, so-named after Sydney Goldstein who wrote early papers on this problem [Goldstein 1948]. Modern computational fluid dynamics (CFD) software is able to overcome this issue either by solving the full N-S equations or employing alternative methods developed in the years following Goldstein's discourse on the problem [Veldman 2009, 2017]. Nevertheless, the breakdown of the boundary layer equations greatly reduces the ability to solve numerous flow regimes, and simulation times for separated flows are much longer than those where the boundary layer remains attached.

If any effort is to be made in preventing it, it is necessary to be able to identify precisely the point at which separation occurs. The definition of the point of separation is the limit between forward and reversed flow of the layer in the immediate neighbourhood of the wall [Schlichting 1987]. This definition is described mathematically in Equation (2.1).

$$\left(\frac{\partial u_t}{\partial n}\right)_{n=0} = 0 \tag{2.1}$$

where n is the normal direction pointing away from the wall, and u_t is the flow velocity component tangential to the wall. Since this definition can apply equally to a point where reversed flow reattaches (reattachment point) as well as to a separation point, sometimes it is necessary to specify the second-derivative also:

$$\left(\frac{\partial^2 u_t}{\partial n^2}\right)_{n=0} \leq 0 \tag{2.2}$$

It can be seen from this definition that at the point of separation, the shear stress on the body will be zero, consequently so will the coefficient of skin friction. These

properties can be used in numerical studies to accurately pinpoint the point of separation. This can be more difficult in physical experimentation, however alternative properties of the separation can be used – in particular the onset of reversed flow. Wu et al. [2004] gives a good overview of the common methods historically used to identify the angle of separation for the flow around circular cylinders at low Reynolds numbers. These typically rely on identifying the point of separation by eye as the point where the recirculatory wake begins at the surface of the body. Visualisation of the flow is often aided by tracers in the fluid, or other imaging techniques including streakline, instantaneous streamline, or density imaging methods, however disparity in experimental setups and the wide variety of methods used results in a fairly large spread in the identified location of separation in the literature. In the paper by Wu et al. [2004], the authors show a spread of up to 10° in the angle of separation from ten different sources of experimental data. This can make it difficult when trying to validate numerical studies with experimental results.

The onset of reversed flow at separation can also be used to identify the point of separation in numerical studies if desired. It is less reliable, however, as reversed flow is not necessarily a result of separation. As noted by Leal [1989], a recirculating wake does not necessarily imply that separation has occurred. This can be seen in the numerical study carried out by Yu et al. [2011] of the flow around permeable cylinders where a recirculatory wake is seen detached from the surface, but no separation occurred at the cylinder. On the other hand, if separation has occurred in a flow, by definition reversed flow must follow. To avoid confusion, it is better to identify the point of separation by the properties of the fluid in the near-wall region, in particular the zero shear rate at the wall at the point of separation (POS).

2.2 FLOW CONTROL

Flow control is an active field of fluid dynamics. The aim of flow control is to design methods that interact with the fluid or geometry of a fluid flow system in order to achieve desired objectives. It lies at the intersection of fluid dynamics, control/stability theory, and engineering design. Control with the objective to delay separation is only a subset of the overall field. A brief picture of this field's history and current state will be given here, followed by a more detailed description of the classification methods, and the specific type of control this thesis is concerned with: suction/blowing of the boundary layer.

2.2.1 A History of Flow Control

For as long as modern fluid dynamics has existed, great efforts have been spent to try and control fluid flows to meet the whims of researchers and inventors. At the

beginning of the Twentieth Century, to test his theory of the boundary layer, Prandtl [1904] performed a series of experiments to control the flow around circular cylinders using suction or rotation of the body. Referring to the three conditions for boundary layer separation above, it can be seen that by removing the low momentum particles in the boundary layer (suction) eliminates Condition 3 (insufficient momentum) while the moving wall reduces the impact of Condition 1 (the no-slip condition). These results supported the hypothesis of BL theory. Since then, the field has been very active. In the lead-up to and during World War II great efforts were made by both axis and allied forces to control the flow around aircraft surfaces so as to get an advantage over the opposing forces. The two volume textbook edited by Lachmann [1961] provides great details over the advances in research during this time. However, since there were easier advancements to be made in the area of geometric improvements to aircraft surfaces, more complex methods like direct flow control were pushed to the side.

This research has continued apace in the peacetime that followed also, and regular reviews have been published since that give details of the advancements since this time. The annual review by Choi et al. [2008] provides an excellent update on the field in the early 21st Century, and the areas that are open for further research. Additional reviews have been made in a variety of journals, usually for the purpose of examining specific applications of flow control. In particular: flow control applications in centrifugal compressors by Tiainen et al. [2017], a review of vortex shedding suppression methods by Rashidi et al. [2016], a review of recent patents for flow control inventions by Kumar et al. [2010], and one on the actuators available for flow control by Cattafesta and Sheplak [2011]. These reviews have shown that since the genesis of this field at the conclusion of the 19th Century, flow control has developed from heavily geometric and steady, to increasingly fluidic and complex with the incorporation of feedback control, computational design, and optimisation of flow control.

2.2.2 Classification of Flow Control

There is a wide variety of active and passive flow control methods, ranging from simple geometric forms such as the splitter plate [Kwon and Choi 1996, Pankhurst et al. 1953] or helical strakes [Scruton and Walshe 1957] to complex active methods like plasma actuators [Sung et al. 2006] and magnetic fields [Rashidi et al. 2015]. It is necessary, therefore, to have a clear classification method to distinguish the principles by which each method works. Two classification styles are quite useful to this end: the first was introduced by Wood [2002] (and used in the review by Tiainen et al. [2017]) and the second was used by Choi et al. [2008] in their review of the field. These are reproduced in Table 2.1 and Table 2.2 below.

Table 2.1 Classification rubric devised by Wood [2002]

Layer	Groupings	Symbolic Grouping
1	Active or passive?	(A) or (P)
2	Geometric or fluidic?	(G) or (F)
3	Steady or unsteady?	(S) or (US)
4	Attached or separated?	(AT) or (SE)
5	Lift, drag, or both?	(L), (D), or (LD)

Active control requires the addition of energy into the system, while passive does not. Geometric control uses actuation that changes the external geometry of the body, e.g. flaps, whereas fluidic control affects the fluid motion directly, e.g. suction. For the third layer, steady and unsteady control are with respect to time. The fourth layer looks at whether the control is used on flow that is still attached or has already separated. The final layer is based on what aerodynamic forces the control hopes to affect.

The rubric from Choi et al. [2008] shares the first layer of classification but further split up the active grouping depending on if it uses open-loop control (i.e. without feedback) or closed-loop control. In contrast, their second layer is only concerned with if the control employs two-dimensional or three-dimensional forcing (e.g. control that acts in the streamwise direction only, or streamwise and spanwise control). Their third layer of classification relates whether the control acts on the boundary-layer or is a direct-control of the wake — this is similar to Wood's fourth layer.

Table 2.2 Classification rubric used in review by Choi et al. [2008]

Layer	Groupings	Symbolic Grouping
1	Passive, active open-loop, or active closed-loop?	(P), (A-OL), or (A-CL)
2	2D forcing or 3D?	(2D) or (3D)
3	Boundary layer or direct-wake	(BL) or (DW)

Choi et al. [2008] highlight the importance of considering both time-varying and spatially-varying control because this has been a large part of research by Kim and Choi [2005], Kim and Bewley [2007]. Though this dimension of control has not gone unnoticed, it is more difficult and computationally expensive to design control that is unsteady and spanwise varying (distributed), so perhaps has not received as much attention as steady, uniform control. The classification described by Wood is useful for describing practical designs in detail, while the groupings by Choi et al. [2008] are useful for highlighting the physical aims and effects of each type of control. Both are used in this thesis.

As can be seen by these classifications, not all flow control is aimed at delaying

or preventing separation. Many flow control methods aim at directly controlling the wake to reduce lateral forces – in these cases, drag reduction is a secondary concern. An example of this type of control are Thwaites' flaps which are plates placed at the trailing edge of an object to prevent mixing of shear layers thus inhibiting the formation of the von Kármán street [Zdravkovich 1997, ch. 21]. This is a passive geometric control method that works directly on the wake, rather than affecting the boundary layer. On the other hand, an example of boundary layer control would be surface roughness, which can be altered to induce early transition to turbulence to delay separation. Some control methods such as slot-injection (suction or blowing) can be used for either purpose.

Suction is typically considered a form of boundary layer control, as it removes low-momentum fluid from the wall surface, delaying separation. Experiments using suction such as those by Shtendel and Seifert [2014], and Chen et al. [2015] exhibit its use as a boundary layer control method. In a 2005 paper by Kim and Choi [2005], however, slot-injection is applied across the span of a cylinder to prevent the von Kármán street forming. This method actually causes separation to occur earlier along the cylinder but is successful at stopping the von Kármán street by blowing/sucking directly out-of-phase with the Strouhal frequency. Therefore, this control method should be classified as direct-wake control as it is the interactions that prevent instabilities in the wake that make it effective, not the early-onset separation.

When it comes to the problem of drag reduction, however, the benefits of preventing boundary layer separation are much greater than merely controlling or stabilising the wake. It would be better to delay separation as this reduces the size of the wake and stabilises greater regions of flow, rather than trying to prevent instability growth directly in an already large wake. Only in scenarios where the point of separation is immovable, such as behind blunt bodies with sharp edges, does this seem futile, for this research the focus was on boundary layer control.

2.2.3 Efficiency of Flow Control

Finally, it is important to highlight the energy-cost of flow control. Early efforts in flow control were mainly focussed on improving geometric designs to achieve the best aerodynamic characteristics [Lachmann 1961], however in the last twenty years a great deal more interest has been paid to novel active methods, as the limitations of simple geometric improvement have been largely reached. But with any active control, the energy used to run the control system must be outweighed by the improvement in performance obtained. When looking to reduce drag, the effective efficiency can be calculated using the following equation as taken from Choi et al. [2008]:

$$\eta_1 = \frac{(F_{d_u} - F_{d_c})U}{\int_A (0.5\rho v_w^3 + p_w\phi)dA}, \tag{2.3}$$

where F_{d_u} is the drag on the body without control, F_{d_c} is the drag with control, U the free-stream velocity, A is the body surface, ρ is the fluid density, p_w is the surface pressure, and v_w is the control velocity (the notation has been changed from the original to match the rest of this thesis). The efficiency, η_1, must be greater than unity for the system to be efficient and, ideally, should be much greater. This calculation only considers the momentum balance – further inefficiencies in realised systems will inevitably have further inefficiencies, decreasing the performance further.

2.2.4 Suction Control

The pertinent question now is what method of actuation has the most potential or should be explored further? Despite the development of modern methods like electrohydrodynamic control or synthetic jets, many of which have great potential, one of the oldest control methods is still very attractive: suction. Suction is an effective boundary layer control method because it removes low momentum particles at the wall surface, which entrains higher momentum particles from the free-stream to replace them. This weakens or eliminates the third condition for boundary layer separation (insufficient momentum). Its counterpart, blowing jets, works in a similar way by directly accelerating the near-wall fluid elements. However, to be effective they must blow tangential to the bounding wall, which can be difficult to implement on curved surfaces such as a cylinder or airfoil. Together, these methods of control are called slot-injection (where suction is negative injection and blowing is positive), though we typically refer to this as suction/blowing control for clarity. Slot-injection is usually implemented using a pump to provide the suction or blowing force. Slots or slits are installed in the body wall, or the wall is replaced entirely with some permeable material to allow the removal or addition of fluid. Both methods have been shown to be highly effective at controlling a variety of flows [Braslow 1999, Huang et al. 2004a, Pankhurst et al. 1953]. Specific examples of slot and uniform suction controls will be detailed for each reference geometry later in this chapter. Here, a brief discussion on non-uniform suction is given, before describing the state-of-the art on autogenous suction control.

2.2.5 Non-Uniform Suction

In recent times, non-uniform suction control has received fresh attention as interest in the optimal control problem has grown. There have been a large influx of papers since the 1990's that have attempted to determine the optimum suction/blowing profiles for different flows to achieve a variety of objectives. To determine the optimum, numerical models are developed which allow any suction/blowing profile to be formed on the body surface. Objective functionals are then defined and optimisation methods employed to try and solve for the best result. Examples for this can be seen for the circular cylinder at low Reynolds numbers ($Re < 200$) with Min and Choi [1999] attempting to minimise

pressure drag, or Li et al. [2003] who succeeded in minimising enstrophy (a measure of vorticity in a flow). Boujo et al. [2019] employed adjoint-based optimisation to find optimal spanwise suction/blowing to stabilise the wake of a 2D cylinder. Each study had success in improving the characteristics of the flow, however, none of these authors investigated how the separation angle changes directly, or whether it can be eliminated. A series of studies by Huang et al. performed parametric simulations of non-uniform suction on a NACA 0012 aerofoil, including using optimisation and genetic algorithms Huang et al. [2004a, b]. By designing numerical studies in this way, a wide variety of parameters can be investigated including the location of suction, its strength, angle of suction, and its profile. The results of all these studies suggest that effective results can be achieved more efficiently using non-uniform suction than its uniform or slot varieties.

2.2.6 Variation of Suction with Flow Conditions

Studies have shown that the effectiveness of suction control is greatly dependent on the Reynolds number of the flow, among other considerations. A 2004 paper by Fransson et al. [2004] investigated the effectiveness of suction and blowing on a porous cylinder in an experimental study similar to Pankhurst et al. [1953] early experiments. The researchers investigated the effects of the suction and blowing over a wide range of Reynolds numbers, nearly the entire subcritical regime ($10^2 \leq Re \leq 10^6$). The researchers found that suction was effective at delaying separation and reducing drag (up to 70%), while blowing (base-bleed) had the opposite effect. An important finding of the paper was that the effect of the suction/blowing could be represented empirically by an effective Reynolds number for the solid cylinder.

Although the relationship found by Fransson et al. may not be appropriate at all Reynolds numbers, it offers a good first estimate for predicting flow behaviour when implementing suction/blowing systems. Further studies have not addressed whether the expression holds up under different conditions, or if a similar relationship can be found for different shapes. Perhaps an arbitrary continuous bluff body might exhibit similar trends. Furthermore, these studies used steady, uniform suction across the entire surface, as has much of the historical research. It stands to reason that due to the varied pressure profile over a bluff body, non-uniform, unsteady, or discontinuous suction/blowing might result in better results. While the optimum suction for reducing drag has been exactly solved for particular cases, such as a flat plate at zero incidence, it has not been for flow in the presence of an adverse pressure gradient [Schlichting 1987, ch. XIV]. In conditions where separation can occur, the relationships between the flow, drag, and suction control are more complex and cannot be easily described.

2.3 AUTOGENOUS SUCTION

The suction control methods described until now are almost all types of active control, requiring a pump to power them. However, it is theoretically possible to generate suction using the energy from the fluid flow alone. Autogenous (meaning 'self-generating') suction has been suggested as a potential solution to this dilemma by researchers Atik and van Dommelen [2008]. This method utilises the energy already in a flow to generate the secondary suction flow. In their paper, Atik and van Dommelen [2008] perform a numerical investigation on whether suction can be autogenously generated to delay the point of separation over a thin airfoil. By connecting the low pressure region shortly before the separation point to a distributed area at a slightly higher pressure in the separated region downstream, a secondary flow can naturally develop. The authors performed this study without physically connecting these regions, but applying appropriate boundary conditions and deducting some pressure to account for losses in a real ducted system. The autogenous suction was able to prevent separation at a range of angles of attack that would have led to stall in the uncontrolled case.

This research offers an exciting prospect for potential passive flow control using suction, particularly because the pressure distribution required for autogenous suction is the same that induces separation. Ergo where separation occurs, autogenous suction should be possible also. The results suggest that to continue to delay the separation point, suction must be spread over the entire rear surface - beginning at where it commences without control. Importantly, also, the researchers found no theoretical limit to the angles of attack at which it could be instigated. This means that the control is possible in very steep APG, provided their model is accurate.

It is important to note that Atik and van Dommelen [2008] took a simplified approach to the control flow. They prescribed a set pressure drop ($\Delta P = 0.1$), and assumed that this would be sufficient to drive the flow. This is because the real pressure drop needed is dependent on any internal ducting and mechanisms incorporated in the design. The authors left these considerations outside the scope of their preliminary study. Furthermore, their study was on an already aerodynamic shape with a relatively kind pressure profile and a steady wake. For bluff bodies like the circular cylinder, these conditions are often not present. Regardless of these missing considerations, the study showed that autogenous suction control was certainly worth further research.

Connecting a point of high-pressure to low-pressure will generate a secondary flow, but difficulty arises when the desired suction profile (one that is known to improve the parameters of the flow, e.g. reduce drag) is located in a low-pressure region. Here, a more complex analysis is needed. The following important considerations are currently unknown in the literature:

- How autogenous suction might be generated in such a scenario (where suction is

needed in the region of lowest pressure)
- Whether autogenous suction can generate an optimal suction profile
- The extent of conditions in which it is effective/can be implemented

One solution to this low pressure suction problem, was put forward in a patent issued to Parikh [2011], and currently held by Boeing. The inventor suggests that when a lower pressure region is not currently present in the flow, a flap may be installed and used for the purpose of manipulating the external flow and generating a localised region of low pressure. No published studies provide details on whether this is actually practical, or if it can be used and still result in improvements to the characteristics of the flow. Additionally, the patent is limited in that the purpose of its control is to relaminarise the turbulent flow over aircraft surfaces. Although this can be greatly effective at reducing skin friction drag (which can be significant in turbulent flows), suction can reduce drag for laminar flows too - by delaying the separation point, or manipulating the pressure profile over the bounding surface, and hence reducing the pressure drag. Additionally, Parikh's patent provides no evidence that such a system as he describes can actually work in practice, or what limitations it has.

In the paper by Atik and van Dommelen [2008], the suction/blowing regime required upstream flow, however another possibility is to generate suction using the same approach but in the downstream direction. An alternative design might take fluid from a high-pressure region and accelerate the flow in order to produce a low-pressure area to provide a suction near the ordinary point of separation. This might be termed an 'accelerated flow' autogenous suction method, while the method studied by Atik and van Dommelen [2008] will be referred to as the 'upstream method'. Figure 2.4 demonstrates possible designs for the cases of a diverging channel and circular cylinder for both potential methods of autogenous suction as were sketched at the beginning of this PhD work. It remains to be seen whether the optimal suction/blowing distributions as found in the papers described earlier might be combined with the concept of autogenous suction to design geometries that achieve optimal control passively. It will be necessary to determine whether this is possible, in what circumstances, and if it would be feasible practically.

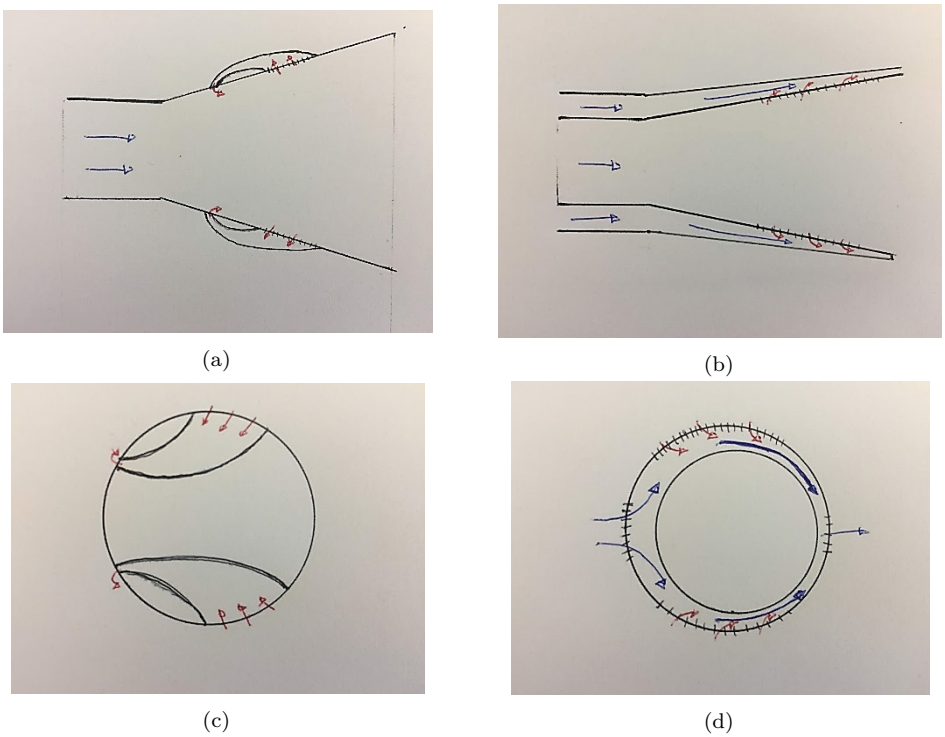

Figure 2.4 Potential applications of autogenous suction using the 'upstream method' from Atik and van Dommelen [2008] (left-hand side) and the proposed 'accelerated flow method' (right-hand side). (a) and (b) show designs for the diffuser while (c) and (d) for the cylinder.

The paper by Atik and van Dommelen [2008], as well as the Boeing patent from Parikh [2011] appear to be the extent of published material on the topic of autogenous suction. Although boundary layer suction has been researched for many years, this particular implementation is new and un-tested. Hence, the great opportunity for novel research and contribution to the field of flow control.

2.3.1 Variable Porosity Skins

In these early works, the design of autogenous control has been considered with the use of ducts and internal transport of the removed fluid. However this approach is problematic due to the large number of parameters and potential designs possible. To reduce the number of design considerations, an approach inspired by nature might be considered – that is the flow through bird feathers. Most birds have a variety of feathers, usually with stiff outer feathers to improve the aerodynamics, and with soft internal down feathers for warmth. Previous studies have shown that these external feathers may operate like flaps that are kicked up when recirculation occurs (after separation) and aids in dampening this recirculating flow [Müller and Patone 1998, Sedghi et al. 2018]. Rippled skin on particular species of sharks (such as the Mako shark) have a similar function [Afroz et al. 2016]. While a very recent study by Ayton et al. [2021] has looked at how the feathers affect flow from a porous point of view.

An alternative to ducted autogenous control, and one which might be much more practically realisable, is the use of overlapping porous skins. Like the bird feathers, imagine a body with two porous layers on top. The inner is highly permeable and – rather than providing insulation – allows fluid to travel from one area to another. The outer has spatially varying permeability. It promotes fluid to move through to the inner layer in particular areas, while in others it is practically impermeable. In this way, similar arrangements to that achieved by internal ducting might be achieved by a more manageable design. Here, the number of parameters are reduced from the combination of porous and duct design, to only the porous materials design. The problem of designing the outer layer with variable permeability is not simple, but a similar approach as the optimisation of suction control could be applied directly to the design problem. Instead of optimising a suction boundary field, the model can be retooled to optimise the permeability of the outer layer. What is more, previous studies have found that even a homogeneous porous layer on its own can improve the characteristics of flow around a circular cylinder [Hsu et al. 2015, Yu et al. 2011]. A 2019 PhD thesis by Pelacci [2019] investigated experimentally a similar system, where 3D woven materials were designed and applied to regions of a circular cylinder with moderate success.

2.4 GEOMETRY 1 – CONICAL DIFFUSER

Boundary layer separation can occur wherever an adverse pressure gradient is present. The simplest geometries where this is the case, are those of internal flows with diverging walls. In particular, the conical diffuser (diverging channel with circular cross-section) and the planar diffuser (diverging channel with straight walls), and the theoretical Jefferey-Hamel (J-H) flow (a 2D semi-infinite diverging channel and for which there is a known analytical solution to the N-S equations). In each of these cases, the pressure is expected to increase monotonically as fluid moves through the channel as the fluid must slow down to maintain continuity of mass. However, the actual flow can often differ substantially from theory as boundary layer separation and instabilities can produce rich and varied flow regimes, usually to the detriment of performance [White 2017, p.404]. Each geometry has practical applications also: the conical diffuser is commonly seen in pipe-flows, biological flows and even turbine engines [Egashira et al. 2019]; the planar diffuser is used regularly for ductwork and has applications as wide-ranging as hypersonic ramjet engines [Su et al. 2018]; while the J-H flow is a simplified version of both these flows and can be relevant to all their applications in certain conditions [Jotkar and Govindarajan 2017].

The conical diffuser was selected for investigating optimal and autogenous suction control in this research as it is the easiest of the three to investigate by CFD simulation, there is a relative plethora of experimental studies on the flow, and it has practical

applications where its improvement would be desirable (e.g. in preventing the failure of heart stents by recirculation [Williamson et al. 2019]). The planar diffuser has many parameters that could be implemented to produce vastly different geometries, aspect ratios and wall lengths. The geometry of the conical diffuser, on the other hand, can be simply described by four parameters: the initial diameter, d, divergence angle, 2α, the expansion ratio, $\beta = D/d$, and its length, L. The Reynolds number of this flow is defined by the average velocity at entry to the diffuser and the entry diameter, $Re = \frac{\rho U_1 d}{\mu}$. In the present work, low-moderate Reynolds numbers were investigated for this flow ($Re \leq 1400$) – a range in which the flow is known to be steady and axisymmetric [Cantwell et al. 2010].

The conical diffuser is a natural geometry for containing and directing the flow of fluids, and as such its use by humans is ancient [Rouse and Ince 1963]. However, the search for a deeper understanding of the resulting flows in this simple geometry is relatively recent, and it is still not fully understood. What follows is an overview of the research into the flow in the conical diffuser, beginning with the flow without any control implemented, a discussion of how its performance and efficiency may be measured, and finally an exploration of the studies investigating suction control to improve diffuser performance. Much of what follows was also described in detail in the co-authored paper 'Effects of boundary layer suction control on flow through an axisymmetric diverging channel' published in the Journal of the Royal Society of New Zealand [Ramsay et al. 2020b]. While the text here is original, it follows much the same structure as this paper and naturally refers to many of the same papers. Additionally, some work from that paper is quoted directly, and is attributed where this is done so in accordance with the copyright permissions of Taylor & Francis [2021].

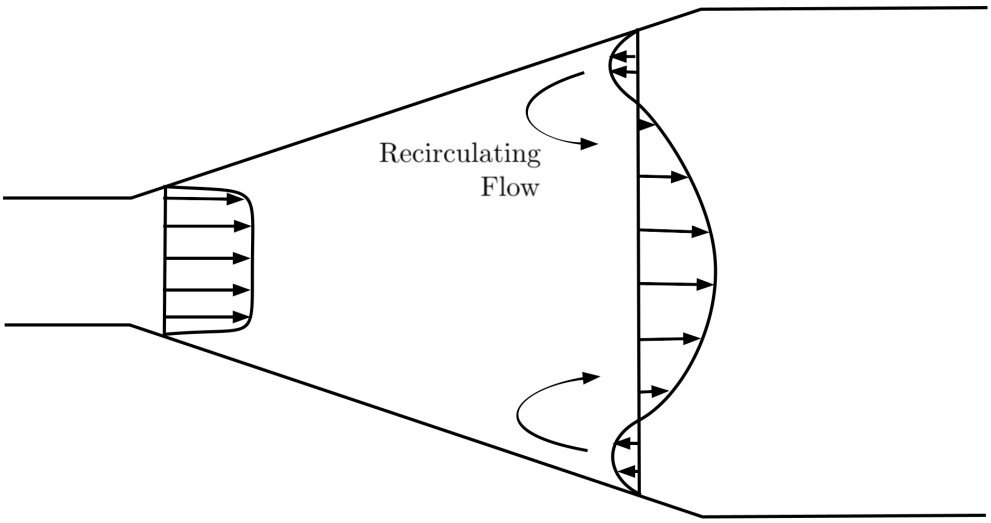

Figure 2.5 General flow structure for badly performing diffuser.

2.4.1 Function of Diffusers

As stated earlier, the conical diffuser has been used by humans since ancient times, with writings from ancient Rome describing the use of diffusers in city water supply systems [Rouse 1983]. The conical diffuser also goes by the name of expanding pipe or axisymmetric diverging channel in the literature; its usual purpose is to convert kinetic energy in a flow to pressure energy [White 2017, p.405]. As the bounding walls diverge, the cross-sectional area of the diffuser increases. Consequently, as the conservation of mass in a given space is a law of nature, incompressible fluids passing through this geometry must slow down as they progress through the diffuser. Since energy must also be conserved also, the kinetic energy of the fluid must be transformed to another form, in this case static pressure energy.

This simple feature of conical diffusers makes them useful in a variety of applications, for example: from controlling the movement of fluid, to store or increase the available energy of a flow, or to mix and distribute transportable materials. In pipework, the first use is exploited using diffusers at outlets to control and adjust flow rates [Armstrong et al. 2003, Rouse 1983]. Turbine engines increase the enthalpy of their combustible fluids before ignition using diffusers [Baya et al. 2010, Ligrani et al. 2017, Marsan et al. 2012]. And in the human body, lymph and venous systems exhibit natural diffusers as, for example, blood is returned from the extremities to the larger vessels near the heart [Egashira et al. 2018, 2019, Madhavan and Kemmerling 2018]. The flow through converging-diverging channels is a popular area of interest currently due to its relevance to 'stenoses' in arteries (blockages/reductions in blood vessel diameter) [Carroll et al. 2019, Fulker et al. 2013, Polanczyk et al. 2018].

2.4.2 Theory of Diffusers

The theory of diffusers has been understood since the early days of hydraulic study [White 2017, p.405]. An inviscid fluid will follow the contour of a diffuser and its characteristics along a streamline will change according to mass conservation and Bernoulli's equation:

$$U_2 = \frac{r_1^2}{r_2^2} U_1, \tag{2.4}$$

$$\Delta P = 0.5\rho U_1^2 \left(1 - \left(\frac{r_1}{r_2}\right)^4\right) = 0.5\rho U_1^2 \left(1 - \frac{1}{AR^2}\right), \tag{2.5}$$

where U is the mean velocity magnitude of the flow, r is the local radius of the pipe, ρ the density of the fluid, AR the area ratio of the diffuser ($AR = \frac{r_2^2}{r_1^2}$), and ΔP is the change in static pressure, while the subscripts denote the location of the flow moving from the diffuser entry (1) to its exit (2). Since the cross-sectional area of the

diffuser increases from location 1 to 2, the flow slows down and the pressure increases (an APG).

However, real flows do not produce smooth flows with the velocity and pressure profiles described by these equations. This is because all real fluids have some viscosity, which coupled with the no-slip condition at the walls cause a boundary layer to form and influence the flow. What's more, due to the adverse pressure gradient that arises in the diffuser, the flow may separate and partially choke the flow. Since, as has been discussed, the occurrence of BL separation depends on the satisfaction of three criteria (no-slip, APG, weak momentum) the flow in a diffuser will sometimes be near the potential flow, and at other times heavily separated and unstable – depending on the geometry, the fluid, and flow characteristics. Of these features and their parameters, the most significant are the diffuser divergence angle, 2α, the Reynolds number of the flow, Re, and the inlet profile [Kline et al. 1959, Latornell and Pollard 1986]. However, researchers have determined that other features also have an effect (though to a much lesser extent), including: the area ratio, AR, the diffuser length, L, the inlet profile and its turbulence [Fox and Kline 1962, McDonald and Fox 1966].

2.4.3 Measuring Performance

The performance of a diffuser is typically measured by its coefficient of pressure-rise, η_{pr} (Equation (2.7)), which is calculated as the average pressure-rise through the diffuser as a ratio of the dynamic pressure available at the diffuser entry. Since the fluid is expected to continue to flow at the diffuser exit and not stagnate entirely, some portion of the dynamic pressure should remain. η_{pr} measures the pressure-rise against that which a theoretically ideal diffuser would achieve with flow continuing at exit, while $C_{pr_{theor}}$ (Equation (2.6)) is the pressure-rise against the entirety of the dynamic pressure at entry (i.e. the performance of a diffuser where flow stagnates at exit):

$$C_{pr_{theor}} = \frac{P_2 - P_1}{0.5\rho U_1^2}, \tag{2.6}$$

$$\eta_{pr} = \frac{P_2 - P_1}{\left(1 - \frac{1}{AR^2}\right) 0.5\rho U_1^2}. \tag{2.7}$$

Though a diffuser may be designed with divergence angle from 0° to 180°, experiments by McDonald and Fox [1966] (among others) have shown that only a limited range gives satisfactory performance. It has been a general rule in hydraulics [Armstrong et al. 2003] for some time that a diffuser with divergence angle of less than about $2\alpha \leq 7° - 10°$ will remain attached, as highlighted by Sparrow et al. [2009] in the introduction to their paper. The experiments by Gibson [1912], Gibson and Petavel [1910] found that for a conical diffuser with area ratio $AR = 2$, the optimum pressure recovery was achieved with a divergence angle in the range $2\alpha = 5.5° - 7°$. This finding was repeated by

other experimenters also, whose work is summarised by Kline et al. [1959]. To add to the experimental results, Schlichting and Gersten [1961] employed boundary layer calculations to diffusers with the same geometry and flow, and calculated the optimal range to lie in $3° \leq 2\alpha \leq 8°$. They found that as Re increases, the optimum divergence angle decreases from 8° to the lower end of the range. On the other hand, experiments by Moore Jr and Kline found that the dependence on the Reynolds number diminishes once Re becomes sufficiently large, above "a few thousand" [Kline 1959, Moore Jr and Kline 1958]. In large part this small range of angles that produce satisfactory results is because of the separation of the flow which occurs when the APG becomes too strong at steep divergence angles.

2.4.4 Flow Characteristics

Interestingly, the best performance in a diffuser is seen, not when the flow remains attached and inviscid-like, but rather at the beginning of the separated regime where small recirculating regions are present near the exit of the diffuser [Kline et al. 1959]. Evidently the flow regime and separation characteristics have a significant effect on the diffuser performance. In their paper, Cochran and Kline [1958], produced a plot of the flow regimes seen within conical diffusers, which is replicated in Figure 2.6. The typical performance curve for a diffuser is shown in Figure 2.7 based on the collated data in Kline et al. [1959]. According to Kline et al. [1959], the best performance for diffusers occurs slightly above the line a-a in Figure 2.6, where small transitory separations occur. Presumably, the recirculating regions help to more efficiently convert the kinetic energy of the flow to pressure energy, without losing too much to viscous effects. These studies all suggest that the best diffuser performance is achieved in this flow regime, and this occurs when the divergence angle is small and the diffuser is long. Unfortunately, in practical cases this is often undesirable due to limitations of space. In these scenarios, either sub-par performance must be accepted, or some other method considered to improve the flow.

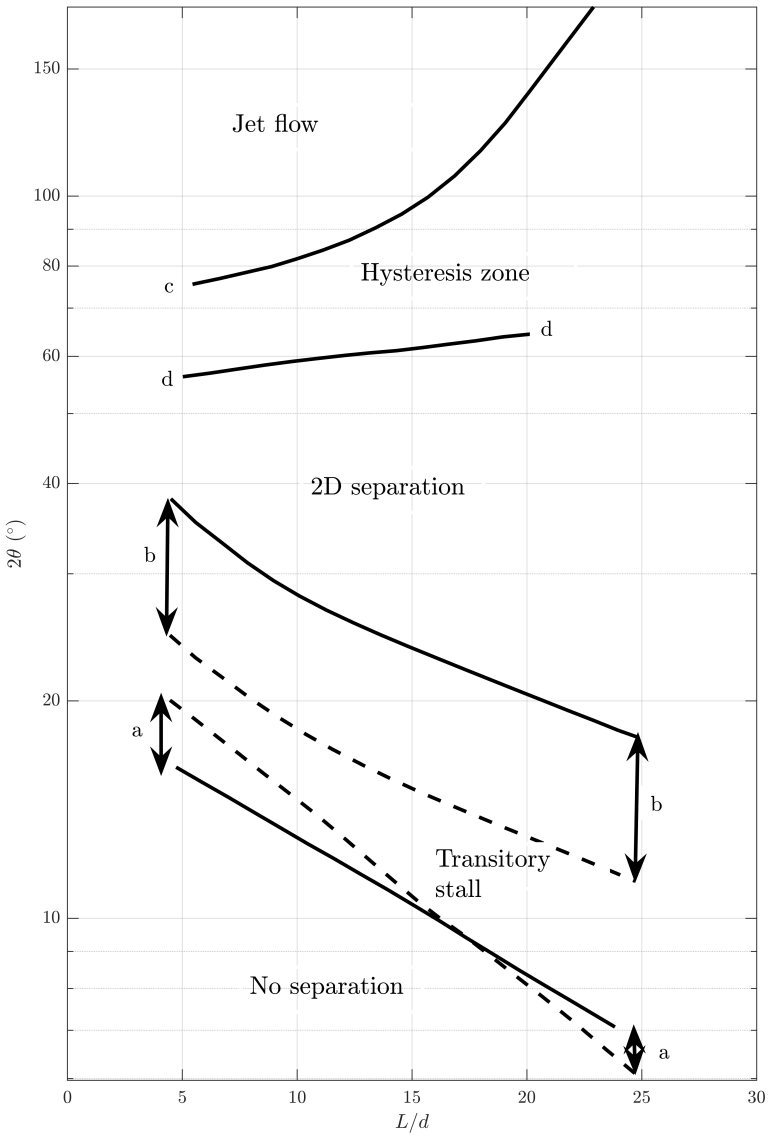

Figure 2.6 Flow regimes and transitions for conical diffuser of varying lengths at constant high Re. Data taken from Cochran and Kline [1958]

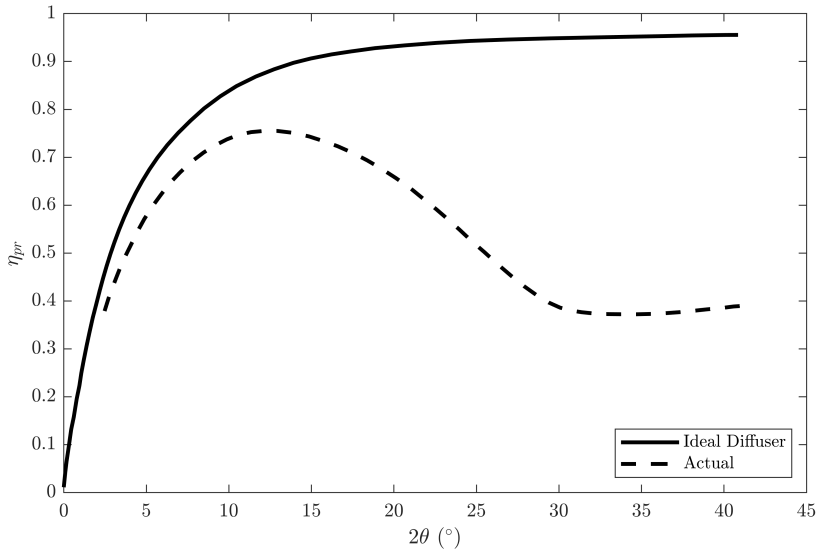

Figure 2.7 Typical performance curves of diffusers. Data is taken from Kline et al. [1959] for the planar diffuser at $Re = 2.4 \times 10^5$ with $L/d = 8.0$, but the curves are similar for the conical diffuser.

One of the interesting features about the flow through diffusers is the contradictory phenomena of re-laminarisation and destabilisation. As was described by Cochran and Kline, the flow through a diffuser often becomes separated and unstable, including the possibility for hysteresis between these different flow arrangements [Cochran and Kline 1958]. Jotkar and Govindarajan [2019, 2017] have recently published results of non-modal instability analysis for both the Jeffery-Hamel (J-H) flow and the diverging channel flow adding more insight. What is interesting is that as a flow moves through a diffuser, particularly a long shallow one, it is slowed greatly due to the increasing area. As the flow slows, the Reynolds number reduces proportionally, prompting the turbulent flow to relaminarise. Cantwell et al. [2010] showed by linear stability analysis that the flow through the conical diffuser is stable up to at least $Re = 1400$, perhaps partly for this reason.

This phenomenon of turbulence dampening has been a key part of the research of Jorge Peixinho and colleagues at the Centre National de la Recherche Scientifique (CNRS) in France [Lebon et al. 2018a, b, Peixinho and Besnard 2013, Selvam et al. 2015, 2016]. After a turbulent flow enters a diffuser, it stabilises as it slows, resulting in bursts of turbulent jets and chaotic motion within the diffuser [Peixinho and Besnard 2013]. This may be a desirable trait in circumstances where enhanced mixing is desired, with a steady outlet flow, e.g. in micro-fluidics applications. While suction control is usually used to stabilise a flow, its reverse (blowing) could similarly be optimised to do the opposite. Recent work by Egashira et al. has been looking at the flow through diverging channels and vessels as part of research into the human lymphatic system [Egashira et al. 2018, 2019, Fujikawa et al. 2016]. This includes the investigation of the effects of minor suction through the vessel walls, as may occur due to the porous

nature of biological materials. Their work is constrained to low Reynolds numbers ($Re \sim O(1)$) at present, but understanding the effects of suction on diffuser walls may have important medical applications.

2.4.5 Summary of Studies on Uncontrolled Diffuser

The present research carried out as part of this PhD thesis was entirely computational. It is of vital importance that CFD simulations are appropriately validated against directly comparable experiments. The literature has many studies that look at the diffuser. Many of these studies employ diffusers of different divergence angles, but the special "sudden expansion" flow (SEF) where $2\alpha = 180°$ is the most common. Fortunately, the trends for flow characteristics are similar regardless of divergence angle, even for the sudden expansion.

Many of the early studies of this flow focussed on the sudden expansion flow (SEF). Experiments by Macagno and Hung [1967], Back and Roschke [1972], Iribarne et al. [1972] and Pollard [1981] provided a useful foundation in the second half of the Twentieth Century. In almost all these cases an expansion ratio of $\beta = D/d = 2$ was used (where D is the diameter of the diffuser exit, and d the diameter of the entry). Through these studies it was found that the length of the recirculation region that forms after the sudden expansion, grows linearly with increasing Reynolds number. This was not completely clear at first due to experimental inconsistencies and imprecision. However, by the time of the paper by Latornell and Pollard [1986] summarising these historical experiments and providing new data, it was clear that this linear trend certainly was seen — at least up until any instabilities developed to the point that the flow becomes asymmetric (as with the J-H flow). Latornell and Pollard [1986] state the formula for the separation growth as

$$L_{sep}/d = 0.048Re, \tag{2.8}$$

where L_{sep} is the length of the recirculation region as measured from the expansion, and Re is the Reynolds number calculated based on the inlet diameter and the bulk flow rate. Here, the length is non-dimensionalised by the entry diameter, but in the original work the step-size was used in its place.

One of the best experimental works on the SEF was performed by Hammad et al. [1999]. This was for a diffuser filled with diethylene glycol and with a fully developed inlet profile (Hagen-Poiseuille profile). The authors used particle image velocimetry (PIV) to observe the flow field and they found that as the Reynolds number is increased for a diffuser of fixed divergence angle and length, the flow is initially attached and then separates near the exit. The recirculating region, which is axisymmetric, then grows linearly with Re, but with a different growth-rate than that given by Latornell

and Pollard [1986]. Instead the relationship was found to be

$$L_{sep}/d = 0.044Re, \tag{2.9}$$

which was quite different. The authors attributed this variance in growth-rate values to a variety of possible differences between studies. In particular the inlet profile, turbulence parameters, and even convective currents. Wang and Lin [1997] noted that if a working fluid of water is used, even a $1°C$ difference in temperature can cause convective effects that change the recirculation region profile, producing an asymmetric result. It appears that the value obtained by Hammad et al. [1999] is most accurate, as stability analysis performed numerically by Cantwell et al. [2010] gave a nearly identical values of 0.0438 (though in their paper the separation length is non-dimensionalised by the step-size ($0.5d$) rather than d so is stated as 0.0867.

It turns out that the same growth rate occurs regardless of the divergence angle, provided the flow is fully-developed on entry. This was demonstrated by computational studies and experimental work by Peixinho and Besnard [2013]. Peixinho and Besnard [2013] also found that though the growth rate does not change, the critical Reynolds number at which the separation begins is shifted – occurring earlier at steeper divergence angles. Furthermore, and unlike the case of $\alpha = 90°$, when the divergence is more gradual the growth of the separated region is not linear near the critical Reynolds number, but grows more rapidly at first.

It is generally accepted that best performance is garnered from a diffuser when the flow enters it with as uniform a profile as possible, but as far as the author is aware, this had not been quantified until this work. Other factors that impact the resulting flow include downstream effects – whether the flow is exhausted to a plenum [Cochran and Kline 1958, Reid 1953] or a tailpipe [Gibson 1912, Shenoy et al. 2019]. In the former the separated region is often not able to fully develop before reaching the plenum.

As for the performance of the diffuser, there are some quantified data charts available. The 'Diffuser Data Book' by P. Runstadler et al. has much, but it is out of print and widely unavailable [Runstadler et al. 1975]. Some of the charts are reproduced in White's textbook 'Fluid Mechanics' and the trends are similar to those collated by Kline et al. [Kline et al. 1959, White 2017, p.407]. These are at very high Reynolds numbers however ($Re \sim 10^5$) as are often seen in HVAC ducting. In this thesis we consider low-moderate Reynolds numbers only.

2.4.6 Suction Control

In cases where satisfactory diffuser performance cannot be achieved with a standard diffuser, one option is to apply flow control. The simplest forms of flow control are those of geometric changes, such as adding vanes or implementing annular designs. Kline

and his colleagues carried out many studies on the use of vanes in conical and planar diffusers, and much of their work has already been referred to [Fox and Kline 1962, Kline et al. 1959, Kline 1959, Moore Jr and Kline 1958]. But since the development of boundary layer theory, the use of boundary layer suction as an alternative method of flow control has been considered for the improvement of diffuser performance.

J. Ackeret, a Swiss experimentalist and one of the earliest aerodynamicists, performed the earliest tests of suction on the flow in a diffuser; Prandtl often referred to his work to demonstrate the importance of the boundary layer [Ackeret 1926, Tietjens and Prandtl 1957]. Ackeret applied suction via a small radial slit about a third of the way down two diffusers of different divergence angles, and found that the pressure recovery was substantially improved, even with only modest suction flow rates – for example, with a suction volumetric flow rate only 2.9% that of the free-stream, an improvement in efficiency from 0.75 to 0.824 was observed. This efficiency measure accounts for the energy of a pump with a modest efficiency of 75% which would exhaust the removed fluid back into the flow downstream of the diffuser at equal pressure. This measure of efficiency is shown in the following section. For the steeper diffuser, an even more substantial improvement was seen with the addition of suction. In the conclusion of his paper, Ackeret stated "The results, as a whole, raise the hope that we may some time succeed in relieving engineers, through the removal of the boundary layer by suction, of the necessity of employing very special shapes." However, his view soon fell out of favour.

Since the studies by Ackeret, other researchers in the 1900's explored the use of suction, or commensurately, tangential blowing in diffusers to improve performance. These studies are summarised in Table 2.3 as reproduced from the paper in JRSNZ co-authored by the present author. While almost all of these found positive results, with efficiency improved by at least 30% almost always – even when accounting for the energy to run the control – the popular outlook on suction control has been that it is too inefficient to be useful [Lachmann 1961, p.8]. This does not appear to be justified, though the report by Braslow on suction control on aircraft highlights some of the difficulties in material science and manufacturing to produce surfaces that allow suction without destabilising the flow, which no doubt contributed to the general pessimism towards suction control [Braslow 1999].

Table 2.3 Summary of key studies on suction/blowing control of a diffuser.

Authors	Control Type	Overall Results	Quantitative Result
Ackeret [1926]	Slot suction	"The values obtained enable us to hope for a favourable result in practice"	Diffuser efficiency increased by as much as 29.5%
Holzhauser and Hall [1956]	Area suction	"...a large increase in total-pressure recovery is obtained with small suction flow ratios."	Separation eliminated entirely ($L_{sep} = 0$) in $2\alpha = 30°$ and 50° diffusers
Yamazato [1969, 1970]	Area suction	"...area suction was effective to improve the diffuser performance..."	Pressure recovery increased by as much as 30% in $2\alpha = 30°$ diffuser
Furuya et al. [1966, 1970]	Slot suction at entrance	"With this optimum suction, the efficiency of these wide angle diffusers approaches that of the diffuser of $2\theta = 10°$"	Loss coefficient reduced to 0.2 for diffusers with $10° <= 2\alpha <= 60°$
Nicoll and Ramaprian [1970]	Blowing at inlet	"The most important information... is the existence of an optimum injection rate for obtaining maximum C_pr and η"	Efficiency increasing by factor of 3 for $2\alpha = 30°$ diffuser
Fiedler and Gessner [1972], Fiedler [1970]	Tangential blowing	"...significant increases in diffuser performance...even when jet blowing power requirements are taken into account."	For $2\alpha = 30°$ diffuser, performance increased up to 30%

2.4.7 Non-Uniform vs Uniform Suction

One of the questions that arises – particularly from a practical implementation perspective – is how the suction should most effectively be applied. In particular is uniform suction best? Or suction distributed over the whole surface but with a varying flow rate? Or is suction in only a small portion of the diffuser necessary? The experiments by Holzhauser and Hall [1956] on area suction of the diffuser found that similar or even improved results could be achieved when the suction was limited to only some regions of the diffuser wall (using tape to cover the other porous areas). They state "it is not necessary, or even desirable from a suction flow standpoint, to apply area suction down

the entire length of the diffuser". On the other hand, Fiedler and Gessner [1972] suggest in the Introduction of their paper that "the best improvement in performance occurs when suction is distributed over the entire surface". Other researchers, in particular Furuya et al. [1966, 1970], and Yamazato [1969, 1970] showed that non-uniformly applied suction was indeed effective. Furuya investigated the effect of slot suction at the diffuser entry, while Yamazato focused on uniform suction applied to small areas (area suction. Both studies found, in their own way, that suction concentrated in the upstream portion of the diffuser was particularly promising, though the suction struggled at higher divergence angles.

It seems reasonable that non-uniform suction be capable of outperforming uniform suction. The boundary layer of an uncontrolled flow is not uniform, so its material does not need to be removed uniformly to achieve the desired result. This has certainly been seen for the flow around the cylinder. However, to the best of the author's knowledge, no work on the optimal suction control of flow through a diffuser has been performed – the ideal suction profile (non-uniform or uniform) has been published.

2.4.8 Change to Performance for Diffuser with Suction/Blowing

The efficiency of suction control is a major concern in order for its implementation to be economical and worth the added complexity. It is not straightforward to fairly determine the performance of a diffuser which has some of its fluid removed. Suction control is effective at increasing diffuser performance because it results in increased pressure at the outlet as the flow more closely follows the contour of the diffuser. However, it also removes energy from the flow as the fluid that is removed is not wholly devoid of energy, and the suction requires energy to operate (unless an exhaust area of lower pressure is accessible to it). The typical performance measure given in Equation (2.7) is not valid because it assumes that the flow rate leaving the diffuser at the exit is the same as at the entry and it does not account for the energy to supply the suction. As we have seen Ackeret adds an approximation of this energy to the denominator, assuming a pump efficiency of $\eta_{pump} = 0.75$.

$$\eta_{Ackeret} = \frac{P_2 - P_1}{\left[1 - \left(\frac{1}{AR}\right)^2\right] h_0 + \frac{C_q P_w}{\eta_{pump}}}, \tag{2.10}$$

where $C_q = \frac{\int v_w \, dA}{\int U_1 \, dA}$, the subscript w refers to the suction parameters (at the wall), the pressure values are the average, and h_0 is the dynamic pressure at the inlet (slightly upstream of the entry). Unfortunately this method makes it difficult to optimise the suction control because the 75% value is arbitrary and the choice of its value will affect the optimal result. Still, it does not account for the volume of fluid no longer exiting the diffuser.

Instead we might perform an energy balance instead of a pressure evaluation. The paper by Nilakantan [1945] shows the derivation of this formula, given as follows

$$\eta_{energy} = \frac{Q_2P_2 - Q_1P_1}{h_1Q_1 - h_2Q_2}. \tag{2.11}$$

Nicoll & Ramaprian modified this equation to account for mass injection by tangential blowing,

$$C_{blow} = \frac{(Q_1 + Q_w)\,P_2 - (Q_1P_1 + Q_wP_w)}{Q_1h_1 + Q_wh_w}, \tag{2.12}$$

$$\eta_{blow} = \frac{C_{pr}}{1 - \frac{1}{AR^2}}, \tag{2.13}$$

where Q_w represents the control flow rate (and a positive value for Q_w represents blowing – adding energy) [Nicoll and Ramaprian 1970]. Comparing to Nilakanatan's equation for the uncontrolled case, we can see they are alike but not identical. Nicoll & Ramaprian considers the energy added by blowing (both its kinetic and static components) as inputs to the diffuser. In the numerator the pressure energy from the blowing is subtracted from the usable pressure energy recovered at exit, and in the denominator its kinetic energy is added to that at entry to represent the available kinetic energy to the flow entering the diffuser. However, Nicoll and Ramaprian did not deduct the kinetic energy still present at exit in the denominator as Nilakantan did, and thus there formula is actually more conservative. Similar equations are also derived by Yamazato [1969, 1970]. Unfortunately the equation of Nicoll and Ramaprian is not usable for the case of suction (where $Q_w < 0$ according to their definition) for here the use of suction would almost always increase the efficiency, regardless of its effect on the outlet pressure (assuming it always improves P_2).

Instead we propose a slightly modified version of their equation, which compares the pressure energy exiting the diffuser (our main measure) and the energy available to it:

$$\eta_{out} = \frac{Q_2P_2}{Q_1(P_1 + h_1) + Q_w\,(P_w + h_w)}. \tag{2.14}$$

We believe this measure of diffuser performance is an effective way of measuring the performance of a diffuser and it was the main value which the suction control was optimised to improve. To quote from our paper in JRSNZ on this measure:

"η_{out} measures the performance of the diffuser as the amount of pressure energy exiting the diffuser as a ratio of the energy put into it. It also assumes that the energy leaving the system via suction contributes to the total energy input, in this way accounting for the minimum energy needed to generate the suction as described by Choi et al. [2008]. Because η_{out} accounts for the energy used to provide the control, any improvement in η_{out} represents a realisable control that is [theoretically] efficient. The components $P_2 - P_1$ – which are expected to increase with suction control and thus increase η_{out} –

are counteracted by the decrease in Q_2 and increase in Q_w which decrease η_{out}). These competing considerations suggest that there will be some optimum suction control where the suction is sufficient to greatly increase the pressure rise in the diffuser, but not so great as to substantially reduce the working fluid in the diffuser or requiring too much energy to run."

2.5 GEOMETRY 2 – CIRCULAR CYLINDER

The following review of the literature for the circular cylinder occasionally quotes the papers co-authored by the present author and published in the International Journal of Heat and Fluid Flow (published by Elsevier) [Ramsay et al. 2020d] and the International Journal of Aerospace Engineering (Hindawi) [Ramsay et al. 2020c]. The text is reproduced here with permission by the publishers according to their copyright permissions policies [Elsevier 2021, Hindawi 2021]. Where these are quoted, the text is italicised.

2.5.1 Uncontrolled Flow

The circular cylinder is one of the most researched geometries in fluid dynamics partly because the flow around it is dynamic and interesting, but also because it represents the most extreme bluff body with no sharp edges. As Shtendel and Seifert [2014] described it, it is an 'archetypal' flow. Investigation of flow around circular cylinders has been earnest since Strouhal described the aeolian tones generated by air moving past circular cylinders, and with the detailed analysis on vortex formations in their wake provided by von Kármán [Strouhal 1878, Von Karman 1911]. The vortex shedding that occurs behind circular cylinders has since come to be known as the von Kármán vortex street (or sometimes, Kármán-Bénard street) . The two volume textbook, 'Flow Around Circular Cylinders', by Zdravkovich provides an excellent review of the important studies in this area up to the end of the 20th Century [Zdravkovich 1997]. This flow, despite its simple geometry, is extremely complex. Numerous flow regimes form as the velocity of the fluid is increased (increasing Reynolds number $Re = \frac{\rho UD}{\mu} = \frac{UD}{\nu}$). Williamson distinguishes the resulting flows into nine regimes, while Zdravkovich uses thirteen [Williamson 1996, Zdravkovich 1997]. Zdravkovich's regimes are delineated in Figure 2.9 below and summarised in Table 2.4.

Table 2.4 Flow regimes delineated by Zdravkovich [1997, p. 17] for the uncontrolled flow around the circular cylinder

State	Regime	Re Lower Bound	Re Upper Bound
Laminar	No Separation	0	4-5
	Closed-Wake	4-5	30-48
	Periodic Wake	30-48	180-200
Transition in Wake	Far-Wake	180-200	220-250
	Near-Wake	220-250	350-400
Transition in Shear Layers	Lower	350-400	1000-2000
	Intermediate	1000-2000	20k-40k
	Upper	20k-40k	100k-200k
Transition in BL	Precritical	100k-200k	300k-340k
	Single Bubble	300k-340k	380k-400k
	Two Bubble	380k-400k	500k-1M
	Supercritical	500k-1M	3.5M-6M
	Postcritical	3.5M-6M	?
Fully Turbulent	Invariable	?	?
	Ultimate	?	?

The general development of the flow progresses as follows: At low Re, the flow is unseparated and steady ($Re < 6$), but in the range of $6 < Re < 47$ the boundary layer separates and a pair of vortices form behind the cylinder; the separation point moves toward the front of the cylinder with increasing Re. At about $Re = 47$, the well-known phenomenon of vortex shedding begins and continues in a two-dimensional manner up until $Re = 188.5$ where the vortex shedding begins to exhibit 3D features (the third dimension being in the spanwise direction). With further increasing Re the wake becomes even more complex as different areas of the flow transition to turbulence, beginning with the wake, moving up the shear layers, and finally the flow transitioning in the boundary layer, which marks the onset of the well-known 'drag crisis', first observed by Eiffel [1912]. At this point, the separation point is delayed significantly, jumping much further aft and producing a substantial decrease in pressure drag. As a consequence of these widely varying flow structures, it is very difficult to design an optimal control over this entire range.

2.5.1.1 Angle of Separation

Despite the continued attention given to the flow around circular cylinders, the importance of the point of separation has gone relatively unappreciated, except for its

influence at the 'drag crisis'. Though some papers publish the separation angle as an output measured in their experiments — for the circular cylinder the *angle* of separation as measured from the leading or trailing edge (LE/TE) is more useful to report than the *point* — even fewer look at attempting to manipulate the separation angle as its own objective. It is commonly held that once the boundary layer has become separated and established it does not change significantly until the drag crisis at $Re = 2 \times 10^5$ where it jumps from about 100° to 60° (as measured from TE) [White 2017, p. 432]. In fact, experiments over a wide range of Reynolds numbers by Weidman [1968] and by Achenbach [1968, 1972], have shown that the separation angle is perpetually changing with Re and not monotonically. Collating data from a variety of experimental and numerical studies in Figure 2.8 shows a complex development of the separated region — accompanying the many changes of the full flow field. Comparing the drag curve from Figure 2.9 to the separation angle curve in Figure 2.8 reveals the coupled relationships between the pressure drag and the separation point. Consequently, as the field of flow control continues to grow and develop, it seems worthwhile to reconsider Prandtl's objective of flow control: to manipulate the boundary layer and try to efficiently delay its separation.

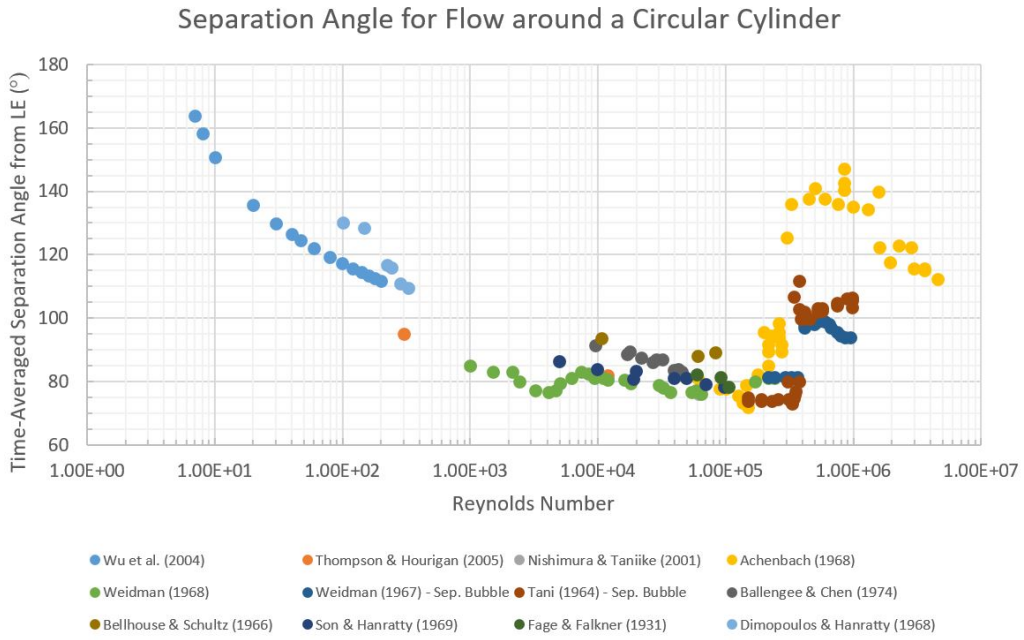

Figure 2.8 Separation angle of flow around circular cylinder using data from the literature Achenbach [1968], Ballengee and Chen [1974], Bellhouse and Schultz [1966], Dimopoulos and Hanratty [1968], Fage and Falkner [1931], Nishimura and Taniike [2001], Son and Hanratty [1969], Tani [1964], Thompson and Hourigan [2005], Weidman [1968], Wu et al. [2004].

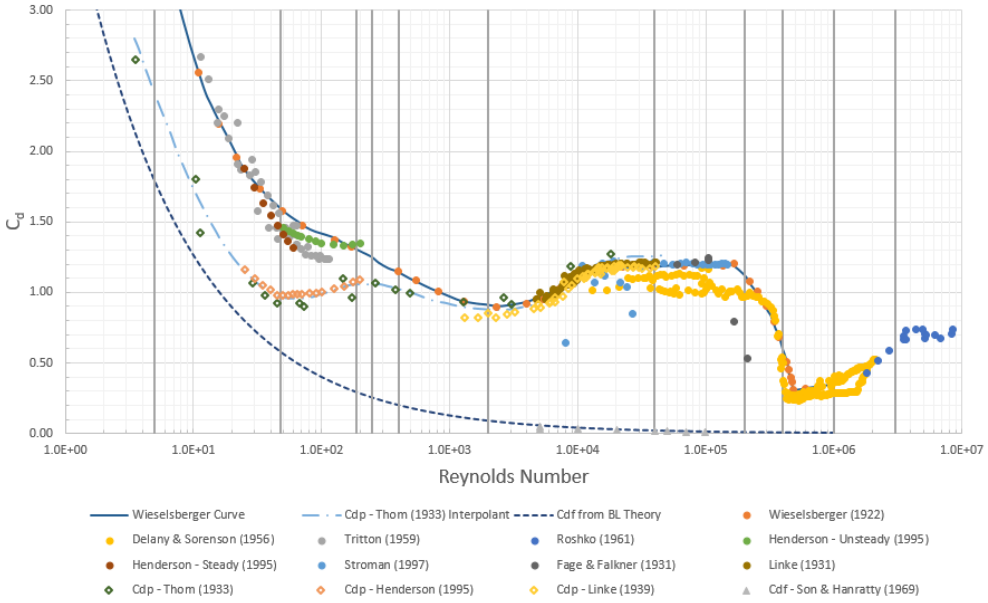

Figure 2.9 Drag coefficient components for flow around circular cylinder with Zdravkovich's regime distinctions shown by vertical lines [Zdravkovich 1997, p.17]. Data taken from the following literature: Data taken from the literature: Wieselsberger [1922b], Delany and Sorensen [1958], Tritton [1959], Roshko [1961], Henderson [1995], Stroman [1997], Fage and Falkner [1931], Linke [1931], Thom and Ingram [1933], Son and Hanratty [1969].

2.5.1.2 Drag

Many flow control studies focus on the minimisation of drag, therefore it is important to have a firm grasp of the drag characteristics of the uncontrolled state. Preliminary approximations of the drag behind objects were developed by Newton in his seminal work, Principia, but these were flawed and did not accurately predict the real behaviour of viscous fluids [Newton 1687]. Various other analytical methods for approximating the drag behind objects were developed in the 19th Century - including Lamb's formula [Lamb 1911] for body resistance in Stokes flow, but it was not until the early 20th Century that the fields of theoretical and experimental fluid dynamics met and accurate measurements and predictions of drag were produced. Some of the earliest experimental measurements on the drag behind a cylinder (and enduringly accurate) were produced by Wieselsberger [1922a, b] over an expansive Re range, and by Relf [1914] over a narrower range. The plot of C_{d_t} over Re produced from the experiments of Wieselsberger is so accurate it is the typical reference used to this day, despite many more experimental and numerical studies on the drag on cylinders. The total and pressure drag coefficients compiled from data of many experimental and numerical studies on the drag of an uncontrolled cylinder in viscous flow is shown in Figures 2.9 and 2.10.

As Figures 2.9 and 2.10 show, the drag on a cylinder changes dramatically over the measured Reynolds range, as do the relative contributions of each drag component. At low Re both the pressure drag and skin friction drag coefficients are large, but the skin

friction component declines asymptotically towards zero as Re increases. This is because the inertial forces dominate the flow at higher Re, even in much of the boundary layer. On the other hand, the pressure drag component does not change monotonically. During the fully attached regimes the pressure drag component decreases, but once separation begins it starts to increase, and undergoes dramatic changes during the unsteady flows that follow at higher Re. This is because of the onset of BL separation which prevents the pressure from recovering on the leeward half of the cylinder, producing a pressure deficit. The example pressure profiles shown in Figure 2.2 for laminar and turbulent flow show how separation manifests a pressure-deficit on the leeward half, and the effect of a turbulent BL in delaying the separation.

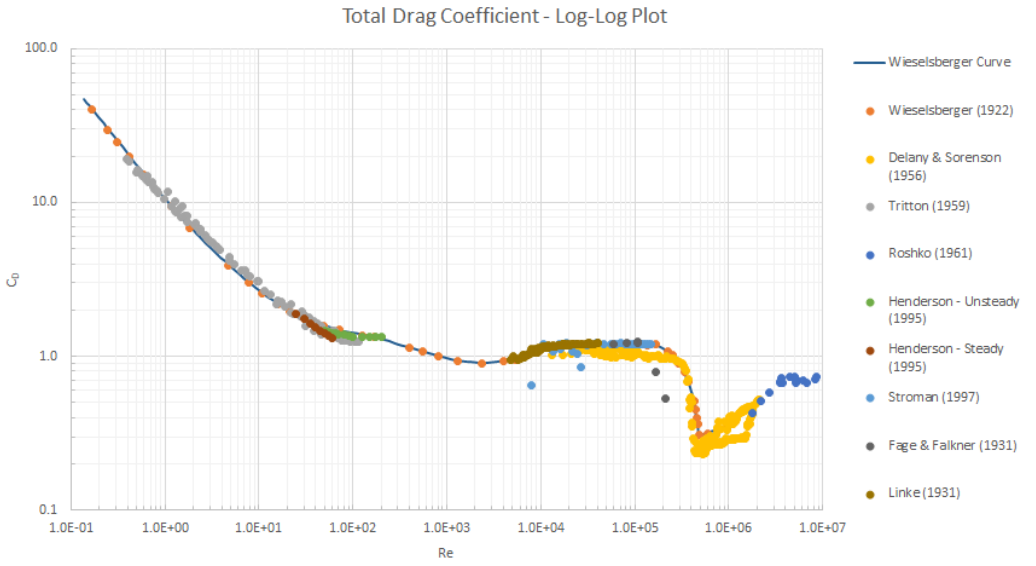

(a)

Figure 2.10 Total drag coefficient data for the circular cylinder. Data taken from the same sources as Figure 2.9

2.5.2 Control of Cylinder

To quote from the co-authored paper in IJHFF in keeping with their copyright practices:

To date, many active and passive methods of control have been investigated to control the flow around the circular cylinder. These range from simple geometric features such as splitter plates [Kwon and Choi 1996] and helical strakes [Scruton and Walshe 1957] to complex active measures like plasma actuators [Sung et al. 2006] or magnetic fields [Rashidi et al. 2016]. Many of these are described in the Annual Review by Choi et al. [2008] or more recently in the 2016 review by Rashidi et al. [2016] Each of these methods have achieved some success at reducing drag or weakening vortex shedding, though often at significant cost. One of the simplest forms of flow control is boundary layer suction. This method removes the low momentum fluid particles at the surface, thus

entraining higher momentum particles from the free-stream to reinvigorate the boundary layer, delaying separation. This method of flow control is as old as the boundary layer concept itself – with Prandtl testing his theory by experimenting on slot suction of a cylinder [Prandtl 1904]. Nevertheless, it is still not a settled matter how this method can optimally control the flow around a circular cylinder, i.e. achieve the control objective with the least suction/fluid removal. Boundary layer suction has many advantages compared to other control methods. For one, the geometry of the body does not have to be changed (although the materials of the surface may). Further, the method is simple and practical – its parameters can be adjusted easily and have a wide range; there is no multi-physicality to this control. And of particular importance to this study, the method is well researched both experimentally and numerically.

Experiments on suction control began in the early 20th Century, and much interest was paid to this subject for the improvement of aerodynamic characteristics for aircraft during the Second World War [Lachmann 1961]. Over this time, two main applications of suction control were investigated: uniform suction over the entire surface of a cylinder with porous walls – as researched experimentally by Thwaites and his colleagues [Hurley and Thwaites 1951, Pankhurst et al. 1953] – and slot suction, where only part of the boundary layer is removed through a slot or series of slots in the cylinder surface. Fransson et al. [2004] determined a relationship between the controlled flow using uniform suction on the cylinder and the uncontrolled flow at a different Reynolds number, and that these could be linked via the Strouhal number. However, the effective Reynolds relationship found by Fransson et al. is only applicable if the control does not entirely suppress vortex shedding which is a common objective for bluff body flow control. Uniform suction has its disadvantages, namely the inefficiency of removing material at all areas of the cylinder – even where it may not be necessary – and its limited control parameters. Slot suction is similarly disadvantaged, being limited in its location of application, the distribution profile of the suction, and the discontinuity of its nature.

A better approach to suction control combines the benefits of each of these methods – non-uniform suction. This method is applied similarly to uniform suction by use of a porous surface, however the suction is applied unevenly, with the possibility of any potential distribution over the surface – continuous or otherwise. Theoretically, this allows much more precise control of the flow, with the possibility to concentrate the suction control at critical areas of the surface and apply no control where it is unnecessary. Because there are so many potential profiles for this method, determining its "optimum" is not straightforward – even when only considering steady, time-independent control. Furthermore the influence of suction on the flow is nuanced. For example boundary layer suction can reduce drag in turbulent flows by relaminarising the flow thus decreasing the skin friction on the surface, whereas when applied to laminar flow it can have the opposite effect – increasing skin friction while decreasing the pressure drag.

2.5.2.1 Suction Control and Optimisation

Some papers on the subject of non-uniform suction have been published, particularly with the focus of utilising it in conjunction with feedback from the flow in order to mitigate the wide-range of potential implementations. Min and Choi [1999] developed and employed sub-optimal feedback control with non-uniform suction and blowing (the optimisation is sub-optimal as it is over a finite, short time-frame). The study investigated the optimised flow and control parameters for three objectives: minimising pressure drag, minimising the difference of the surface pressure profile to that for inviscid flow, and maximising the square of the pressure gradient. The researchers successfully reduced the drag on the cylinder, and their results showed that the choice of objective had a large impact. The pressure drag objective did not result in the best drag reduction nor, surprisingly, did it result in the smallest pressure drag for a given set of conditions. The researchers showed that this was due to the balance of skin friction drag and pressure drag which were influenced in different ways by the control.

Though the researchers presented the separation points of the controlled flows in some instances, they did not investigate its potential as a control objective or how it relates to the optimised control parameters. They also limited their study to two Reynolds numbers, thus the potential changes of suction/blowing profiles change depending on the characteristics of the flow were limited. The sub-optimal suction/blowing profiles that achieved the most drag-reduction consisted of strong blowing near the rear of the cylinder and lesser suction near the top and bottom of the cylinder (90° and 270°). A later paper by Kim and Choi [2005] also found that at $Re = 100$, the flow was most sensitive to control by spanwise distributed slot suction. In the remainder of that paper the control was applied at this 90° location for a wide range of Reynolds numbers, although the best location for suction control may move with Re.

Li et al. [2003] performed a similar numerical study as Min and Choi [1999], and carried out a complete adjoint optimisation procedure with unsteady, time-dependent simulations. The researchers achieved a complete control of vortex shedding for up to $Re = 110$. They also found that the optimal controls were insensitive to initial conditions if the control was applied for time-scales longer than the vortex shedding period. The researchers used objectives for the error between the flow field and potential flow field, the enstrophy of the flow (to suppress vortex shedding), and the minimisation of drag. The separation angle of the flow was not investigated. Very recently, the optimum spanwise-varying suction/blowing control of a 3D circular cylinder in 2D flow was determined using eigenmode analysis by Boujo et al. [2019]. Due to the nature of this method, though, it can only be used to optimise for stabilisation or frequency modification which does not necessarily coincide with minimised drag or the elimination of separation. All of these studies were performed by numerical methods; non-uniform suction has not been explored substantially by physical experimentation.

Some of the difficulties of designing suction/blowing flow control should be highlighted for the geometry of the circular cylinder. Firstly, unlike some other geometries, the constantly varying convex surface of the cylinder makes it very difficult to enact control that sucks or blows through the surface at any incidence other than normal. This limits the potential control. Just as suction control can delay separation by increasing the momentum in the boundary layer, blowing tangential to the surface can likewise benefit the flow by adding momentum (directly rather than enticing fluid from the free-stream). This would be very difficult for the circular cylinder, and many studies that have investigated blowing control have found that it tends to promote separation rather than delay it [Fransson et al. 2004, Kim and Choi 2005]. Though, some attempts have been made for tangential blowing jets as described in Volume 2 of Zdravkovich's textbook [Zdravkovich 1997, p.949]. Secondly, the pressure profile over the surface of the cylinder is quite complex. For potential flow, its profile is given by $C_p = 1 - 4\sin^2(\theta)$, however in reality, it is even more complicated as viscous effects and boundary layer separation disturb the pressure recovery. This makes it difficult when considering autogenous suction, as the locations of lowest pressure varies with Re. Finally, the phenomenon of vortex shedding adds an additional complication. From $Re > 47$ the wake of the cylinder becomes dynamic and therefore time-dependent control may be more appropriate than steady action. Each of these concerns must be considered when designing control for this flow.

While many studies have investigated the use of suction and blowing control on bluff bodies, there is still not clarity on what the best solution is. Furthermore, there has been little interest in the separation point as a potential parameter to control, despite it having a close relationship with the pressure drag (which dominates bluff body flows). Even ignoring the relationship with the body drag, there are cases where eliminating separation is desirable. For example, preventing heart stents from bursting due to Dean vortices [Williamson et al. 2019], concealing wakes behind ships [Chan et al. 2019, Trevorrow et al. 1994], and maintaining steady flow behind obstructions.

Finally, the efficiency of suction control is important for this flow. Bluff body flows are often used as analogues for more complex vehicles, and in transportation the economic and power cost of flow control is a critical parameter. Choi et al. [2008] presented a useful metric for measuring the theoretical efficiency of suction/blowing control, but this does not account for the additional weight, complexity, and performance of any pumps or machinery needed to drive it (instead looking only at the static and dynamic pressure power of the control). To the author's best knowledge, no studies have investigated autogenous suction control for the circular cylinder. The tools to develop such a control have not been produced and unique challenges are presented for this flow, such as the dynamic wake and complex pressure profile. Nevertheless, there has never been a stronger drive to produce flow control that improves the drag on bluff bodies.

Chapter 3

METHODOLOGY

3.1 OVERALL PROCEDURE

The objective of this thesis was to determine the optimal suction control to minimise separation or drag on two reference separated flow-cases, and then attempt to produce such a control autogenously. The detailed methodology for the simulations, optimisation and design approach are outlined in this chapter. Here is a brief summary is given of the general procedure that was undertaken to achieve this and answer the research questions.

Firstly, computational fluid dynamics (CFD) models were developed for the reference flows without control, usually using the CFD software package COMSOL Multiphysics. Since experiments were not conducted to validate the models, their results had to be closely matched to values already published in the literature instead. The models had to be robust, valid, and efficient even before any control was applied to them.

Next, these models were coupled with optimisation methods. Objectives, control parameters, and constraints were defined for each, and appropriate solvers were implemented to solve them. The control usually consisted of suction imposed by boundary conditions on the bounding walls, and a variety of approaches were taken. These included defining specific suction profiles, functions whose parameters could be altered to adjust their shape, strength and location. Alternatively, a suction field was defined which was discretised and whose strength at each point could be adjusted. Lagrange shape functions were used to interpolate the profile at non-nodal points. This stage of research was the most substantial in this thesis.

After determining the optimal (or near-optimal) suction control, boundary condition functions were defined that would mimic autogenous suction control, where suction and blowing are balanced both in flow rate and pressure. Parametric and optimisation procedures were used to determine the best arrangement of this control, and to satisfy these constraints. The development of autogenous control – even with the simplified approach of imposing boundary conditions to produce their effect – is not simple, as the pressure profile changes when the control changes.

Finally, real autogenous control with a physical implementation was designed and modelled. While the boundary condition simulations of autogenous suction control revealed much, they relied on many assumptions – some of which are tenuous. A likely physical implementation would involve the use of porous surfaces and secondary ducting to redirect the flow. As such the CFD models were altered to solve flows that involved unbounded flow and porous media flow. Various approaches for autogenous suction designs were developed and tested in the effort to uncover a workable control design. To aid in the duct-design, it was desirable to understand the relationship between duct geometry and the resulting suction. Iterative and randomised CFD simulations were used to train a neural network to design geometries to produce a desired suction profile. This network could then be probed, inputting a desired suction velocity profile, and receiving as output a wall profile to accomplish it. This stage of research was at the intersection of fluid physics and engineering design. The potential avenues of approach were plentiful, though not necessarily fruitful.

The precise models used in each part of this research will be described in their relevant sections. This chapter gives a general outline of the methods used and the background necessary to understand them. The chapter consists of the following: Firstly, the two models for the reference geometries are introduced and the control strategies. Secondly, the procedures of CFD and the finite element method are described. Then, the theory behind optimisation and a few specific algorithms employed are described. In the same section, the objectives investigated in this research are detailed, and how they were evaluated in the CFD models. Third, the particular control profiles that were investigated for the non-autogenous control of the cylinder and diffuser are stated. Then, an alternative to optimisation – the training of neural networks – is outlined as well as its theory. And finally, our approach for developing autogenous suction control is explained.

3.2 THE TWO MODELS

Two flow-cases with boundary layer separation were investigated to optimise non-uniform suction control and develop autogenous suction control: the circular cylinder (external flow) and the conical diffuser (internal flow). These flows were modelled numerically, using the Finite Element Method (FEM), and a variety of methods were employed to develop optimal suction control and effective autogenous suction control. A schematic of each geometry and some of the suction/blowing control designs that were implemented are shown in Figures 3.1 and 3.2.

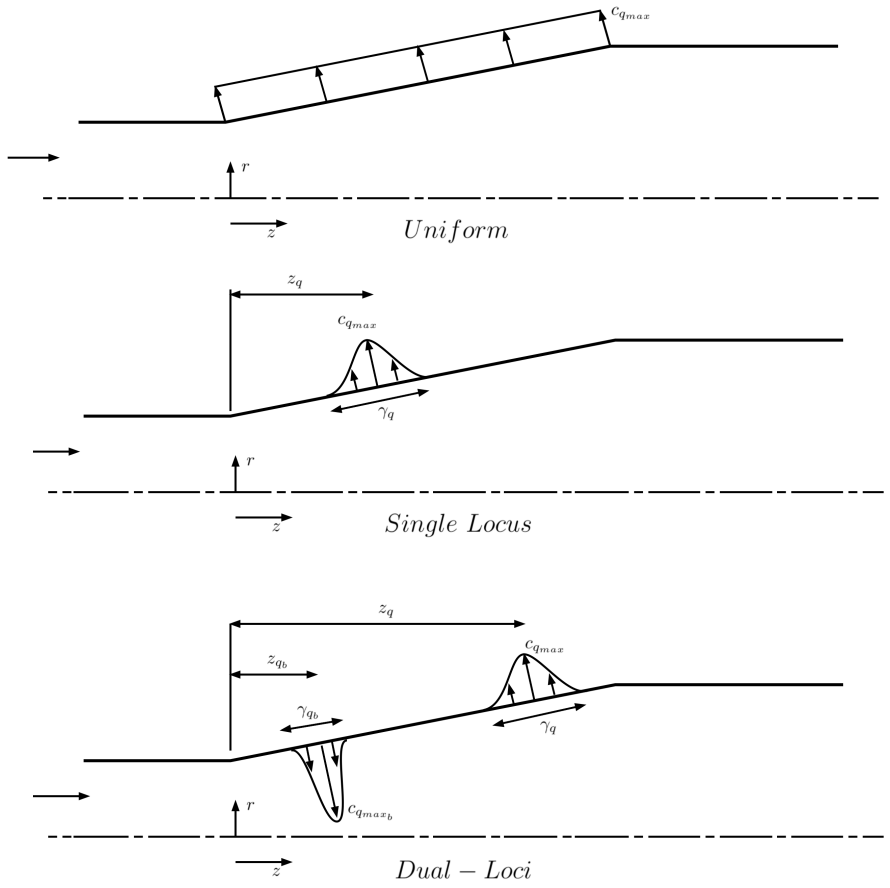

Figure 3.1 Schematic of flow through the conical diffuser model with key suction/blowing profiles shown.

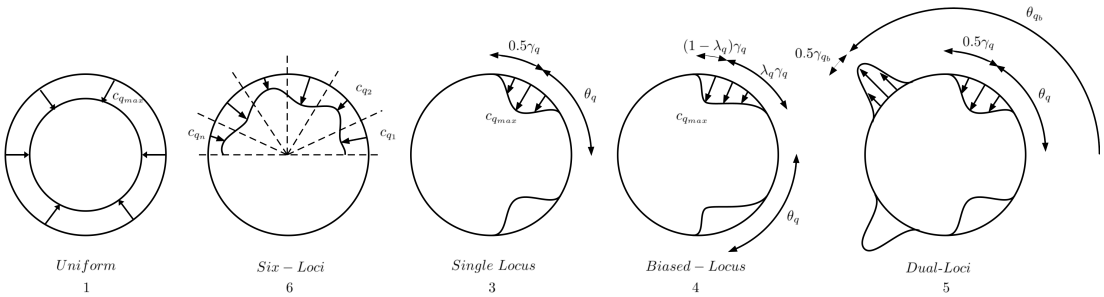

Figure 3.2 Suction/blowing profiles for control of the circular cylinder.

The conical diffuser was modelled as a 2D axisymmetric domain, whereas the cylinder was modelled as a 2D domain. The flow was expected to have these traits (2D axisymmetric and 2D) at the simulated Reynolds numbers as described in Chapter 2. Schematics of each domain are shown in Figures 3.3 and 3.4 with further details in their relevant chapters. Each model was first validated by simulating the uncontrolled flow over the range of parameters being investigated (Reynolds number, divergence angle, etc.) and key characteristics compared to data from the literature.

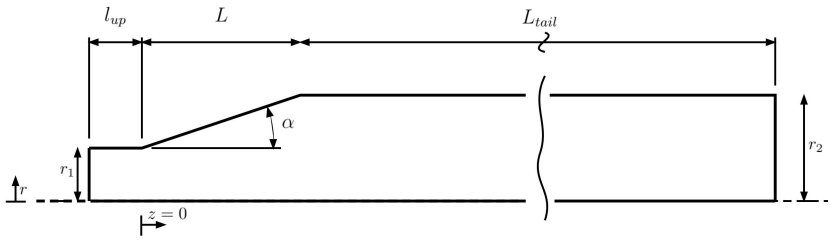

Figure 3.3 Schematic of computational domain for the conical diffuser. The bottom axis is the line of axisymmetry. More details in Chapter 4

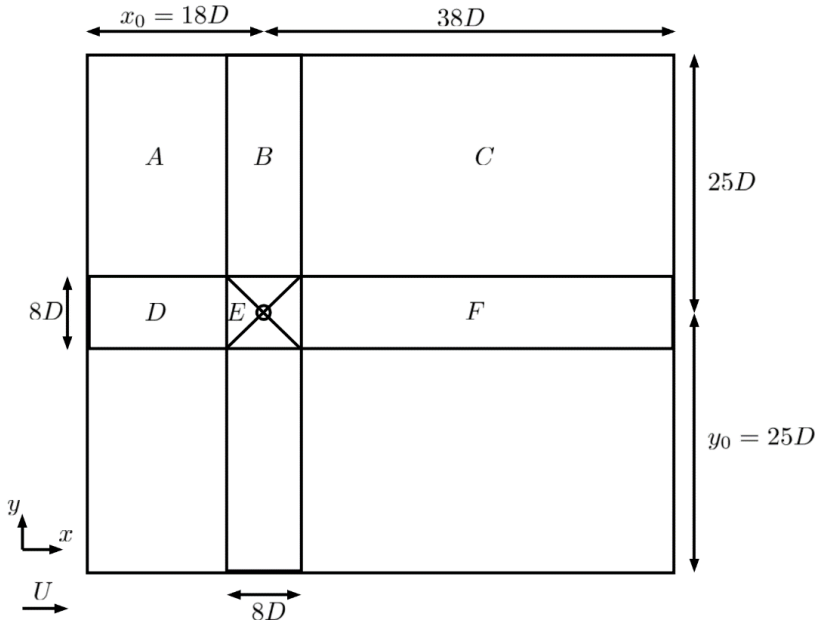

Figure 3.4 Schematic of computational domain for the flow around the cylinder. The flow moves from left to right. More details in Chapter 6.

Once the models were validated, uniform and non-uniform suction control was implemented by adjusting the boundary conditions on the relevant walls. For non-uniform suction, pre-defined functions and a discretised field approach as will be described later in this chapter. These controls were investigated with parametric studies as well as being optimised using the Nelder-Mead or SNOPT algorithms.

To develop autogenous suction control, flow-rate balanced suction and blowing regions were needed. The 'dual-loci' control – as seen in Figures 3.1 and 3.2 – was developed for this purpose. Dual-loci control consists of a contained locus of suction and a contained locus of blowing, each with their own control parameters which can be kept independent (unbalanced dual-loci control) or coupled (Q-balanced and P-Q-balanced dual-loci control). Investigations were performed on the dual-loci control with either no coupling between the suction and blowing, flow-rate balanced constraints, and flow-rate and pressure constraints (fully autogenous). Finally, the cylinder model was adjusted to have internal ducting and porous walls so as to test whether an autogenous suction

flow does develop when expected.

In addition to these investigations, an investigation into how arbitrary non-uniform suction profiles could be induced by internal duct geometries was performed for a simple case: the flow through a straight 2D channel. The model for this is shown in Figure 3.5. Rather than just taking a direct optimisation approach for this – which would limit the results to only one suction profile – artifical neural networks (ANNs) were trained on randomised CFD data to produce appropriate suction-inducing geometries. The theory for each of these research steps are outlined in this chapter.

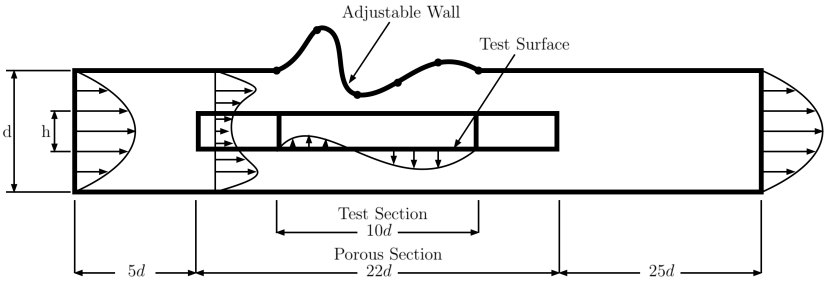

Figure 3.5 Schematic of computational domain for the suction-inducing geometry studies. More details in Chapter 5.

3.3 MODELLING FLUID FLOW - COMPUTATIONAL FLUID DYNAMICS (CFD)

3.3.1 Navier-Stokes Equations

The flow of a viscous fluid is described by the set of coupled non-linear partial differential equations (PDEs) known as the Navier-Stokes (N-S) equations. These are named after two independent physicists who developed them in the 19$^{\text{th}}$ Century [White 2017, p. 5]. The N-S equations are an application of Newton's Second Law of Motion to the flow of fluids. They are typically a set of three systems of equations stating the conservation of mass, the conservation of momentum, and the conservation of energy for a fluid control volume in mathematical form. For the case of an incompressible and isothermal flow – as is investigated in this thesis – the equation describing the conservation of energy is not needed, and several terms in the first two equations are simplified. These equations are as follows:

$$\frac{\partial \mathbf{u}}{\partial t} + (\mathbf{u}\cdot\nabla)\,\mathbf{u} - \nu\nabla^2\mathbf{u} + \frac{1}{\rho}\nabla p = \mathbf{f} \tag{3.1}$$

$$\nabla\cdot\mathbf{u} = 0 \tag{3.2}$$

where $\mathbf{u}$ and p are the velocity vector and scalar pressure fields respectively (the dependent variables), $\nu = \mu/\rho$ is the kinematic viscosity, ρ is the fluid density, and

$\mathbf{f}$ is the vector for all external forcing terms. The ∇ symbol represents the gradient operator. The N-S equations are usually employed to solve an initial value problem, where boundary conditions and initial conditions are imposed on a domain in order to achieve a solution to the dependent variables ($\mathbf{u}$ and p) within that domain. The equations are usually not directly integrable. Solving involves determining the specific values for the dependent variables at all points in the domain and all times.

Each term of the N-S momentum equation can be considered to describe a phenomenon of the real fluid flow. The first term in Equation (3.1) is how the velocity field changes over time, the second is the effect of convection, the third that of diffusion, the fourth from changes due to internal sources (only pressure in this case) and finally the external forcing. The continuity equation (Equation (3.2)) enforces the constraint that mass is conserved in any given control volume, so the divergence of $\mathbf{u}$ must be zero everywhere for an incompressible fluid.

Since the N-S equations are only rarely integrable, they are usually solved numerically by discretising the domain and using iterative solver methods to approximate the values of the dependent variables. There are many approaches for achieving this, the most popular of which are the Finite Volume (FVM) and Finite Element (FEM) methods, though there are many others. Both commercial and open-source computational fluid dynamics (CFD) software are available that resolve fluid flows with one or more of these methods. For example, FVM is used to model fluid flow in ANSYS Fluent, OpenFoam and StarCCM+, while FEM is used by COMSOL, FEniCS, nektar++ and nek5000. In this research, COMSOL was the main CFD software tool. This was due to its strong capabilities, accuracy, and availability in the Mechanical Engineering Department at the University of Canterbury. Since COMSOL was the primary code used for modelling the fluid flows explored in this thesis, only the finite element method will be explained here.

3.3.2 Finite Element Method

3.3.2.1 From Navier-Stokes to Finite Element

The finite element method consists of discretising a physical domain into finite subdomains (elements) defined by a mesh (in 2-D these are flat shapes, while in 3-D they are volumes, etc.). Each element has nodes – typically on its edges – which are where the dependent variables are evaluated. Thus what is in reality a continuous field with infinite points is turned into a finite discrete domain for the numerical solution. The values of the dependent variables within each element are evaluated by interpolating from the nodal values using shape functions. The finite element method does not solve the governing PDEs directly, but instead evaluates a 'weak' (variational) form of the equations.

A brief summary of how the finite element method is constructed and then how it is applied to the case of fluid flow, will be described here.

General Solving Process To summarise: the finite element equations are derived from the governing equations by the following process:

1. The domain, Ω, is discretised into subdomains (elements).
2. For each element and each dependent variable, shape functions, N_i, are developed which have the property of being equal to 1 at their node, and 0 at all other nodes within their element. These are usually polynomial functions. The order of their function is an important factor.
3. The governing equation is converted into variable form. This is achieved by multiplying each term of the equation by the shape functions (or perhaps a different weighting function), integrating across the domain, and reducing higher order terms (using integration by parts).
   In this context, the shape functions (or the weighting functions) are sometimes referred to as the *test function.* With this terminology, the approximate solution produced by the finite element analysis, $\widetilde{\mathbf{u}}$, is the *trial function*
4. All elements are then assembled together using linear algebra and commonalities between nodes.
5. The full system is then solvable using linear algebra, $\mathbf{f} = K\mathbf{u}$

Example of Simplified Navier-Stokes to Finite Element – Stokes Equations

Governing Equations Now we will look at an example more closely related to the present investigations – deriving the Finite Element formulation of the Navier-Stokes equations. This discussion is based on the seminar given by Burkardt [2011]. To simplify matters, we will consider a steady Stokes flow, which removes the non-linear and time-dependent terms of the Navier-Stokes equations. For a derivation of the variational form for the full N-S equations, the reader is directed to an excellent walkthrough in the FENICS Tutorial [Langtangen and Logg 2016, p. 56]. The incompressible and steady Stokes equations in 2-dimensions are as follows:

$$-\nu\left(\frac{\partial^2 u}{\partial x^2}+\frac{\partial^2 u}{\partial y^2}\right)+\frac{\partial p}{\partial x}=0, \tag{3.3}$$

$$-\nu\left(\frac{\partial^2 v}{\partial x^2}+\frac{\partial^2 v}{\partial y^2}\right)+\frac{\partial p}{\partial y}=0, \tag{3.4}$$

$$\frac{\partial u}{\partial x}+\frac{\partial v}{\partial y}=0, \tag{3.5}$$

where the pressure, p, is scaled by density, and the velocity components, u & v, give the mass velocity.

Discretisation Let us consider the flow across a simple 2D rectangle with flow from left to right, with the top and bottom edges representing no-slip walls. We discretise the mesh using triangular elements. Employing the Frontal-Delaunay method produces a mesh as shown in Figure 3.6 and Figure 3.9.

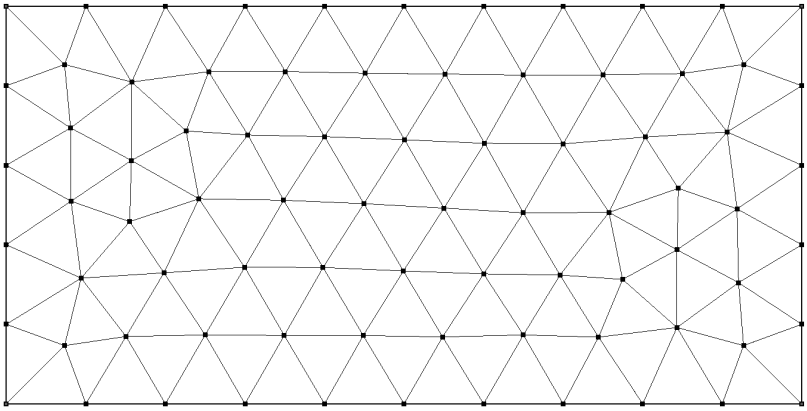

Figure 3.6 Discretised domain using a triangular mesh for the rectangular domain, generated in Gmsh. Only first-order nodes are shown.

Shape Functions The next step is to define the shape functions. Since there are two dependent variables (the vector velocity field, ($\mathbf{u} = u, v$), and the scalar pressure field, p) this will require two sets of shape functions. Unlike for other PDEs, there is a known complication with the Navier-Stokes equations where unstable oscillating solutions will be produced for particular combinations of shape functions for the velocity and pressure variables. The typical way to address this is to use Taylor-Hood pairs of shape functions where the pressure shape function is usually one order lower than that for the velocity. We typically use P2+P1 for our simulations in COMSOL (second-order velocity, first-order for pressure), so that is what will be used here.

For the pressure shape functions, the mesh produced above is appropriate. Each triangular element has three nodes, one at each corner. We will call these p-nodes to distinguish them from the nodes on the mesh used to define the velocity test functions, u-nodes. The shape functions must be defined such that they are 1 at their nodes, and 0 at all others (within their element), and we have chosen to use first-order (linear) shape functions (P1) for this purpose. Figure 3.7 and Figure 3.8 shows one element and the shape functions defined on it. Their general formula is given below, and can be derived from geometry:

$$N_c\left(x,y\right) = \frac{1}{2A_e}\left(\left(x_a y_b - x_b y_a\right) + \left(y_a - y_b\right)x + \left(x_b - x_a\right)y\right). \tag{3.6}$$

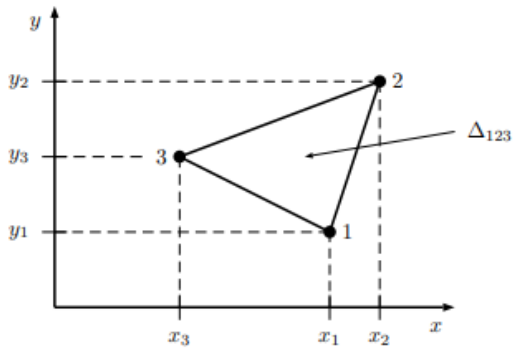

Figure 3.7 First-order 2D element.

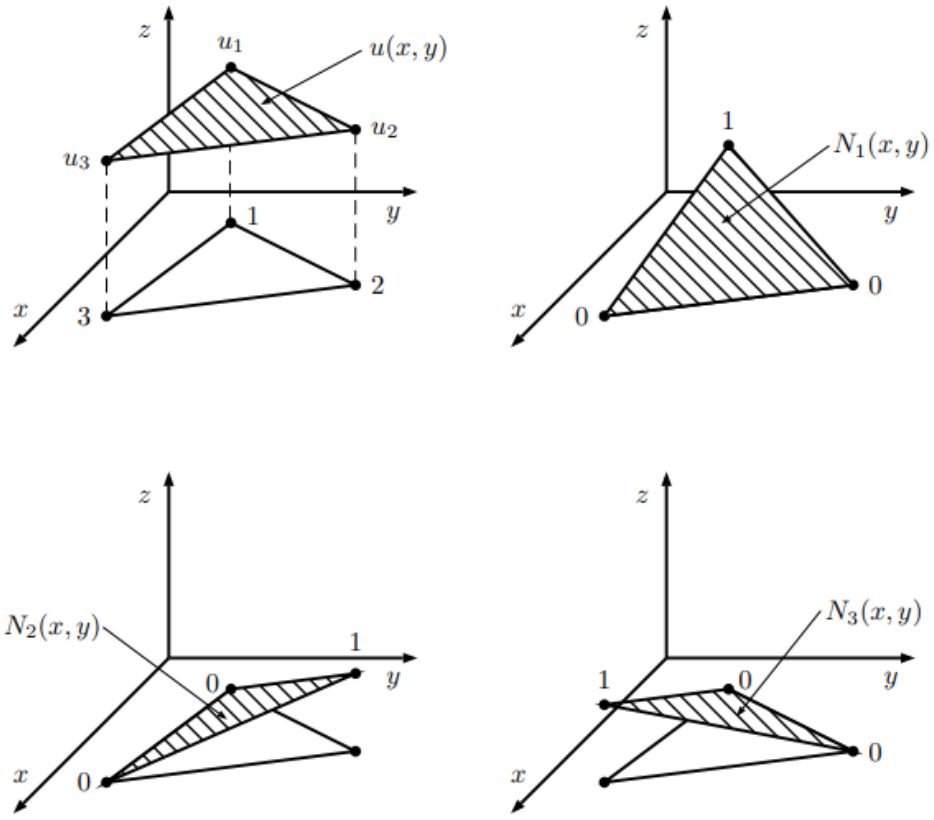

Figure 3.8 Linear shape functions produced for this element.

The velocity shape functions are a little more complicated as they are of a higher order. These second-order elements require more nodes which are placed between the existing corner nodes. This produces six u-nodes per element. The nodes for the second-order elements used for the velocity variables are shown in Figure 3.9. Note that the pressure values will not be defined at the middle-nodes as the pressure is solved on the first-order elements.

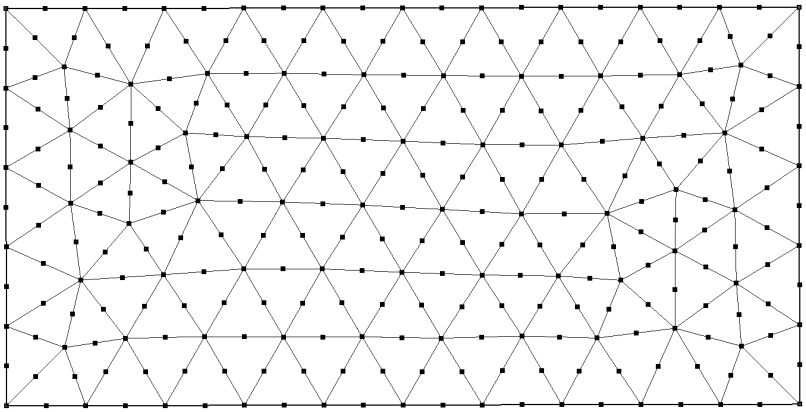

Figure 3.9 The same discretised domain, but with second-order nodes shown.

The velocity shape functions are second-order polynomials. Let us take our element from before as an example, and add these extra nodes. We label the node between n_1 and n_2 as n_4, the node between n_2 and n_3 as n_5, and the last as n_6. Rather than deriving the second-order shape functions from scratch, linear formulations can be combined to produce second-order shape functions with the necessary traits. For example, to produce a second-order shape-function that is zero at n_3, we can produce a linear function, $A(x, y)$, that is zero at n_1, n_4, n_2 and another, $B(x, y)$, that is zero at n_5, n_6. Combining these, we produce a quadratic equation that is zero at all nodes except n_3. We want the function to be 1 at n_3 which can be achieved by normalising the function by the same function evaluated at the n_3 co-ordinates:

$$M_3(x, y) = \frac{A(x, y)\, B(x, y)}{A(x_3, y_3)\, B(x_3, y_3)}. \tag{3.7}$$

Here M is used to denote a shape function for the velocity, to distinguish the u-node shape functions from the p-node ones. This same approach for generating the second-order shape functions is applied for all the nodes in an element. Remember that the approximation to the dependent variable field within the element is derived using the shape functions:

$$p = \sum_{i=1}^{p-nodes} p_i N_i(x, y) \tag{3.8}$$

$$\mathbf{u} = \sum_{i=1}^{u-nodes} \mathbf{u}_i M_i(x, y) \tag{3.9}$$

Mapping Functions Each element needs to be logically connected and "placed" appropriately in the overall domain. This is a matter of programmatic book-keeping so will not be elaborated on here.

Variational Form The variational form of the governing equations can now be produced by multiplying the governing equations by the appropriate shape functions and integrating over the domain.

$$\int_\Omega \left(-\nu \left(\frac{\partial^2 u}{\partial x^2} + \frac{\partial^2 u}{\partial y^2} \right) + \frac{\partial p}{\partial x} \right) M_i \, dx \, dy = 0 \tag{3.10}$$

$$\int_\Omega \left(-\nu \left(\frac{\partial^2 v}{\partial x^2} + \frac{\partial^2 v}{\partial y^2} \right) + \frac{\partial p}{\partial y} \right) M_i \, dx \, dy = 0 \tag{3.11}$$

$$\int_\Omega \left(\frac{\partial u}{\partial x} + \frac{\partial v}{\partial y} \right) N_i \, dx \, dy = 0 \tag{3.12}$$

It should be noted that the continuity equation – which is multiplied by the pressure shape functions, N_i – does not explicitly refer to the pressure. However, it is this equation which implicitly constrains the pressure field. As it stands, there are second-order derivatives, so these are removed by integration by parts (Green's Theorem) resulting in

$$\int_\Omega \nu \left(\frac{\partial u}{\partial x} \frac{\partial M_i}{\partial x} + \frac{\partial u}{\partial y} \frac{\partial M_i}{\partial y} \right) + \frac{\partial p}{\partial x} M_i \, dx \, dy = \int_{\partial\Omega} \frac{\partial u}{\partial n} M_i \, ds \tag{3.13}$$

$$\int_\Omega \nu \left(\frac{\partial v}{\partial x} \frac{\partial M_i}{\partial x} + \frac{\partial v}{\partial y} \frac{\partial M_i}{\partial y} \right) + \frac{\partial p}{\partial y} M_i \, dx \, dy = \int_{\partial\Omega} \frac{\partial v}{\partial n} M_i \, ds \tag{3.14}$$

$$\int_\Omega \left(\frac{\partial u}{\partial x} + \frac{\partial v}{\partial y} \right) N_i \, dx \, dy = 0 \tag{3.15}$$

where $\partial\Omega$ defines the boundary of the domain. Since the shape functions are required to be zero at the boundaries, the right-hand side disappears. The boundary conditions are incorporated as the boundary nodal values are explicitly defined or incorporated in the derivatives. By substituting in the approximations for u, v, p (more accurately, $\widetilde{u}, \widetilde{v}, \widetilde{p}$) as defined by their shape functions within each element, the system becomes fully defined by the nodal values.

Assembly The full system of equations can now be assembled. Most nodes are shared by other elements, and some nodes (u-nodes) do not have pressure values for them. Therefore, when assembling, careful book-keeping is essential. When considering the contribution to the coefficient for each node, one has to consider:

- All the *elements* associated with that *node*
- All the *nodes* in those *elements*
- All the *variables* associated with those nodes

Despite this complexity, if appropriately coded, the process is straight-forward, and eventually a full system of equations is produced with a large stiffness matrix, which when multiplied by the dependent variables gives the forcing vector:

$$K\mathbf{u} = \mathbf{f} \tag{3.16}$$

This is then solved by linear algebra methods, producing the values for the dependent variables at each node. The overall field can be described by interpolating using the shape functions.

3.3.2.2 From Deriving Equations to Software Packages

Of course, it would be far too burdensome to re-derive the finite element equations for each new model, mesh or problem. The steps described above are all automated within many robust FE solvers, such as those outlined earlier. In most cases, it is only necessary to define the geometry, materials, boundary conditions, and mesh. All of the assembly and solving is taken care of by the software package – though usually with the possibility to adjust these steps. Often post-processing of the results is incorporated too. This makes modelling and analysing fluid flows much more accessible.

3.3.2.3 COMSOL Multiphysics

COMSOL Multiphysics is a commercial software package produced by COMSOL Inc. that is designed to solve a variety of physics or Multiphysics problems using the finite element method. Since much of the physical phenomena of the world are described by partial differential equations, it is a very useful tool for many fields, not just fluid dynamics. As a commercial package, COMSOL often operates as a black box, with the 'heavy-lifting' taken care of in arranging and reformulating the governing equations to suit the model defined, and refining the algorithms used to solve them. It consists of several 'Physics Modules' which contain the tools for performing analysis in that field. For CFD, this is the Fluid Dynamics Module. Within this module are many sub-models which can be selected individually or combined to model complex flows. These include turbulent models, non-isothermal flows, multiphase flows, flows through porous media and more. In this work the sub-models used were predominantly from the 'Single-Phase Flow' and 'Porous Media and Subsurface Flow' modules. The Mathematics module was also used in order to couple optimisation methods to the CFD, as will be discussed later in this chapter.

COMSOL works like most other CFD software. Setting up a model consists of several stages: creating the geometry, defining the materials properties and boundary conditions, generating a numerical mesh, and selecting/modifying the solver method.

3.3.3 Laminar Flow vs. Turbulent Flow

While the N-S equations appear to accurately model the behaviour of all Newtonian flows – even turbulent ones – they can become prohibitively expensive to solve when the range of length and time scales of a flow become too broad [Argyropoulos and Markatos 2015]. This is usually the case for turbulent flows. Turbulence occurs in most natural flows, and is chaotic fluid motion in which cascading eddies form throughout the flow [Barkley 2016]. Because such flows exhibit eddies with a wide length-scale range (from large eddies stretching over much of the free-stream domain, to tiny eddies on the Kalmagorov scale) and a wide range of time-scales, in order for a numerical mesh to capture all the details of the flow, a very fine mesh with very fine time-stepping is needed over a large domain. Furthermore, turbulent flows are inherently three-dimensional, increasing the domain size and computational demands.

It appears that all flows become turbulent when their inertial forces dominate their viscous forces to a sufficient degree. This ratio of influencing forces is described by the Reynolds number, Re, a non-dimensional number that is omnipresent in fluid dynamics (Equation (3.17)). Named after the experimentalist Osborne Reynolds (1842-1912) it gives a strong indication whether a flow will be turbulent or not (although this is usually calibrated for particular flows based on past empirical evidence only). Reynolds [1883] showed that flow through a pipe will become turbulent (as observed with a dye tracer in the flow) at a Reynolds number of roughly $Re{\approx}2300$ while the flow around a circular cylinder becomes fully turbulent (including in the boundary layer) at a Reynolds number of roughly $Re{\approx}3 \times 10^5$ (however, as described in Chapter 2 the wake and shear layers become turbulent at much lower Re).

$$Re = \frac{\rho UL}{\mu} = \frac{UL}{\nu}, \tag{3.17}$$

where L is the relevant length scale of a particular flow (e.g. for flow around a cylinder, this is its diameter while for a diffuser it is the entry diameter).

Turbulent flows are rarely resolved directly with the full Navier-Stokes equations – such a simulation is described as Direct Numerical Simulation (DNS) – and instead simplifications are made so that coarser meshes can be used. As turbulent flows are unstable and chaotic systems, even tiny eddies can have a substantial impact on the overall flow over time, and so there is substantial risk of inaccuracy in failing to resolve them. Nevertheless, their impact can be approximated by models rather than being fully resolved. One approach is to solve the time-averaged Navier-Stokes to approximate the average flow (RANS), while another is to filter the N-S equations to resolve many of the smaller eddies (LES and DES), and only model the very smallest. The particular method(s) used to account for the unresolved eddies in a numerical scheme are called 'turbulence models', of which there are a great number, each of differing validity. Table

Table 3.1 below details a few of the most common in increasing order of accuracy (but also increasing computational cost).

Model	
RANS Reynolds-Averaged N-S equations	Increasing computational cost ↓ / Increasing approximation ↑
URANS Unsteady Reynolds-Averaged N-S equations	
SAS Scale Adaptive Simulations	
DES Detached Eddy Simulations	
LES Large Eddy Simulations	
DNS Direct Numerical Simulations	

Table 3.1 Summary of turbulence resolving approaches.

For this research, the flows that were studied were predominantly laminar. Since turbulent flows are much more computationally expensive to resolve, it would be time-consuming to perform many studies in the turbulent regimes. Optimisation studies require many iterations of the forward problem (solving the N-S equations), even when gradient-based methods are employed. The aim of this thesis is to determine the feasibility of autogenous suction control and uncover any relationships between the uncontrolled characteristics (particularly the separation values) and the optimal control. Much more can be achieved through many studies in well-behaved laminar flows than with time-consuming turbulent ones.

3.3.4 Two-Dimensional or Three-Dimensional Flows

Similar to the discussion of whether to study laminar or turbulent flows, it is in many instances possible to simplify a numerical model by reducing the number of spatial dimensions involved. This is not feasible when the flow is turbulent and highly three-dimensional, but for laminar flows a two-dimensional approximation is often reasonable when appropriate boundary conditions are applied. The flow around a circular cylinder is two-dimensional up until $Re = 188.5$ according to the review of experimental studies by Williamson [Williamson 1996]. At $Re = 188.5$, the vortex shedding begins to have spanwise periodicity. Similarly, the flow through a conical diffuser exhibits symmetry about its central axis up until about $Re = 2000$ for gradual expansions [Cantwell et al. 2010]. As such many of the studies in this thesis make use of these simplifications in the flow.

3.3.5 Modelling Porous Flows

Any practical implementation of suction control requires a way for the fluid to be pulled through the body surface. This is typically achieved through the use of slots or porous materials. Since we are particularly interested with non-uniform suction profiles, which are much more efficient, the porous option is best. In order to test more physical designs of suction control – and in particular for the development of autogenous suction control – the CFD models had to be modified to be able to resolve flow through porous materials as well as unrestricted (free) flow.

The study of flow through porous materials has a long history, mostly in the civil engineering field where water transport through soils and ground materials is of high importance. In its modern study, Henry Darcy (1803–1858), a French engineer, was the pioneer. His studies of flow through a packed porous bed of sand found that the flow was directly proportional to the pressure gradient and to a variable describing the propensity for the material to conduct flow through it – the permeability, κ [Darcy 1856]. The equation he derived from these experiments now bears his name, Darcy's Law:

$$\mathbf{u} = \frac{-\kappa}{\mu}\nabla p, \tag{3.18}$$

where κ is the isotropic permeability (m^2). Integrated over cross-sectional area, A, the equation is

$$Q = \frac{\kappa A}{\mu L}\Delta p, \tag{3.19}$$

where Q is the total volumetric flow rate ($\frac{m^3}{s}$), A the cross-sectional area (m^2) and L the length over which the pressure drop is measured.

These equations are only valid where the flow is entirely moving through the porous material and is normal to it. They also assume that the flow is relatively slow. The present application is for the case where flow through a porous medium is only part of a greater free-stream, and where the flow is not necessarily normal to its surface. Additionally, the flow may be fairly quick in order to achieve flow rates that will have a substantial effect on the flow. The model must be able to seamlessly solve for free flow and flow in a porous medium that are adjacent.

Considering these factors, the Brinkman equations are more appropriate for such a case. Introduced by Brinkman [1949], the equation is an extension of Darcy's law to account for the kinetic energy lost due to viscous shear effects as a flow moves through a porous medium, and is defined as

$$\mathbf{u} = \frac{-\kappa}{\mu}\nabla p + \beta\nabla^2\mathbf{u} \tag{3.20}$$

where, $\beta = \frac{\widetilde{\mu}}{\mu}$ is an effective viscosity term, and ∇^2 is the Laplacian operator. The advantage of this variation on Darcy's law, is that the Navier-Stokes equations can be simplified to a similar equation under particular circumstances, and so the flow field between the two regions can be unified. Since the flow is expected to be fast, it makes sense to include the Forcheimer drag term also [Nield and Bejan 2013, p. 10] which accounts for form drag (pressure drag) arising in the porous medium. This is the last term in the following extended equation:

$$\mathbf{u} = \frac{-\kappa}{\mu}\nabla p + \beta\nabla^2\mathbf{u} - c_f k^{\frac{-1}{2}}\rho(|\mathbf{u}|\cdot\mathbf{u}) \tag{3.21}$$

where, c_f is a dimensionless form-drag constant, and k is the inertial permeability. One can see the resemblance between the Forcheimer drag term (the last term) and the typical drag calculation for a body in fluid.

COMSOL has a ready-to-use porous media module in their CFD package with this functionality available. The 'Free and Porous Media Flow' solves the velocity field and pressure throughout the domain using the Brinkman equations in porous regions, and the Navier-Stokes in free-stream domains. Since the Brinkman equations are also solved to give the velocity field and the pressure field, no special boundary conditions or treatments are needed [COMSOL Multiphysics® 2020a, p.407]. However, this is only the case when the free-stream flow is laminar, so turbulent studies could not be conducted with this approach. All that needs to be done to solve the free and porous flow is to import the module, define the material characteristics, and specify which equations to solve in which zones. It is even possible to define anisotropic permeability if desired.

Due to the varying materials and the flow through the body, evaluating the drag by integrating the shear and normal stresses on the surface of the body is no longer viable. Therefore, the drag was evaluated using the momentum integral approach which will be described shortly.

3.3.6 Validation of CFD

Any computational approach to modelling fluid flow must be accompanied by experiments that can validate that the results are physically correct. With the numerical methods and algorithms discussed above, an appropriately described boundary value problem can usually be solved – but that does not guarantee that the results are actually physically relevant. Many errors can accumulate in CFD models, so validation is a key part of the process. Typically, a base model is developed and validated against experiments – either performed in tandem with the simulations, or drawing upon historical results from the literature. The model can then be used with some surety that the results are at least within a fair tolerance range. Obviously not every CFD simulation

should be matched by experimental studies, as the reasons to use CFD in many cases is to perform a great number of tests that could not otherwise be run by experimental means (e.g. a parameter sweep with 1000 iterations, which would take many weeks in a wind tunnel or the like). Therefore, once a model has been validated it is extended. However, if the flow is expected to become drastically different, it would be advised to confirm the results by experimentation again. The approach taken in this research was to validate each major CFD model against values from the literature. The relative accessibility and abundance of past experimental and numerical results for the reference geometries was an important reason for their selection, as highlighted in the Chapter 2.

For the circular cylinder and the conical diffuser, models were first developed and then validated against values from the literature for the uncontrolled cases. Where such data was available and replicable without too great a change to the models, controlled flows were also compared. Then mesh independence studies were performed so as to optimise the mesh and confirm the numerical stability of the converged results. Once these tasks were achieved, the models were considered valid and could be extended to numerical experimentation on suction and blowing control. The details of these processes and their results are provided in each relevant chapter.

In some cases, the implementation of suction control produced results that were unusual. In such cases, the assumptions made in each model were usually reduced to see if the results remained. For example, in simulations of suction control of the diffuser, some parameter ranges resulted in no convergence or else performances that appeared to be outliers. The assumption that the flow was steady was relaxed, and time-dependent simulations were performed with the control either ramped up or down. This revealed that hysteresis in the flow was occurring, and the method of solving the steady-state equations influenced what result was achieved (if any at all). This sort of approach was used in all our CFD work. Whenever possible, results were verified by simulations involving fewer assumptions – e.g. time-dependent or 3-dimensional.

3.4 OPTIMISATION OF FLOW CONTROL PROCEDURE

The general procedure of optimisation has been described in Chapter 2, so in this section the objectives for the optimisation studies, how they were evaluated, and the specific algorithms used for the optimisation will be described.

3.4.1 Optimisation Objectives

There were three objectives that were predominantly investigated in this research:

1. Minimisation of separation angle, θ_s, or the length of the recirculation region, L_{sep}
2. Minimisation of total drag coefficient, C_{d_t}

3. Minimisation of pressure drag coefficient, C_{d_p}

These were chosen as to find results for the research questions – particularly to uncover any relationship between the separation characteristics and the drag. Since pressure drag is the dominant contributor for bluff bodies and high Re flows, this was also investigated as its own objective also. The methods for evaluating these parameters will briefly be discussed, as there are often many different ways of doing so for each.

3.4.1.1 Separation Parameters

The point of separation occurs where the gradient of the velocity tangential to the wall (and evaluated at the wall) with respect to the direction normal to the wall is zero:

$$\frac{\partial u_t}{\partial n} = 0. \tag{3.22}$$

It is at this point that the flow in the BL has stagnated. However, since this relationship will occur when the flow reattaches also, a further condition is needed to distinguish a point of separation from a point of reattachment: the second derivative of the tangential velocity with respect to the normal direction:

$$\frac{\partial^2 u_t}{\partial n^2} < 0. \tag{3.23}$$

Upstream the flow still moves forward (though greatly retarded), while downstream the flow will be reversed near the wall. A streamline defined along the wall will separate from it at this point, and since the local skin friction is directly proportional to the normal gradient of the flow, this too will be zero. All these features can be potentially be measured in order to ascertain where separation has occurred. In experiments, some features are easier to detect than others, but for computational simulations they are all similarly accessible. We define and ascertain the separation point in the typical way for CFD: as the first point on the bounding wall where the above gradients are observed. In COMSOL, there is not a simple way of evaluating this point so a custom MATLAB function was coupled with the CFD model which performs this analysis and returns either the angle of separation, θ_s, (as for the flow around the circular cylinder) or its distance from a reference point, z_s (as for the flow through the diffuser). For the internal flow simulations, the length of the recirculation region was desired, L_{sep}. To calculate this, the first reattachment point is also needed, and this was evaluated in a similar way but with the opposite sign for the second derivative. Below are the full equations for separation objectives for the cylinder and for the diffuser

$$J_{s,cyl} = \theta_s = max\left(\theta\left(\left.\frac{\partial u_t}{\partial r}\right|_{wall} = 0, \frac{\partial^2 u_t}{\partial r^2} < 0\right)\right), \tag{3.24}$$

$$J_{s,div} = L_{sep} = |z_s - z_r| \tag{3.25}$$

where J is used to denote an objective functional, *min* and *max* are used in case several separation regions are present. For Equation (3.25), z_s and z_r are given by

$$z_s = min\left(z\left(\left.\frac{\partial u_t}{\partial r}\right|_{wall} = 0, \frac{\partial^2 u_t}{\partial r^2} < 0\right)\right), \tag{3.26}$$

$$z_r = min\left(z\left(\left.\frac{\partial u_t}{\partial r}\right|_{wall} = 0, \frac{\partial^2 u_t}{\partial r^2} > 0\right)\right). \tag{3.27}$$

3.4.1.2 Drag Evaluations

Drag can be considered in two ways: as a force experienced by a body in fluid flow, or as a pressure and skin friction distribution over that body. In experimentation, this first feature is often used to measure the drag, using a simple force probe where the body is attached to its support. CFD resolves the entire flow field, so it is usually easiest to evaluate the drag by integrating its constituent parts – the pressure and skin friction over its surface. However, the total stresses on the body could be integrated (instead of their tangential and normal components) to determine the total drag directly. The total drag coefficient is therefore given by

$$C_{d_t} = C_{d_p} + C_{d_f}, \tag{3.28}$$

where C_d represents a drag coefficient ($C_d = \frac{F_d}{\frac{1}{2}\rho U^2}$, and the subscripts t, p and f denote whether it is the coefficient for the total, pressure or skin friction drag components. These components are evaluated as following

$$F_{d_p} = -\oint p dx \tag{3.29}$$

$$F_{d_f} = -\oint \mu \frac{\partial \mathbf{u}}{\partial n} dx \tag{3.30}$$

where, x represents the direction of the drag axis, and n is the direction normal to the bounding wall. Combining these we get the objective functionals for total drag and for pressure drag for the circular cylinder:

$$J_{d_t} = C_{d_t} = C_{d_p} + C_{d_f} = \frac{1}{\frac{1}{2}\rho U^2 D}\oint \left(-p\left(\theta\right) + \mu \frac{-\partial u_t\left(\theta\right)}{\partial r}\right)\cos\left(\theta\right) R d\theta, \tag{3.31}$$

$$J_{d_p} = \left|C_{d_p}\right| = \left|\frac{1}{\frac{1}{2}\rho U^2 D}\oint -p\left(\theta\right)\cos\left(\theta\right) R d\theta\right|, \tag{3.32}$$

where R the radius of the cylinder, and θ the angle measured anti-clockwise from the trailing edge.

Another method, developed by B.M. Jones [Schlichting 1987, p.761], is also useful for evaluating drag: the momentum balance. This is useful in both experimentation and CFD, particularly where the boundary layer may not be fully resolved, e.g. if wall functions are used in turbulence models, or in the present case when the use of porous materials on/in the body complicate the pressure and skin friction evaluations. Since every action has an equal and opposite reaction, the drag force imposed on the body is equally and oppositely applied from the body to the fluid, therefore the net flow downstream has less momentum than before encountering the body. This knowledge can be used to determine the drag by measuring the flow field upstream and downstream of the body. By considering a control volume surrounding the body, the drag will then be the difference in the streamwise momentum integral (plus the integrated pressure difference if there is one) at the downstream end and the upstream one. When the drag is evaluated in this way, it is usually referred to as the wake drag. Referring to Figure 3.10, the equation for the drag is

$$\oint_{abhi} \rho(\mathbf{u}\cdot\vec{n})\ \mathbf{u}\cdot\vec{i}\ dA + \oint_{abhi} p\ \vec{n}\cdot\vec{i}\ dA = -D. \tag{3.33}$$

Which gives the following evaluation of the coefficient of drag:

$$C_{d_u} = -\frac{\oint_{abhi}\rho(\mathbf{u}\cdot\vec{n})\ \mathbf{u}\cdot\vec{i}\ dA + \oint_{abhi} p\ \vec{n}\cdot\vec{i}\ dA}{1/2\rho U^2 A}, \tag{3.34}$$

where this coefficient, C_{d_u}, is called the wake drag coefficient.

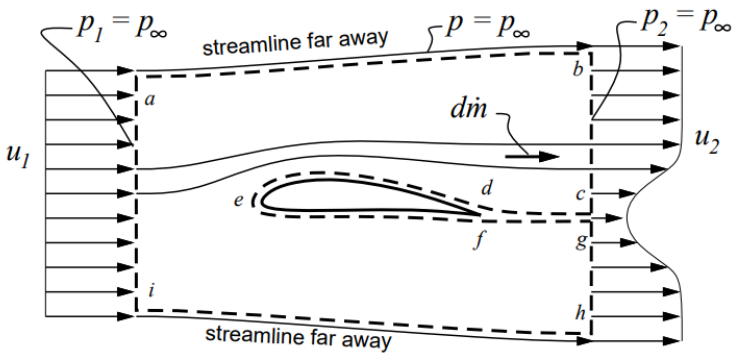

Figure 3.10 Control volume for evaluating the drag from fluid momentum change. Taken from Paolo Lozano's MIT lectures on fluids with permission [Lozano 2008].

In the simulations conducted for this thesis, the drag was usually evaluated by

integration over the body surface. Where relevant, the lift forces were evaluated in the same manner but with the principal direction in the vertical instead. When porous surfaces and internal ducting were implemented to try and achieve autogenous control, however, this method was no longer reliable. Instead the momentum balance approach was used. There is usually a slightly higher error with this calculation than the boundary integrations because the mesh is more refined near the walls rather than where the control volumes are defined. However, this error was found to be small enough to be negligible ($< 1\%$).

When suction is applied to a body in a fluid, the drag calculation is complicated slightly. The usual momentum balance assumes that fluid only enters and exits the control volume upstream and downstream. When suction is applied, it also exits through the body wall. As described in the textbook by Schlichting [1987, p. 387], the drag contribution of boundary layer suction on a body is

$$C_{d_s} = 2C_q, \tag{3.35}$$

where C_q is the suction volume coefficient $C_q = \frac{v_w}{U}$. If the drag is evaluated using the momentum approach, it would be necessary to add this to the wake drag to determine the total drag. However, the pressure and skin friction profiles respond to the suction and they still give an accurate evaluation of the total drag when evaluated (Newton's Third Law still applies and the forces on the body are in the form of pressure and friction, regardless of whether there is suction or not). For a more detailed discussion of these evaluations of drag, see the paper by Beck et al. [2018] on Drag Reduction by Laminar Flow Control. Thus one can develop the following equivalent evaluations of drag:

$$J_{drag} = C_{d_t} = C_{d_p} + C_{d_f} = C_{d_w} + 2C_q \tag{3.36}$$

where, the subscript w denotes the wake drag.

3.4.1.3 Diffuser Performance

As was discussed in the Chapter 2, there are many measures used to quantify the performance of a diffuser. The matter is further complicated when fluid is added or removed to the system by suction or blowing control. As such, we employed a relatively simple and conservative measure of the performance: the ratio of pressure energy exiting the diffuser to the total energy entering it (including any energy added or used by the control). This is given by the following equation:

$$\eta_{out} = \frac{Q_2 P_2}{Q_1 \left(h_1 + P_1\right) + Q_w (P_w + h_w)}, \tag{3.37}$$

where, the pressures are the average pressure over their relevant regions, h is the dynamic pressure and the subscripts $1, 2$ and w refer to the entrance, exit and control regions of the diffuser respectively. When the pressures are measured relative to the entrance pressure, P_1, this is simplified to

$$J_{perf} = \eta_{out} = \frac{Q_2(P_2 - P_1)}{Q_1 h_1 + Q_w \left(P_w - P_1 + h_w\right)}. \tag{3.38}$$

3.4.1.4 Pressure and Flow Rate Balancing (Autogenous Control)

Determining the optimum suction profiles to minimise drag or eliminate separation is a major objective, but important to the present work is whether these characteristics can be improved without adding energy to the system, i.e. passive control. For an autogenous suction to be generated, the system needs to involve both suction and blowing – for the removed fluid must be exhausted back into the flow. A coupled suction/blowing control system must be considered. The flow rates must be balanced, but also, if the control flow is to be driven passively using the energy in the system, the pressure gradient from suction location to blowing location must be favourable. In other words, the average pressure where suction is applied must be higher than where it is exhausted at the blowing location, and ideally this pressure differential would be such that it drives the control flow at the optimal flow rate. What exactly this pressure differential should be is not known a priori as it depends on the way that the control is implemented (ducting geometry, porous materials, etc.).

To address this, either a set pressure drop can be specified, as in [Atik and van Dommelen 2008], and the control parameters optimised to satisfy this. Or a broad constraint can be applied – e.g. that the pressure difference must be greater than some value (but not equal to a particular value). We call this the *minor* objective in cases where it is used, for it is only a step in the overall objective of maximising performance. Figure 3.11 shows the flow chart of the optimisation procedure to determine the best autogenous suction control to maximise performance within the conical diffuser. The minor objective is:

$$J_{auto} = P_s - P_b - \Delta P, \tag{3.39}$$

where ΔP is the desired pressure differential to be achieved (must be positive for the flow to be naturally driven), the subscripts s and b denote the suction and blowing locations, and the pressures here are averaged over the control locus (represented by a capital P). In most cases, we employ $\Delta P = 0$. In other cases this objective is not included, but a constraint like the following is employed, coupled with the major

objective:

$$dP = P_s - P_b \geq 0. \tag{3.40}$$

The difference between dP and ΔP is that the former is the actual pressure drop evaluated from the resulting flow, while ΔP is the desired pressure drop.

Given the hypothetical case that there may be several arrangements for the same suction control where a pressure and flow balanced blowing locus could be setup. Therefore, it is important to include the performance or drag objective in the minor optimisation also:

$$J_{minor} = J_{auto} + J_1. \tag{3.41}$$

For completeness, the constraint that the flow rates of the suction and blowing components are equal also is given by:

$$|C_{q_s} + C_{q_b}| = C_q \leq 10^{-4}. \tag{3.42}$$

A tolerance rather than an equality is used due to numerical imprecisions that are always present.

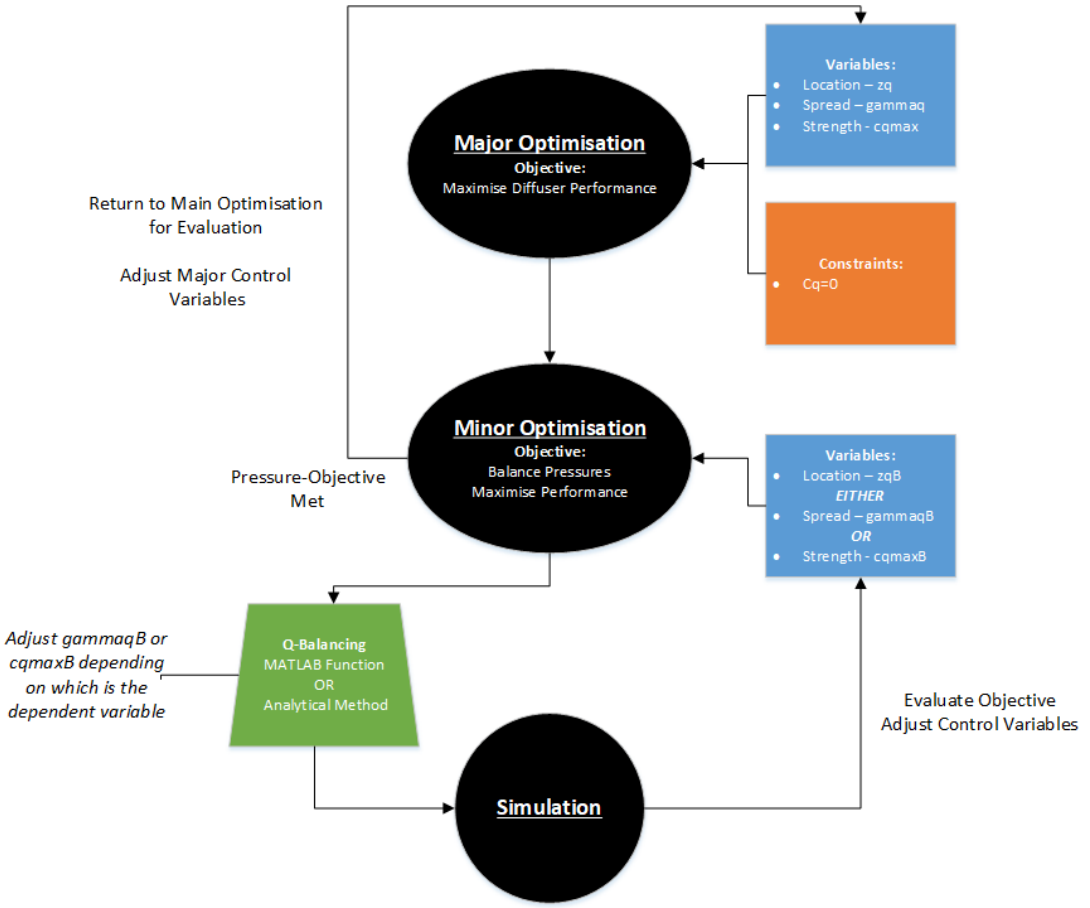

Figure 3.11 Flow chart of a program to optimise autogenous control within the conical diffuser. In this case, a secondary MATLAB function was used to find the appropriate profile of suction or blowing in order to match the other due to the changing geometry within the diffuser.

3.4.1.5 Balancing Objectives

The type of optimisation problem that will be addressed in the following investigations is typically of the multi-variate and multi-objective variety. Several control parameters are relevant to the solution, several objectives are considered simultaneously, and the effect of each parameter has a unique effect on each objective. Often, in cases such as this, there is no one true optimal solution to the problem but rather a set of parameter combinations that provide the same global objective value. By improving one objective, the others are worsened producing the same net result. This set of parameters and their objective values is called the Pareto Front, and it defines the edge of the objective values where improving one objective worsens the others such that no further improvement can be made in the total objective. Therefore it is important to have clear goals when designing the optimisation study, with which objectives are most important. Sometimes we combine an objective to minimise drag with another to minimise the control effort. Appropriate weighting of contributing objectives is key. For each model, further details of the specific control parameters and objectives are described.

3.4.2 Optimisation Methods

3.4.2.1 Nelder-Mead Method

The Nelder-Mead (N-M) method is a derivative-free optimisation algorithm created by John Nelder and Roger Mead in 1965 [Nelder and Mead 1965]. While it does not evaluate the gradient of the objective at any point, it creates a pseudo understanding of the local objective space topography by the use of several points stored in memory each iteration. The Nelder-Mead algorithm creates a simplex (a shape with $n+1$ vertices – where n is the number of dimensions in the parameter space) and evaluates the objective at each point of the simplex (referred to as a test point). It then extrapolates the trends from these $n+1$ points throughout the rest of the domain and determines how to move next by removing one test point and replacing it with another.

Its first attempt is to move the worst point, reflecting it through the weighted location of the other points. If this improves the objective function value, then it tries to extend it further in that direction. If those attempts are fruitless, it will contract the worst point towards the others but not past the centroid of the other locations. If this too does not improve upon any of the points, then the algorithm will shrink the whole simplex towards the best point. Here is a summary of the basic Nelder-Mead algorithm:

1. Order according to the values of the objective functional, $f(x)$, at the vertices: $f(x_1) \leq f(x_2) \leq \ldots \leq f(x_{n+1})$. If the tolerance has been reached, terminate and return the best value, $f(x_1)$.
2. Calculate x_0 the centroid of all points except the worst, x_{n+1}
3. Compute the reflected point, $x_r = x_0 + \alpha(x_0 - x_{n+1})$ where $\alpha > 0$. If the value at the reflected point is not the best, but is better than the second-worst, replace the worst point with this reflected point and return to (1)
   If $f(x_1) \leq f(x_r) \leq f(x_n)$ then replace x_{n+1} with x_r and return to (1)
4. If the reflected point is the best, then proceed to (5)
   If $f(x_r) < f(x_1)$ then proceed to (5)
5. Compute the expanded point, $x_e = x_0 + \gamma(x_r - x_0)$ with $\gamma > 1$
   (a) If the expanded point is better than the reflected point, replace the worst point, x_{n+1}, with the expanded point, x_e, and return to (1)
   If $f(x_e) < f(x_r)$ replace x_{n+1} with x_e and return to (1)
   (b) Otherwise replace the worst point, x_{n+1}, with the reflected point, x_r, and return to (1)
   Else replace x_{n+1} with x_r and return to (1)
6. If the reflected point, x_r, is not better than the second-worst point, x_n, then we reach this step. Instead of reflecting through the centroid, instead contract the space between the worst-point and the centroid (contract). $x_c = x_0 + \rho(x_{n+1} - x_0)$ with $0 < \rho \leq 0.5$.

If the contracted point, x_c, is better than the worst point, x_{n+1}, then replace the worst point with it.
If $f(x_c) < f(x_{n+1})$ then replace x_{n+1} with x_c and return to (1)

7. None of the above options have found an improved point than the worst in the simplex. Instead, shrink all points closer to the best point, x_1.
Replace all points except x_1 with $x_i = x_1 + \sigma(x_i - x_1)$ with $\sigma < 1$ and return to (1)

There are many variations on this method. The values of the reflection, expansion, contraction and shrink coefficients (α, γ, ρ, and σ) are all important as to the functionality of the algorithm and can be overdamped or underdamped. Usually one would expect to find an improvement in the reflected point as it is somewhat a move in the pseudo-downhill direction, but is not guaranteed.

In COMSOL, the initial simplex is generated by taking a fixed step in each dimension direction. If bounds have been defined for the parameters (which is usually the case) it will take one of the bounds as the second point along that dimension (in addition to the specified initial value for that dimension). The optimality tolerance used in the implementation by COMSOL is that if there is no improvement over the current best estimate "with steps in the scaled control variables of relative size larger than or equal to the optimality tolerance" then the solver will stop. It is important that the control variables are scaled appropriately therefore, so that the optimality tolerance works appropriately.

The Nelder-Mead method is useful for fluid flows because it does not require the reformulation of the governing equations. Many control arrangements may result in complicated mathematical boundary conditions which would be hard to rearrange into adjoint form. On the other hand, NM is only effective when the number of control parameters are relatively few ($\leq$10). Like many other optimisation methods, the NM simplex will readily converge on local (not global) minima depending on the starting points. What is more, it can also converge on non-stationary points (points that are not even local minima), whereas adjoint methods will not.

3.4.2.2 SNOPT Algorithm

The SNOPT (Sparse Non-linear OPTimiser) algorithm is one of the gradient-based methods available in the Optimisation Module provided by COMSOL [COMSOL Multiphysics® 2020b]. The algorithm, published by Gill et al. [2005], employs sequential quadratic programming (SQP) methods which is very effective for constrained optimisation problems. The method works by approximating the objective function as a quadratic polynomial (and the constraints as linear functions) at a point – this step is referred to as an *outer* iteration. These are then iteratively solved for the minimum – the *inner* iterations – which then is used to determine the next step in the control

parameters for the next major iteration. To generate the quadratic approximations to the objective function, the gradient at each test point is needed. Hence, SNOPT is a gradient-based method. As discussed earlier, this can be efficiently calculated using the adjoint equations calculated analytically, or the gradients can be determined numerically (with a perturbation and solving the forward problem again), though this is more time-consuming. The algorithm will not be detailed in full here, instead the reader is directed to the original user's guide [Gill et al. 2005].

3.5 CONTROL SETUP

3.5.1 Non-uniform Profiles

The focus of this thesis was suction control. Suction can be simply implemented in a CFD model through the use of a Dirichlet condition (either of the velocity or pressure) defining flow out of the domain. The strength and shape of the suction can be further specified by defining functions dependent on the spatial coordinates and the control parameters. Many non-uniform suction profiles can be defined depending on the function implemented, so it is important that appropriate and useful ones are employed. Alternatively, a control field can be defined over the boundary which is discretised and interpolated with shape functions. The values of this discretised field are defined and can be altered individually. This approach works best with gradient-based optimisation methods as the number of parameters can be very large (10,000's) depending on the discretisation of the control field.

For the flow around the cylinder, uniform and non-uniform suction profiles were modelled, and both function-defined and field-based control implementations were used. It might do well to ask why one would choose to define a non-uniform profile rather than just using the field-based approach. After all, if the optimisation procedure is efficient, it should determine the best profile, while not being constrained to a particular one which may be less than optimal. We chose to define particular suction profiles for a few reasons. Firstly, evidence in the literature had suggested that particular profiles were most effective, based on the results of field-based approaches [Flinois and Colonius 2015, Li et al. 2003, Min and Choi 1999]. Secondly, while a field-based approach may determine a highly effective control profile, it is also likely to generate profiles that simply cannot be replicated in reality. Defining particular profiles constrains the control to achievable possibilities. However, both approaches were employed and, in fact, we found that the field-based approach converged on control profiles very similar to our defined functions after all. The profile-defined approach is much faster and more reliable, so this was used in many more of the studies.

Three main non-uniform suction profiles were investigated for the cylinder, which were named: single locus, biased locus, and segmented control. For the diffuser, the

single-locus was the main non-uniform profile investigated. In all instances uniform suction was also implemented as a point of comparison for the efficiency of non-uniform contro. These profiles are illustrated in the schematics Figure 3.2 and Figure 3.1.

3.5.1.1 Single Locus Profile

For all the suction profiles it was desired to have smooth, continuous profiles – at least where sections of suction are applied – and for the edges and maximum point of each region to have a zero-gradient. Additionally, the single locus profile was to be symmetrical about the maximum point. This is in many respects similar to the flow profile that one might expect from a slot. The no-slip condition at the edges of the suction region would provide a zero-value and zero-gradient, and the Hagen-Poiseuille flow case has a peak in the middle which also has zero-gradient. In reality though, the tangential pressure gradients in the external flow may make the suction profile asymmetric, but this is ignored for this case though the biased locus can mirror such behaviour. The single locus profile was constructed from two sections of a cubic profile. Thus each section would have two stationary points – the endpoint and the shared maximum.

Such a profile can be described using three control parameters. The location of the centre of suction is denoted by θ_q for the cylinder case, and z_q for the diffuser. Its strength at the maximum point (at θ_q) is denoted $c_{q_{max}}$ and the spread is denoted γ_q in both cases. These are illustrated in Figure 3.2 and Figure 3.1. Let us consider the cylinder case, and use θ as the spatial dimension. To simplify the equations, a parameter for the lower-bound of the suction (the first endpoint) can be defined, $lb = \theta_q - \frac{1}{2}\gamma_q$, and likewise for the upper bound, $ub = \theta_q + \frac{1}{2}\gamma_q$. Thus, the following conditions are produced for the lower half of the profile, where c_q is the local suction coefficient:

$$c_q\left(\theta = lb\right) = 0 \tag{3.43}$$

$$\frac{dc_q}{d\theta}\left(\theta = lb\right) = 0 \tag{3.44}$$

$$c_q\left(\theta = \theta_q\right) = c_{q_{max}} \tag{3.45}$$

$$\frac{dc_q}{d\theta}\left(\theta = \theta_q\right) = 0. \tag{3.46}$$

The upper half has a similar form, but with the first two equations evaluated at the upper bound. This forms a system of equations which can fully define a cubic profile of the form

$$c_q = A\theta^3 + B\theta^2 + C\theta + D \qquad \text{for } lb \leq \theta \leq ub. \tag{3.47}$$

Solving the system for the lower and upper half, the following coefficients are found:

Table 3.2 Coefficients for single locus function.

Region	Lower Half (1)	Upper Half (2)
Range	$lb \leq \theta \leq \theta_q$	$\theta_q \leq \theta \leq ub$
A	$\frac{2c_{q_{max}}}{lb^3-3lb^2\theta_q+3lb\theta_q^2-\theta_q^3}$	$\frac{2c_{q_{max}}}{(\theta_q^3-3\theta_q^2ub+3\theta_q ub^2-ub^3}$
B	$\frac{-3c_{q_{max}}(lb+\theta_q))}{(lb^3-3lb^2\theta_q+3lb\theta_q^2-\theta_q^3}$	$\frac{3c_{q_{max}}(\theta_q+ub)}{ub^3-3\theta_q^2ub+3\theta_q ub^2-ub^3}$
C	$\frac{6c_{q_{max}}lb\theta_q}{lb^3-3lb^2\theta_q+3lb\theta_q^2-\theta_q^3}$	$\frac{-6c_{q_{max}}\theta_q ub}{(\theta_q^3-3\theta_q^2ub+3\theta_q ub^2-ub^3)}$
D	$\frac{(c_{q_{max}}lb^2(lb-3\theta_q))}{lb^3-3lb^2\theta_q+3lb\theta_q^2-\theta_q^3}$	$\frac{c_{q_{max}}ub^2(3\theta_q-ub)}{\theta_q^3-3\theta_q^2ub+3\theta_q ub^2-ub^3}$

When these coefficients are used in the appropriate ranges, the single locus profile is fully-defined:

$$c_q(\theta) = \begin{cases} A_1\theta^3 + B_1\theta^2 + C_1\theta + D_1 & \text{if } lb \leq \theta < \theta_q \\ A_2\theta^3 + B_2\theta^2 + C_2\theta + D_2 & \text{if } \theta_q \leq \theta < ub \\ 0 & \text{else} \end{cases} \tag{3.48}$$

This function is fully continuous and differentiable. The conditionals can be imposed using Boolean calls within the CFD software so the appropriate functions are applied at the right locations. It is important to note that c_q is the local suction coefficient, $c_q = \frac{v_w(\theta)}{U}$, and the equation must be multiplied by the free-stream velocity to give the dimensional velocity at each location. The net suction coefficient is given by the average value of this variable over the cylinder $C_q = \frac{1}{\pi D} \oint \frac{v_w(\theta)}{U} d\theta$.

In order to evaluate the net suction produced by this profile, one must integrate under the function. This gives the following formula

$$C_q = \frac{\gamma_q c_{q_{max}}}{360}, \tag{3.49}$$

where the angles are measured in degrees.

While the single locus profile has the same formulation for the conical diffuser (just replacing the θ's with z's), the formula for evaluating the net suction coefficient is not the same. The local volumetric flow rate of fluid removed through the diffuser walls varies along the diffuser due to the increasing surface area. Thus, the formula for C_q does not work for this case. While a complex piecewise analytical formula can be derived for this, it is simpler to numerically integrate the boundary condition.

3.5.1.2 Biased Locus

The biased locus is a simple extension from the single locus form. It adds a parameter, λ_q, which defines how skewed the profile is toward the leading edge. In this case, θ_q no longer defines the center of the suction control, but rather the location of the peak suction. The equations for c_q and its coefficients do not need to be changed. The bias is simply incorporated by changing the upper and lower bounds:

$$ub = \theta_q + (1 - \lambda_q)\gamma_q, \tag{3.50}$$

$$lb = \theta_q - \lambda_q\gamma_q, \tag{3.51}$$

where γ_q has values of $0 < \gamma_q < 1$. The larger λ_q is, the closer the peak suction is to the leading edge, and vice versa.

3.5.2 Autogenous Control – Dual-Slot Approach

When autogenous suction control is implemented there must be one or more suction regions and one or more blowing regions where the removed fluid is exhausted back into the flow. As discussed earlier, these flows must have balanced flow rates and pressures (this is only a concern when the control is being implemented by boundary condition). To keep matters simple, a 'dual-loci' profile was developed by reusing the single locus control functions for the suction and blowing components, and superimposing them to produce the suction/blowing control. This has the advantage of keeping each control parameter independent to adjust, while they are treated as a single boundary condition within the CFD program. For the case of the circular cylinder, these control parameters were $\theta_q, \gamma_q, c_{q_{max}}, \theta_{q_b}, \gamma_{q_b}$, and $c_{q_{max_b}}$ where θ_q is the angle from the trailing edge where the control is centred, γ_q is its spread, and c_q its maximum strength (the b subscript denotes where these parameters refer to the blowing control). Two variations on the dual-loci control were used. The first is an 'unbalanced' form, where the suction and blowing loci parameter are entirerly independent. The second is a flow-rate balanced 'Q-balanced' variety, where the blowing parameters are coupled to the suction ones so that $C_{q_s} = -C_{q_b}$. More details for this are provided in the relevant chapters (Chapters 4 and 7).

3.6 NEURAL NETWORK APPROACH

An alternative to optimisation methods, and one that is becoming increasingly popular and the subject of much interest, is the use of artificial neural networks to design near-optimal control. To understand why, first consider the advantages and disadvantages of parametric studies (where particular parameters are altered systematically) and

optimisation. Parametric studies are the traditional way of experimenting on fluid flows. When performing an experiment in the wind tunnel, a researcher will methodically change the parameters of interest, measure the results, and repeat – for example the angle of attack of an airfoil. By plotting and comparing these data-points, a fair idea of the influence of this parameter, and a good approximation of its optimal value can be made. However, this process is tedious, time-consuming, and does not extend well when many coupled parameters are in the picture. Optimisation, on the other hand, performs a similar process but instead of changing the parameters methodically, it makes more educated guesses of what might be the best next change in an effort to always improve some objective. It is often very effective, can handle many control variables, but often leaves the researcher with a weaker understanding of the overall behaviour and is left with only one final potential design. If other influencing factors are then changed, or it is desired to extrapolate the results out to a different scenario or environment, the optimisation may have to be performed again in its entirety. Both methods have their benefits and detriments, and each has a particular place in the study and design of fluid flows. The neural network approach attempts to combine the advantages of both these methods.

3.6.1 How it Works

The neural network approach works by coupling CFD simulations (or a body of experimental data-points) with an artificial neural network which is then trained to predict some value or vector of interest when prompted by a relevant input. For example, in this research, a neural network was trained to design the geometry of an internal duct so as to achieve a prompted suction profile in another area of the flow. It was trained by performing thousands of CFD simulations where the duct geometry was randomised (or parametrically investigated) and evaluating the suction profile in the relevant region. Values for both features were then stored, and fed to the network for training, validation and testing. Then the network can be used to design the geometry that will achieve some desired suction profile. Simply input to the network appropriate values representing the suction profile, and it will output the geometry values it believes will achieve it with the least effort. This is demonstrated by the flow chart in Figure 3.12.

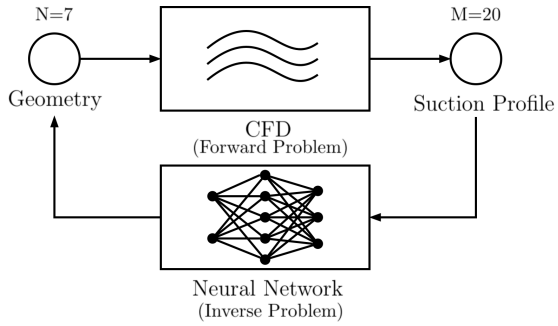

Figure 3.12 Flow chart for CFD-ANN coupled workflow for designing suction-inducing geometries in this study. More details in Chapter 5.

This is a relatively straight-forward approach to training the network as only one set of parameters was altered in the underlying studies (the wall geometry). Its advantages over a simple parametric study are perhaps not as demonstrable here (although at least seven parameters were used to define the wall geometry, and to get a decent picture using parametric studies would require many thousands of studies). In a more challenging test, many parameters might be altered at once (whether at random or methodically) and the network should theoretically be able to find reasonable trends in the output behaviour.

In this research, the artificial neural network was designed, trained and used through the MATLAB Machine Learning Toolbox, specifically the 'Neural Net Fitting' tool. 'Livelink for MATLAB' was also used, which is a COMSOL extension that allows COMSOL to be called and run within a MATLAB script. This made it easier to perform the forward simulations and extract the relevant data from which the networks were trained. Further details on the specific parameters and network features will be described in Chapter 5.

3.6.2 Advantages/Disadvantages

The neural network approach is attractive for a variety of reasons. Firstly, this approach can handle many parameters at once and find cohesive patterns even amongst sparse studies. Secondly, while an optimisation approach can do likewise, it is not capable of then extrapolating that information out if the objective is changed. In our example, if a different suction profile is desired than initially thought, one need only probe the neural network again and receive a new design in seconds. Whereas, the optimised result is no longer useful for the changed objective, and the optimisation process must be performed again (although perhaps with a much improved starting point – the previous optimum). Third, it is relatively simple to use. Instead of carefully designing a parametric study which will use minimal iterations but still give a good picture of the response to the parameters, the parameters can simply be randomised, or the best attempt made, and the network will respond to it extremely well. Fourth, it is new and there is much

more improvement in efficiency and usefulness to be found, if the improvements in optimisation theory are anything to go by.

3.6.3 Implementation to Suction Control Design

The neural network approach was used to aid the design of a physical autogenous control design. While two regions of appropriate pressure can be connected to drive a rough secondary flow, it may be possible that further improved autogenous control might be achieved through more complicated means. For example, the downstream approach proposes that perhaps suction can be implemented in a region of very low pressure (where otherwise it could not be) by producing a flow from further upstream to further downstream, and using a venturi-like effect to pull the fluid through the desired region in between them. This is a complicated design, and the neural network approach was used to get a better idea of whether it was feasible. The coupled advantages – the versatility of a parametric study with the flexibility of an optimisation study – were ideal for such a problem.

3.7 DESIGNING AUTOGENOUS CONTROL FEATURES

The general approach taken in this research was to first determine what kind of autogenous suction control was theoretically possible and if it was worth pursuit, then to try and implement that specific control physically. However, this approach is limited based on the assumptions that are made in that first step, the details of which will described shortly. Furthermore, the approach to the primary question looked at upwind autogenous control only (where the control flow moves from downstream to be exhausted upstream to make use of the adverse pressure gradient in the streamwise direction). In reality, alternative approaches may be possible, but it would be near impossible to design an accurate model where their effect is simulated by boundary conditions without first designing such a system and testing its validity. Therefore a systematic approach to designing potential autogenous control systems was needed – either to test already determined theoretical designs, or to develop new ones. This section describes the investigation into these problems. First, the difficulties in designing autogenous control are described without looking at any one particular design, then the approaches taken to design upwind and downwind autogenous control are described in order.

3.7.1 Difficulties in Designing Autogenous Control

There are several difficulties in designing a physical implementation of autogenous control. The most important ones are the following:

- Number of parameters to investigate. The design space of internal (or external) ducting is practically limitless, and the chosen design will affect the pressure drop needed, and the flow rates and profiles that result
- Non-normal suction/blowing. Most studies on boundary layer suction assume that the suction is normal to the bounding wall. In reality, due to the strong gradients in the tangential direction, it would be difficult to generate a normal suction without a very strong pressure drop to dominate the flow (as a pump would produce)
- Transitioning from the uncontrolled flow (with its pressure profile) to the controlled stable autogenous one (with its own, different pressure profile). Since autogenous control relies on the pressure contours available in the flow and does not generate its own, there is a significant problem in how the control can be started. The pressure profiles of the uncontrolled flow and ideally autogenously controlled flow are (or at least should be) drastically different. How can the uncontrolled flow be transitioned to the controlled one?
- Time-varying flow field. Most flows of practical use are unsteady. Above $Re = 47$ the flow around a cylinder has a dynamic wake, and consequently the pressure profile along its wall varies with time. As was found in our study on the cylinder, improvements in drag are only really achieved by suction above $Re = 47$ – here, the flow is time-varying [Ramsay et al. 2020d]. While an upwind autogenous control system could be designed for the cylinder flow when it is steady at $Re < 47$, it would be of little practical use. Autogenous control is already hard to design for a steady flow, but the time-dimension adds another difficulty.

These all bear significant challenges that make the development of autogenous control difficult. Many of the assumptions made in the proposed boundary condition simulations are likely to be invalid in a real physical system. So what is the best way to address these issues? It is to run simulations of the real physical cases and then to adjust from that basis. Boundary condition simulations (where the effect of idealised autogenous control is imposed on the flow) can be guided by these physical simulations instead of the other way round. Or better yet, a combination approach is applied.

3.7.2 Upwind Autogenous Control

The study by Atik and van Dommelen [2008] had shown that it was theoretically possible to passively drive suction and blowing on an airfoil, and by that control, delay separation. This was achievable by designing the system so that the control flow (or secondary flow) moves upstream. This makes use of the adverse pressure gradient in the streamwise direction. We choose to call this autogenous suction control *upwind autogenous*. Those authors did not attempt to implement such a system, nor design a physical system (ducting etc.) that might accomplish it. This upwind autogenous control should be

the simplest possibility though. Theoretically one need only to connect the suction and blowing regions, using a suitably designed porous material to achieve the desired profile, and then the naturally arising pressure profile should drive the secondary flow. In practice though, it is not as simple as this, with some of the potential issues already described. The design of the ducting has a strong impact on the pressure drop from the suction to blowing regions – due to skin friction and minor losses that may occur. Figure 3.13 demonstrates some of the potential ductworks for the case of a cylinder with dual-slot control.

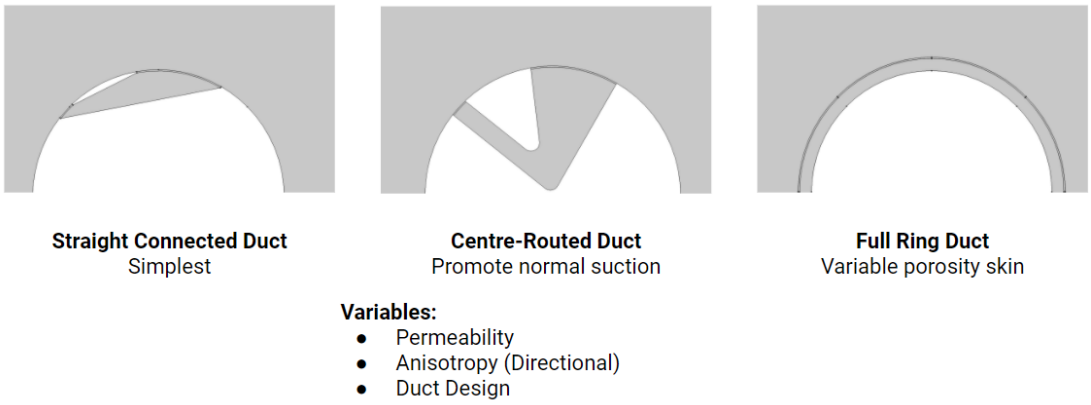

Figure 3.13 Potential designs for internal ducting for autogenous control on the circular cylinder.

The approach taken in this work for the design and testing of such a system was to use a porous skin on the surface of the cylinder or diffuser, and then design some ducting between the regions. There are obviously many parameters at play here, from the porous material characteristics to the design of the ducts. A parametric sweep is not particularly useful for such a problem where so many parameters are involved, while an optimisation approach would likely be too constrained. Instead, the engineering approach is better suited. To manually perform simulations on potential designs, measure the performance, and adjust based on the results. We performed such studies on both the steady cylinder flow ($Re < 47$) (despite the control not being useful in this range, and on the unsteady 2D laminar cylinder flow ($47 < Re < 188.5$).

Chapter 4

CONTROLLING INTERNAL FLOWS - CONICAL DIFFUSER

4.1 SUMMARY

In this chapter, the results for simulations of flow through the conical diffuser with and without suction/blowing control are presented.

Since the experimental results in the literature for this flow are varied and mostly focussed on either very slowly diverging diffusers or the sudden expansion case, first a thorough investigation of the uncontrolled flow was performed over a wide-range of diffuser parameters: the diffuser semi-divergence angle, α, the Reynolds number, Re, and the inlet profile, n were varied in a parametric study.

Following this, suction control was investigated beginning with a study of uniform suction over the length of the diffuser. Parametric and optimisation studies were performed. While these studies were undertaken with diffusers of many divergence angles, complications such as the development of hysteresis meant that much of the focus was initially on the diffuser with semi-divergence angle $\alpha = 5°$. After this, it was endeavoured to find the optimal uniform suction flow rate to improve the diffuser efficiency or to eliminate separation. This was performed over the range of semi-divergence angles $5° \leq \alpha \leq 85°$ and with Reynolds numbers up to $Re \leq 2000$ (though typically $Re \leq 1400$). Uniform suction was usually able to improve the performance even when its own effort was considered in the balance. For example at $\alpha = 5°, Re = 1000$ the performance was improved from $\eta_{out} = 0.4335$ to $\eta_{out} = 0.4720$ (a 9% improvement). Hysteresis of the fully-developed flow was observed in the range of $25° \leq \alpha \leq 35°$ for certain suction flow rates and Re.

After confirming that suction control could increase the performance of a diffuser – even when its own energy requirements are considered – an optimisation of non-uniform suction control was carried out. This involved the field-based approach and a variety of non-uniform profiles. Again, it was found that non-uniform suction control is more effective and efficient than uniform control. The field-based control produced a performance of $\eta_{out} = 0.6758$ and the single locus $\eta_{out} = 0.665$ – both improving on

the uncontrolled diffuser by over 50% – while using less suction than the optimised uniform case ($C_q = 0.159$ for single locus vs. $C_q = 0.145$ for uniform). While trends in the most effective use of suction in the diffuser were discovered – such as the preference for strong suction near the diffuser entry – no reliable relationships with the separation parameters were uncovered.

The major focus of our investigation into non-uniform control for the diffuser was that of autogenous control. It was desired to see if upwind autogenous control could be effective. The pressure profile within the diffuser increases throughout (after an initial dip as the flow enters and turns the corner) and often continues to rise in the exhaust pipe before reaching its peak and decreasing with the linear trend of flow through pipes. Therefore, a secondary control flow could be driven with suction downstream and blowing upstream. The boundary condition approach described in the Methodology chapter Chapter 3 was used here to match pressures of the suction and blowing regions, as well as their flow rates.

Unfortunately, though this arrangement of suction downstream and blowing upstream certainly is possible, our investigation found it has little use in improving the performance of the diffuser. On the other hand, if the pressure requirement is ignored, the dual-loci suction/blowing control could produce tremendous performance. For the unbalanced case (i.e. net removal or addition of flow by the control) a performance of $\eta_{out} = 0.8283$ was achieved (a 91% improvement over the uncontrolled case). The flow-rate balanced control (no net removal of fluid) achieved a slightly worse performance ($\eta_{out} = 0.5820$) than the suction-only case, but still greatly improved on the uncontrolled performance. For the P-Q-balanced study, though little or no gain in performance was achieved it should be stressed that this was only for one diffuser and flow, and with one type of limited autogenous control setup. For example, our study only considered the case with the blowing region exhausted normal to the diffuser surface. On the other hand, it is known that blowing tangential to the boundary is usually beneficial to the flow and delays separation by stimulating the BL. Further investigation using directional suction/blowing may overcome these issues of poor performance.

Much of the analysis and results presented here were previously published in the Journal of the Royal Society New Zealand [Ramsay et al. 2020b]. In particular the model details of the uniform suction case, and the results for the 5° diffuser. At times, this article is quoted directly while at other times it is paraphrased (this is in accordance with the copyright guidelines of the publisher [Taylor & Francis 2021]).

4.2 MODEL SETUP

4.2.1 Geometry

The flow through the conical diffuser was modelled using COMSOL Multiphysics with the Laminar Flow and Optimization modules (see Chapter 3 for details). The simulations were predominantly 2D axisymmetric and steady-state as previous studies had suggested that the flow has these features and is stable up until at least $Re = 1400$ [Cantwell et al. 2010]. Time-dependent studies were also performed when the flow began to exhibit hysteresis. In the following discussion, all values are non-dimensionalised using the parameters in Table 4.1.

Table 4.1 Non-dimensionalising scales for the flow.

Dimension	Non-Dimensional Scale
Length	$d = 0.002m$
Velocity	$U = Re\frac{\nu}{d}$
Pressure	$h_0 = \frac{1}{2}\rho U^2$

A schematic of the axisymmetric model geometry and the regions used to define the mesh is shown in Figure 4.1. For all simulations, the area ratio was $AR = \frac{A_2}{A_1} = 4$, and the expansion ratio $\beta = \frac{D}{d} = 2$, where the subscript 1 refers to the entry and 2 to the exit of the diffuser. The diffuser length, L, was adjusted to provide the specified semi-divergence angle, α, which was varied in the following studies. Trigonometry gives the relationship $L = \frac{D-d}{2\tan(\alpha)}$. For the special case of the sudden expansion flow, $\alpha = 90°$, Zones 2 and 3 disappear and there is no diffuser length, L. As such a separate model was developed for this case as it cannot be handled by the same geometric features as the gradually diverging diffusers.

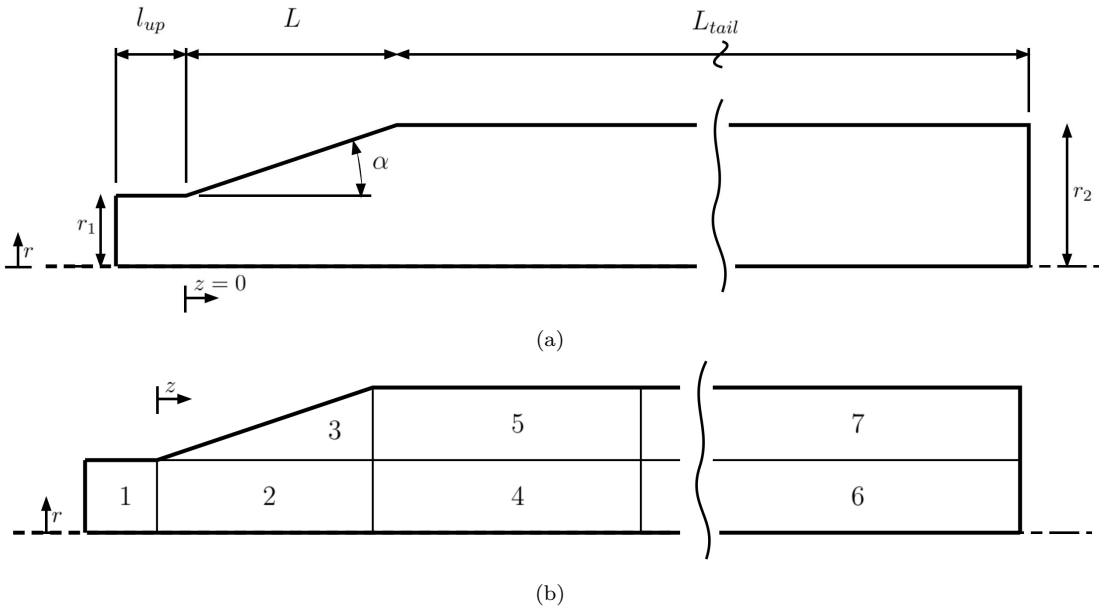

Figure 4.1 Geometry (a) and layout of the numerical domain (b) for the flow through the conical diffuser.

The inlet flow cannot be imposed directly at the diffuser entry because it naturally varies depending on the downstream conditions and a solution to the N-S for this flow is not known *a priori* (unlike for the Jeffery-Hamel case). Therefore a small inlet pipe is attached upstream so the flow can develop naturally at the diffuser entry, but so that a variety of inlet profiles can still be utilised without their effect being wiped out by the flow fully developing to the Poiseuille solution before reaching the diffuser entry. A length of $l_{up} = 0.2$ was used.

The flow through the diffuser exits into a long tailpipe so the flow can be observed until it is fully developed. The condition for this was when the difference between the theoretical and actual centreline velocity at the outlet was less than 0.1%. Its length, L_{tail}, was made to vary depending on the flow characteristics (the Reynolds number) and diffuser geometry (divergence angle) in order to reduce computational expense. Flows at higher Reynolds numbers have longer recirculation regions as it takes time for the free-stream flow to diffuse back into these regions. For the $\alpha = 5°$ case, the range was $33 \leq L_{tail} \leq 60$ for $20 \leq Re \leq 1400$ and for $\alpha = 85°$, the range was $40 \leq L_{tail} \leq 104$.

4.2.2 Numerical Mesh

As taken from the JRSNZ paper: *"Referring to Figure 4.1, all areas of the domain except Zone 3 (the expanded portion of the diffuser) were meshed with structured rectangular elements. Within Zone 3, triangular elements were employed except for the boundary layer inflation layers. The major gradients in the flow are near the walls and at the shear layer between the separated and unseparated flow, therefore, the element distribution*

was defined to provide finer resolution in these areas (Zones 3 and 5). Eight inflation layers with expansion ratio of 1.2 were applied to the walls to fully resolve the boundary layer." For the sudden expansion flow (SEF) case, Zones 2 and 3 are absent and it was possible to use a structured mesh throughout.

Since the domain changes depending on the divergence angle and the Reynolds number, a computational mesh was constructed which scaled according to the changing dimensions. In the structured areas, distributions were defined along the key edges and the number of elements were proportional to the lengths of each. The aim was to have roughly the same sized elements at the key areas of the flow (entry to the diffuser, shear line, recirculatory regions). In Zone 5 a symmetric bias of 5 was applied in the radial direction so that the elements were more refined at the edges than the centre. A bias ratio of 10 was used in the axial direction of the first section of the outlet (Zone 4 and 5) so that the elements are heavily biased towards the diffuser end and coarser elements could be used in the final outlet section where the flow is fully reattached. In addition to the biased distributions, a boundary layer inflation was applied to all wall boundaries (including the suction boundary of the diffuser) with 8 layers and an inflation of 1.2.

In the unstructured triangular mesh region, the 'advancing front' algorithm was used so that the structured distributions on the domain edges dictated the structure of the triangular mesh region. The maximum element size was restricted to 0.003 and 2×10^{-7} (in dimensionless units) The same distributions defined on the right and bottom boundary of Zone 3 used to define the structured regions of Zone 5 and 2 also applied to the triangular mesh in Zone 3, so good consistency between the regions was observed with no sudden jumps in growth rate. Table 4.2 gives the total number of elements and the number of triangular elements at the two extremes investigated.

Table 4.2 Number of elements for representative meshes

		$\alpha = 5°$	$\alpha = 85°$
Re=20	Triangular Elements	15,062	161
	Total Elements	41,588	16,037
Re=1400	Triangular Elements	15,044	175
	Total Elements	51,519	40,040

Mesh convergence studies were carried out on the flow by uniformly scaling the elements and measuring any changes to the separation length, diffuser performance, and net skin friction along the external walls. These variables changed by no more than 0.01, 0.001, and 0.0004 respectively for the final mesh resolutions. Figure 4.2 shows examples of the final mesh for the 5° and 85° diffuser at $Re = 1400$.

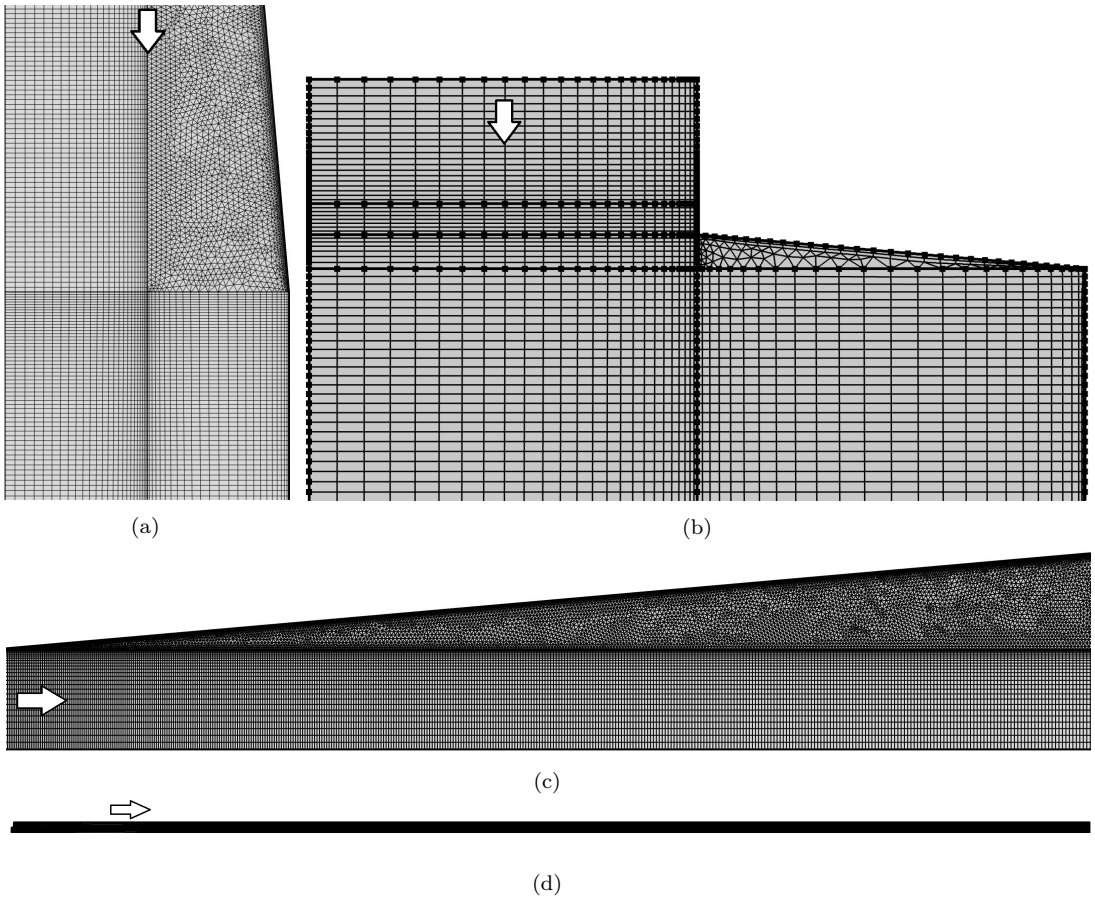

Figure 4.2 Examples of mesh regions: (a) 5° geometry at diffuser exit, (b) 85° geometry showing the diffuser and inlet region, (c) 5° geometry showing most of the extent of the diffuser, and (d) the entire domain for $\alpha = 85°$ at $Re = 1400$. Arrows indicate the direction of flow for each mesh.

4.2.3 Boundary Conditions

The following is also taken from the JRSNZ paper: *"In order to solve the governing equations, the domain needs to be fully bounded. An axisymmetric boundary condition was applied along the pipe centreline. The outlet (right boundary in Figure 4.1) is a zero relative pressure Dirichlet boundary condition. The boundary condition on the diffuser wall was defined as a fixed velocity outlet, the strength of which could be adjusted to achieve any desired suction through its surface – out of the domain. All other walls (upper horizontal surfaces) were prescribed no-slip boundary conditions.*

The suction velocity was fixed as normal to the wall with zero tangential velocity and defined by the following equation:

$$v_w = C_q U r_w \quad \text{for} \quad 0 \leq z \leq L. \tag{4.1}$$

Here v_w is the suction velocity normal to the surface at any point on the diffuser wall, C_q is the total suction flow coefficient $\left(C_q = \frac{Q_w}{Q_1}\right)$, U is the average free-stream

velocity at the inlet, and r_w is the area ratio for the diffuser wall to the diffuser entry to scale the volumetric suction coefficient for use in the axisymmetric model $\left(r_w = \frac{3L}{r \tan \alpha}\right)$. *For the case of no suction ($C_q = 0$), the boundary condition is the same as a no-slip condition. This equation could be easily altered to achieve non-uniform profiles too by replacing C_q with a local flow coefficient which varies withz, $c_q(z)$, similar to previous work by the present authors [Ramsay et al. 2020d]*

A near-uniform velocity profile was prescribed to the inlet (left boundary). While many studies of the uncontrolled diffuser employ a fully-developed profile (parabolic Hagen-Poiseuille), a flat profile is more typically seen in practical use, e.g. in turbine engines [Baskharone 1991]. If the pressure increase in the diffuser is important, efforts are made to shrink the boundary layer before the flow enters the diffuser as this greatly improves the flow and performance – typically achieved using contractions or screens directly upwind of the diffuser [Yamazato 1969, 1970]. An important note also is that boundary layer suction will have little effect, or even a detrimental effect, if the boundary layer is too large. If the fluid momentum is too spread out, the boundary layer is not adequately stimulated by free-stream particles even when the low-momentum particles are removed near the wall by suction. The fully developed profile is effectively one where the boundary layer takes up the entire pipe, and so suction control only removes valuable momentum from the flow without the benefits of re-stimulating the boundary layer [Schlichting 1987, White 2017, p.406]. The equation for the near-flat profile employed in this study is given in Equation (4.2)

$$u(\lambda) = \left(1 + \frac{2}{n}\right) U(1 - \lambda^n) \quad \text{for} \quad 0 \leq \lambda \leq 1, \tag{4.2}$$

where $\lambda = r/r_1$ and n is any even positive integer and represents a scaling term defining how flat the profile is. The higher n is, the more "flat" the profile, while a value of $n = 2$ recovers the Hagen-Poiseuille profile for fully developed pipe flow. A value of $n = 1000$ was used in this study, giving an effectively flat profile with a "boundary layer" thickness of 0.0025 at the inlet. The inlet was situated a distance $l_{up} = 0.2$ upstream of the diffuser entry. This allows the flow to develop naturally in the diffuser without being constrained by the imposed inlet boundary condition.

Except for the suction boundary condition, the same boundary conditions were applied in all cases, regardless of divergence angle and Reynolds number. Additionally, the value for n for the inlet profile was altered when its effect was studied. For the suction boundary condition, the C_q value was indeed replaced with a local coefficient $c_q(z)$ which was used to impose whatever non-uniform profile was desired. Additionally, the boundaries where the suction condition were applied was also adjusted in some simulations. For the case of the SEF, for example, it seemed unlikely that suction on the now vertical "diffuser wall" would provide the best benefit to the flow, so it was also trialled using the suction profile on the upper wall instead. And for others, other

locations of suction were also experimented. For autogenous control it was sometimes desirable to draw fluid from regions in the tailpipe, in which case the suction condition was extended to apply to the downstream walls also. Since this boundary condition replicates the no-slip condition wherever $c_q = 0$, this causes no [implementation] issues.

4.2.4 Optimisation

4.2.4.1 Control Parameters & Objectives

Uniform Suction For the studies of uniform suction, only one control parameter was under investigation: the volumetric suction coefficient: C_q. This was bounded with the limits $0 \leq C_q \leq 1$ which mark the extreme cases of no suction and complete exhaustion of the incoming fluid respectively. The Nelder-Mead method was employed, which has been described in detail in Chapter 3.

Two objectives were investigated:

1. Minimise the separation length, L_{sep}
2. Maximise diffuser performance, η_{out}

For the case of the separation length, an additional objective was included but only as a very minor contribution:

3. Minimise amount of suction to achieve these objectives, C_q

This was included with a scale factor of 0.001 so the separation would have to be effectively eliminated before it had any substantial effect over the main objective.

Non-Uniform Suction The same objectives as for the uniform case were employed for the non-uniform suction investigations. However, the control parameters and optimisation approach were different. When the local suction coefficient, c_q, is used to define a non-uniform profile its values need to be defined, either directly at each node (and shape functions for in-between) or as the output of a function. Previous experiments had found that suction concentrated near the entrance to the diffuser was particularly effective [Furuya et al. 1966, 1970] and that suction spread over the diffuser wall was effective at smaller divergence angles [Yamazato 1969, 1970]. While a few different pre-defined profiles were investigated (including linearly and exponentially varying profiles) only the case of the single locus will be discussed in this thesis. The control parameters and general equation for the single locus and field-based approach are listed here:

- Single locus
  - $c_q(z) = Az^3 + Bz^2 + Cz + D$

    - Control parameters: $z_q, \gamma_q, c_{q_{max}}$
- Field approach
    - $c_q(z)$
    - Control parameters: c_q (discretised using linear discontinuous Lagrange shape functions)

For optimising the function-defined profiles, the Nelder-Mead algorithm was employed again. For the field-based control, a gradient-based method is needed due to the large number of control parameters so the SNOPT algorithm was used for these simulations.

Autogenous Control For the autogenous control studies, the dual-loci profile was employed. This employs two oppositely signed single locus profiles superimposed to produce a suction locus and a blowing locus. The parameters of each locus can be controlled independently. The key control parameters and function formula are summarised below (though full details were provided in the Chapter 3):

- Dual-loci
    - $c_q(z) = c_{q_s}(z) + c_{q_b}(z)$
    - Control parameters: $z_q, \gamma_q, c_{q_{max}}, z_{q_b}, \gamma_{q_b}, c_{q_{max_b}}$

Flow-Rate Balance (Q-Balanced Dual-Loci) Autogenous control requires equal flow-rates in the suction and blowing regions (net-zero mass removal) and a pressure gradient to drive the control flow. The flow-rates of a suction and a blowing locus could be balanced a priori since their velocities were imposed directly as boundary conditions. Since the surface area of the diffuser varies along its length though, the parameters of each control locus will be different - $z_q, \gamma_q, c_{q_{max}}, z_{q_b}, \gamma_{q_b}, c_{q_{max_b}}$. Let's take the case where the suction parameters are pre-defined, thus we know C_q, and need to determine the blowing parameters, $z_{q_b}, \gamma_{q_b}, c_{q_{max\,b}}$ so that the condition $C_{q_b} = C_q$ is satisfied. Looking ahead, z_{q_b} is likely to be dictated by the pressure profiles in the flow so it is best to take this as an independent variable (a control variable), and manipulate γ_{q_b} and $c_{q_{max_b}}$ to balance the flow rates. This is not a fully bounded problem as there are many combinations of these two parameters that could conceivably achieve the required equality $C_{q_b} = C_q$. Therefore, we must choose one to be under the purview of the optimisation algorithm – a control parameter – and the other to be determined as a function of the other parameters and the geometry of the diffuser to achieve the flow rate equality.[1] Alternatively, both could be made control parameters with an accompanying constraint.

[1] An alternative option exists which might fully bound the system. That is to assume that the flow through any connecting duct (the control flow) will develop the profile of Poiseuille flow in an annular

There was no particular difference in the effectiveness of the optimisation procedure based on which parameter was chosen to be the control parameter, and the other the dependent variable. Typically it was taken that $c_{q_{max_b}} = c_{q_{max}}$ in order to simplify the possible control designs and accelerate convergence of the optimisation. γ_{q_b} was then calculated using the dual-loci cubic profile definitions analytically.

Pressure Balance (P-Q-Balanced Dual-Loci) The pressure profile along the length of the uncontrolled diffuser is shown in Figure 4.3. There is a very small radial variation in the pressure field; both the pressure along the wall and the centreline are shown in the line-plot. Because the pressure profile is monotonically increasing along the diffuser length, autogenous suction control should be readily achievable with with suction downstream of blowing.

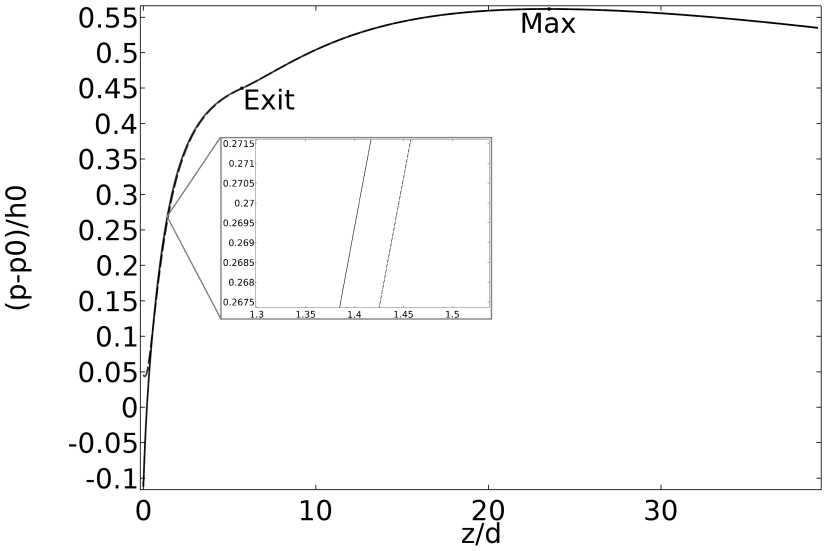

Figure 4.3 Unbalanced pressure profile through the $\alpha = 5^\circ$ diffuser at $Re = 1000$, normalised by the average entry pressure. Dotted line is pressure along the centreline while the solid line is pressure along the wall. The differences are small, mostly seen at the entry; an inset shows a magnified view.

The approach for balancing the pressures of a dual-loci control system was described briefly in Chapter 3. The general approach is summarised as follows:

1. A suction locus is applied to the flow, $z_q, \gamma_q, c_{q_{max}}$. These are the major optimisation control parameters.
2. Blowing parameters are devised – partly by the minor optimisation algorithm and partly from the flow-rate balancing, $z_q, \gamma_q, c_{q_{max_b}}$. These are the minor optimisation control parameters.
3. The forward model is simulated
4. The average pressure difference between the loci is evaluated, $dP = P_s - P_b$.

section. In this way, the maximum velocity (at its centre) might be related to the width of the relevant control locus.

5. A minor optimisation is performed by iterating through steps 2-4 until the objective (usually to maximise η_{out} is achieved subject to the constraint $dP > 0$
6. The major optimisation continues back at Step 1 until the optimality criteria are met (typically to maximise diffuser performance).

It is not clear what dP should be in order to provide sufficient pressure drop to drive the desired flow. Through the control channel there will be losses due to porous media flow (through the diffuser wall) and friction losses. An approximation could be made assuming the flow is that of annular Poiseuille flow, and a similar approach was taken for the cylinder case (assuming duct flow). However, for this model it was assumed that $dP > 0$ is a sufficient requirement.

In addition to this approach, a second method was used: an optimisation of all parameters at once. Rather than separating the suction and blowing control parameters into two coupled optimisation procedures, they can be kept together in one overall optimisation. The constraint of $dP > 0$ is applied as a strict penalty.

4.2.4.2 Constraints

In all non-autogenous cases, the potential control was constrained so that $0 \leq C_q \leq 1$ which limits the control so its maximum strength is that where all the fluid is exhausted out the control area. At times appropriate bounds were made directly on the control parameters so as to accelerate the optimisation. In the dual-loci case, this was modified to C_{q_s} as the net control volume coefficient should be zero.

4.2.5 Outline of Studies

4.2.5.1 Uncontrolled Flow

Parametric studies were performed to determine how the uncontrolled flow through the conical diffuser is affected by the Reynolds number, divergence angle, and inlet profile. These parameters were adjusted via a parametric sweep with the values provided in Table 4.3.

Table 4.3 Parameter sweep values.

Parameter	Symbol	Parameter Sweep
Semi-Divergence Angle	α	5°:10°:85°
Reynolds Number	Re	20:20:180 & 200:200:2000
Inlet Profile Flatness	n	2, 1000

Additionally, to determine the optimal Reynolds number for diffuser performance in this Re range, an optimisation was performed at each α for $n = 1000$.

4.2.5.2 Uniform Suction

Parametric and optimisation studies were performed for the case of uniform suction, varying the suction strength, C_q. The inlet profile was always flat, $n = 1000$ for these studies, but the Reynolds number and semi-divergence angle were altered.

First, the $\alpha = 5^\circ$ diffuser was investigated in detail with a parametric study with $C_q = 0, 0.3, 0.6, 0.9$ at each Reynolds number as was used in the earlier study on the uncontrolled diffuser (Table 4.3). Then optimisation studies were performed at each Re optimising C_q for each objective described earlier. Second, these optimisation studies were extended to steeper diffusers ($\alpha \geq 5^\circ$). However, since hysteresis was found to occur, for some Re, α time-dependent models were used for the optimisation.

4.2.5.3 Non-Uniform Suction

Brief studies of non-uniform suction on the $\alpha = 5^\circ, Re = 1000, n = 1000$ diffuser were performed. Firstly using the single locus profile, then employing a field-based control. These results were compared to the uniform case for this diffuser/flow.

While it is useful to know the best-case non-uniform suction profile, it is also important to arrive at designs that are practical. For this aim, the single locus profile offers a more compelling option than the arbitrary field developed by the adjoint-based optimisation process. After all, the velocity profile from the single locus is similar to that produced when a slot is implemented in the body surface. Optimisation of the single locus parameters was carried out with three objectives – to maximise the performance of the diffuser, minimise the separation length, and to maximise the performance of the overall system (taking the maximum average pressure at any point in the diffuser or tailpipe as the point to measure the performance). The third objective arose because upwind autogenous suction control naturally favours suction in the high pressure regions downstream. If some useful effect can be generated in the tailpipe region, it may be beneficial overall.

4.2.5.4 Autogenous Suction Control

Finally, investigations on autogenous suction control were performed for the same diffuser as the non-uniform suction studies. The dual-loci control was optimised to maximise performance of the diffuser using the two approahces described above.

4.3 UNCONTROLLED DIFFUSER RESULTS

4.3.1 Validation of Model

To quote again from the JRSNZ paper: *"The computational model was validated against experimental and numerical studies of similar geometries by comparing the growth of the recirculation region with increasing Reynolds number. Much of the experimental data in the literature is constrained to the extreme case of* $\alpha = 90°$*, for which the experimental work by Hammad et al. [1999] and numerical work by Cantwell et al. [2010] represent the most accurate results. For the case of* $\alpha < 90°$ *which we are interested in here, numerical work by Peixinho and Besnard [2013] and Selvam et al. [2015] showed the same growth rate but with a delay in the separation onset (a translation along the x-axis). All these studies employed a fully developed inlet condition,* $n = 2$*.*

The validation of our model was made using a plug factor of $n = 2$ *to match these studies, while a plug factor of* $n = 1000$ *was used for the actual investigations. Figure 4.4 compares the growth of the separation bubble as a function of Reynolds number for* $n = 2$ *for* $\alpha = 5°, 85°$*, as well as* $n = 1000$ *for* $\alpha = 5°$ *to the data from the literature. As can be seen, it matches extremely well when the same conditions are replicated. Furthermore, the x-intercept for the* $\alpha = 5°, n = 2$ *case – i.e. the Reynolds number where separation commences – matches exactly with that found by Peixinho & Besnard:* $Re_c = 138.6$ *compared to* $Re_c = 138$ *from the study. The growth rate of the separation for* $n = 2$ *is* $L_{sep}/Re = 0.0447$ *which matches well with the result of Hammad et al. [1999], though is slightly higher than values found by Cantwell et al. [2010] The separation growth for the case where the inlet profile is effectively flat (*$n = 1000$*) is also shown in Figure 4.4 too. The growth rate is much slower as the diffuser operates more effectively with the momentum of the flow evenly spread across the pipe. At lowRe as the separated flow regime develops, the growth of the recirculating region is not linear as in the fully-developed case. Once the separation is developed, a linear fit gives an approximate growth-rate of* 0.0118*."*

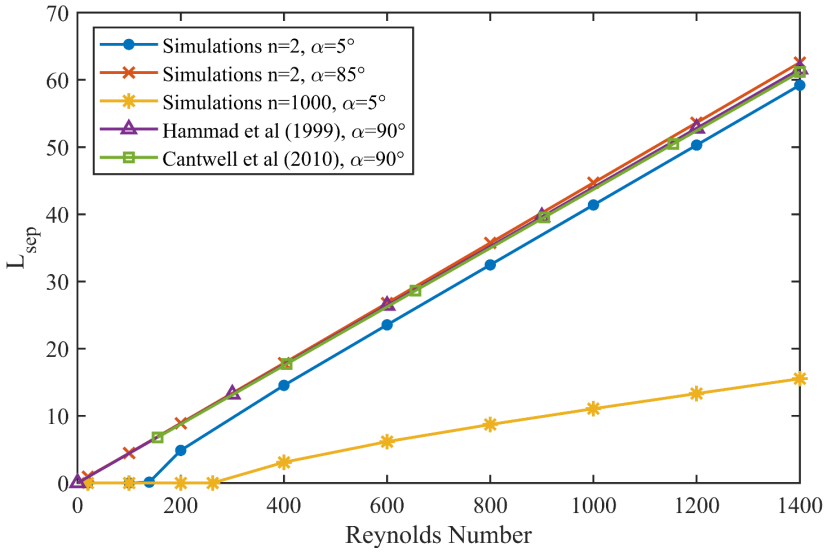

Figure 4.4 Separation growth with Reynolds Number compared to values from the literature.

4.3.2 Characteristics of Uncontrolled Diffuser

4.3.2.1 Flow Structure

Consider the structure of the flow through the diffuser for different semi-divergence angles as the Reynolds number is ramped up. At very low Reynolds numbers, the flow within a gradually expanding diffuser remains fully attached throughout the diffuser and tailpipe. However, for diffusers with steep divergence, $\alpha \geq 45°$, and a flat profile the flow is virtually always separated even at $Re = 1$. The combination of parameters (low momentum, strong APG) prevents the flow ever remaining fully attached. Once separation begins an axisymmetric recirculation bubble forms near the exit of the diffuser. With increasing Re it stretches further down the tailpipe and upstream into the diffuser, though the latter effect is much stronger. The separation length grows linearly with Re. At a sufficiently high enough Re, the flow will then become unstable and jet flow will develop with asymmetric recirculation regions, though the present axisymmetric simulations are not capable of capturing this behaviour.

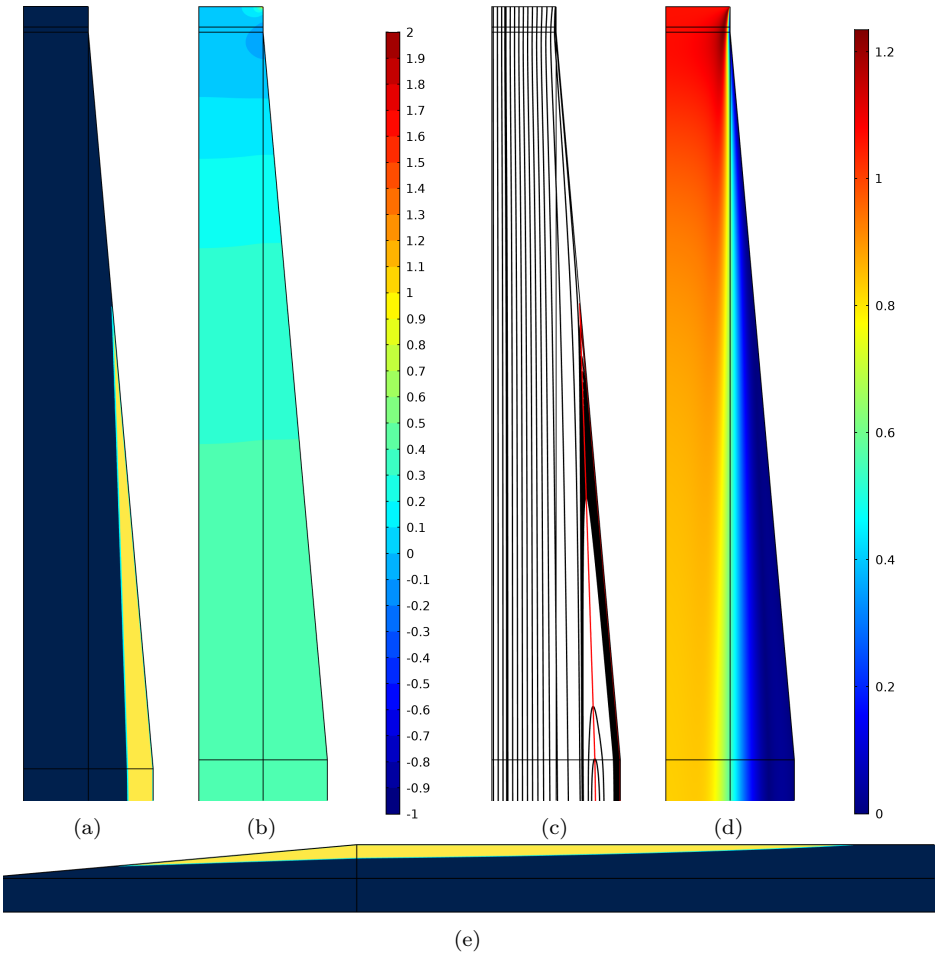

Figure 4.5 Example of the flow structure in a conical diffuser – here for $\alpha = 5°, Re = 1000, n = 1000$, showing the axisymmetric plane. Figure (a) shows the reversed region of flow (yellow) and, (b) shows the pressure contours (normalised by average entry pressure), (c) gives streamlines with density of 20 and separatrix shown in red, and (d) shows the velocity magnitude surfaces. The extent of the separation region is shown in (e). The features of this flow-field were typical for all the uncontrolled flows simulated in this chapter.

4.3.2.2 Separation Length

When the velocity profile of the flow is not fully-developed on entry to the diffuser, the separation length is dependent on Re and α. After an initial parabolic growth phase, the separation length continues to grow linearly with Re, just with different growth rates depending on the divergence angle. These trends can be seen in Figures 4.6 and 4.7. We can understand the linear growth of the separation bubble by considering the balance of convection and diffusion of the flow through the diffuser and tailpipe.

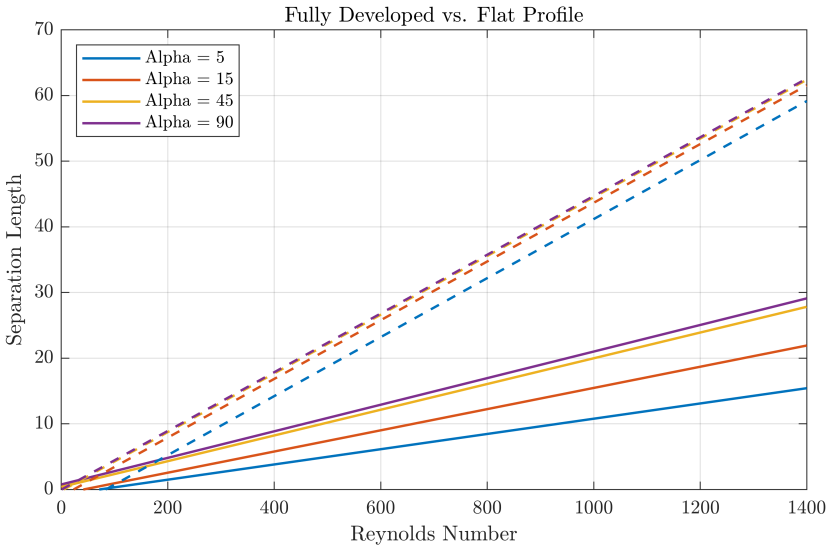

Figure 4.6 Comparison of recirculation region growth for fully-developed $n = 2$ profile (dashed lines) and flat $n = 1000$ profile (solid lines).

One might wonder why increasing the Reynolds number does not aid the situation, after all the flow then has more momentum. Firstly, with a larger velocity on entry to the diffuser, the flow has less time to react to the change in geometry before it is convected downstream. Secondly, this same issue causes the recirculation region to grow with increasing Re. After separation, with a higher Re the forward flow in the centre of the pipe travels much further before the diffusive action completes its effect of gradually eliminating the recirculation bubble. It is expected that at the transition to turbulence, and the development of a turbulent boundary layer, there will be a drop in separation length as the turbulent boundary layer has higher momentum to push further against an APG. However apart from this, increasing the Reynolds number only increases the convective distance of the free-stream, lengthening the recirculation region.

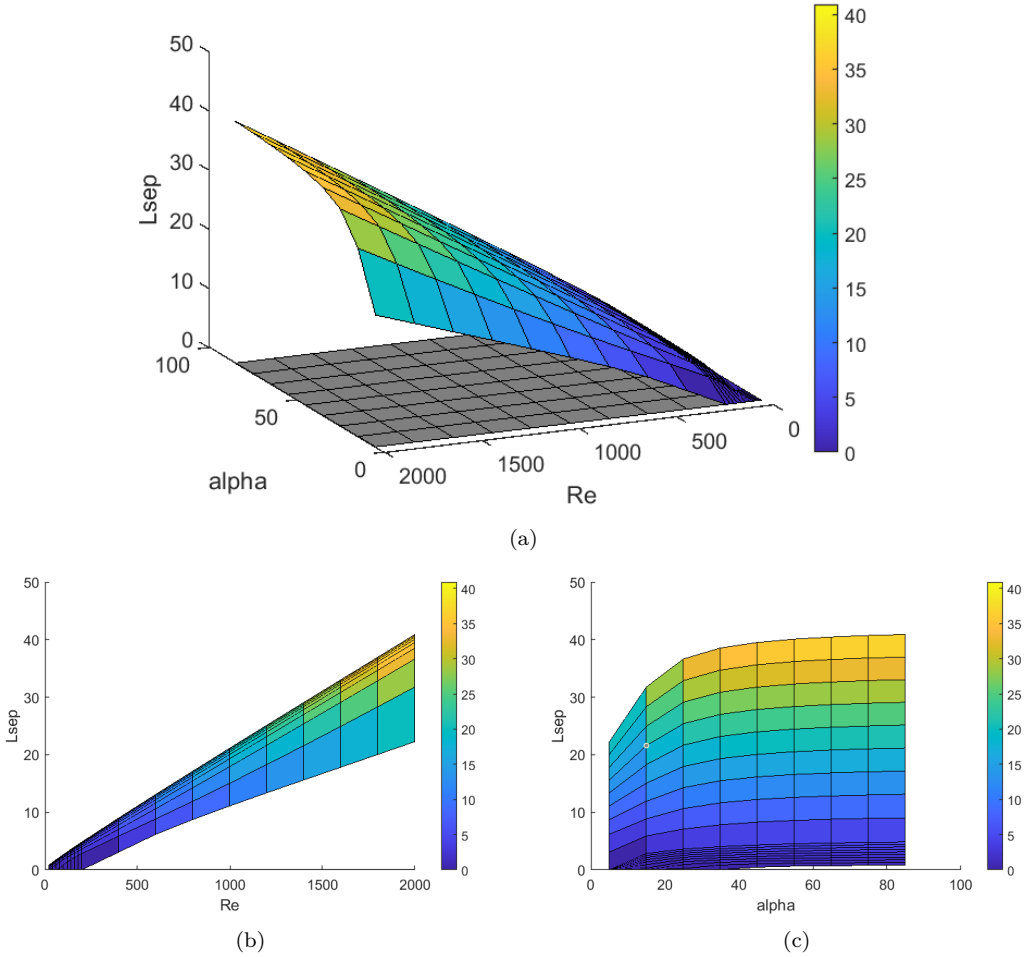

Figure 4.7 Separation growth as shown by (a) surface plot, (b) against Re and (c) against α

Finally, the initial non-linear growth phase of the recirculation region bears discussion. This trend occurred regardless of α, but was more apparent for the slowly diverging diffusers (particularly $\alpha = 5°$) where the separation growth is more gradual. This non-linear (parabolic) growth at the onset of separation is consistent with the results of Selvam et al. [2015], as shown in their validation figure. The initial growth-phase appears to occur as the recirculation region establishes itself, and linear growth begins once the separation point has retreated from the exit to about halfway through the diffuser. The non-linear growth likely occurs because a very small recirculation region would be much less stable than a larger established one with a larger surface area along the shear layer and therefore grows much faster.

4.3.2.3 Separation Onset

For a diffuser with $\alpha = 90°$ (SEF) the separation point is located at the corner of the entry into the expanded region. As α is decreased, the separation point (always located at the wall) moves further away from the entry for the same Re. From the present

simulations, it can be seen that – for a given α – the separation appears to instantiate at the corner of the diffuser exit and works its way upstream as Re is increased, as shown by the peaks at low Re in Figure 4.8 (f). This movement is rapid at first and then slows down, apparently approaching the corner with the entry asymptotically. As was stated before, for some divergence angles, there appears to be no Re where separation does not occur, i.e. $\alpha \geq 45°$. As shown in Figure 4.5, at higher Re the separation region begins part-way through the diffuser and continues far into the exhaust pipe.

Figure 4.8 shows a surface and 2D plots of the separation point, z_s, against the Reynolds number and semi-divergence angle. Here, the separation point is non-dimensionalised by d as all distances were. Since the length of the diffuser contracts with increasing α (as β is held constant), the separation point can be better interpreted if non-dimensionalised by L (the length of the diffuser) instead of by d (the diameter of the inlet pipe). The results for this case are also shown in Figure 4.8. In all plots, when there is no separation the data-point for z_{s_L} and its parameters is omitted. The following conclusions can be made from these plots:

1. Separation commences at higher Re for diffusers with lower semi-divergence angles. This is particularly dramatic at very low semi-divergence angles $\alpha < 10°$.
2. The separation point moves closer to the entry as either Re or α are increased.
3. It appears that separation commences at or very near to the diffuser exit ($z_{s_L} = 1$). While not all peaks in the surface plot (Figure 4.8 (b)) appear to occur at $z_{s_L} = 1$, this is likely due to the coarse nature of the parametric sweep (commencing at $Re = 20$ and increasing in increments of 20). For the cases where separation begins before this value, the onset of separation has not been captured and presented. Similarly for where it commences between parameter steps.

The second point bears further highlighting. There is a dramatic difference in the values and trends for the case of $\alpha = 5°$. Not only does the separation commence at much higher Re, but the movement of the separation point upstream is much slower than at any other semi-divergence angle. As was discussed in Chapter 2, uncontrolled diffusers have a clear optimal geometry with the divergence angle less than $7-8°(\alpha \leq 4°)$ [Schlichting and Gersten 1961, Sparrow et al. 2009]. It is interesting though, that the optimal geometry for the case of a flat inlet profile appears to be very similar to that of a fully developed inlet profile. The behaviour of the recirculatory region likely is a significant reason why these very slowly diverging diffusers are so notable. We may expect to see a relationship between the separation characteristics and the performance of the diffuser at converting the energy of the flow from dynamic to static pressure.

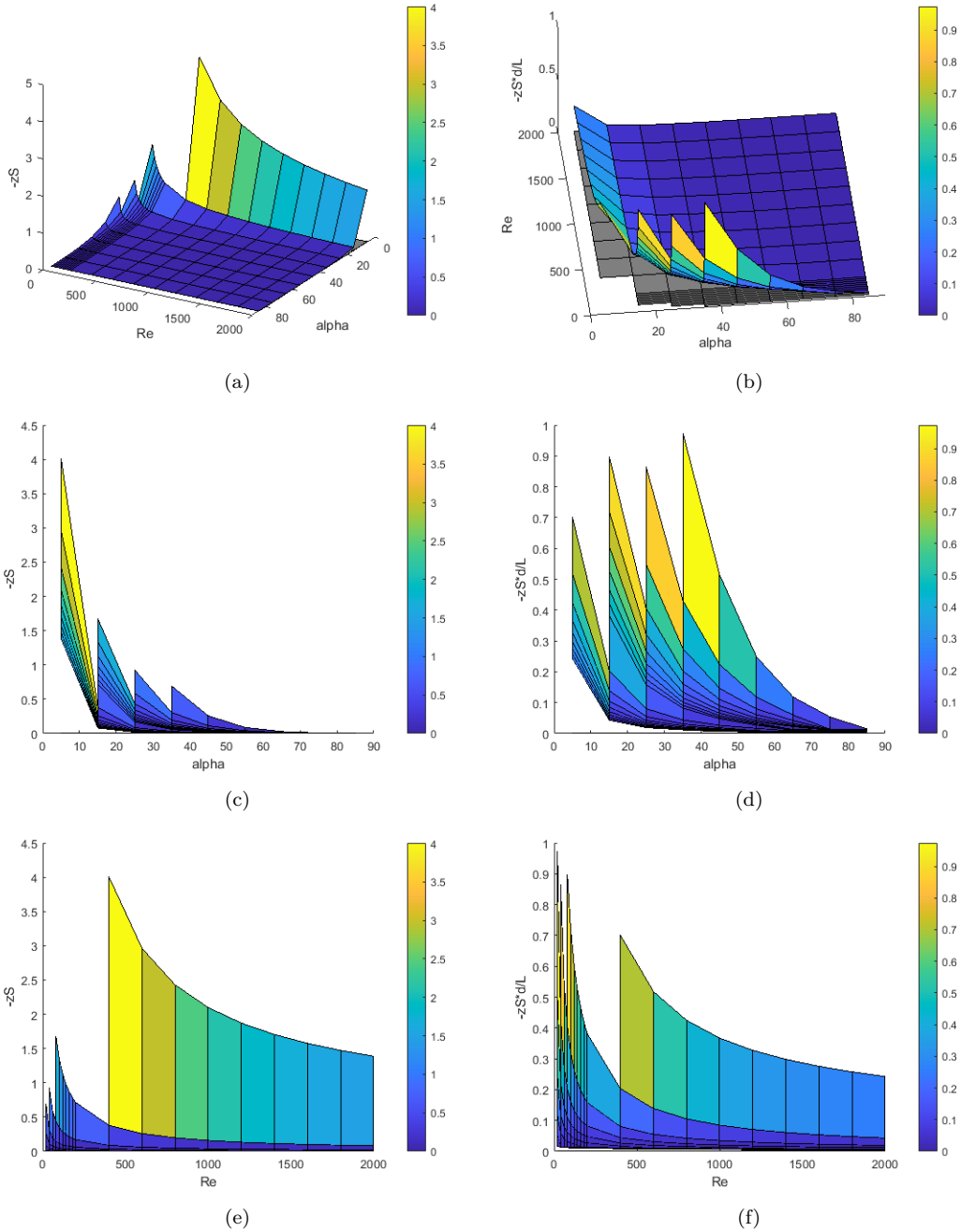

Figure 4.8 Onset of separation, z_s non-dimensionalised by d (left) and by diffuser length (right)

4.3.2.4 Effect of Inlet Profile

The inlet profile has a dramatic effect on all characteristics of the flow in the conical diffuser. Figure 4.6 shows how the separation length growth changes for a selection of semi-divergence angles and with two different inlet profiles – fully developed ($n = 2$) and flat ($n = 1000$). It is clear to see that when the inlet profile is flat, the growth rates have a dependency on the semi-divergence angle unlike when the profile is fully-developed.

Where the fully developed inlet profile results in separation growth with the formula $L_{sep} = 0.088Re$, when the inlet is flat the growth varies depending on α, and the coefficients for each divergence angle studied is shown in Table 4.4. Now, more detail for the flow characteristics will be provided for the case of $n = 1000$.

Table 4.4 Parameters for growth of separation length for flat profile $n = 1000$ inlet at different divergence angles.

α (°)	Growth Rate	y-Intercept	Re_{crit}
5	0.0116	-0.8364	72.03
15	0.0161	-0.6773	41.96
45	0.0196	0.3862	0
85	0.0202	0.7613	0

4.3.2.5 Performance - η_{out}

Let us now consider the performance of the uncontrolled diffusers through the parametric sweep. Here, the η_{out_s} values is used as the performance measure. Surface and 2D plots of the diffuser performance against Re and α are presented in Figure 4.9.

From the surface plot, it can be seen that generally the performance of an uncontrolled conical diffuser at a given Re increases with decreasing α for a given Re. However, at low Re the best performance is not achieved with the lowest semi-divergence angle, but rather an intermediary one. Once the Reynolds number is at a suitable level, though, the $\alpha = 5°$ diffuser becomes the best performing by far. This trend of increasing diffuser performance with decreasing divergence cannot continue to $\alpha = 0°$ as a straight pipe cannot increase the pressure of a flow. This again is in keeping with the literature and the optimal diffuser geometries previously determined [Schlichting 1987, p. 629].

At low Reynolds numbers each diffuser has negative performance measures. This is because when the Reynolds number is very small, the pressure rise associated with the slowing of the flow in the diffuser is smaller than the energy lost to viscous forces. Consequently, the performance is less than zero as the static pressure on exit is *less* than on entry. This is only for very low Re and exacerbated when the diffuser is long (low α if β is fixed). Indeed, for some of the diffusers ($\alpha \geq 75°$) the performance is always negative in the Re range investigated. Since the divergence is so steep, the fluid flows through this geometry with a jet-like flow and experiences none or very little of the flow expansion which results in a slowing of the velocity and increasing of the pressure. At lower Re, though the jet flow may be diminished, the viscous losses are too large. The pressure in such a diffuser is likely to increase downstream in the tailpipe as the recirculation region is gradually damped out, but a different performance measure would be needed if such behaviour were acceptable for a diffuser.

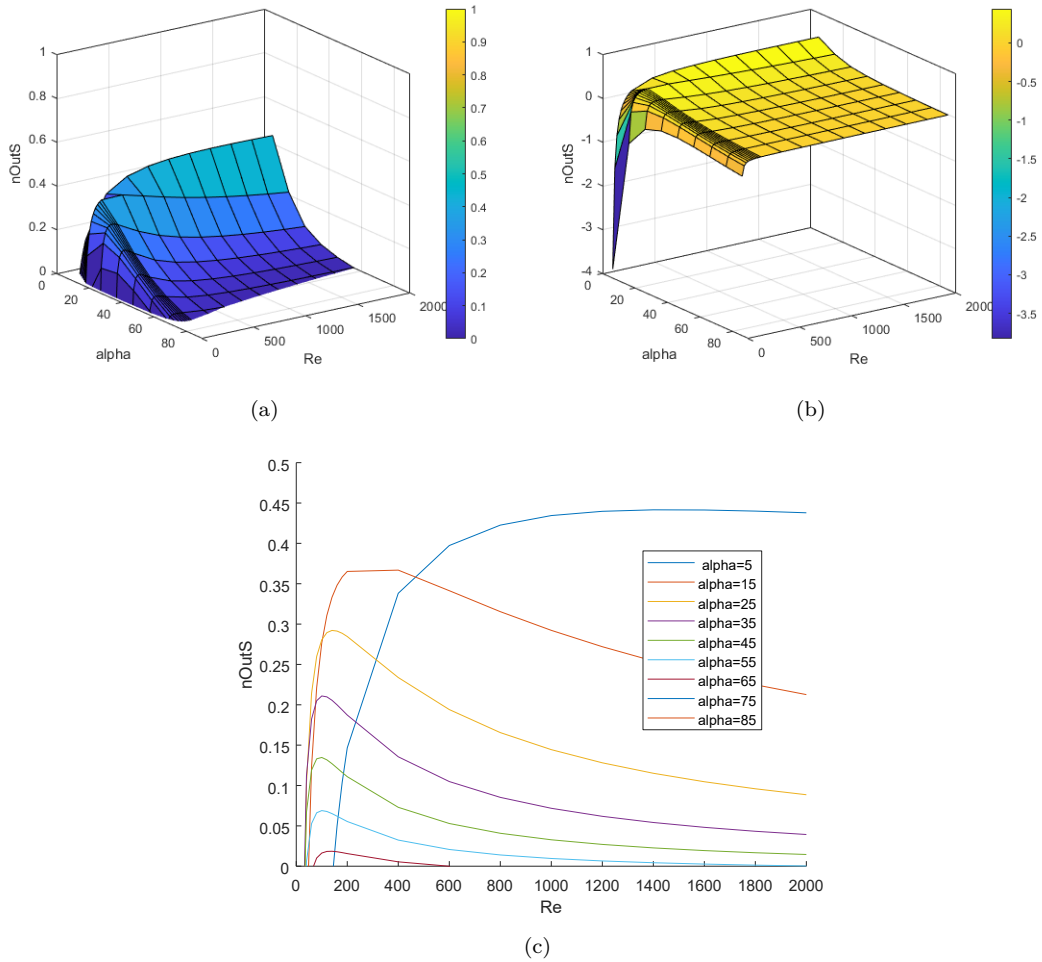

Figure 4.9 Uncontrolled diffuser performance against Re and α: (a) surface for values above 0, (b) entire surface, and (c) 2D plot against Re sorted by α.

4.3.2.6 Maximum Efficiency

The above parametric study shows that there is a clear optimum flow for achieving maximum performance in each uncontrolled diffuser. However, the resolution of the parametric sweep is not sufficient to capture these peaks with accuracy. Therefore, a simple one-parameter optimisation with the objective of maximizing the efficiency by adjusting the Re was devised. Performing this optimisation on each angle allows the peak performance to be captured (if it lies within the permitted Re range, $1 \leq Re \leq 2000$). In addition to the diffusers simulated above, further low-angle diffusers were also modelled to get a better impression of the best performance achievable for uncontrolled flow (which is expected to occur at $\alpha \leq 7°$ even with a flat inlet profile compared to a fully-developed one). The difference in maximum performance based on inlet profile was also compared. Since there does not appear to be specific values in the literature for the peak performance of diffusers at low/moderate Reynolds numbers, we performed this optimisation for inlet profiles with $n = 2, 100, 1000$ and compiled the results in

Tables 4.6 and 4.7. Apparently, the $Re = 2000$ upper bound for the optimisation is too restrictive, however to allow higher flow rates would ignore the physicality of these flows and the likelihood that the flow no longer remains axisymmetric. Therefore, wherever a $Re_{opti} = 2000$ result is produced, better performance is likely achieved at an even higher Re.

Table 4.5 Optimal parameters for uncontrolled conical diffusers. Values in bold are best overall, cases where the upper bound of $Re = 2000$ were reached are italicised.

α (°)	$n = 2$		$n = 100$		$n = 1000$	
	$\eta_{out_{opti}}$	Re_{opti}	$\eta_{out_{opti}}$	Re_{opti}	$\eta_{out_{opti}}$	Re_{opti}
2	**0.3977**	**448.44**	*0.4000*	*2000.00*	*0.4014*	*2000.00*
3	0.3960	299.90	*0.4272*	*2000.00*	*0.4359*	*2000.00*
4	0.3939	225.44	**0.4295**	**1690.00**	***0.4432***	***2000.00***
5	0.3916	180.32	0.4278	1256.10	0.4417	1471.70
6	0.3890	151.46	0.4245	978.63	0.4382	1128.60
7	0.3862	130.13	0.4201	788.82	0.4334	901.32
8	0.3832	113.59	0.4149	652.65	0.4275	727.65
9	0.3799	104.22	0.4091	551.50	0.4209	620.31
10	0.3765	89.67	0.4027	473.88	0.4138	523.29
15	0.3565	67.43	0.3670	266.73	0.3745	283.34
25	0.3024	35.77	0.2892	140.07	0.2921	140.07
35	0.2491	35.21	0.2101	110.48	0.2109	110.48
45	0.1865	36.37	0.1357	95.32	0.1350	95.32
55	0.1292	38.60	0.0708	101.27	0.0690	101.27
65	0.0819	42.40	0.0213	133.49	0.0186	133.49
75	0.0461	50.75	*-0.0107*	*2000.00*	*-0.0138*	*2000.00*
85	0.0219	75.63	*-0.0133*	*2000.00*	*-0.0164*	*2000.00*

Table 4.6 Separation characteristics of uncontrolled diffusers operating at peak performance. Italicised values are those where the Re was at the upper bound.

α (°)	$n = 2$		$n = 100$		$n = 1000$	
	L_{sep_L}	z_{s_L}	L_{sep_L}	z_{s_L}	L_{sep_L}	z_{s_L}
2	0.622	0.6309	*1.523*	*0.4375*	*1.449*	*0.4508*
3	0.631	0.6270	*2.388*	*0.3317*	*2.249*	*0.3461*
4	0.639	0.6235	2.751	0.2998	*3.050*	*0.2856*
5	0.643	0.6217	2.610	0.3042	2.873	0.2894
6	0.663	0.6133	2.496	0.3072	2.716	0.2929
7	0.673	0.6090	2.405	0.3090	2.604	0.2940
8	0.675	0.6081	2.332	0.3096	2.474	0.2973
9	0.744	0.5819	2.275	0.3092	2.447	0.2928
10	0.662	0.6122	2.230	0.3080	2.363	0.2936
15	0.947	0.5131	2.148	0.2912	2.224	0.2789
25	0.841	0.5357	2.409	0.2293	2.380	0.2274
35	1.744	0.3208	3.293	0.1483	3.270	0.1457
45	2.905	0.1961	4.469	0.0952	4.448	0.0932
55	4.661	0.1140	7.101	0.0506	7.071	0.0494
65	7.911	0.0592	14.057	0.0229	13.987	0.0227
75	16.710	0.0134	*309.680*	*0.0042*	*303.933*	*0.0039*
85	76.620	0.0139	*952.275*	*0.0049*	*934.948*	*0.0040*

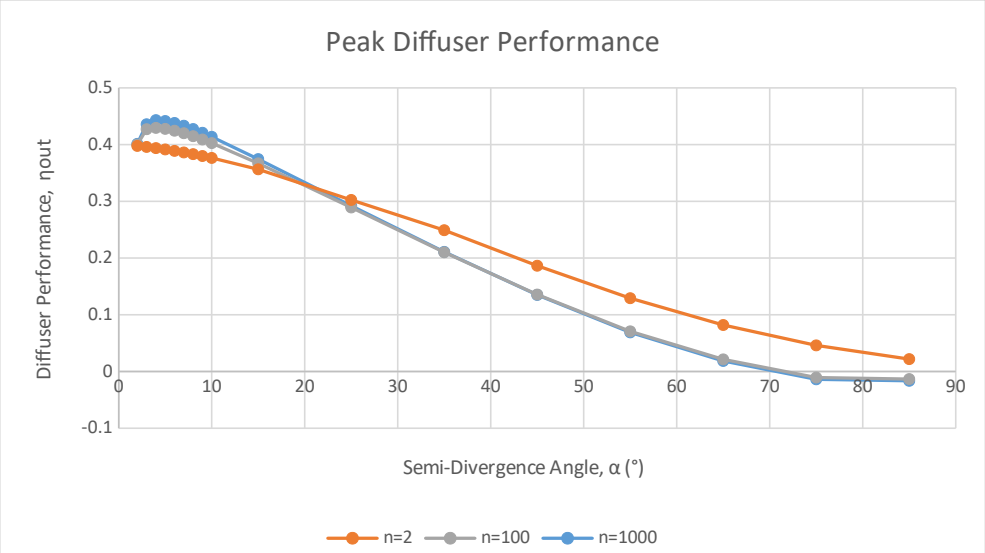
Peak Diffuser Performance
Diffuser Performance, ηout
0.5
0.4
0.3
0.2
0.1
0
-0.1
0 10 20 30 40 50 60 70 80 90
Semi-Divergence Angle, α (°)
n=2 n=100 n=1000

(a)

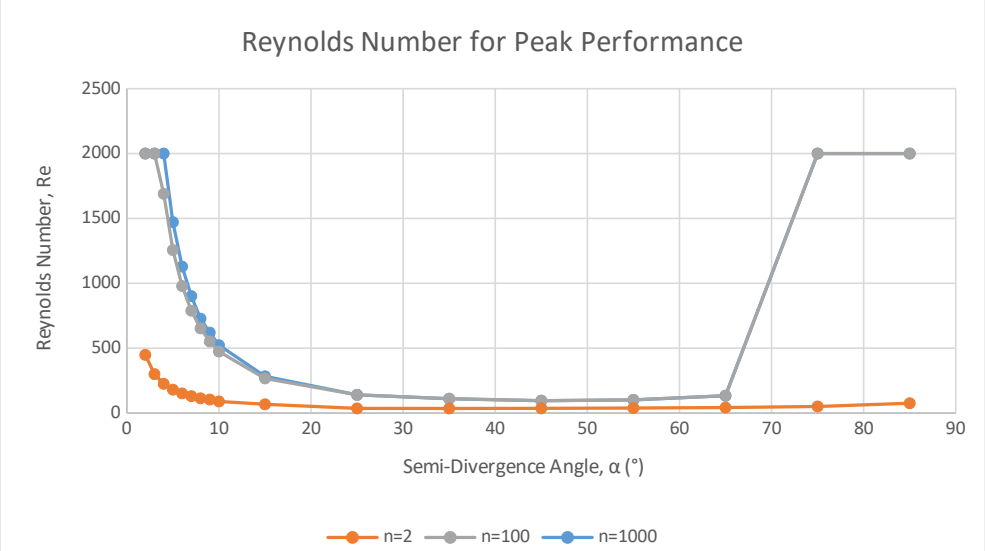
Reynolds Number for Peak Performance
Reynolds Number, Re
2500
2000
1500
1000
500
0
0 10 20 30 40 50 60 70 80 90
Semi-Divergence Angle, α (°)
n=2 n=100 n=1000

(b)

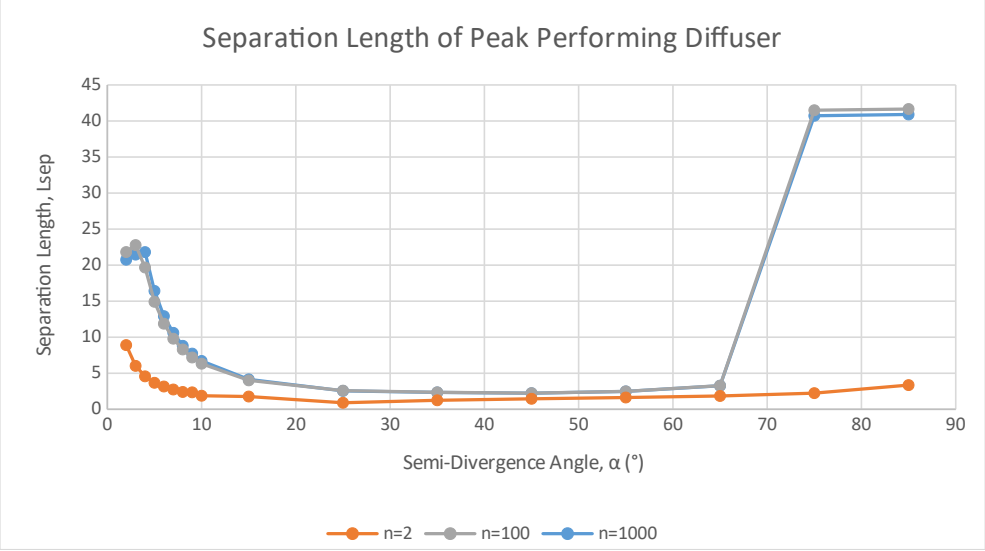
Separation Length of Peak Performing Diffuser
Separation Length, Lsep
45
40
35
30
25
20
15
10
5
0
0 10 20 30 40 50 60 70 80 90
Semi-Divergence Angle, α (°)
n=2 n=100 n=1000

(c)

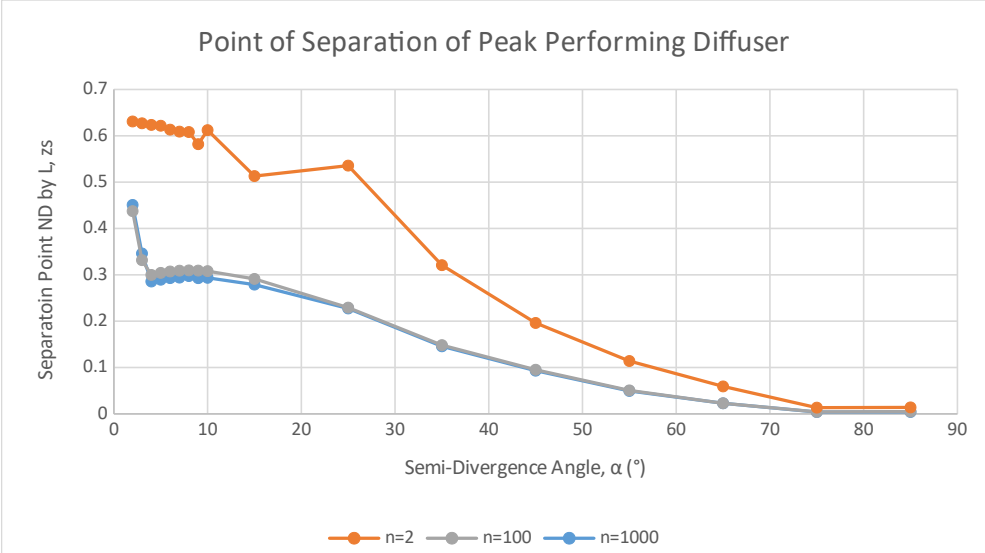

(d)

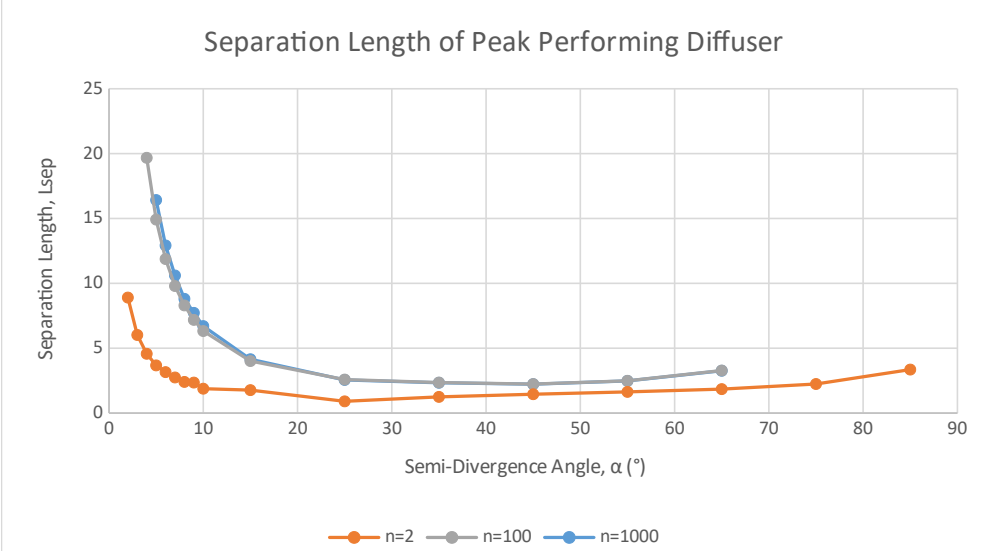

(e)

Figure 4.10 Key characteristics of optimal uncontrolled diffusers.

The diffuser performance peaks at $\eta_{out} = 0.4432$ when $\alpha = 4°$ with Re in the upper range of values. This is as expected, as the optimal divergence angle was stated many times in the literature, as $2\alpha \leq 8°$. However, there is a noticeable effect from the inlet profile on how effective that peak performance is. The plots from Figure 4.10 show that the best performance occurs for diffusers with the flattest profile ($n = 1000$) but only when α is low. It is interesting that at high α, the flatter profiles ($n = 100, 1000$ are unable to achieve positive performance ($P_2 < P_1$) whereas the simulations with a fully-developed inlet profile can. The fully-developed flow has low momentum near the walls and so can follow steep changes in the wall profile more easily than flow with high momentum. Naturally, this following of the wall profile does not continue far into

the diffuser due to the early onset of separation, but it performs better than the flat profiles in this instance. This may be a useful finding. It takes conscientious effort to flatten the velocity profile of flow through a pipe before it enters a diffuser. These results suggest that for higher semi-divergence angles, the fully-developed profile may be preferred. In order to get adequate performance at these α, control would have to be applied, but this does add one more reason why making steep diffusers capable of reasonable performance more attractive.

4.4 UNIFORM SUCTION CONTROL RESULTS

4.4.1 $\alpha = 5°$ Diffuser

In this section, the JRSNZ paper will be quoted directly, then a summary of the results provided at the end to link it back to the main objectives.

"In this section, the results of the computational studies are presented and discussed. These will be presented in two sections discussing: firstly, the separation characteristics; then, the diffuser performance. The results from simulations of the uncontrolled diffuser, parametric studies with suction strengths $C_q = 0.3, 0.6, 0.9$, and the optimisation of the control are presented together.

4.4.1.1 Separation Characteristics

Figure 4.11 shows the separation length against the Reynolds number. The figure shows that there is a substantial dependence on Re for the effectiveness of suction control. For Re > 600, separation can be prevented entirely – although the amount of suction necessary drastically alters the overall flow. Figure 4.12 shows how dramatically the flow is changed when the optimal suction control to eliminate separation is provided. The velocity surfaces show how suction control allows the diffuser to behave much closer to the 'ideal diffuser' with a more gradual and even velocity spread. However, because of the extreme suction, this is by no means optimal for diffuser performance.

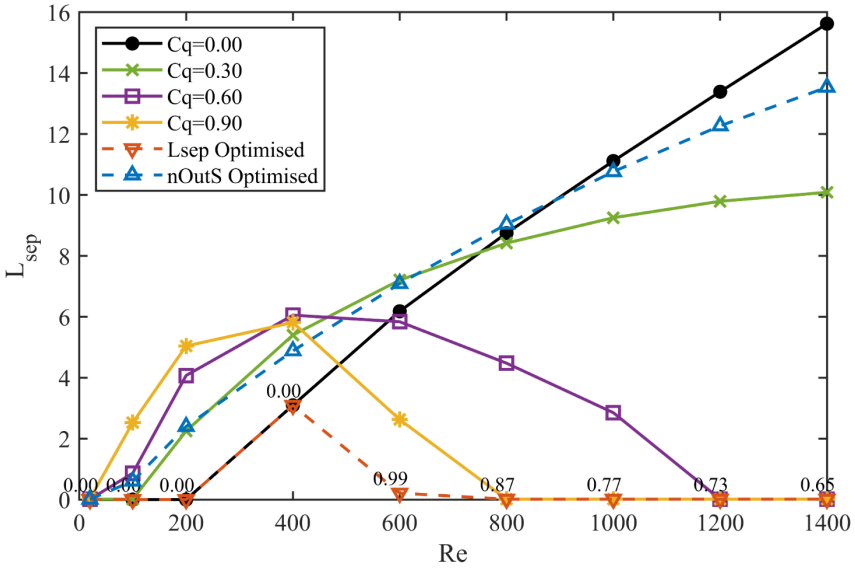

Figure 4.11 Growth of the separated region with Reynolds number for a variety of suction strengths. For the optimally controlled cases, the suction strength is annotated above each data-point.

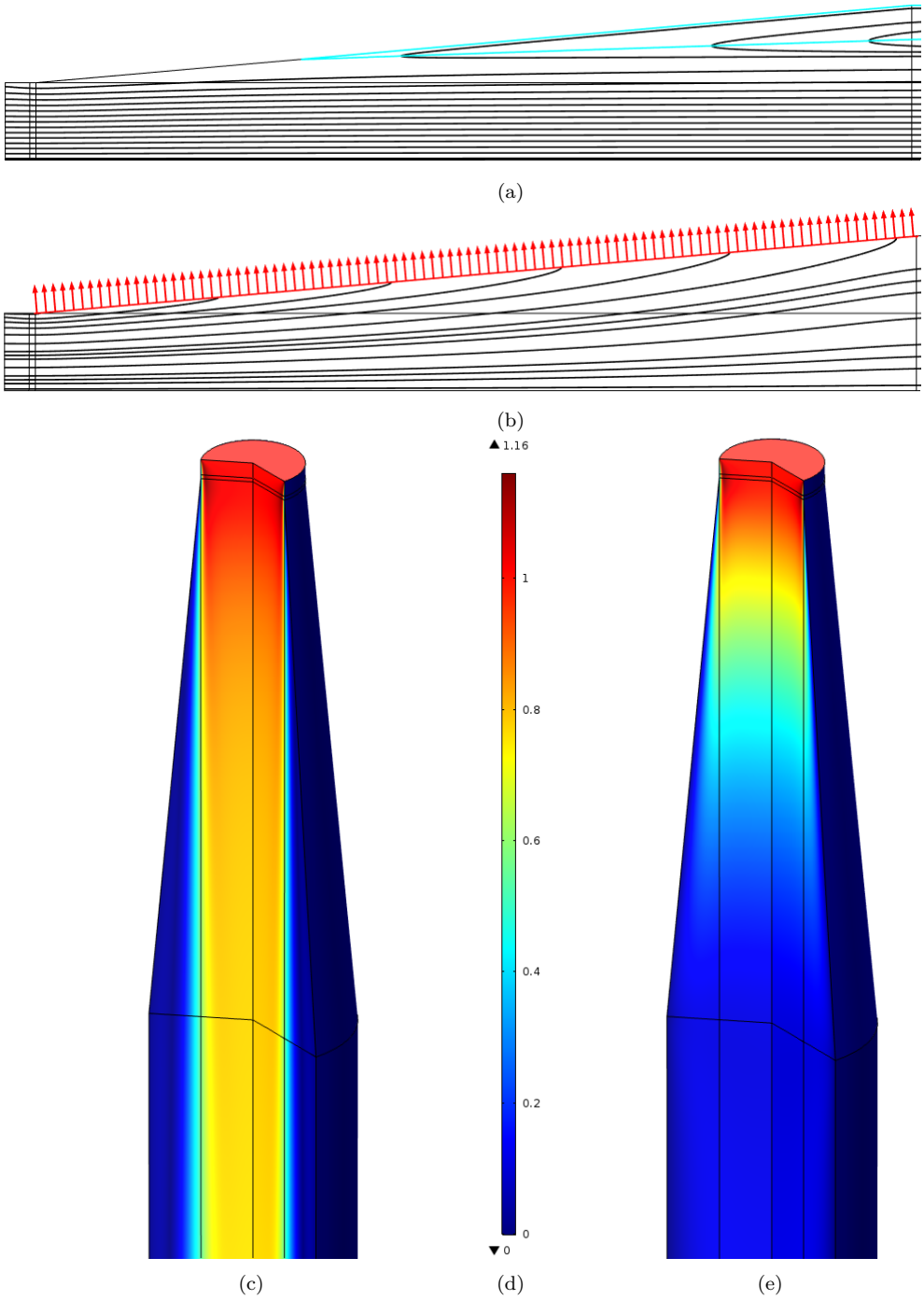

Figure 4.12 Flow at $Re = 1400$ through the (a, c) uncontrolled diffuser and (b, d) optimally controlled diffuser for minimal separation length. Streamlines (a,b) where the separation line is marked by a cyan contour line, or non-dimensionalised velocity magnitude surface plot (c, d).

As Re increases, less suction is needed to eliminate separation. This is shown by the x-axis intercepts for the parametric curves in Figure 4.11, and the decreasing values of C_q shown for the L_{sep} objective curve. These trends suggest that the $C_q = 0.3$ curve and the η_{out} curve, in Figure 4.11, will eventually peak and curve down to meet the x-axis at some higher Re. In other words, as Re continues to increase, the same amount

of suction will result in a smaller and smaller recirculatory region. This is perhaps seen more clearly in Figure 4.13 where the $C_q - Re$ curve for the separation objective decreases approximately linearly. This is because at higher Re the momentum of the free-stream is greater, and so the stimulation of the boundary layer is stronger when the low-momentum particles are removed at the diffuser wall. An important caveat however, is that the onset of turbulence is likely to affect this trend, and the results should not be directly extrapolated into the turbulent regime. However, this is promising for the application of suction control on diffusers. Most diffusers in real applications usually experience high Re flows, so if less suction is needed to achieve these objectives at high Re, the use of this control is more attractive.

The optimisation of the L_{sep} objective should result in the flow with the shortest separation length possible. Consequently, it is interesting to note that this curve shows that it is not always possible to improve upon the uncontrolled flow. For $Re \leq 400$, applying no suction, results in the shortest separation length. This is arbitrary for $Re < 200$ where separation has not commenced, but is interesting for the case of $Re = 400$ where separation is present but cannot be eliminated, or even reduced, by suction control. This is due to the balance of viscous and inertial forces in the flow. At low Re, the flow has little momentum and is much more sensitive to viscous effects. Consequently, as the low Re fluid moves through the diffuser it loses a lot of its energy through viscous effects, and there is little momentum available to move from the free-stream to the boundary layer. Additionally, the velocity profile will develop more in the short inlet pipe before reaching the diffuser, reducing the capabilities of BL suction control. This can be seen in Figure 4.14 (b), and is an unavoidable feature of the flow which has a natural influence on the effectiveness of control.

Finally, the curve for the η_{out}-optimised flow in Figure 4.11 shows two interesting features. First, is that the curve appears to follow a smooth parabolic curve. We can infer from this that there is a relationship between the optimum performance and the separation length, with an apparent polynomial correlation. As Kline et al. [1959] discussed in their review of 'optimum diffuser design', diffusers perform best when there is a small recirculatory region to aid in the energy transformation. It appears that – at least in this low Re range investigated – the size of this ideal recirculatory region varies. Interestingly, the directionality of the L_{sep} change is not consistent, as shown in Figure 4.14. For $Re \leq 800$, the η_{out}-optimised control results in a longer recirculation length than the uncontrolled case, but still provides better performance. For $Re > 800$ it is a shorter L_{sep} that gives the best performance.

The different changes in L_{sep} can be explained by considering the two effects that suction control has on the flow. Firstly, it should delay BL separation by removing low-momentum flow which gets replaced by high momentum flow from the free-stream. Secondly, in this case, it provides a radial force on the fluid body. This helps the fluid momentum to spread in the diffuser, increasing the pressure energy. At low Re, the first

effect is not really felt – in fact, the opposite effect is seen because boundary layer is too big initially and grows too quickly that high momentum from the free-stream cannot be transferred adequately. The boundary layer is much larger on entry to the diffuser at the lower Re, as shown by Figure 4.14 (b). Therefore, it must be the second effect that produces the improvement in performance. At higher Re, the boundary layer effects can be seen, but eliminating the separation entirely is not ideal – so there is a balance that results in the relationship seen here. The value of Re≈800 for this transition is a factor of the inlet length, flow conditions and control setup, but the trend of crossing the x-axis as in Figure 4.14 (a) is expected to always occur at some point. This study repeated with an inlet length of $l_{up} = 0.05$ (compared to 0.2 here) found the same trend, but the critical Re where a suction of $C_q = 0.3$ always reduced the separation length decreased to Re≈600.

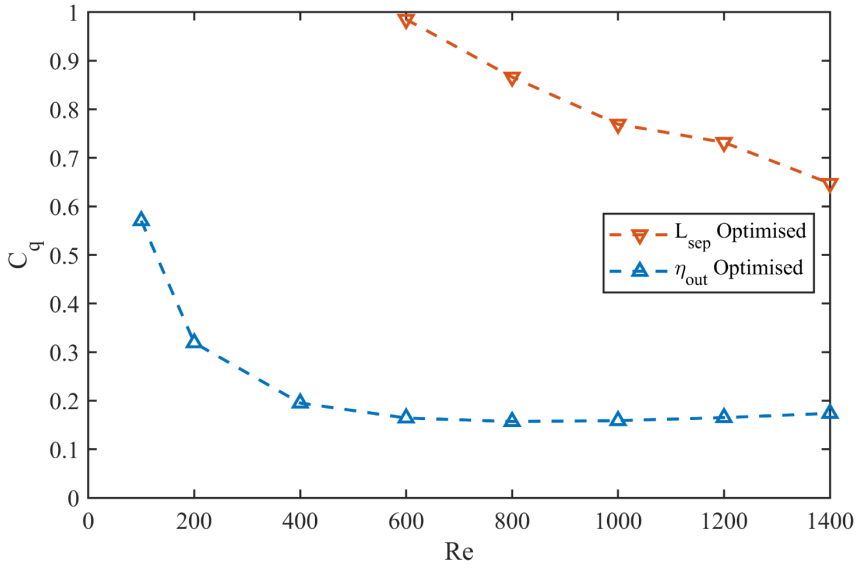

Figure 4.13 Suction effort required for optimised flows. A best linear fit for the L_{sep}-optimised curve has the equation $C_q = 1.205 - 0.000405Re$ for $Re \geq 600$ and has a fit quality of $R^2 = 0.9712$.

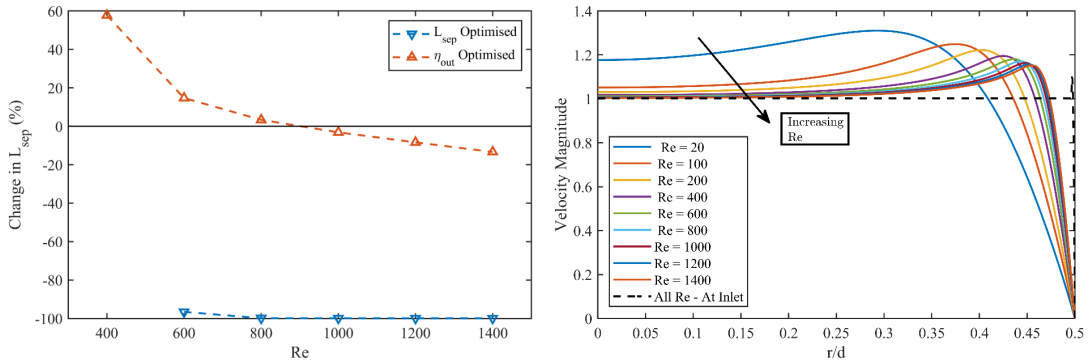

(a) (b)

Figure 4.14 Change in separation length from the uncontrolled case for $Re > 400$, (a), and the velocity magnitude at the diffuser entry for the uncontrolled flow, (b).

4.4.1.2 Performance of Diffuser

For the case of the 10°-diffuser ($\alpha = 5°$ with uniform suction, it was found that the performance and efficiency of the diffuser could always be improved by applying suction. Figure 4.15 below shows how η_{out} varies with Re for each control applied.

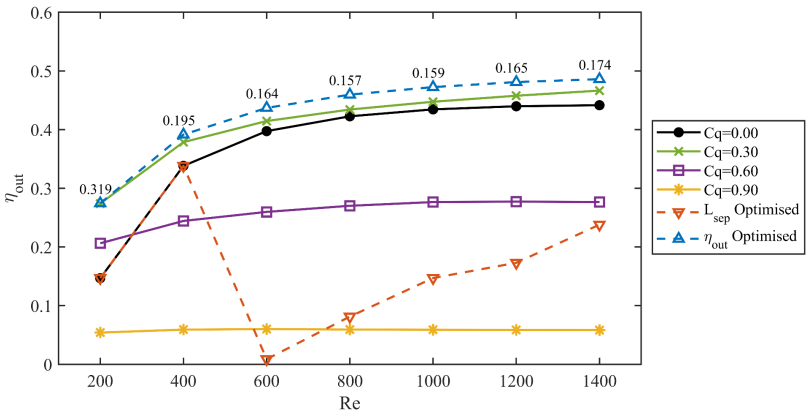

Figure 4.15 Performance of diffuser with differing amounts of uniform suction control. For the η_{out} objective, the C_q value is printed above each data-point. Values for $Re < 200$ are omitted as the strong viscous effects give a *decrease* in pressure through the diffuser.

As can be seen in Figure 4.15, the performance of the uncontrolled diffuser increases with Re over the entire range investigated. The application of uniform suction could always improve the performance further – even though this measure accounts for the power to apply the control. In other words, efficient suction control of the conical diffuser is indeed achievable and economical. The C_q values printed above the η_{out}-optimised curve (blue triangles) show that the controller effort to achieve the optimal case varies with Reynolds number. For $Re > 600$ once the uncontrolled separated flow has become fully established, the controller effort increases slightly with Re, however, the improvement in performance increases slightly here also. Once the flow has become fast enough that viscous effects no longer dominate the performance and pressure rise – i.e. $Re \geq 400$ – the suction control gives a near-consistent 10% improvement in diffuser efficiency (see Figure 4.16).

The performance of the optimally controlled flow follows the same trend as the uncontrolled flow. This is useful for its implementation in engineering practice. The engineer looking to design a diffuser for an application needs to only follow a simple two-step process: first, design the diffuser for optimal performance without control within the design constraints, second, apply and optimise the suction control for further improvement.

One interesting insight into the control can be seen in images of the reversed flow in the diffuser as shown in Figure 4.12 (a) and (b). The suction control results in the separated region becoming shorter, but slightly thicker. Additionally, the speed of the reversed fluid is faster as it is driven by the suction at the walls. For the uncontrolled

flow, the separated fluid forms half of a vortex defining the recirculatory region and surrounding the separatrix. On the other hand, because of the centripetal force generated by the suction on the diffuser walls, the vortex for the controlled flow is technically centred at the corner of the diffuser entry. Only half of the vortex is present in the flow as the material is removed from the domain by the suction. Inevitably, the thickest part of the separated region is therefore collected at the exit of the diffuser, as the centripetal force is removed once the fluid has entered the tailpipe, and the vorticity can diffuse. The use of directional suction might allow even more efficient control.

Unlike the η_{out}-optimised suction, the L_{sep}-optimised control dramatically reduces the diffuser performance. This is understandable given the large amount of material that is removed from the domain to eliminate separation at low Re. The performance of the diffuser at $Re = 600$ when $C_q = 0.99$ is near zero as almost all the fluid has been removed from the domain. However, less and less suction is needed to eliminate separation as Re increases, and as shown in Figure 4.16, it appearst that eliminating separation will improve performance at higher Re (approximately $Re = 2100$ at the current rate). Unfortunately the onset of a bistable solution (hysteresis) at higher Re complicates the situation and is more difficult to resolve numerically. When one considers that, for the uncontrolled diffuser, the separated region continues to grow and choke the flow, it makes sense that removing this obstacle would improve the performance.

Finally, the parametric curves in Figure 4.15 demonstrate the non-linear relationship of suction control on the flow. A small amount of suction improves the flow, as seen with the $C_q = 0.3$ curve, but too much and the performance rapidly decreases. There is a natural balance between improving the flow and removing too much material.

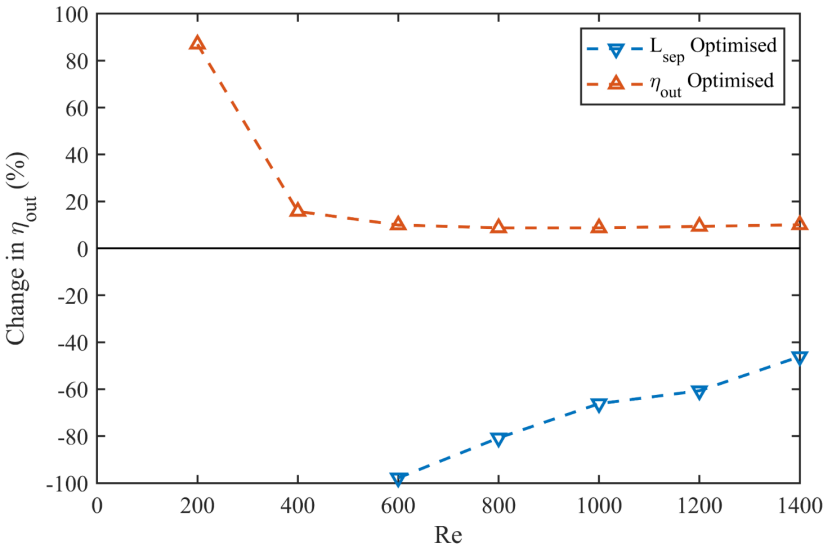

Figure 4.16 Change in diffuser performance from the uncontrolled baseline. Only data-points where the suction is active and where η_{out} is positive are shown.

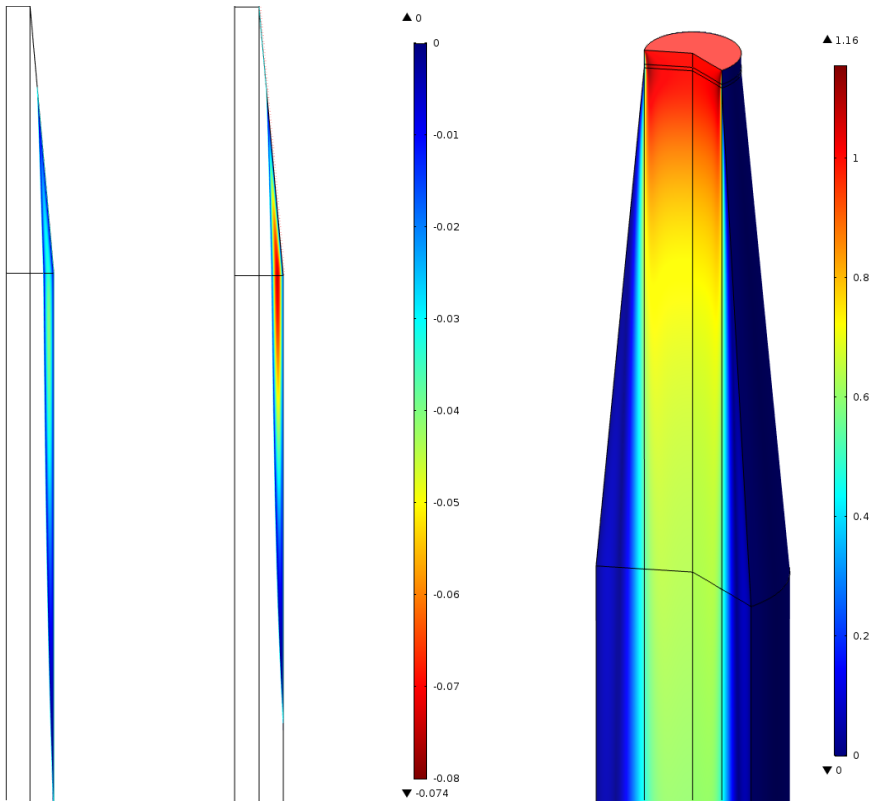

Figure 4.17 Surface plots of the reversed streamwise velocity in the separated region for the (a) uncontrolled diffuser and (b) diffuser optimised for η_{out}. The velocity magnitude profile for the entire flow for the η_{out}-optimised case is shown in (c).

4.4.1.3 Continuing On from JRSNZ Paper

The studies performed and published in the Journal of the Royal Society New Zealand showed that uniform suction applied to the diffuser wall could be very effective at increasing performance or controlling the separation characteristics for a diffuser with semi-divergence angle $\alpha = 5°$. However, there were aspects of suction control of the diffuser that were not shown or discussed in that paper (due to limitations of space, and further research performed after its writing). This includes: the optimal performance of diffusers of different semi-divergence angles, hysteresis that occurs in the controlled flows at some $Re, C_q, \& \alpha$, and, of course, control by non-uniform suction. These will now be discussed in that order.

4.4.2 $\alpha \geq 5°$ Diffuser

4.4.2.1 Initial Optimisation Results

The optimisation procedure was carried out on the range of Re and α outlined earlier to determine the optimal uniform suction coefficient, C_q. The objectives of eliminating

separation and maximising performance were both investigated. Figure 4.18 show surfaces of the performance or separation length of the optimised flows for each objective. As can be seen in the figure, several data-points are missing. This is because the solver failed to converge for some combinations of Re, α, C_q and therefore the optimisation failed. 2D plots in Figure 4.19 provides more detail of the results for each semi-divergence angle. This will be discussed in further depth shortly.

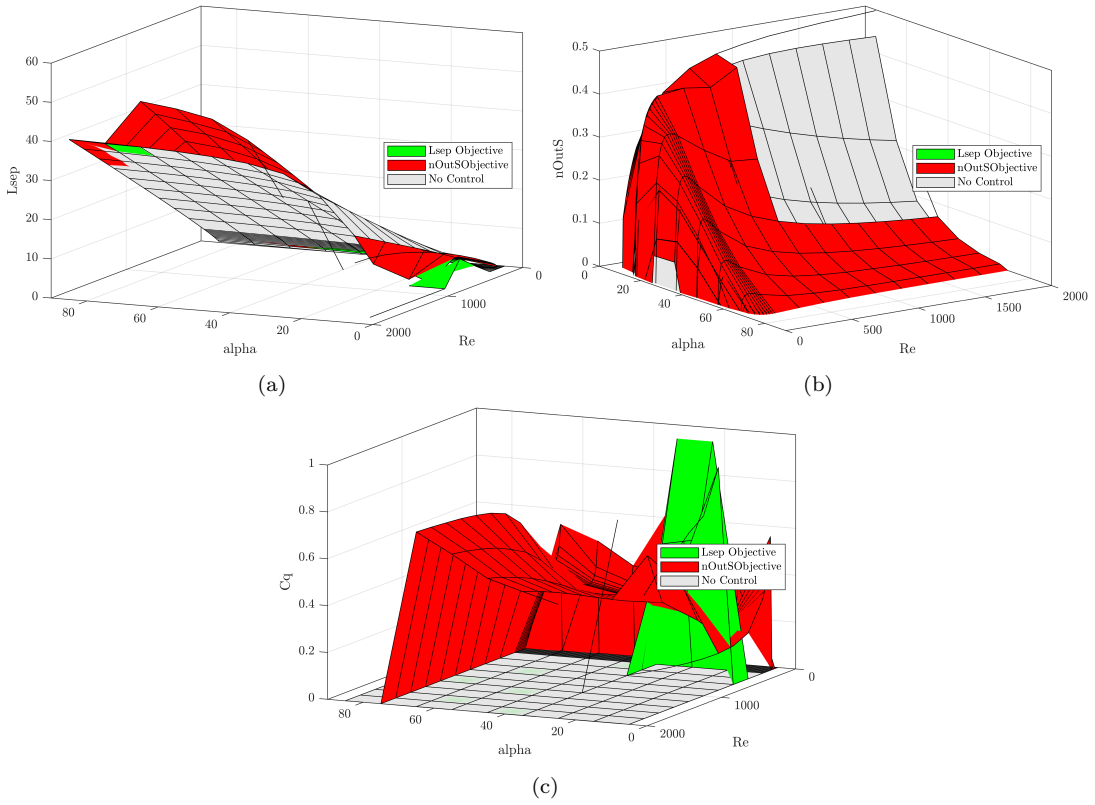

Figure 4.18 Surface plots of the optimised results for $n = 1000$ compared to the uncontrolled case.

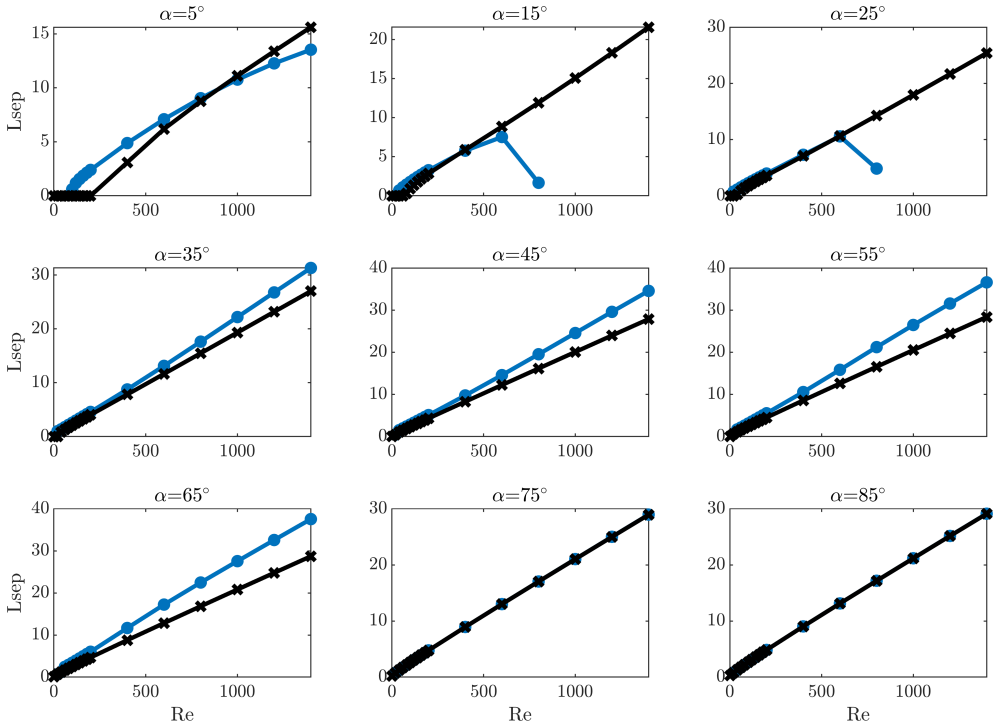
α=5°
α=15°
α=25°
α=35°
α=45°
α=55°
α=65°
α=75°
α=85°
Lsep
Re

(a)

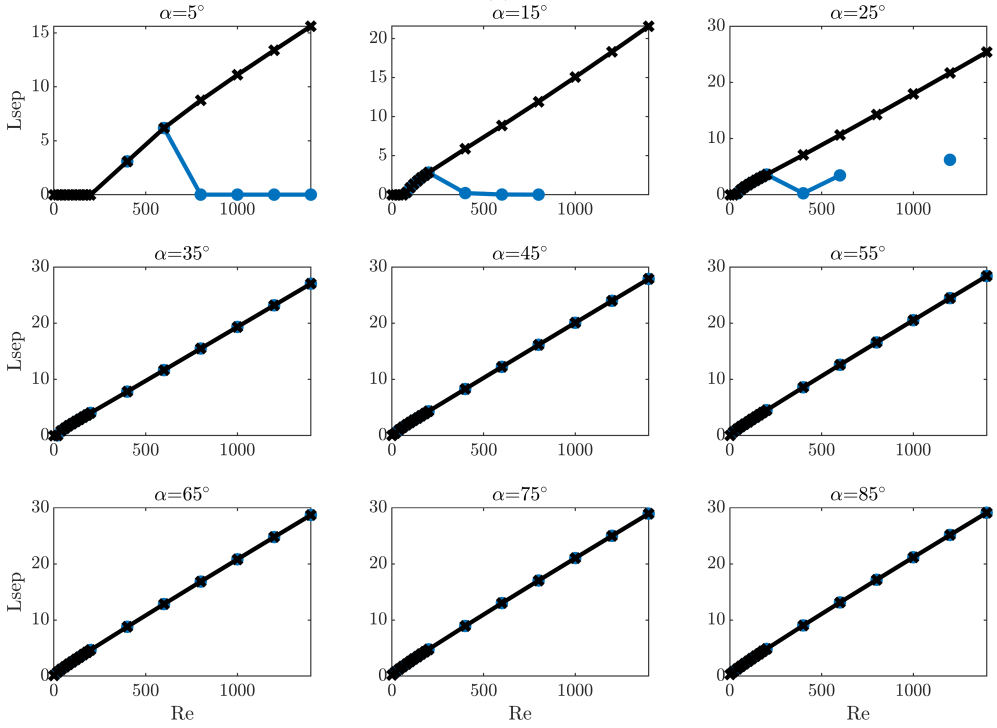
α=5°
α=15°
α=25°
α=35°
α=45°
α=55°
α=65°
α=75°
α=85°
Lsep
Re

(b)

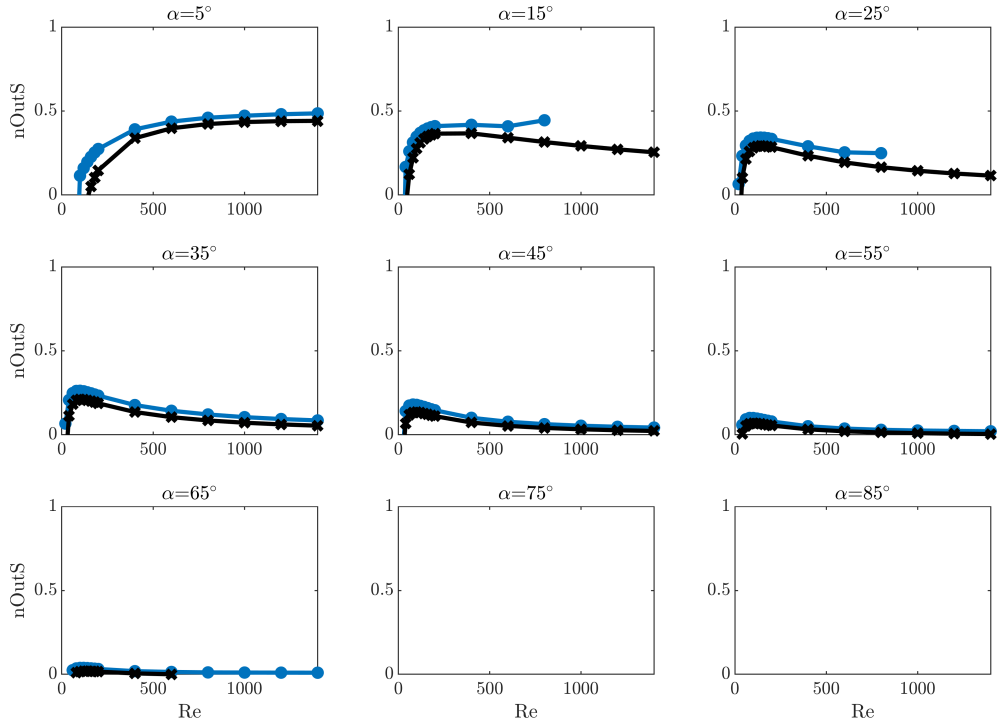
α=5°
α=15°
α=25°
α=35°
α=45°
α=55°
α=65°
α=75°
α=85°
nOutS
Re
0
0.5
1
500
1000

(c)

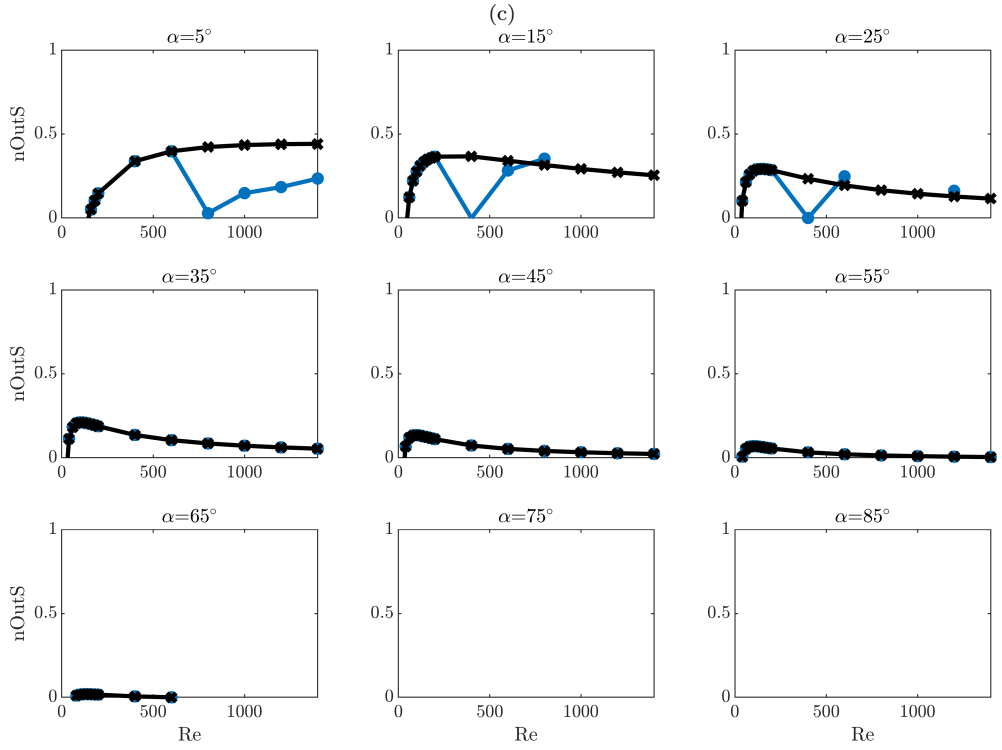
α=5°
α=15°
α=25°
α=35°
α=45°
α=55°
α=65°
α=75°
α=85°
nOutS
Re
0
0.5
1
500
1000

(d)

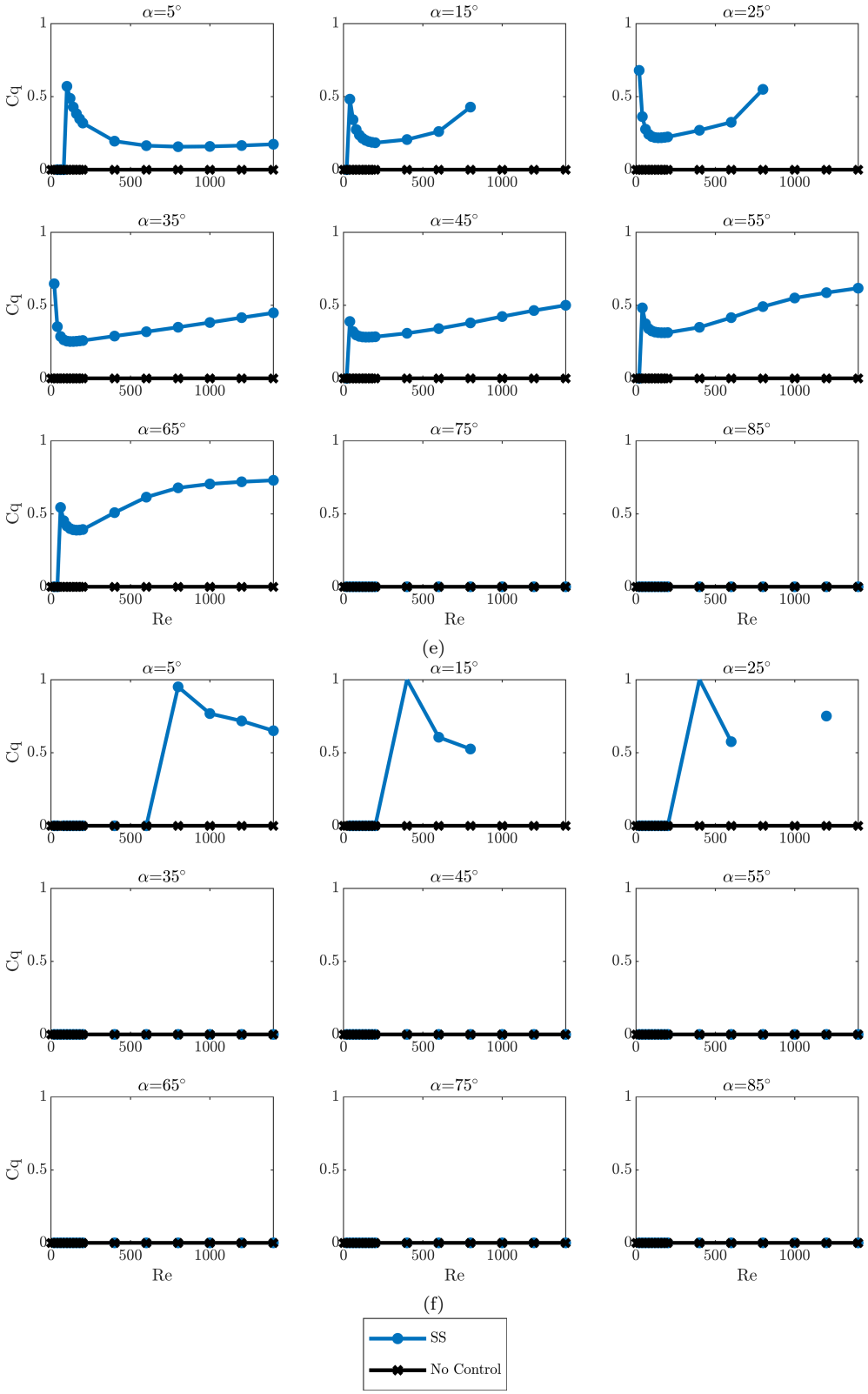

Figure 4.19 Key characteristics of optimised result for η_{out_s} objective (a,c,e) and L_{sep} objective (b,d,f) from steady-state simulations. Note for the η_{out} plots at high angles ($\alpha \geq 75°$) no data-points are shown because the performance is never positive (the y-axis is bounded from 0 to 1).

4.4.2.2 Convergence Issues

During the optimisation runs, it was found that many parameter combinations failed to generate converged results. In other words, the solver methods were unable to find satisfactory velocity and pressure fields that satisfied the governing equations. There were never any convergence issues for the uncontrolled case, so this suggests that the implementation of suction control either destabilises the flow, or affects it in some way such that the solver is unable to find its way to the correct solution. This failure to find the solution for a subset of parameters becomes a major problem for an optimisation process. An optimisation algorithm can be made to continue even when an error in the forward-problem solving occurs (non-convergence), however this missing data-point may contain useful information and possibly even the desired optimum.

The convergence errors occurred only for some of the diffusers ($\alpha = 15°, 25°, 35°$) and only for particular combinations of Re and C_q. To uncover roughly over what range of parameters these errors occurred, a parametric study was performed as in the JRSNZ paper. Plotting the planes of C_q against α & Re in Figure 4.20, missing data points show where the solver failed to converge. These results show that there appears to be a ballooning region of parameters where the flow fails to converge. Beginning at $\alpha = 15°, Re = 1400, C_q \approx 0.35$ and growing as Re is reduced and α increased. Unfortunately, these are particularly interesting diffusers and flows – with the most potential to improve by suction control. Therefore, it was important to uncover what was causing these convergence issues and to remedy them for the optimisation process.

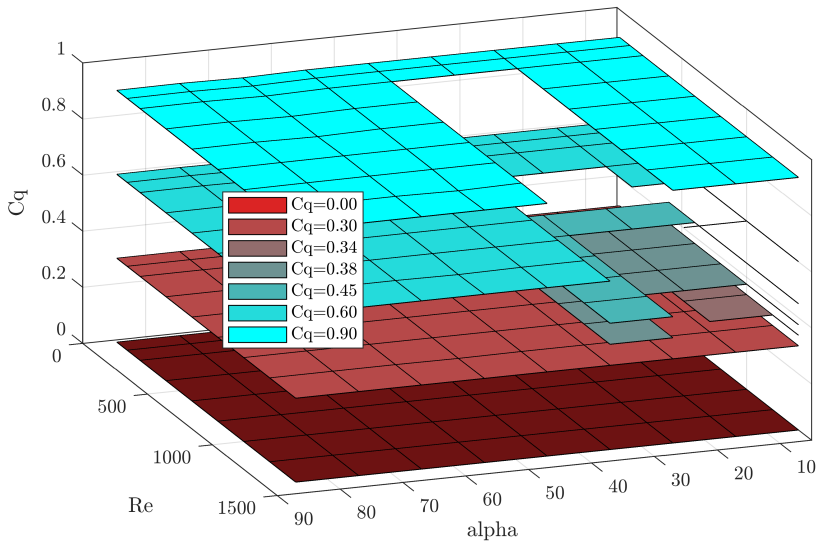

Figure 4.20 Convergence failing data-points (areas where surface is broken). Note that for $C_q = 0.45$ & 0.38 smaller planes were used so only the missing data-points within these planes are where convergence failed.

The most likely causes of convergence issues are: the underlying assumptions no

longer being valid (time-dependent flow instead of steady; 3-dimensional instead of 2D; turbulent flow instead of laminar), the initial guess being poor (though a zero-velocity field initial value is usually robust), or the solver algorithm getting trapped or stuck along a diverging solver path. To determine the cause of the errors, parameter combinations which were unable to be solved with the steady-state axisymmetric model, were applied to a time-dependent case.

4.4.2.3 Hysteresis in the Flow – Cause of Convergence Issues

Suction control was alternately ramped up or down for parameter combinations which resulted in non-convergence for the steady-state case. When ramped up, the suction begins at $C_q = 0$ whereas when it is ramped down, it begins from $C_q = 1$. The ramping occurs over one convective time-unit $t^* = \frac{d}{U}$ after a small period of modelling the pre-ramped flow (which was always steady). The objective of this investigation was to uncover if the resulting flow actually was steady-state.

The conclusion of these studies was that the flow does indeed reach a steady-state once fully developed. However, it was discovered that the flow that results from the control depends on whether the suction is ramped up or down. There is hysteresis in the flow. Figure 4.21 shows the fully-developed flow for the 'ramped up' and 'ramped down' cases at $\alpha = 25°, Re = 1400, C_q = 0.5121$.

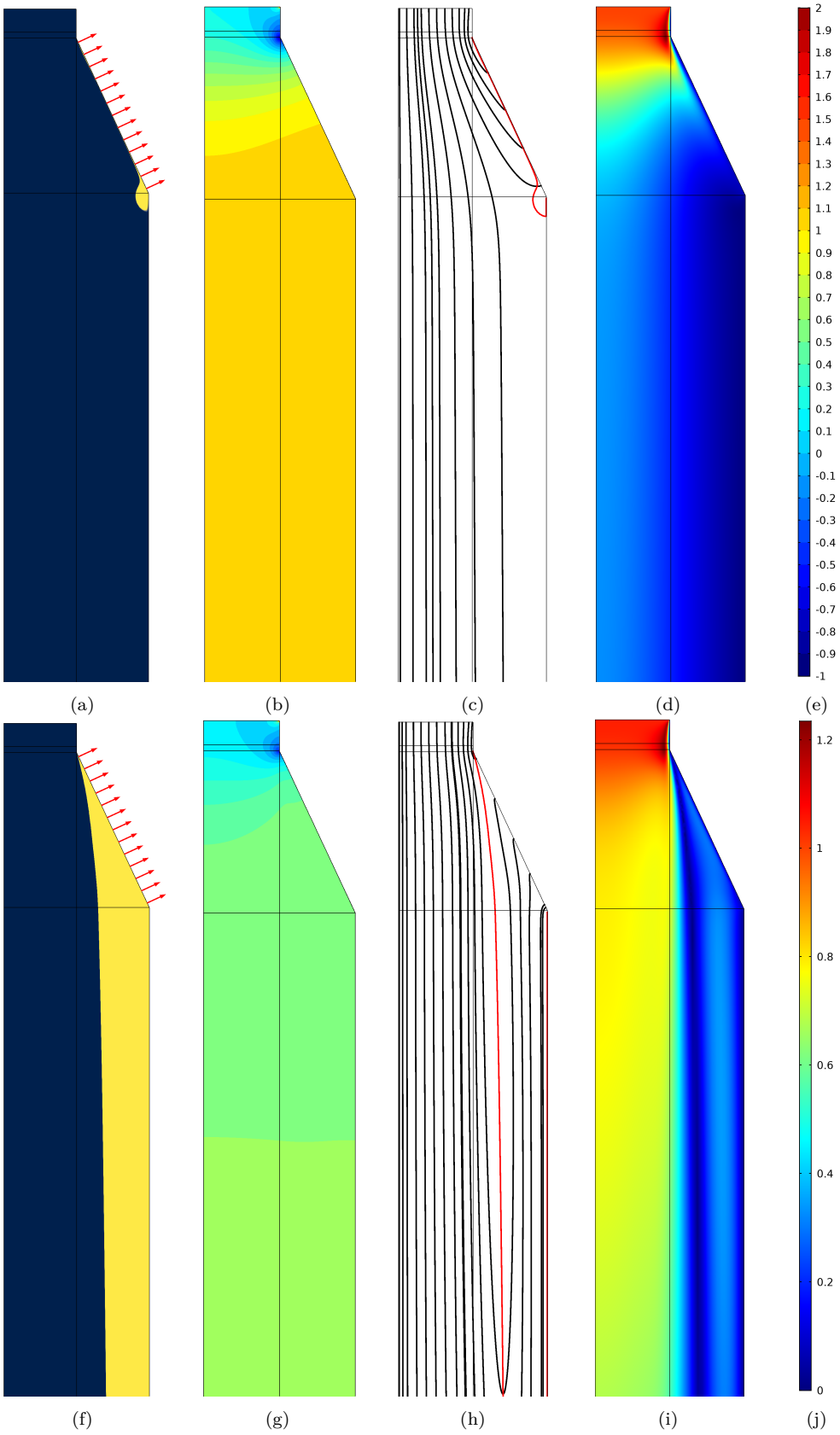

Figure 4.21 Hysteresis in fully-developed flow for $Re = 1400, \alpha = 25°, C_q = 0.5121$ diffuser either ramped down from $C_q = 1$ (above) or ramped up from $C_q = 0$. Figures (a,f) show the reversed region of flow and suction vectors, (b,g) show the pressure contours (normalised by average entry pressure) with colourbar given in (e), (c,h) streamlines with density of 20 and separatrix shown in red, and (d,i) give velocity magnitude surfaces with colourbar in (j).

It is this hysteresis that causes the convergence issues for the steady-state solver. To confirm this, a 'load-ramping' approach was applied to the steady-state simulations. The inlet velocity was ramped up from 0 (by a series of iterative steady-state simulations where the solution from the previous is used for the proceeding one), while the suction control was held steady (replicating the 'ramp down' time-dependent simulations as the suction control is effectively stronger when the inlet flow is weaker). The load-ramping enabled the flow to be resolved with parameters that had previously been unable to converge. However, the flow that was resolved was actually that of the case where suction is ramped up (in the time-dependent simulations). Attempting to load-ramp in the alternative direction (reducing the inlet velocity from a higher one, or increasing the suction coefficient) resulted in failure to converge upon a solution. This may suggest that the 'ramped up' flow is stable, whereas the 'ramped down' flow is unstable – though this evidence is insufficient. The load-ramping was only effective when the suction was stronger than the point where hysteresis begins to be exhibited. Therefore it could not be used reliably. Time-dependent simulations are needed to reliably resolve the hysteretic flow.

To test the stability of the flow, a perturbation was added to the controlled flow in the time-dependent simulation of the $\alpha = 25°, Re = 1400, C_q = 0.5121$ flow. A $0.01U$ and $0.2U$ radial perturbation was applied to the inlet velocity over a short time-period, pushing the flow away from the walls to the diffuser axis. It was found that for the 1% perturbation both flows were stable, but for the 20% perturbation the ramped down case became disturbed and developed into the ramped up case after a long period of time. This coarse approach to testing the stability of the flow is by no means rigorous, but it gives some indication which final flow is more stable. The research of the uncontrolled SEF by Cantwell et al. [2010] performed linear stability analysis of the uncontrolled flow. They found that the flow was stable until at least $Re = 1400$ and likely much higher. While that happens to be the Re simulated here, we know that the hysteresis occurs at much lower Re for this semi-divergence angle and others when suction is applied. It is possible that the application of suction control accelerates the development of flow instability and bifurcation. Partly due to the generally accelerated flow – especially in the boundary layer – partly due to the oppositional force (relative to the free-stream flow) generated by the suction forces normal to the diffuser wall, and partly due to the momentum removed from the overall flow.

4.4.2.4 Optimal Control in the Presence of Hysteresis

To demonstrate how the hysteresis affected the optimisation procedure, the regular optimisation procedure was carried out on the time-dependent model and the steady-state model under two parameter sets: one where the steady-state model has no issues, and the other where it has convergence issues. These are $\alpha = 25°, Re = 400$, and

$\alpha = 25°, Re = 1400$. The objective of maximising performance was used. For the time-dependent optimisations, both ramping up and ramping down were tested. The objective is evaluated at the final time-step for the time-dependent optimisation studies. In all cases the fully-developed flow was steady. Each data-point obtained during the optimisation studies were then plotted, as shown in Figure 4.22.

As can be seen in the figures, at $Re = 400$ – where the steady-state model had no convergence issues – there was no hysteresis in the flow. However, at $Re = 1400$ – where convergence issues were present – the flow exhibited hysteresis and the ramped down diffuser performed much better. For this flow, load-ramping had to be applied for cases where $C_q > 0.51$ in order to actually resolve the flow. The performance of the diffuser changes significantly depending on which flow regime is developed by the suction control (which approach is taken in the hysteresis). The flow from the ramped down case is much better. The separated region is dramatically smaller than the ramped up case, and the performance is better as was shown in figures Figure 4.21. Consequently, in order to determine the optimal performance of the diffuser with uniform suction, time-dependent simulations must be carried out in the parameter ranges where hysteresis is present.

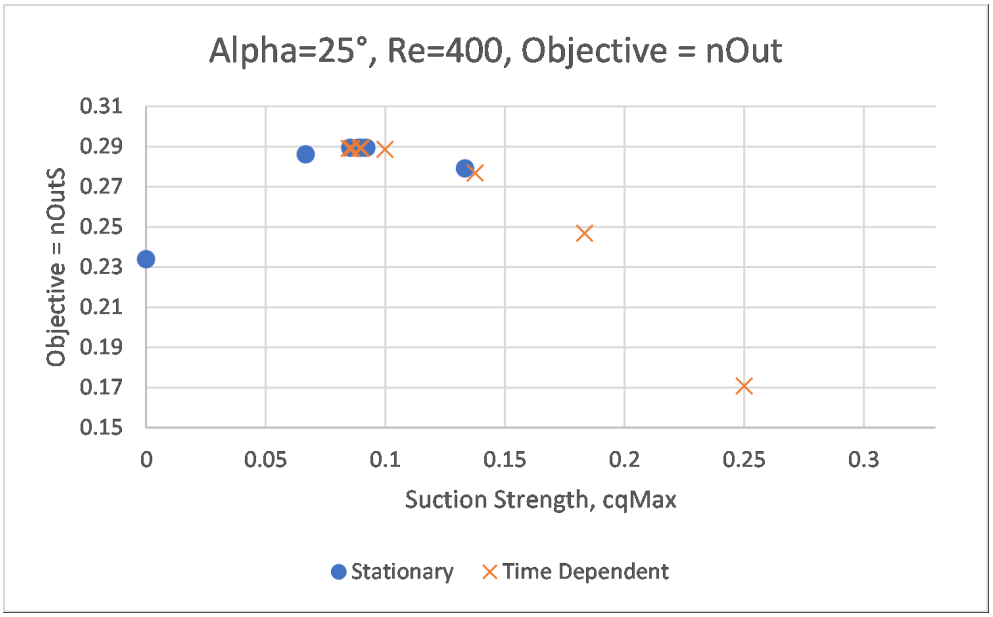

(a)

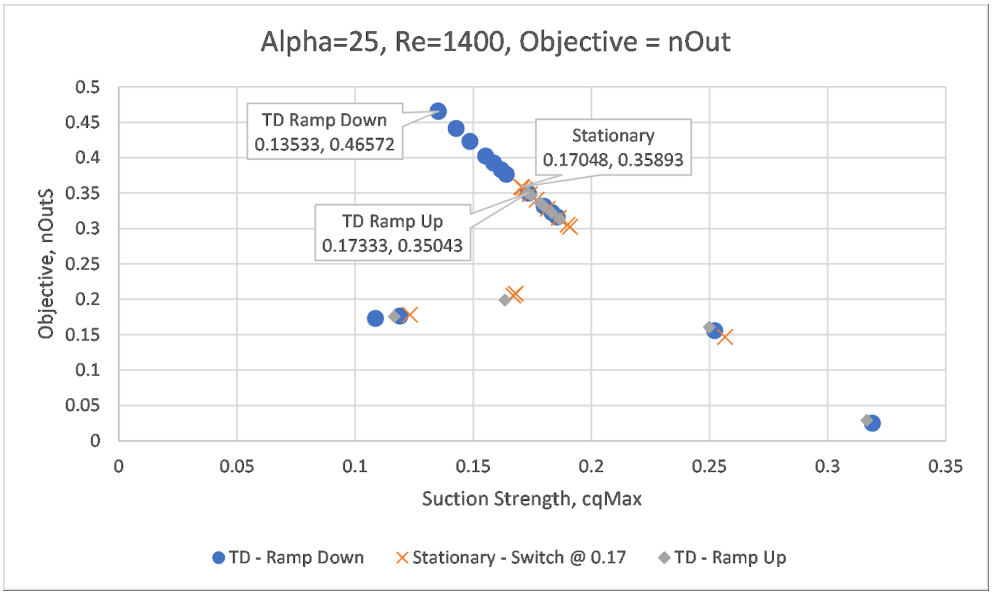

(b)

Figure 4.22 Result of optimisation process for steady-state, ramping control up, and ramping control down at $Re = 400$ and $Re = 1400$. Here $cqMax = \frac{1}{3}C_q$. Note that there is no hysteresis for the $Re = 400$ case.

4.4.2.5 Optimal Control by Uniform Suction

The optimisation process was repeated for the Re, α combinations which produced errors (hysteresis) in the steady-state optimisation up to $Re = 1400$. For these troublesome points, time-dependent simulations were performed with the control either ramped up or ramped down. Combining the data of the time-dependent optimisation with those converged points from earlier, the following results were achieved as summarised in

Figure 4.23.

The ramped down control produces a dramatic improvement on the performance of the $\alpha = 25°$ & $35°$ diffuser, as shown in Figure 4.23 (c). The η_{out}-optimised control for these diffusers is almost as good as for the $\alpha = 5°$ case, however the control effort required, C_q, is much greater (see Figure 4.23 (e)). Similarly, the separation is greatly reduced – or even eliminated – when the control is optimised for these moderately steep diffusers (Figure 4.23 (b)). The suction effort to produce optimal performance increases with Re after an initial decrease at low Re forming a v-shaped curve, as can be seen in Figure 4.23 (e). It is interesting to note that the control optimised with the ramp-down approach uses more suction than the ramp-up optimised control at $\alpha = 35°$ but the reverse at $\alpha = 25°$. In the $\alpha = 25°, Re = 1400$ example above (Figure 4.22) it is clear that less suction is needed for better results from the ramped-down flow, but evidently this is not the case for higher divergence angles. It appears that the ramp down C_q curve will intercept the ramp up C_q curve at $\alpha = 35°$ at higher Re. This trend was also seen at $\alpha = 25°$ but just occurred at lower Re.

Overall the results are very promising. Diffusers with divergence angles as steep as $\alpha = 35°$ can be made to produce performance nearly on par with the optimal $\alpha = 5°$ diffuser with appropriate uniform suction. This is an important result because even though the semi-divergence angle is only different by $20°$, the $5°$ diffuser for an expansion of $\beta = 2$ is eight times longer than the $\alpha = 35°$ diffuser.

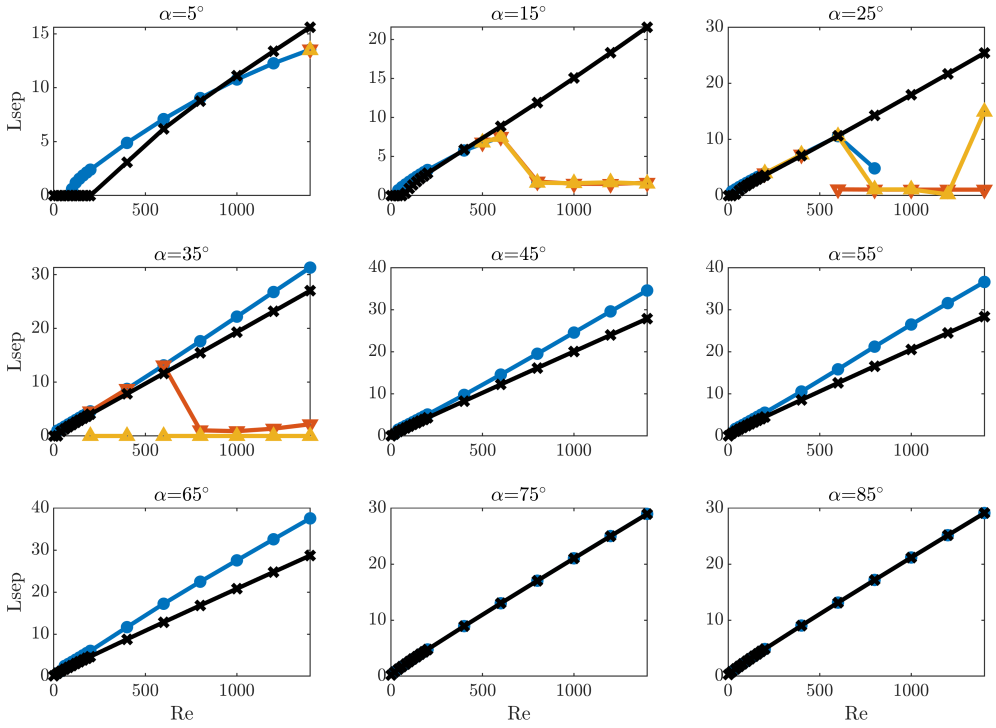
α=5°
α=15°
α=25°
α=35°
α=45°
α=55°
α=65°
α=75°
α=85°
Lsep
Re

(a)

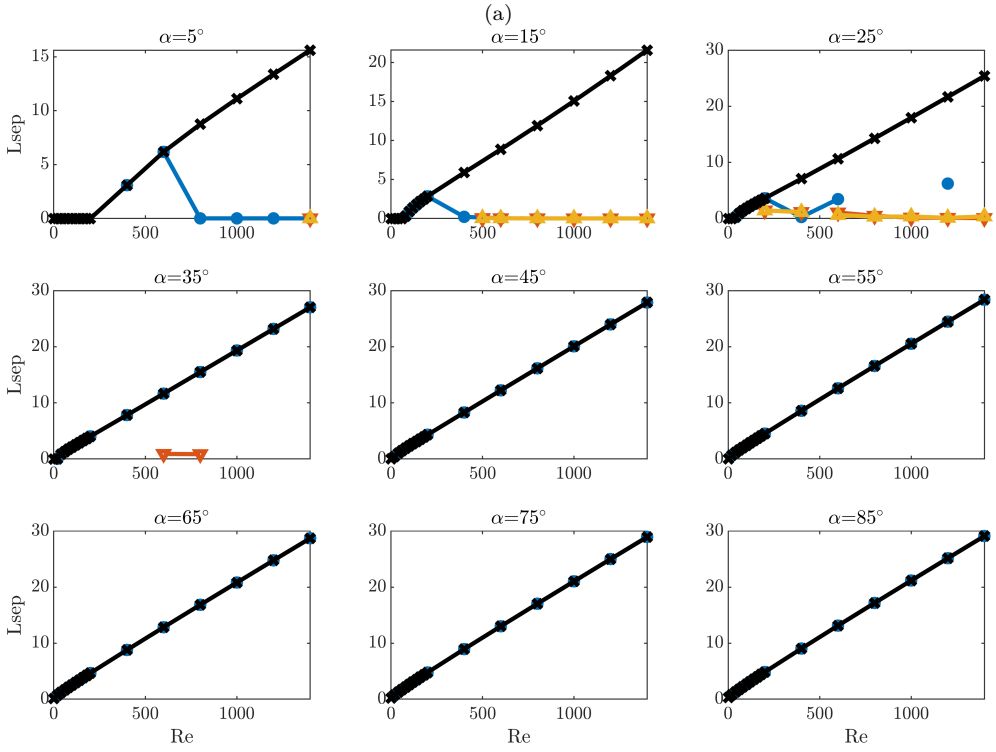
α=5°
α=15°
α=25°
α=35°
α=45°
α=55°
α=65°
α=75°
α=85°
Lsep
Re

(b)

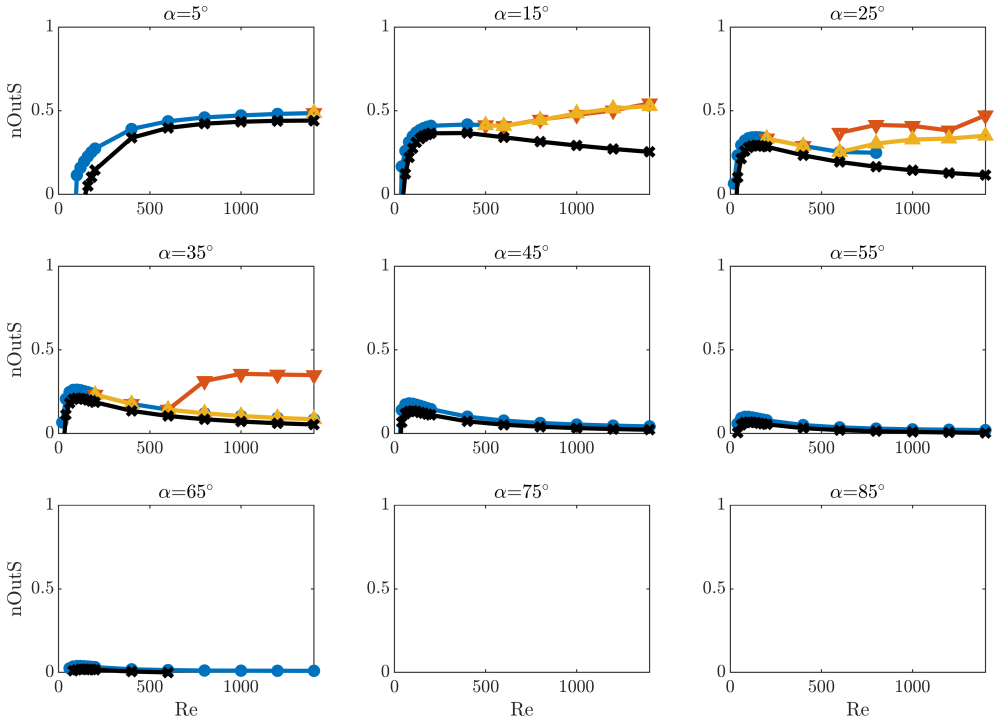
α=5°
α=15°
α=25°
α=35°
α=45°
α=55°
α=65°
α=75°
α=85°
nOutS
Re
0
0.5
1
500
1000

(c)

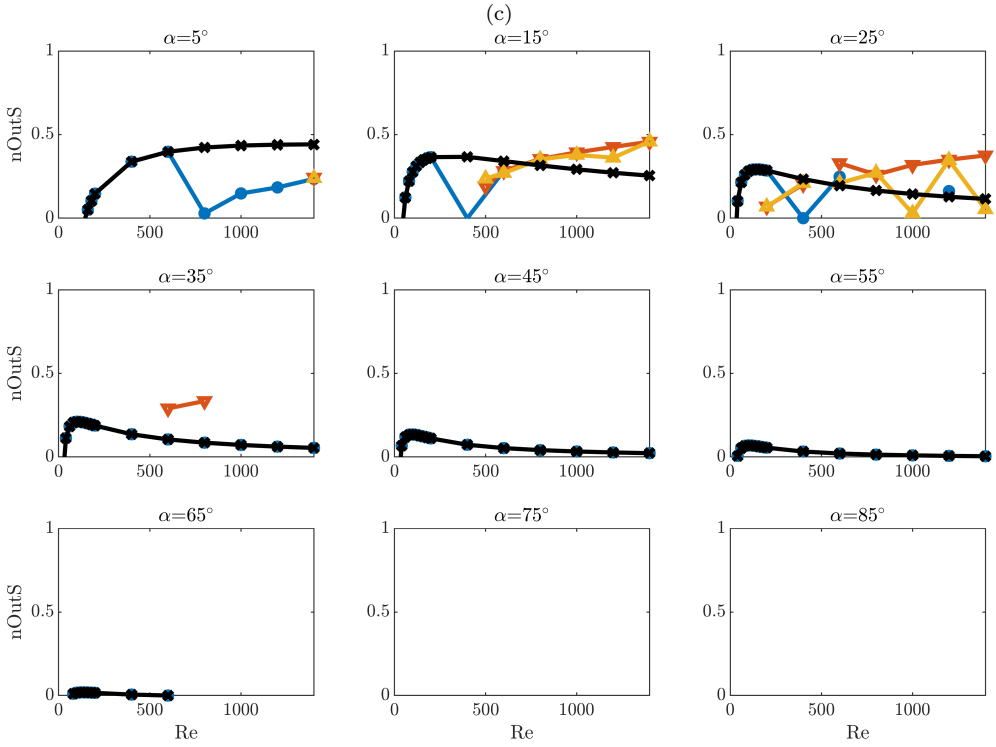
α=5°
α=15°
α=25°
α=35°
α=45°
α=55°
α=65°
α=75°
α=85°
nOutS
Re
0
0.5
1
500
1000

(d)

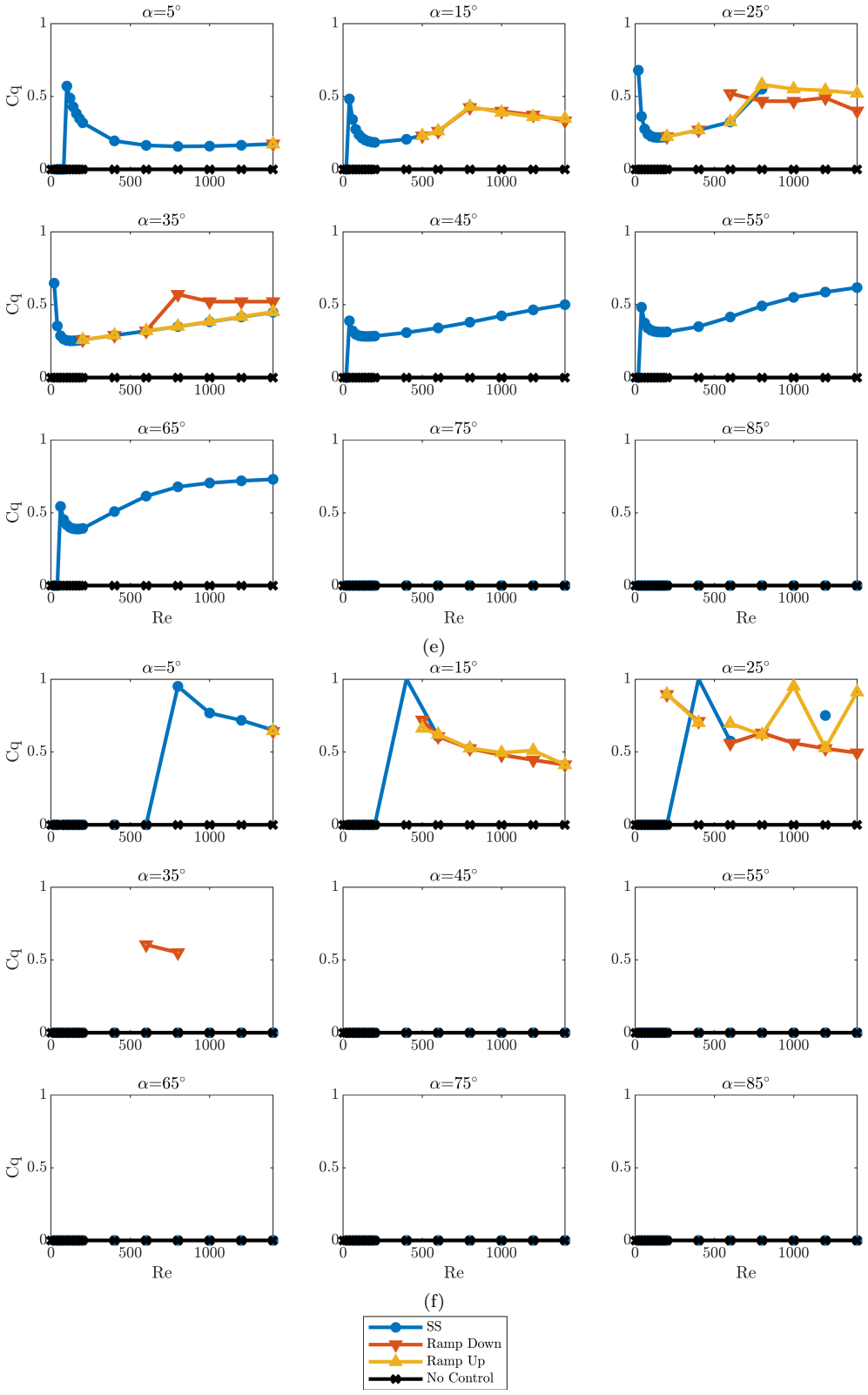

Figure 4.23 Results of optimised control: (a,c,e), η_{out} objective, (b,d,f), L_{sep} objective with suction ramped up or ramped down compared to the original result.

4.5 NON-UNIFORM SUCTION INVESTIGATION

For these studies, only the $\alpha = 5°$ diffuser was considered. Additionally, a much more restricted range of parameters was investigated, in many cases just looking at the $Re = 1000$ flow case, with $n = 1000$ for the inlet profile. The processes used to determine the optimal non-uniform suction control for the $\alpha = 5°, Re = 1000, n = 1000$ diffuser could easily be applied to all others (bearing in mind the possibility of hysteresis development). A summary of the key results is given in the following list:

- Non-uniform suction control was more effective than uniform suction control. Performance of diffuser increased by up to 53% over the uncontrolled case and 34% over the diffuser with uniform suction.
- Less suction is needed to achieve the same or better results than uniform suction. The net suction coefficient, C_q, to achieve a maximum performance of $\eta_{out} = 0.495$ with uniform suction was $C_q = 0.159$ whereas only $C_q = 0.145$ was needed for the single locus profile to achieve performance of $\eta_{out} = 0.665$.
- Suction biased towards the entry of the diffuser produces the best results. However, this arrangement is hard for upwind autogenous control to generate
- Optimised field-based control gave $\eta_{out} = 0.6738$ which is slightly higher than the single locus performance, $\eta_{out} = 0.665$ but required about 25% more suction.

4.5.1 Field-Control Optimisation

Theoretically, optimising a control field should result in non-uniform suction profiles that are the best as there are no constraints on the shape of the control profile. The optimisation ran smoothly and the optimised flow is shown in Figure 4.24 with the reversed flow, pressure and velocity magnitude surface plots. Linear Lagrange shape functions were used to define the control field, c_q, and while the regularisation term helped to smooth the final profile – there is still some refinement that could be done to the resulting profile shown in Figure 4.25. The final profile is very similar to the biased-locus profile.

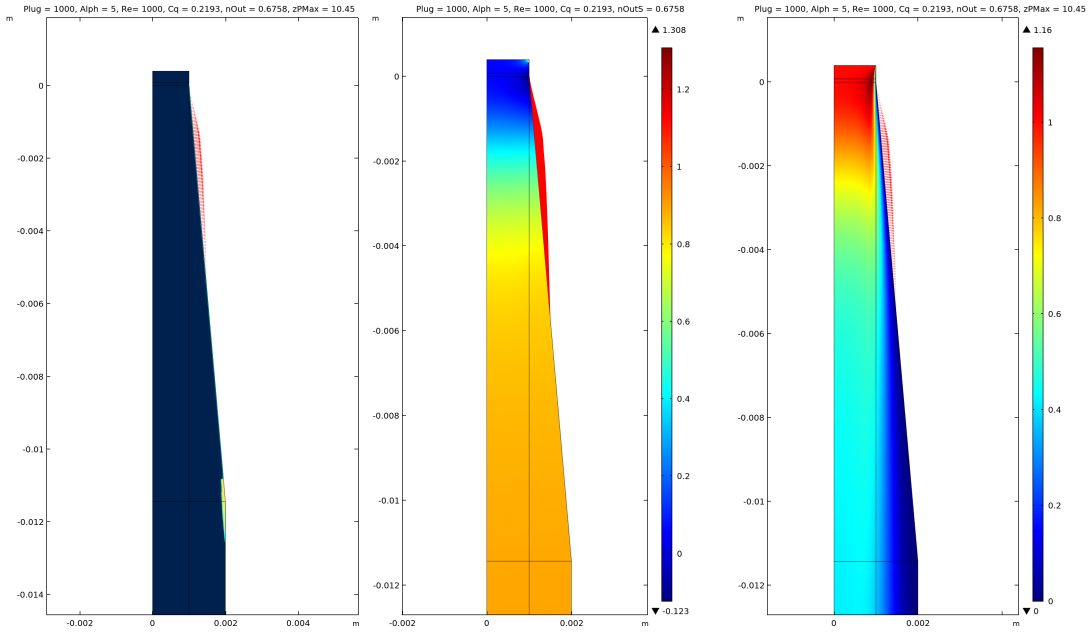

(a) (b) (c)

Figure 4.24 Performance-optimised field-based control surfaces, (a) reversed flow, (b) pressure contour, and (c) velocity magnitude for 5° diffuser at $Re = 1000$.

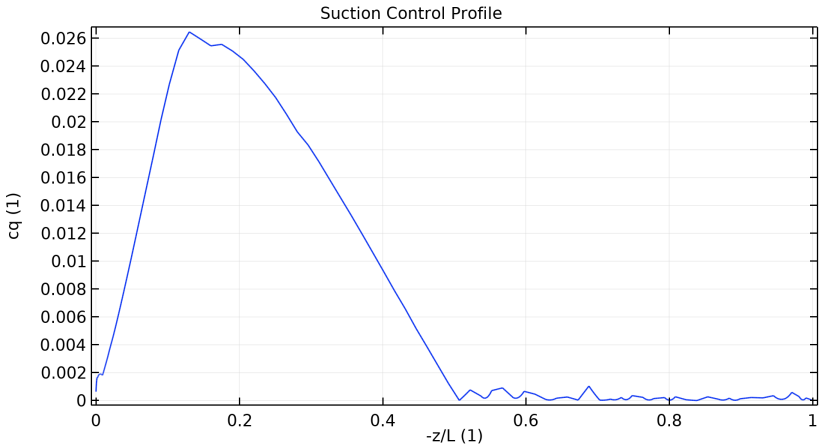

Figure 4.25 Field-based suction profile for best performance.

4.5.2 Single-Locus Optimisation

The results of these optimisation studies are shown in the plots below Figure 4.26. Firstly, the general structure of the suction profiles are shown by displaying the reversed flow surfaces. Magnified vector arrows are also plotted to show the location, spread and strength of the optimised single locus profile for each objective. The values of the key flow characteristics are then plotted in the following bar charts, as well as their improvement over the base, uncontrolled, steady flow. As can be seen in Figure 4.26 the location of the optimised suction is similar for both the η_{out} and L_{sep} objectives. It is

located shortly after the entry to the diffuser, $z_s = 1.2047$ ($z_{s_L} = 0.211$) and $z_s = 1.3245$ ($z_{s_L} = 0.232$) respectively. For the $\eta_{out_{max}}$ case though, the control is situated after the exit of the diffuser, and the maximum pressure point is achieved downstream of the portion of the domain shown in the figure. Realistically, the usefulness of the control in this case is limited as the maximum pressure point occurs so much further downstream, $z_{P_{max}} = 18.84$ ($z_{P_{max_L}} = 3.297$).

The location of peak suction for the η_{out} objective was very similar as for the optimised field control profile. Likewise, the improvement in performance using the single locus was substantial, improving on the uncontrolled case by 46% ($\eta_{out} = 0.6357$ compared to $\eta_{out} = 0.4335$). The key results are summarised graphically in Figure 4.27. However, this is not quite as good as the performance achieved by the field-based control at $\eta_{out} = 0.6652$. Though they are close, for a much simpler profile, and with less control applied for the single locus case ($C_q = 0.1455$ vs. $C_q = 0.2442$). Non-uniform suction was equally capable of improving the separation objective, entirely preventing separation at the studied Re.

Interestingly, blowing (even when it is arranged normal to the wall) was also able to greatly improve the separation characteristics (though not the other objectives). It nearly eliminates the recirculation region when situated just downstream of the separation point. This is interesting as one might expect normal blowing to promote separation by forcing the boundary layer away from the wall. However, since the boundary layer has already separated, the blowing instead acts to oppose the reversed flow and disrupt the separation bubble. On the other hand, blowing on its own was never useful for improving the performance of the diffuser. When only blowing was allowed, the optimisation found that the best control was no control at all. Blowing within the diffuser leads to an acceleration of the flow, instead of a slowing and diffusing of it. This is detrimental to the efforts of converting dynamic pressure to static pressure.

These results bode poorly for the use of autogenous suction control. With the basic upwind autogenous control, fluid removed by suction must be returned to the flow at a point of lower pressure. In the diffuser this arrangement is suction downstream (near the exit) and blowing upstream (near the entry). It appears that this is the reverse of the optimal case however. Will the effect of suction downstream be as pronounced? Can a combination of suction and blowing result in an improvement, even though blowing (normal to the surface) is always detrimental to the diffuser performance?

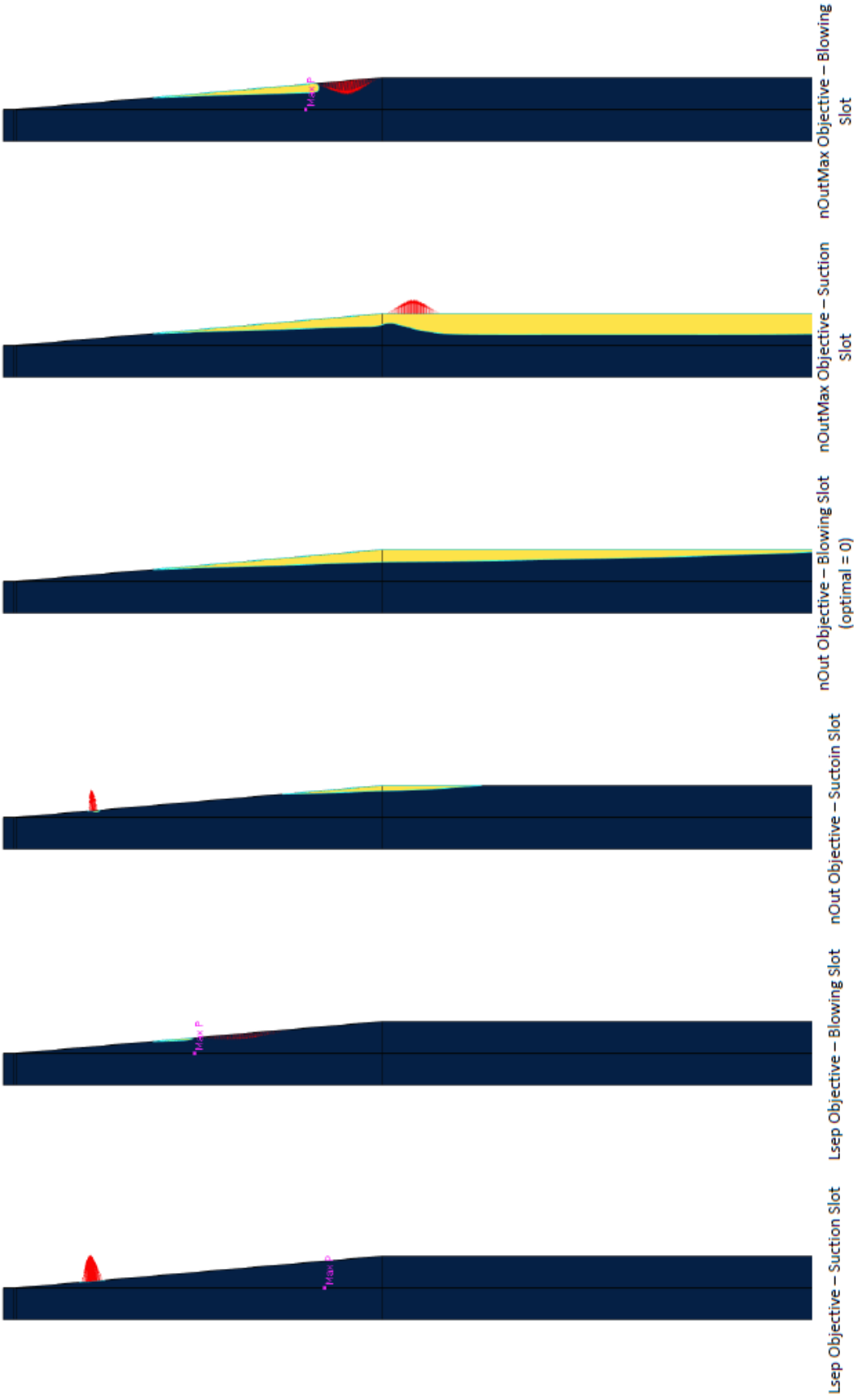

Figure 4.26 Reversed flow for optimised control with different objectives and control methods.

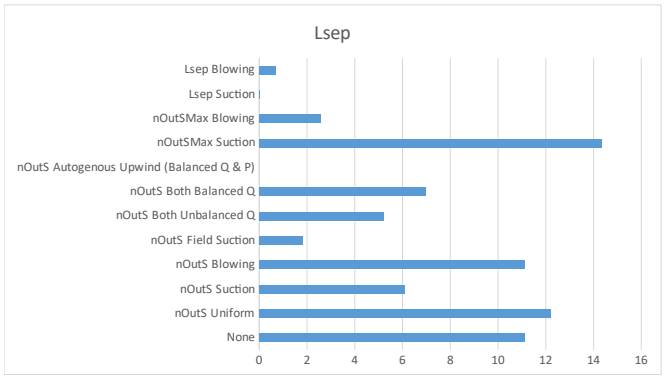

(a)

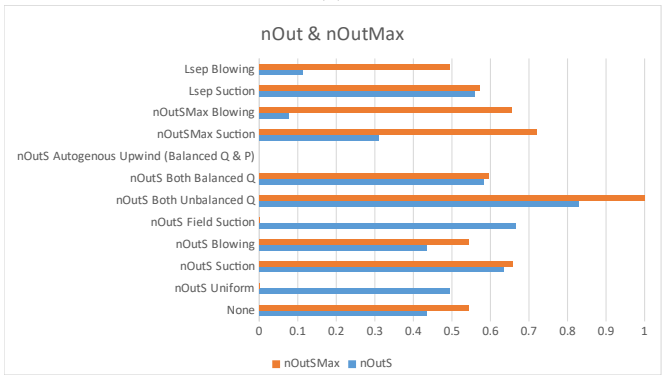

(b)

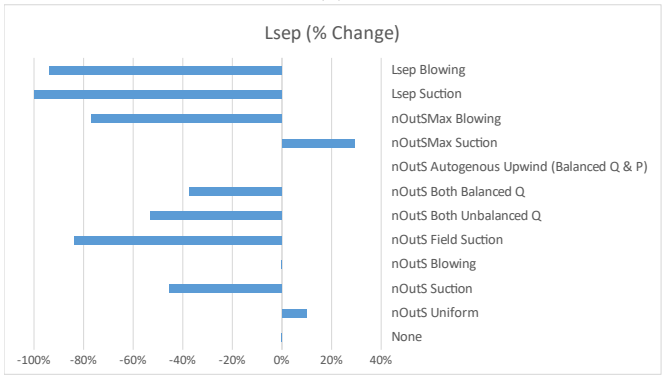

(c)

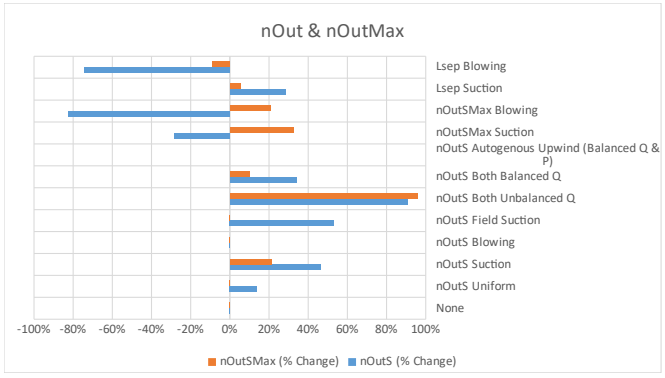

(d)

Figure 4.27 Key results for optimised flows and their percentage change.

4.6 AUTOGENOUS CONTROL ATTEMPTS

4.6.1 Flow-Rate Balanced (Q-Balanced) Dual-Locus Control

The Q-balanced dual-loci control was able to greatly improve the diffuser performance over the uncontrolled case (η_{out} = 0.5820 vs. 0.4335). However this is a worse performance than the single locus (suction only) case (0.665). The optimised Q-balanced dual-loci control employed a small but strong suction slot shortly downstream of the diffuser, and a thinner blowing slot downstream. If the suction and blowing loci were permitted to have different flow rates – equivalent to an open system with net fluid being added or removed – the performance could be improved over the suction-only case. In fact, very strong performance was achieved by this unbalanced approach with $\eta_{out} = 0.8283$. The parameters for the two control loci are given in Table 4.7 below.

Table 4.7 Optimised control parameters and performance for dual-loci control. Note, uncontrolled performance of this diffuser is $\eta_o ut = 0.4335$

Control Parameter	Q-Balanced Value	Unbalanced Value
z_q	0.8739	1.3297
γ_q	0.2183	0.1847
$c_{q_{max}}$	0.2009	0.3539
z_{q_b}	7.6049	5.6125
γ_{q_b}	0.1258	0.6406
$c_{q_{max_b}}$	-0.2009	-0.3624
C_q	-5.87E-05	-0.7606
η_{out}	0.5820	0.8283

4.6.2 Pressure and Flow-Rate Balanced Dual-Locus Control

4.6.2.1 Effect of Suction/Blowing on Pressure Gradient

Before discussing the results of producing a pressure-balanced upwind autogenous control, it would be useful to also show what happens to the pressure profile when suction or blowing is applied. The pressure plots below Figure 4.28 show the development of the pressure profile through the whole domain with suction being applied either at $z_q = 1, 5, 10, 15$ and with blowing applied in the opposite trend $z_{q_b} = 15, 10, 5, 1$. In Figure 4.28 (a), the spread of the blowing locus, γ_{q_b}, is fixed and $c_{q_{max_b}}$ is adjusted to match the flow rates, while in Figure 4.28 (b) the opposite approach is taken. In both plots the pressure profile of the uncontrolled diffuser is also shown as the black line.

Both plots show practically the same results, demonstrating the relative unimportance (to the free-stream flow) of how γ_{q_b} and $c_{q_{max_b}}$ are arranged. What is clear on

first glance is that there is a great dependency on the location of the control. When suction is applied near the entry of the diffuser, there is a very large increase in static pressure (all along its axis), but when the suction is applied further downstream the effect is much more muted. The effect of blowing follows the same trend but generates the contrary effect – significantly lowering the static pressure at and downstream of its position. Wherever suction or blowing is applied, there is a slight and temporary dip in static pressure though it is felt predominantly at the wall and very little at the centreline.

While the results are for only a few limited cases, it seems that achieving an increase in static pressure is only likely when suction is located upstream of the blowing, and particularly when located close to the entry (where the pressure is lowest). Evidently such an autogenous suction arrangement is feasible, given the highly accessible pressure gradient in the flow; whether it can be arranged in such a way to improve the diffuser performance is another matter.

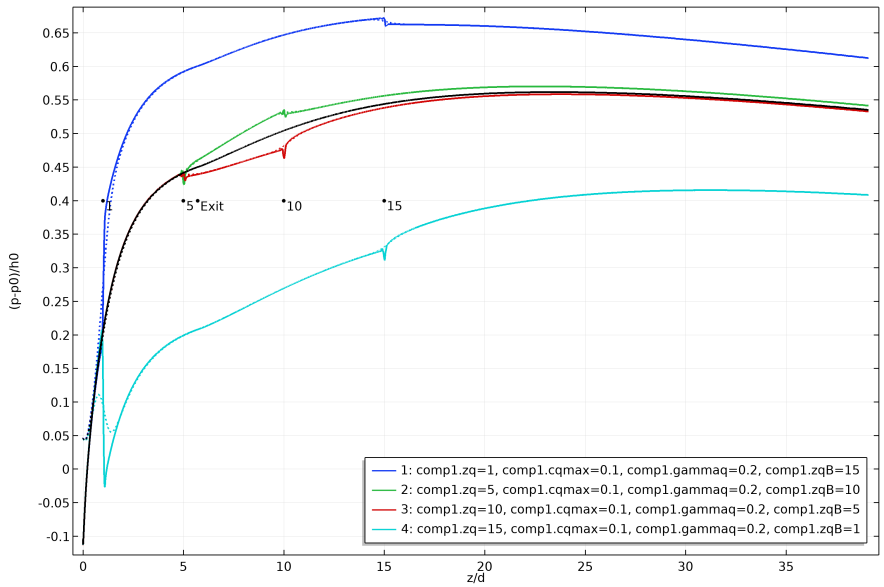

(a)

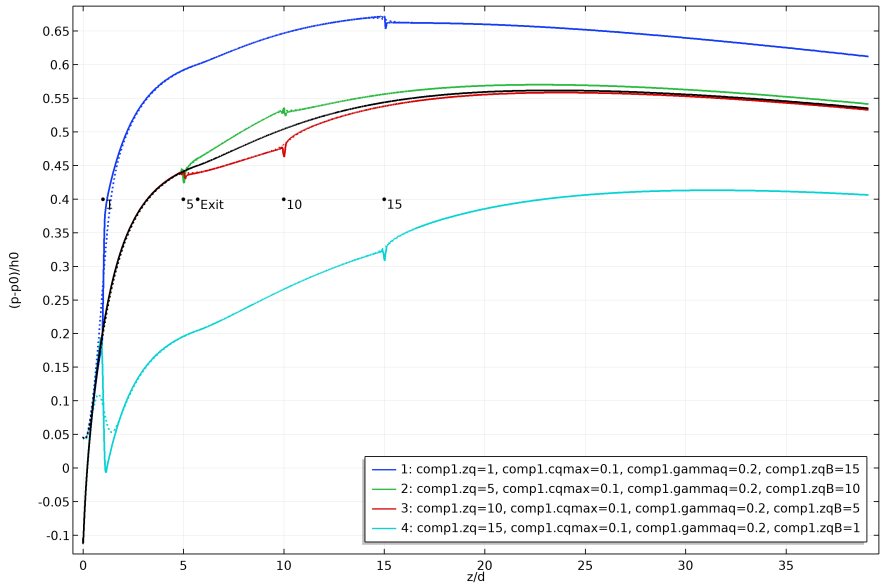

(b)

Figure 4.28 Pressure profiles from parametric dual-loci control with constant suction parameters. Blowing strength, $c_{q_{max_b}}$, is adjusted so the suction and blowing flow rates are equal.

4.6.2.2 Pressure-Balanced (Q-P-Balanced) Upwind Autogenous Control

The optimised pressure-balanced dual-loci control to maximise performance consisted of no control, whether by the coupled-optimisation approach or all-in-one. In other words, the Q-P-balanced dual-loci control was unable to produce a benefit to the flow through the diffuser (at this Re and α). It is a disappointing result, however it is by no means representative of all possible autogenous suction controls for this – or other – diffusers. The suction control is unable to have a major effect on the flow downstream as the free-stream flow is too far away from the wall to feel its impact. In order for

it to be effective at these locations, the suction would have to be very strong, which produces a greater pressure drop where it is applied, and thus makes it harder for the pressure constraint to be satisfied. Additionally, the optimisation study may have missed parameter combinations that could improve the flow. Therefore, further research is needed before the potential for autogenous control can be ruled out. However, the results presented in this chapter – from the parametric studies to this final optimisation – suggest that if upwind autogenous control is possible, the range of potential control parameters where it would be successful is limited.

4.6.2.3 Downwind Autogenous Suction Control

The alternative approach is to try and induce suction in the low-pressure region by the Venturi effect or otherwise in a carefully constructed duct and "blown" back into the main flow downstream. If part of the incoming flow can be diverted and used to this purpose, improvements in the overall flow may be seen. Success in this endeavour is likely to be much harder than for the flow around the circular cylinder though, because the pressure profile (when the diffuser is working correctly) continues to increase in the z-direction and never decreases again, so the suction and blowing loci would likely have to be very close together if it is to work at all. Attempting to design such a system in-situ and against these headwinds is difficult. Additionally, there are a large number of parameters at play. Therefore, the toy problem of testing Venturi-induced suction design using parallel plates was devised as a first step (this is the subject of the following chapter). Later, attempts were made to generate downwind autogenous suction in the more viable case of flow around the circular cylinder.

4.7 CONCLUSIONS

Numerical simulations were performed of the flow through conical diffusers with a wide-range of geometric and flow parameters, and controlled to maximise their performance – their ability to efficiently convert kinetic energy to static pressure. First, a great number of simulations were performed of the uncontrolled diffuser to determine the relationships between the flow characteristics, diffuser geometry, separation characteristics, and the performance of the diffuser. While much data is available for the flow through the conical diffuser, much of this is experimental and limited to only a few data-points for each setup. The effect of inlet profile on the resulting flow had not been addressed by numerical simulations (which allow for much more control and manipulation of the inlet profile) in the literature before – though, in the interceding time a paper to this effect has been published by Debuysschère et al. [2020] for the planar sudden expansion flow. Our numerical simulations exposed the dominating trends that affect the flow within the diffuser.

Second, uniform suction was applied to the diffuser wall and its strength optimised to either eliminate separation or maximise separation. Strong improvements in performance and the elimination of separation was usually possible, except at very low Re and some divergence angles. An interesting finding was that for certain combinations of $\alpha, Re, \& C_q$ the controlled flow exhibits hysteresis. When the suction is ramped down from a higher suction flow rate, a much improved flow with smaller recirculation region and better performance results, compared to if the suction is ramped up. However, it appears that the ramped down flow is somewhat unstable. Great depth on the controlled flow and optimisation of the flow was provided for the case of $\alpha = 5°$, though the key results for the optimised flow at other divergence angles were provided also.

Third, the suction control was modified to implement non-uniform suction profiles for the case of $\alpha = 5°, Re = 1000, n = 1000$. In particular the single locus profile and an unconstrained field-based profile were employed. Non-uniform suction was found to be much more effective at increasing the performance ($\eta_{out} = 0.6652$ vs. $\eta_{out} = 0.6357$ vs. $\eta_{out} = 0.4948$ vs. $\eta_{out} = 0.4345$ for the performance-optimised field-based control, single locus control, uniform control, and uncontrolled flows respectively).

Finally, methods for implementing flow-rate balanced suction and blowing control were devised and implemented. Then optimisation was carried out to maximise performance of the dual-loci control – unbalanced, Q-balanced, and P-Q-balanced. While the unbalanced control greatly improved the performance than any other control investigated, and the Q-balanced control also 34% better than the uncontrolled diffuser, when the pressure constraint was imposed the control was no longer able to produce a benefit. The key results for the optimised controls of the $\alpha = 5°, Re = 1000, n = 1000$ diffuser are summarised in Table 4.8

Table 4.8 Comparison of $\alpha = 5°, Re = 1000, n = 1000$ diffuser with different optimised controls. Note the P-Q-balanced control was unable to improve the performance.

Control	η_{out}	% Change	C_q
Uncontrolled	0.4335	-	-
Uniform	0.4720	9%	0.159
Field	0.6758	56%	0.220
Single-Locus	0.665	53%	0.145
Unbalanced Dual	0.8283	91%	-0.761
Q-Balanced	0.582	34%	0
P-Q-Balanced	-	-	-

Overall, though, the results bear good tidings for the use of suction control for the flow through diffusers. The performance of diffusers could be improved greatly by the use of suction control – both for diffusers that already perform well ($\alpha < 10°$) and for those that are unusable when uncontrolled ($25° \leq \alpha \leq 45°$). The simulations were all performed on laminar flow at low-moderate Reynolds numbers. It is known both that the dependency of the flow on Re dies out at high Re and that the effectiveness of BL suction control increases with Re, which suggests that these findings will prove only more useful in more practical flow conditions. While the efforts to generate autogenous flow control have not been fruitful for this flow – particularly upwind autogenous suction – there is the possibility of devising effective downwind autogenous control. Additionally, the models of autogenous control were fairly limited – with symmetrical suction/blowing profiles rather than more distributed and free profiles. Future work employing less restricted autogenous control setups, looking at higher semi-divergence angles, or investigating the use of the Venturi-effect (as will be described in later chapters) shows promise for improving the overall flow by passive means.

Chapter 5

SUCTION-INDUCING GEOMETRIES

5.1 SUMMARY

Generating non-uniform suction profiles is not as simple as connecting a pump to a slot, careful design of control ducting is required. To aid this design process, single-layer feed-forward artificial neural networks (ANN) were created and trained to design suction-inducing geometries. The purpose of this investigation was to ascertain whether non-uniform suction profiles could be generated by appropriate design of adjacent control ducts due to the Venturi effect. This would be a step toward practical autogenous suction control. It was found that non-uniform suction profiles could indeed be induced by appropriate geometry design, which bodes well for the application of non-uniform suction profiles generally. It was also found that ANNs could be trained for this purpose very successfully. In this toy problem of the parallel channels, the error of the networks within-dataset were very small (NMSE < 0.013–where 0 is a perfect fit) while their ability to achieve an arbitrary profile depended on the input profile and the geometry setup used in training, but could often give a good first-approximation (NMSE $= -0.6042$).

The general procedure was as follows: The flow through a 2D rectangular channel with a porous medium dividing the flow along the centreline was modelled. The flow in the lower-half represents the flow to be controlled, and the upper-half was the control channel. When no changes to the geometry are made, the flow moves through the channel with no spanwise flow, and two Poiseuille-like flows in each channel with a small streamwise component in the porous medium. Geometries of the upper wall were randomly modified within a test region and the consequent flow resolved. The flow profile normal to the porous divider (equivalent to suction/blowing for a real flow) was recorded as well as key geometry parameters. After repeating N times, this data was then used to train a neural network to solve the reverse problem: given a desired suction profile in the test region, what wall geometry is needed.

A variety of general geometry arrangements were tested – in particular regarding the constraints on the outlet of the control channel. Three setups were investigated, one

where the upper channel must return to its original dimensions after the test region and the upper wall could only be expanded (*Expand* model), one with the same criteria but the upper wall could be contracted also (*Expand/Contract* model), and the last where the upper wall could expand or contract, and the final parameter for the channel height would be maintained after the test region also (*Changing Outlet* model). In other words, the last height in the test section is maintained to the far-right boundary of the domain. The *Changing Outlet* was found to be most effective at achieving suction profiles alike those found in the optimisation of non-uniform suction studies.

Compared to a direct optimisation, the ANNs proved both effective and quick. Decent first-approximations at geometries to induce both realistic and unrealistic suction profiles were produced in milliseconds from the trained networks, including our single locus profile. While much of the information produced by an optimisation study is forgotten (as only the optimal point is pursued), the ANN approach efficiently stores key information about the flow and control which may be used at a later date. This study found that the geometries required to induce non-uniform suction profiles were complex, even in a simple toy problem like the parallel channel flow. The present results found that the ANN approach is a good supplement to existing optimisation and parametric study techniques.

5.2 INTRODUCTION

The optimisation studies of suction control on the diffuser and cylinder showed that non-uniform suction was much more effective than uniform suction. However, it is not always simple to develop a non-uniform suction profile. For the single locus case, it was argued that this profile is similar to the case for a slot, however as the slot reaches large sizes, this is less plausible. As such, it bears investigating how such non-uniform suction profile may be generated. The design of any ducting system on the internal (or external) body is critical, and there are many influencing parameters at play, as is the case for nearly all design problems. Additionally, as the purpose of this thesis was to test designs of autogenous control, a method for inducing these non-uniform suction profiles with the flow characteristics already in the free-stream was desirable.

Rather than designing a specific ducting system to produce a specific profile, it was thought a more general approach would be advantageous. One idea was to exploit the Venturi effect to produce the non-uniform suction profiles. This has three key benefits: 1) if the principle works, it could be applied for any non-uniform profile, 2) no machinery is needed to produce the Venturi suction if appropriate flow inputs/outputs can be used, and 3) The Venturi effect can produce a suction normal to the overall free-stream flow and the controlling flow (useful for autogenous cases in the cylinder).

The Venturi effect is a natural phenomenon arising from the conservation of momentum and mass, and is most well-known for its use in carburettors. When an

incompressible fluid flow is constricted, it must accelerate, as such static pressure in the flow is converted to dynamic pressure creating a region of lower pressure. This can then be reversed by gradually expanding the geometry downstream. Fluid from another area of the system can be 'pulled' into the flow due to the low pressure region at the choke point. This concept could be used to generate non-uniform suction profiles and even to produce downwind autogenous suction control. The simple Venturi consists of a linear convergence, before a linear divergence (though the converging-diverging angles are often quite different) – but what if segments of the bounding walls converge at different rates? How is the suction affected?

The Venturi approach has another advantage. Many of our studies on the optimisation of non-uniform suction control of separated flows found that the suction is often most effective when placed in regions of low pressure within the flow. This makes it difficult to naturally produce upwind autogenous suction control. To elaborate: in order to drive this suction, a region of lower pressure must be connected to the control area to drive the fluid through. If this is not available already in the flow, then perhaps it can be artificially generated through the use of the Venturi effect.

Suction may be generated in the low pressure region over the cylinder or within the diffuser through this effect. With reference to Figure 5.1, the arrangement to achieve this is best conceived by considering three key locations: the suction location, (S), the source of the controlling flow, (1), and the exhaust of the controlling flow (blowing region), (2). For the cylinder, these likely correspond to the suction area determined by the optimisation studies, the region near the leading edge, and the region around the trailing edge respectively. With this arrangement, high pressure fluid can be pushed through the leading surface at (1), have its pressure lowered by the Venturi effect such that it will draw fluid from (S) at the choke (C), and then continue to be exhausted at (2). This section from (C)-(2) will require the flow to move against an adverse pressure gradient (just as in the external flow), however the control flow may have sufficient momentum to continue through this region without separating if it has been accelerated sufficiently.

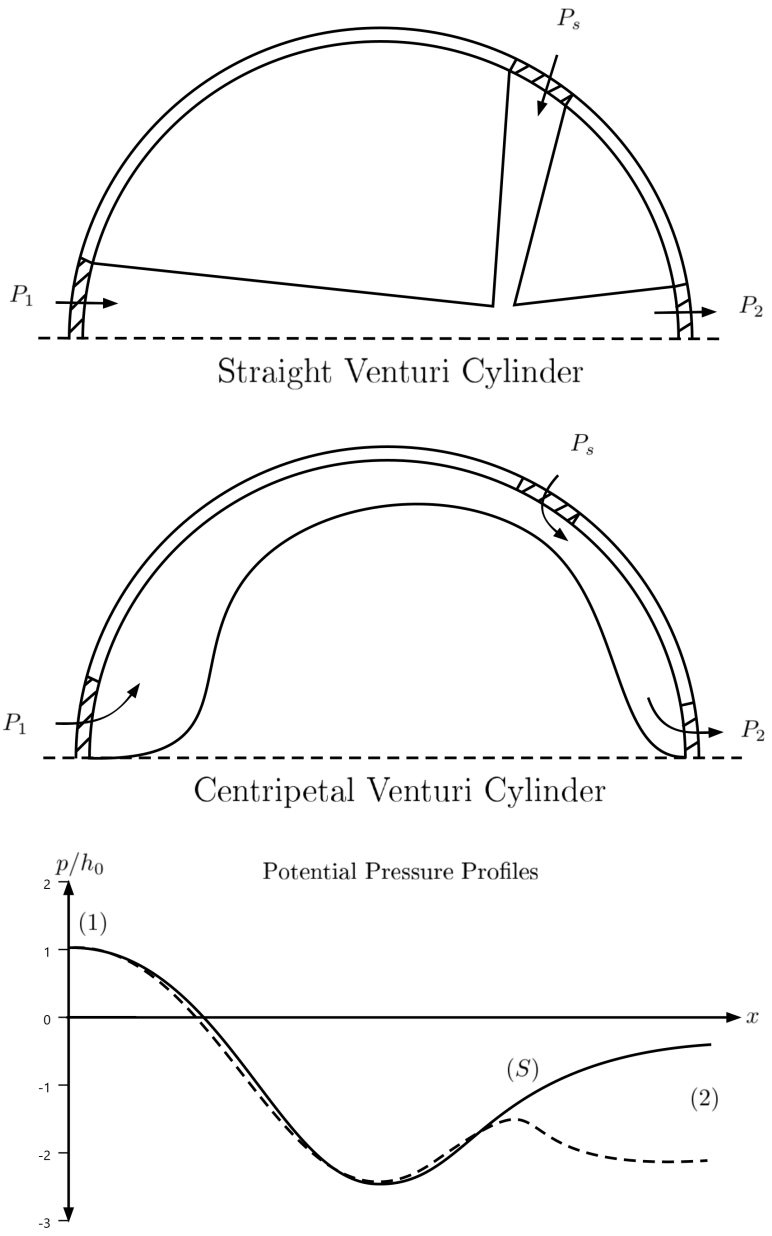

Figure 5.1 Schematic of potential Venturi duct to generate non-uniform suction in cylinder.

5.2.1 Aim of Study

The aim of this study was to investigate whether inducing non-uniform suction profiles using the Venturi effect was possible or realistic. To begin with, a simple toy problem of the flow through a parallel channel divided by a porous material was investigated. The objective was to produce a desired suction velocity (spanwise flow through the porous material) by manipulating the geometry of the upper wall. In order to get a better idea of the overall possibilities, and to investigate the use of neural networks to aid in the design of such systems, an alternative approach to optimisation was employed. Instead, randomised CFD studies were performed of the forward problem (geometry to flow),

and the collected data from these studies was then used to train neural networks for the reverse problem (desired suction/blowing profile to geometry) in MATLAB. Thus, there were three objectives: 1) Determine whether the Venturi effect could be exploited to induce arbitrary non-uniform suction profiles, 2) Build an understanding of the control duct geometries needed to produce each type of suction/blowing profile, 3) Ascertain whether ANNs would be useful for designing control ducts in real control flow cases.

5.2.2 Structure of Chapter

This chapter describes the methodology and results for designing suction-inducing geometries using ANN and comparing them to optimisation methods. First the ANN approach is described and presented, then compared to the direct optimisation which used the Nelder-Mead method to shape the upper wall directly. The influence of the ANN structure (the number of neurons) is discussed also. Finally, the key conclusions are reiterated and suggestions for further improvements provided.

Some of the results of these investigations were published in a peer-reviewed conference paper for the Australasian Fluid Mechanics Conference 2020 (AFMC) [Ramsay et al. 2020a] The conference papers were collected and published under an open-source licence. In this chapter, sections from this paper will be quoted directly, and denoted by italicised text. This is in agreement with the copyright terms of the publisher [UQ 2020].

5.3 MODEL AND METHODOLOGY

5.3.1 *Methods & Modelling*

The study involved two modelling processes: the CFD model, which includes the implementation of the geometry and resolving of the flow; and the ANNs trained on the CFD data. The details of each model are described briefly in this section. The general modelling process is shown in Figure 5.2 and proceeded as follows.

1. *The geometry constraints and data to be exported are defined and implemented in the CFD model*
2. *The geometry and mesh are generated, and the forward problem solved.*
3. *The suction profile and wall geometry data points are extracted and saved.*
4. *Return to Step 2 until sufficient data has been gathered (1000 simulations, in this study).*
5. *Training of neural network with the data from Step 3.*
6. *Test performance of network with a desired suction profile outside the existing data set ('test spike profile') and running the resulting geometry through the CFD model.*

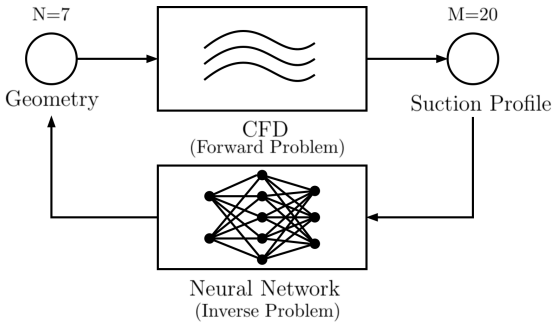

Figure 5.2 Flow chart for the modelling process

5.3.2 CFD Model

The flow domain and geometry is shown in Figure 5.3. It consisted of a 2D channel divided by a porous medium located centrally. While there is only one channel overall, in this paper the upper half will be referred to as the 'upper channel', and vice versa. Flow enters from the left boundary with a fully developed laminar profile, and exits at the right boundary with a zero relative pressure Dirichlet condition with no backflow. The middle 50% of the porous region defines the 'test section' where the shape of the upper wall is modified to induce spanwise movement of the fluid through the porous region – the 'suction'. The upper and lower boundaries were defined as no-slip walls, while the divider is defined as a porous region with porosity and permeability given in Table 1. This setup allows the flow to develop fully in all areas so each section does not interfere with those up- or downstream.

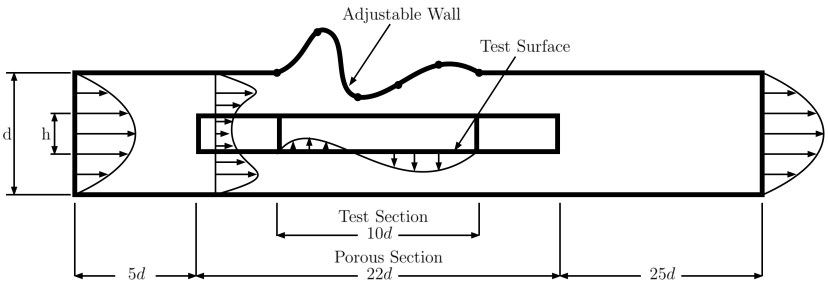

Figure 5.3 Schematic of fluid flow domain

The important input of this study was the geometry of the wall and the output: how it influenced the 'suction' observed on the lower interface of the porous divider in the test section. The upper wall was generated using N-pairs of coordinates evenly spaced in the x-direction of the test section which an interpolation curve is fitted to. The y-coordinate for each of these was randomised with a uniform probability distribution, with maximum deformation from the base case of $+1d$ or $+-0.5d$. The value of N was varied in some investigations, but was always 7 for the results presented here (including the two points at the ends of the test section).

Three geometric setups were tested. These are described as: 'Expand', 'Expand/-

Contract', and 'Changing Outlet' and are ordered in increasing complexity. Examples of resulting geometries for each of these can be seen in the Results section. 'Expand' limits the test wall to only move upwards (expand) and not contract in on the upper channel, 'Expand/Contract' allows both, and 'Changing Outlet' allows both movements but also the outlet height of the upper channel to change too (following the y-value of the Nth coordinate). In all cases, the same inlet dimensions are used where the upper channel up to the test section is identical to that of the lower channel.

The mesh consisted of predominantly triangular elements with three inflation layers on each wall surface and stretching factor of 1.2. The triangular elements had a minimum and maximum size of $\frac{x}{d} = 4.33 \times 10^{-4}$ *&* 0.04865 *respectively, with a maximum growth rate of 1.1. The mesh was generated with the default free distribution. This allowed for rapid meshing of the frequently changing geometries, and gives stable non-skewed distributions. An example mesh is shown in Figure 5.4.*

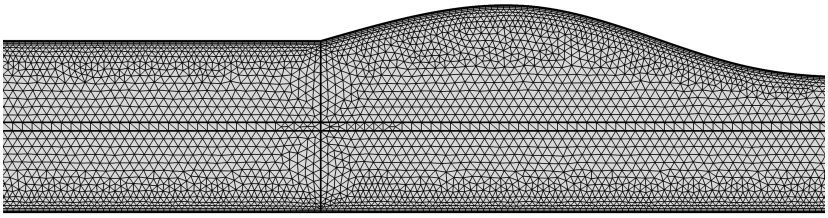

Figure 5.4 Example of mesh for Expand/Contract model showing the entry to the test section.

The flow in the 2D channel was solved using COMSOL Multiphysics (a commercial CFD package) using the 'Free and Porous Media Flow' module. COMSOL solves the governing equations using the Finite Element method, employing the PARDISO solver algorithm in this case. In the defined problem, fluid flows through porous media and in free space. The selected module solves the Navier-Stokes equations for flow in unconstrained free-space, and the Brinkman equations in the porous domain. The same velocity and pressure fields are solved for in both domains, therefore continuity is preserved and no special interface method is needed. For the sake of brevity, the governing equations are not presented here, but can be found, along with detailed discussion, in the paper by Le Bars and Worster [2006].

Table 5.1 Key parameters for the CFD model.

Feature	Symbol	Value
Channel Height	d	$0.002m$
Divider Height	h	$0.0001m$
Reynolds Number	Re	100
Maximum Velocity	$U_{max} = 1.5U$	$0.05m/s$
Porosity	ϵ	0.8
Permeability	κ	$1 \times 10^{-8}m^2$

5.3.3 ANN Modelling

The neural network was developed, trained and tested using MATLAB's built-in Machine Learning Toolbox with the Neural Net Fitting application. Simple feed-forward single-layer networks were constructed. The number of neurons in the hidden-layer was 10 except when the effect of the number of neurons was tested. The Levenberg-Marquardt method was used to train the network, with 70% of the data used for training, 15% for validation (testing for overfitting and terminating when this is the case), and 15% for testing. The purpose of the network was to solve the inverse-problem, and so it takes the suction velocity profile as its input, and outputs the co-ordinates for the upper-wall curve that should produce the suction flow (for the corresponding CFD model). The resolution of the inputs and outputs is obviously an important factor, as it is all the network sees – it knows nothing of the physical problem it is being used to interpret. M-data points were taken of the normal velocity along the test-surface, where M was 20 in this study. N-data points were used for the output.

The typical training process consists of feeding M-inputs to the neural network, these inputs are fed to each neuron which apply a sigmoid function with the neuron's weighting before passing the result as an output to the output neurons, which are N-neurons with linear activation functions. The output of the network is then compared to the real data values from the CFD model and error-metrics evaluated, in particular the normalised mean-squared-error (NMSE). Once fully trained, the network state is saved as a callable function. This can be probed by inputting a desired suction profile to the network, which will almost instantaneously return its best approximation of the coordinates that describe the upper wall to achieve that flow in the forward model.

5.3.4 ANN Testing

The effectiveness of the trained ANNs were tested on new velocity profiles that had not been generated by any of the randomised geometries. Indeed, for one of the test profiles – the spike test – it is unclear whether any geometry can physically produce it.

This out-of-dataset testing is a better method for checking the usefulness of the ANN in real cases. As such, a velocity profile using the single locus profile was also tested. In each case, desired suction velocities at each of the M probe points were input to the networks. The output co-ordinates for the upper wall were then applied to the CFD model and the forward problem solved. The resulting velocity profiles could then be compared visually and statistically.

5.3.5 ANN Structure Testing

One influencing parameter on the effectiveness of the trained ANNs, is their network structure. The networks used in this study were single-layer feed-forward networks with ten neurons in the hidden layer. This means that there is only one layer of neurons which process the data from the input layer and feed them to the output layer after applying their operations. The processor neurons in the hidden layer do not feed data to each other, so non-linear behaviour is harder to capture. The ANN performance might feasibly be improved, therefore, by changing the structure of the network. A multi-layer perceptron (MLP) network is a common ANN which is similar but has multiple hidden layers where the neurons feed each other. This was not readily accessible in the MATLAB Neural Net Toolbox, and as a study of ANN-CFD relationships was not the primary focus of this study, it was decided not to pursue this possibility. However, one variable that could be easily changed and tested was the number of neurons in the hidden layer of the single-layer ANN. One would presume that with too few neurons, the network would be relatively impotent and unable to produce complex geometry profiles. While on the other side of the spectrum, adding more neurons past an optimal point is likely to have little benefit. There is likely a optimal point appropriate for this particular problem.

To test this, the same 1000 training data for the Changing Outlet simulations were used to train and test the in-dataset (recreating geometries from their output velocity profiles) and out-of-dataset performance (producing geometries for untested velocity profiles) of single-layer feedforward ANNs with different numbers of neurons in the hidden layer. Networks with 1 to 10 neurons (in steps of 1) were tested as well as with 15, 20, 40, 50, and 100 neurons. The in-dataset performance is provided from the test procedures carried out when training the networks, while the out-of-dataset performance was measured by inputting the spike test profile to each network, simulating the resulting geometry, and comparing the velocity profile produced.

5.3.6 Direct Optimisation

The alternative approach to training artificial neural networks is, of course, to perform a direct optimisation of the geometry. Therefore, the Changing Outlet geometry was optimised within COMSOL using the same $N = 7$ points to define the upper wall,

and interpolating between the points. To get a better understanding of what model parameters could be improved in future studies, an additional study using 22 points to define the upper wall were also used. These will be referred to as the 7-point NM and 22-point NM studies. The objective was to minimise a least squares objective, comparing the velocity profile to the 'spike' profile as measured at the $M = 20$ points on the lower porous surface. The Nelder-Mead (NM) method was employed with an optimality tolerance of 10^{-7}.

5.4 RESULTS

As expected, in all cases, modifying the upper wall in the test region induced spanwise fluid motion through the porous medium. Some geometric set-ups allowed more control over the suction profile than others. In this section the results will be presented by briefly analysing the raw inputs/outputs to the neural network model, then discussing how effectively the networks achieve an arbitrary suction profile.

5.4.1 Raw Inputs/Outputs of CFD Model

The displacement of the randomised upper wall geometries (y-coordinates) and their resulting suction profiles are shown in Figure 5.5. While there is too much data to make sense of, the general trends of the plots illustrate a few features that show how changing the geometry affects the induced spanwise flow.

Firstly, the Expand setup always results in suction (+ve) at the start of the test section, and blowing (-ve) at the endpoint. This suggests that unlike the Venturi Effect, where the cross-sectional area is reduced to lower pressure and induce suction, in this case the flow appears to follow the direction of the upper wall – moving up when the wall expands, and moving downward when it contracts back to its original size at $\frac{x}{d} = 10$. *As will be discussed later, this is an oversimplification. The Expand setup greatly restricts the potential suction profiles achievable, particularly near the endpoints. The Expand/Contract, on the other hand, allows more variable profiles, including suction flow at the end of the test section, while the Changing Outlet has an even greater spread and allows strong spanwise movements at the test section end. The overall trends of all three setups show that producing a 'blowing' profile is easier than inducing a suction, as shown by the spread on the y-axis of the suction profiles. However, in all cases, suction is possible.*

Finally, these plots suggest that allowing the upper wall to expand further does not increase the suction strength. The Expand setup allowed expansions up to a length of $1d$ *– effectively doubling the channel height – however, the maximum suction velocity was actually less than the cases where the geometry changes were limited to* $0.5d$ *and where contraction was permitted.*

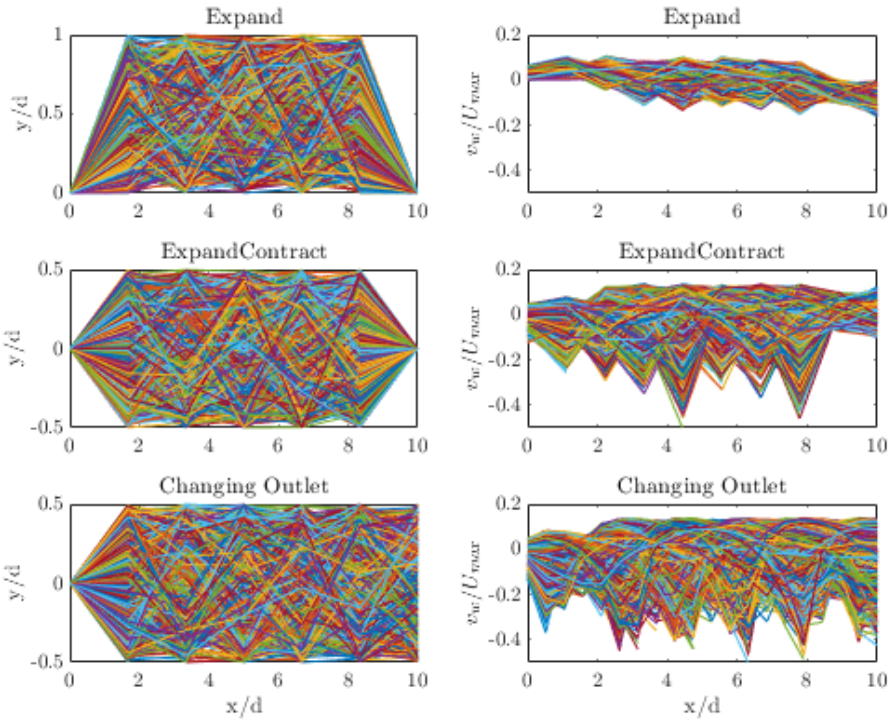

Figure 5.5 Randomised upper wall geometries (left) and the resulting probed suction profiles (right). Straight connections between probed points (as opposed to the actual interpolated or full resolution curves).

5.4.2 Network Effectiveness

The data shown in Figure 5.5 was then used to train three artificial neural networks as the output and input to the networks respectively. Once fully trained, the networks were tested on data reserved from the original dataset and their effectiveness measured by the normalised mean-squared error (NMSE) of the output compared to the actual values (normalised by the mean of the reference data). An NMSE value of 0 represents a perfect fit, 1 means a fit no better than a straight-line, and $-\infty$ bad fit. This is shown in the second column, giving a measure of the difference between the recovered geometry from a velocity profile and the true one, as taken from the test dataset.

The purpose of creating these networks was to use as a design-aid for achieving complex non-uniform suction profiles. These suction profiles may be quite complex, may be impossible to achieve with the geometry constraints used in training the networks, or may not be physically achievable at all. Therefore, the networks were also tested using an arbitrary (and quite unphysical) velocity profile target to determine how effective the networks are as a design-aid in such a case. The corresponding output of the networks, are shown in Figure 5.6, and the suction profiles they induce when run through the forward CFD models are shown alongside the target profile in Figure 5.7. In addition, the difference in pressure between the lower and upper surface of the porous divider is

shown below in Figure 5.8. The error between the desired profile and that achieved by the ANN-designed model is shown in column 3 of Table 2.

Table 5.2 NMSE of the three networks for the test portion of the generated data, and for the out-of-dataset arbitrary test profile.

Geometry Setup	**NMSE for Recreating CFD Geometry**	**NMSE for Achieving New Profile**[1]
Expand	0.0025	-4.0827
Expand/Contract	0.0106	-0.5696
Changing Outlet	0.0123	-0.6042

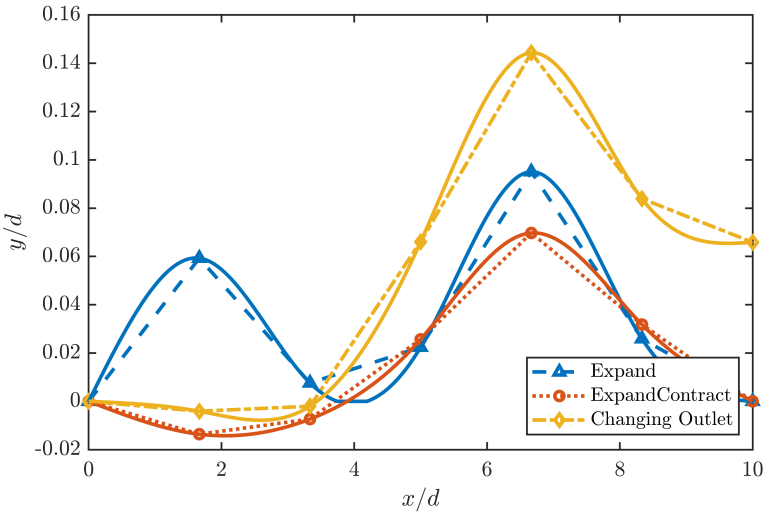

Figure 5.6 Geometries generated by the trained neural network to achieve an arbitrary 'spike' suction profile. Solid lines show the final geometry generated in the CFD models.

[1] These values differ from those published in the original article, after they were recalculated and found to be incorrect.

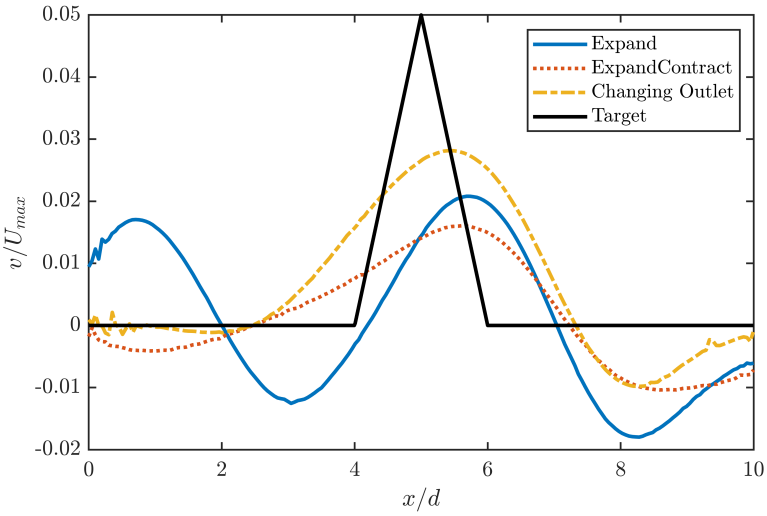

Figure 5.7 Resulting 'suction' profiles from the geometries generated by the trained neural networks

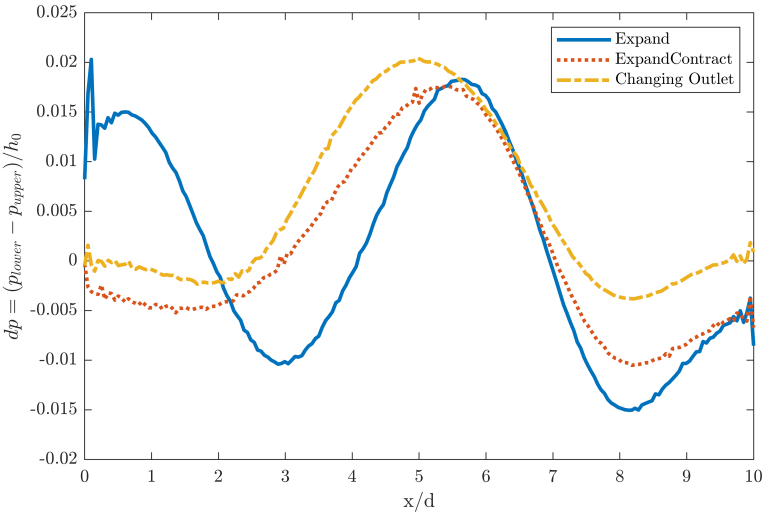

Figure 5.8 Pressure difference between lower and upper surface of the porous divider in the test section.

Figure 5.7 shows the effectiveness of the geometries designed by the neural networks, while their NMSE are also given in Table 2. It is evident from the figure and table, that the Changing Outlet setup is the most effective. While the strength of the peak suction is less than half that of the desired profile, it follows its shape well. The sharp target profile would be difficult, if not impossible, to achieve with the limitations on all the models investigated, therefore the damped nature of the resulting suction profiles is unsurprising. The Expand/Contract method is also fairly close to the target profile, achieving a single spike, but suffering from more severe troughs due to the geometry having to contract at the endpoint. The ability of the Changing Outlet setup to remain expanded/contracted allows it to achieve near-zero spanwise flow before/after peaks. The Expand model, on the other hand, has very poor performance for this target profile,

mostly due to the effects of its additional constraints. Overall, these results show that the neural networks give a good approximation of the desired suction profile – and do so, with relatively little training. Importantly, it is the scale that is the major issue, whereas the more difficult aspect – the shape – is captured appropriately by the two best networks. This is a promising result for the aims of this study.

The geometries that produce these suction profiles, shown in Figure 5.6, display similar trends between the different ANN outputs. All three peak at the $N = 5$ *point at* $x/d = 6.67$ *with an expansion on the order of* $0.1d$ *which is about twice the maximum velocity of the target profile* $v/U_{max} = 0.05$*. Due to the interpolation used in the CFD model, the final peak does not always correspond with the peak from the ANN models. Nevertheless, it is interesting that in all cases the peak is downstream of where the peak suction is desired, even though the corresponding coordinate point at* $x/d = 5$ *was available to the networks to control. This suggests that the velocity effects are felt slightly upstream of the geometry disturbances.*

The spanwise and pressure surface plots of these flows are shown in in Figure 5.9 and Figure 5.10 respectively. These show that the suction/blowing is pressure driven with a staggered pressure profile forming between the upper and lower channel when the upper wall geometry is altered. [This is easier to see in Figure 5.8 where the difference in lower and upper pressure on the porous surface is plotted directly. It is apparent that the mechanism by which the geometry induces the suction flow is by producing a favourable pressure gradient from the lower to upper channel.] *While an expansion of the upper wall gives fluid from the lower chamber room to move into, the tangential flow in the upper chamber slows due to the area increase, resulting in an increase in pressure. These two factors are in opposition which makes it difficult to design the appropriate geometry. An example of the complexity this produces is that, based on the results of these tests, a small contraction before the major expansion is needed so that the static pressure in the upper chamber is lowered before a downstream expansion can draw fluid from the lower channel without the increase in pressure undoing its work. The pressures then equalise again, and the suction stops. This is a nuanced feature that could easily be missed and it is encouraging that the ANNs capture these features.*

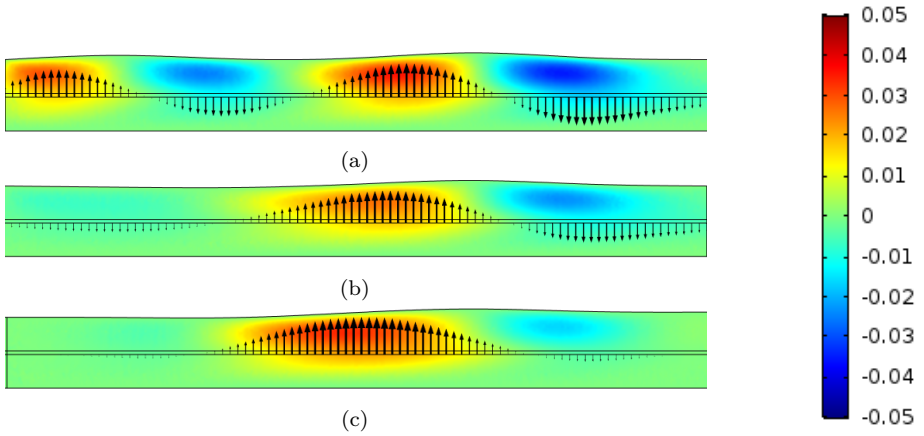

Figure 5.9 Spanwise velocity (v/U_{max}) surface plots with arrows showing spanwise velocity through the lower porous surface for (a) Expand, (b) Expand/Contract, (c) Changing Outlet geometries.

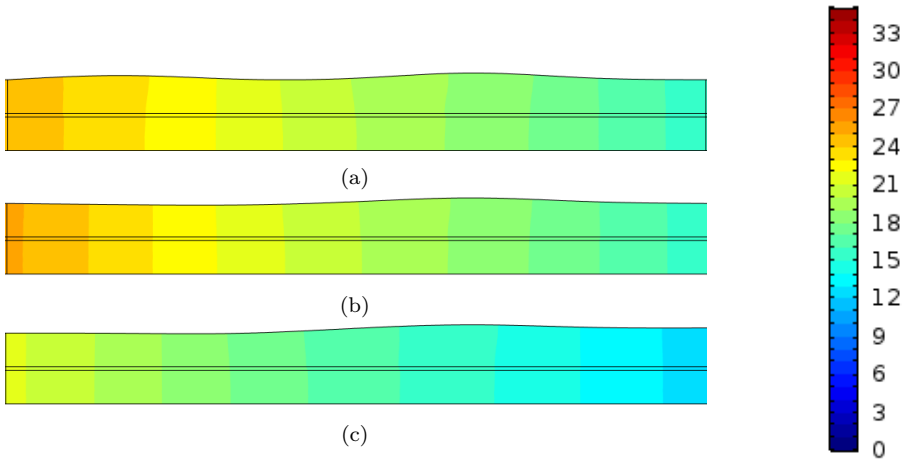

Figure 5.10 Pressure profiles in the test region for each setup. The backward-slanted contour lines before the expansions show that at the same x-coordinate the upper channel is at a lower pressure, providing an upward pressure force.

5.4.3 Comparison to Direct Optimisation

The results for the 7-point and 22-point optimised profile are compared to the ANN result for the Changing Outlet geometry in Figure 5.11 and Figure 5.12. The resulting geometry and flow for the 7-point NM optimisation is practically identical to the ANN-designed geometry. It is apparent, when comparing these to the 22-point optimised profile, that the restriction on the number of geometry points was hampering the algorithms from achieving the spike profile. The 22-point NM optimised geometry appears starkly different to those for the 7-point, however they show the same trends, just magnified. The same mild contraction and large expansion occur, just in a tighter area.

Comparing the 22-point and the 7-point results, it is clear that the number of points used to measure the geometry and velocity profile were insufficient in the ANN tests. The choice of $N = 7$ was made to reduce the number of simulations needed for training, produce reasonable geometries when randomised, and have a decent resolution. The same logic was used for using $M = 20$ points for the velocity profile. Therefore, the recommended approach – after these studies – would be to randomise with N 10 but record many more points for training the network ($N \sim 100$) as there is little cost to do so. In this way, the effects of each point in the geometry on the flow is embedded into the ANN without the downside of generating unrealistic geometries and requiring many more randomised simulations. For the velocity profile, one may as well record all the points along the test region ($M \sim 1000$ as there is little space requirements needed to store simple text files of the vectors along here.

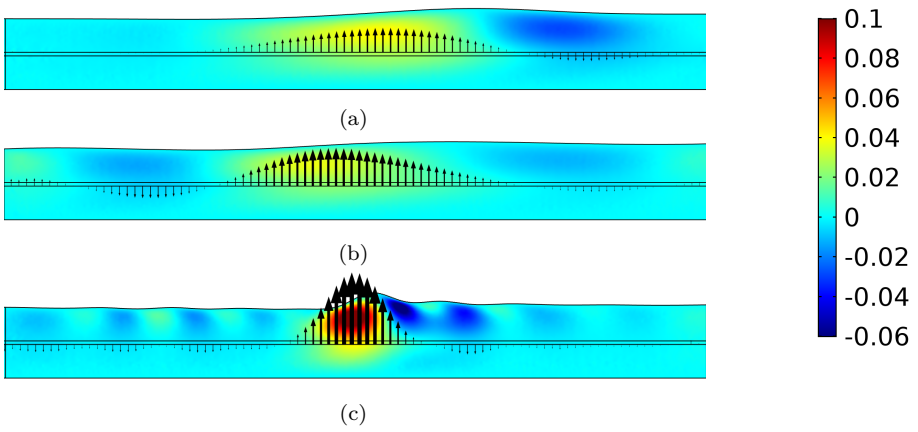

Figure 5.11 Spanwise velocity (v/U_{max}) surface plots with arrows showing spanwise velocity through the lower porous surface for (a) 7-Point ANN, (b) 7-Point NM optimisation, (c) 22-point NM optimisation produced geometries.

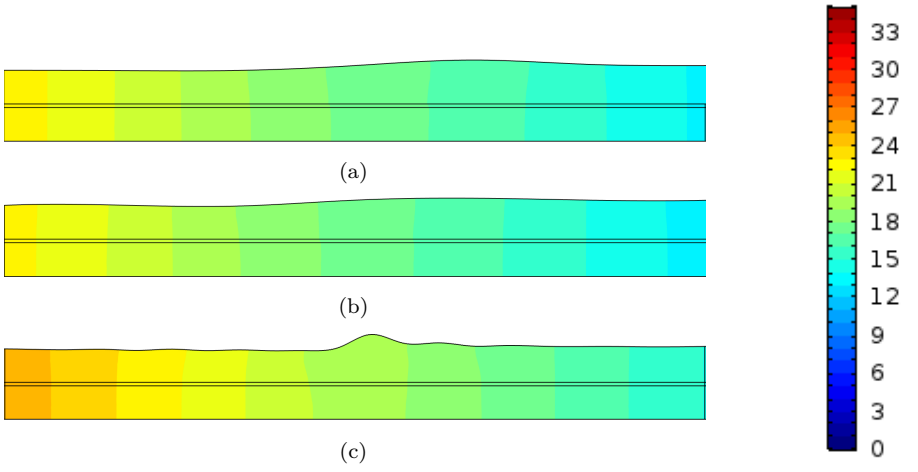

Figure 5.12 Pressure profiles in the test region for each setup.

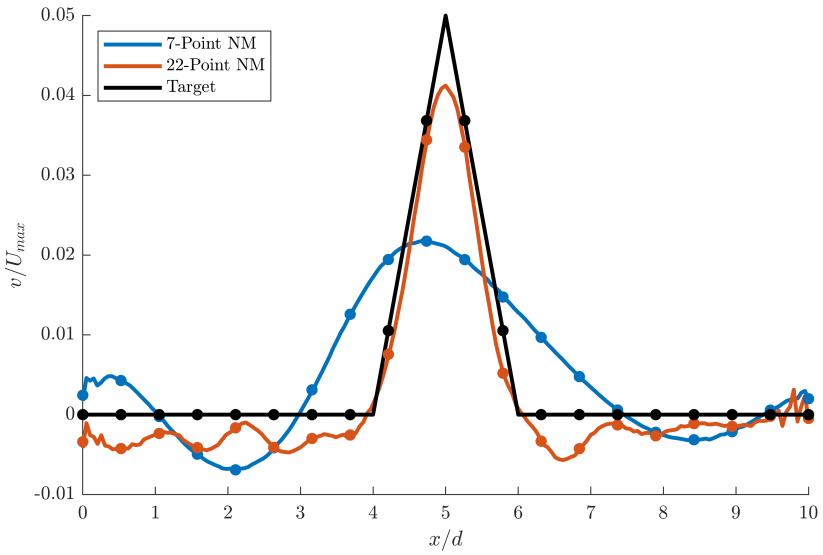

Figure 5.13 Suction velocity profiles from the direct optimisation results. The points are those where the velocity was probed for the objective (as for the ANN studies).

	Number of Simulations	**NMSE**	**Peak v/U_{max}**
7-Point ANN	1,000	-0.6042	0.024351
7-Point NM	246	0.5382	0.021824
22-Point NM	842	0.9265	0.041226

Table 5.3 Comparison of ANN approach to direct optimisation. Note the desired peak v/U_{max} was 0.05.

The number of simulations needed for the optimisation could be improved by using gradient-based methods like SNOPT or MMA. These are more complicated when performing shape-optimisation because the numerical grid must be consistent between the simulations. In this case a moving mesh approach is needed, and often shape functions (such as Bernstein polynomials) are employed to define the geometry. Even then, the limitation of optimising for a single suction profile is still present.

5.4.4 Effect of Network Parameters

The performance is shown for each network in Figure 5.14. It can be seen the figure that the in-dataset error decreases with the number of neurons (and presumably would reach a minimum when the same number of neurons as data-points are used). However, the out-of-dataset error – for achieving the spike test profile – shows that the error levels off after about 8 neurons in the network. The network with 10 neurons is very close to that with the minimum error (50 neurons) and has excellent performance for the out-of-dataset test.

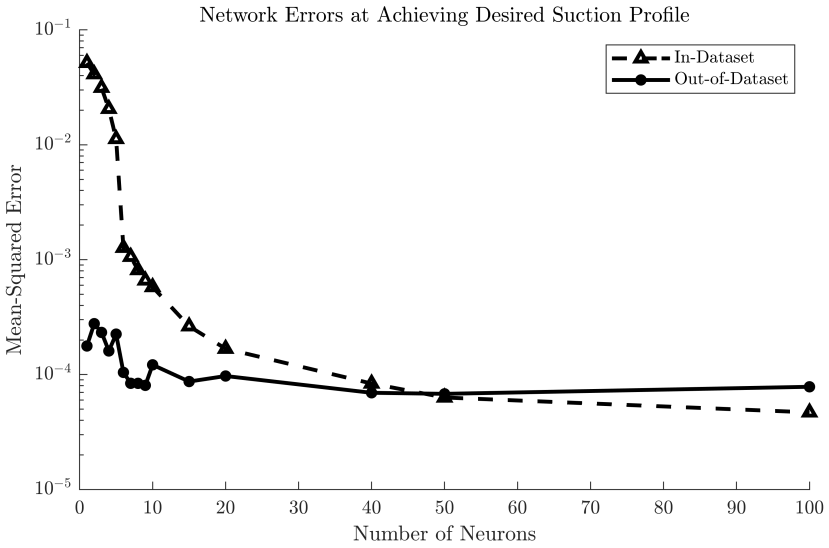

Figure 5.14 MSE for in-dataset and out-of-dataset tests of ANNs with different number of neurons in their hidden layer.

The suction velocity profiles achieved by each network is shown in Figure 5.15. It appears that the neurons stack in a similar way to the Fourier series, with low neuron networks resulting in very periodic profiles in the final velocity profile, while the higher neuron networks produce more nuanced geometries resulting in better matches for the velocity profile.

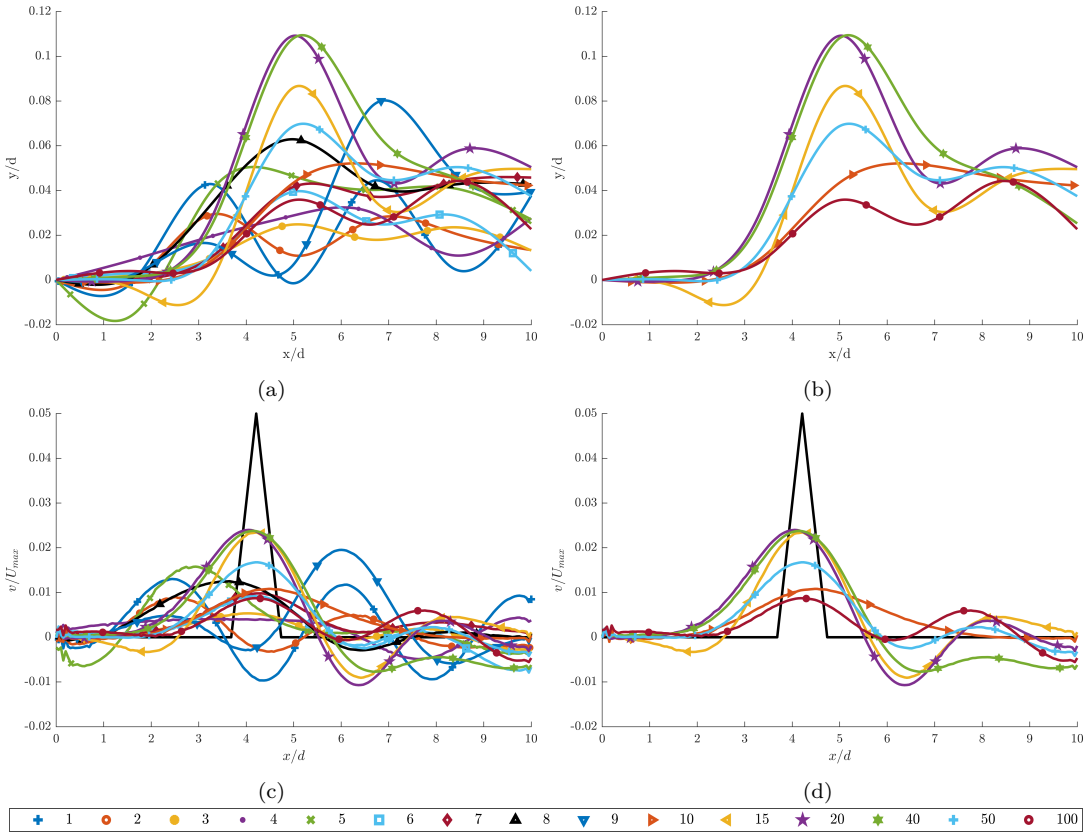

Figure 5.15 Output of ANN with varying neurons in hidden layer (a,b) for achieving the 'spike' test velocity, and the resulting suction velocity achieved by these geometries (c,d). Figures (b,d) plot fewer profiles so the changes can be seen more clearly. The legend shows the number of neurons in the networks.

5.4.5 More Realistic Profiles

The spike test profile is too unrealistic to feasibly be achieved by the present control formulation. Unfortunately, the potential suction profiles that can be tested are limited by the resolution of the velocity profile used in training the networks ($M = 20$) and the number of geometry points ($N = 7$). However, it is still possible to test something like the single locus or biased locus profiles, and we would expect a closer match to these from the trained networks. Below are the results for each geometry setup to achieve a single locus profile with parameters: $z_q = 5$, $\gamma_q = 5$, $c_{q_{max}} = 0.05$. It is important to bear in mind here that the full single locus profile is not 'seen' by the networks, only 20 points are used to define it. As can be seen in Figure 5.16, the resulting velocity profiles match much better with the desired suction profile. Even the Expand geometry, which did very poorly in the spike test, matches the peak velocity very well in terms of size and location. The Changing Outlet approach though, remains by far the best. It matches extremely well with the desired profile. The NMSE values are compared in Table 4, and while the values suggest that the Changing Outlet is little better than a straight line (which has $NMSE = 1$) this actually reflects a very good fit. The desired

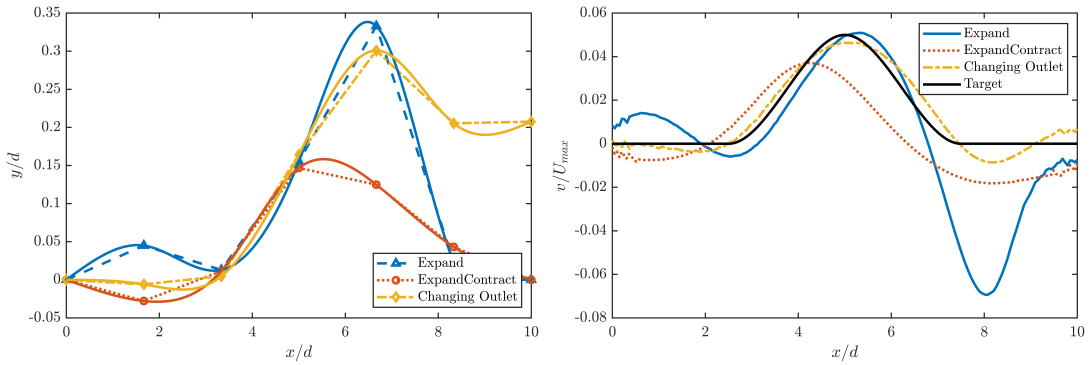

(a) (b)

Figure 5.16 The ANN geometry generated (a) and the resulting suction velocity (b) for the single locus target profile.

velocity profile is 0 at most of the x-coordinates so a straight-line is a very good fit.

The same behaviour of the geometry are seen here as for the spike test: a small contraction before the expansion to reduce pressure, then a large expansion to draw the fluid through. Here the expansion is much more gradual and lasts longer, but it is also more extreme. Where for the spike test the maximum y/d value was 0.12, here it is almost three-times higher. Presumably this is because a greater volume of fluid is being pulled through here with the spread out single locus profile. Interestingly, for the Changing Outlet case, in order to stabilise the spanwise flow, the final height of the upper wall is roughly 0.2. This is a reduction of one-third from its peak, which is the same proportion as for the spike test case too. While two examples of this phenomenon is too few to suggest a strong relationship, it is worth noting for further studies.

Table 5.4 Normalised errors for the two test profiles.

Geometry Setup	**NMSE for Spike Test**	**NMSE for Single Locus**
Expand	-4.0827	-0.8299
Expand/Contract	-0.5696	0.3217
Changing Outlet	-0.6042	0.9313

5.5 CONCLUSIONS AND FUTURE WORK

5.5.1 Conclusions

From AFMC: *"Non-uniform suction profiles for controlling separated flows are much more efficient than uniform or slot suction. Using the main body flow to generate the controlling flow (in the pursuit of passive fluidic control) requires complex geometries that are difficult to design. In this study, ANNs have been used to generate geometries*

that successfully give a first-approximation of arbitrary suction profiles. The best performing setup was that with the least constraints (Changing Outlet) and allowed for the geometry to remain expanded. None of the networks exactly matched the desired profile – particularly in magnitude – however, they give a good first-approximation, especially qualitatively. The networks could be improved by using more training data, increasing the number of geometry points under control (N) and the number of objective data points employed (M). These results suggest that using ANN in conjunction with optimisation would be a beneficial synthesis of both methods. The ANN, having been trained on a broader range of possibilities can give a strong starting point for a more thorough direct optimisation, and in combination a more versatile and rapid process can be employed."

The number of data-points used to record the wall geometry and the velocity profile are important factors. Using more data-points would allow the networks to produce more refined geometries and produce more complex velocity profiles. However, using more points to define the upper wall also causes problems for producing the training dataset for the networks. If 20 points are used, many more simulations have to be performed to get a representative dataset. Therefore, the best approach would be to use only a few points to randomise the geometry, but store many more points along the wall for training the network. In this way, the network gets a higher fidelity understanding of the geometry, without sacrificing the efficiency of producing the training set.

The design of ducts to induce non-uniform suction profiles is not as simple as exploiting the Venturi effect blindly. The results of this study show that complex non-uniform suction profiles can be produced by clever geometric design. These are particularly effective for more gradual suction profiles (like the single locus) as it was hard for the peak velocity to be produced for sharp velocity profiles (like the spike test). While we were able to make a few general conclusions about the necessary geometry alterations to produce a particular suction effect – e.g. a slight contraction before a desired suction area in order to lower the pressure and using expanding regions to pull fluid through – it would still be difficult to design a geometry manually for a given velocity input. The ANN approach takes out much of the work and provides good results.

5.5.2 Future Work

This toy problem provided confidence that this approach could be useful in the design of suction-inducing geometries which couples nicely with the work on optimal suction/blowing control. Extending this approach to a more complex geometry – such as the cylinder – or introducing an adverse pressure gradient would provide further useful information. The latter task would be particularly useful as the results of suction-only control found that the best improvement in drag and separation characteristics usually

occurred when the suction is concentrated in low pressure regions.

Chapter 6

CIRCULAR CYLINDER WITH SUCTION CONTROL

6.1 SUMMARY

Reliable relationships between the location of optimal suction and the flow and separation characteristics were uncovered. Contrary to conventional wisdom, it was found that the location of optimal suction was not always at or near the separation point – but moved with Re and in the opposite direction to the separation point. Unfortunately, for the prospect of effective autogenous suction control, the location of optimal suction was typically in areas of very low pressure within the flow (both before and after control). This threatens the usefulness of upwind autogenous control. Unlike for the diffuser, though, the prospect of downwind autogenous control has more potential for this flow. This is due to the varying and non-linear pressure profile providing appropriate sources of pressure energy available up- and down-stream of the control location. Efforts to achieve this type of autogenous control will be described in Chapter 7, but details of the pressure profiles before and after control are applied are outlined in depth here.

The results of these studies were published in two journal articles: one in the International Journal of Aerospace Engineering (IJAE) [Ramsay et al. 2020c] and the other in the International Journal of Heat and Fluid Flow [Ramsay et al. 2020d]. Sections of these papers will be quoted directly in this chapter (with attribution) in accordance with the copyright permissions of both publishers [Elsevier 2021, Hindawi 2021]. To produce a chapter that is easy to follow the logical development of these studies, the papers will be quoted in sections rather than in entirety, and conjoined by further new writing. Direct quotes are italicised and are preceded by the journal initials to indicate which paper the quote is taken from. The figure, table, and reference notations have been updated to be consistent throughout this chapter. It should also be noted that the notation used was slightly different in these papers for the suction coefficient C_q. In the IJAE paper, the subscript q is capitalised, and in both papers the value is $100\times$ the value of C_q in this thesis (reflecting the percentage of the free-stream directly rather than as a decimal).

6.2 MODELS

The numerical models for this flow were constructed and solved using COMSOL Multiphysics, the details of which have already been described in Chapter 3. Here, specific details for the cylinder model are provided briefly – quoted directly from the published papers.

6.2.1 Geometry and Mesh

From IJHFF: *The computational domain and mesh are shown in Figure 6.1. This domain was based on that employed successfully by Wu et al. [2004].*

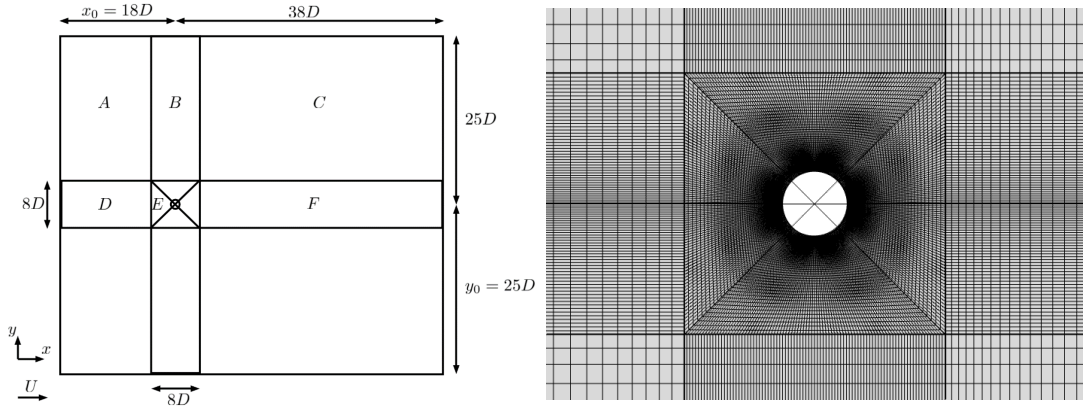

Figure 6.1 Sketch of (a) computational domain and (b) close-up view of element mesh around the cylinder

The inlet (left-boundary) was assigned a uniform flow boundary condition with velocity, $u = U = \frac{\nu Re}{D}, v = 0$. *The upper and lower boundaries were modelled as no-slip moving walls with the same velocity profile as the inlet. This minimises any potential blockage effects that may result from the artificially bounded domain. The actual domain has blockage ratio,* $BR = \frac{1}{50} = 0.02$ *which was shown to reduce the error in separation angle to below* 0.2% *by Wu et al. [2004]. A pressure outlet condition was imposed on the outlet (right-boundary) with zero relative pressure. The cylinder walls were modelled as a fixed-velocity outlet with defined normal outflow velocity,* $u_n = v_w, u_t = 0$, *where* u_n *and* u_t *are the normal and tangential velocity components at the wall, respectively. This boundary condition made it possible to define any suction or blowing profile on the cylinder wall by only changing the function that defines* v_w, *the suction velocity. In keeping with the terminology typically used in the literature, the non-dimensional suction coefficient,* $c_q = \frac{v_w}{U} \times 100$, *was used as the control parameter, from which* v_w *was defined. In this paper* c_q *with a lower case 'c' refers to the local suction coefficient at any particular point on the cylinder, while* C_q *refers to the net suction coefficient of the cylinder as a whole,* $C_q = \frac{1}{2\pi} \oint c_q d\theta$. *The two definitions will be useful given*

that non-homogeneous suction profiles are the subject of this investigation. With this boundary condition, locations where no suction is applied have the same definition as a no-slip wall.

Fluid properties for water at $20°C$ *were used for the model, employing the above equations. The PARDISO solver algorithm was used for both the steady and unsteady models [Schenk and Gärtner 2004]. For the time-dependent models, the implicit Backward Differentiation Formula (BDF) with variable order was employed for time-stepping [Brayton et al. 1972]. In these cases, 'Intermediate' time-stepping was used to reduce the Courant–Friedrichs–Lewy (CFL) restrictions while preventing the solver from dampening the instabilities that induce vortex shedding. A time-step giving 30 steps per vortex shedding period were found to give accurate results for the mesh described in Figure 6.1 and Table 6.1. With this time-step, dt is defined as* $dt = \frac{1}{30}T = \frac{1}{30}\frac{D}{USt}$*, where* T *the period of vortex shedding and St is the Strouhal number. The 'Intermediate' time-stepping setting forces the solver to take at least one time-step within each interval, but it may automatically use more time-steps within these bounds to improve convergence.*

Table 6.1 Characteristics of mesh found to be independent for steady-state and transient solutions.

Region	Number of Grid Points (x × y)	Number of Elements	Average Quality	Minimum Quality
A	20x20	400	1.000	1.000
B	90x20	1800	1.000	1.000
C	60x20	1200	1.000	1.000
D	20x90	1800	1.000	1.000
E	49x90	4410	0.843	0.500
F	60x90	5400	1.000	1.000
Total		31640	0.904	0.500

6.2.1.1 Modelling Approach

In both sets of studies, the optimisation investigations were predominantly undertaken using steady-state solvers – even in the known time-dependent regime ($Re > 48$). The justification for this was that the application of suction control was expected to stabilise the flow and therefore effectively controlled model would be resolved. To confirm that this assumption was correct, the final optimised models were simulated using the appropriate time-dependent Navier-Stokes equations.

6.2.1.2 Control Setups

In the IJAE paper, a particular focus was paid to optimal uniform suction control and using that as a baseline for comparison against non-uniform profiles. In particular,

non-uniform suction profiles composed of multiple-loci stitched together by piecewise functions – a sort of low-resolution field-based approach – were investigated in this paper. In the IJHFF paper, the best control setup from the IJAE studies – the six-loci approach – was extended to the rest of the Re in the range of present interest. In addition, more refined non-uniform suction profiles were investigated, in particular the single locus and its biased form which were described in Chapter 3.

IJAE: *The variables altered by the optimisation algorithm were the local suction coefficients, c_q, used to define the suction velocity over defined regions of the cylinder wall. To allow non-uniform suction, and impose any arbitrary profile, the suction coefficient at any point on the cylinder wall was made the output of a piecewise function. The function specifies the suction coefficient in any defined arc on the cylinder, which is then used as independent control variables. With a piecewise constant function, sharp transitions at the boundaries of the suction profile often lead to small separation bubbles. To minimise this occurrence, continuous second derivative smoothing between each data-point was used, as in [Delaunay and Kaiktsis 2001]. This provides a continuous distributed suction profile across the entire cylinder surface.*

With this method, the suction profile over the cylinder wall can be broken into as many discrete segments as desired without altering the geometry or boundary conditions - only redefining the piecewise function. Figure 6.2 gives an example of the cylinder divided into 36 arcs by the piecewise function, and an arbitrary suction profile. To avoid the suction profile imposing any asymmetry in the cross-flow direction, it was imposed that the suction profile on the lower half of the cylinder always mirrored that on the upper along the central x-axis. Therefore, a scenario with the cylinder broken into 36 segments, as in Figure 6.2, really only has 18 control parameters and will be referred to as an 18-segment control case.

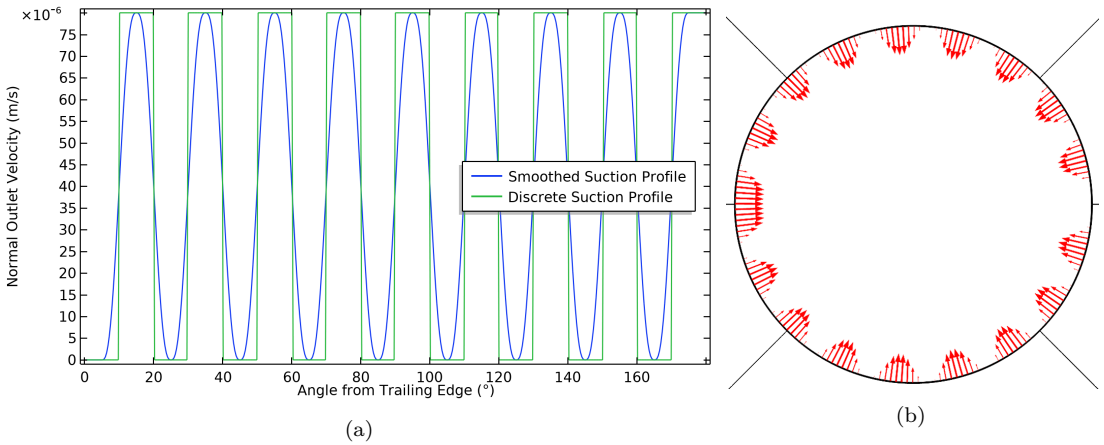

Figure 6.2 Cylinder with 18 segments alternating between $c_Q = 0$ and $c_Q = 50$: (a) Piecewise function, (b) arrow plot of velocity profile at cylinder wall.

IJHFF: *. . . three methods for applying non-uniform suction profiles were devised.*

These are summarised in Figure 6.3. The values underneath each configuration show the number of control parameters for each distribution.

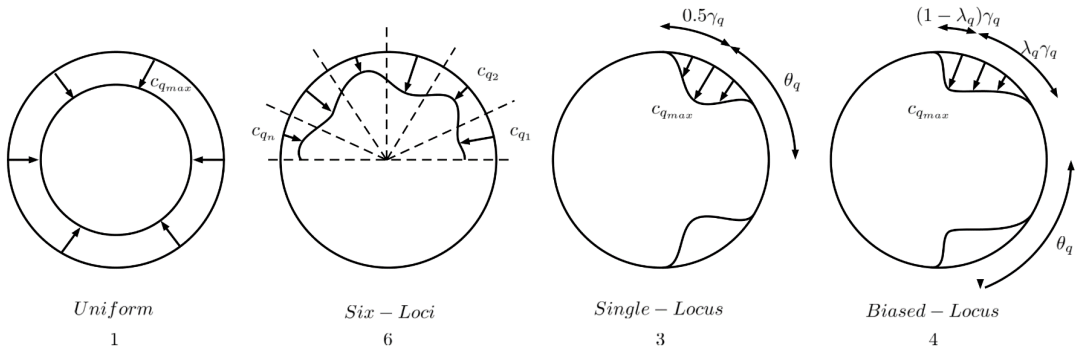

Figure 6.3 Schematic of the types of control methods investigated.

The "six-loci" control configuration can model non-uniform suction with a single locus (location of peak suction) or multiple, and thus has the most flexibility of the non-uniform suction profiles presented here. For this distribution, the upper half of the cylinder was divided into six equal segments and the suction coefficient defining the suction velocity at the centre of each was used as the control variables, c_{q_n}. As we were not concerned with the lift or lateral forces of the cylinder, the lower half of the cylinder control were set to mirror the upper half. To create a continuous suction profile from the six discrete values, pointwise interpolation with a continuous second-derivative constraint was applied. In this way, a suction profile with multiple loci of suction could be modelled. Earlier trials of using more "segments" found that six segments resulted in the best control. Using 9 and 18 loci did not improve the control while taking longer to converge to an optimised solution. At $Re = 80$ for instance, these took 35% and 135% longer to solve than the six-loci system respectively, and achieved the objective with 6% more suction than the 6-loci solution.

Earlier investigations also found that the final suction profiles from the optimisation typically have only one locus of suction. The "single-locus" control was defined to generate this type of distribution using fewer parameters. Here three control parameters are used: the maximum local suction coefficient, $c_{q_{max}}$, centre of suction, θ_q, and spread of suction, γ_q. To create a smooth suction profile, a cubic polynomial was defined from these parameters and the condition of zero-gradient was applied at the edges and centre of the profile. Thus, a distribution with compact support can be generated and its location can be varied easily by the optimisation system.

The "biased-locus" distribution was identical to the single-locus profile except for the addition of a fourth control parameter: a bias factor, λ_q. This allowed the suction profile to be asymmetrical. This does introduce the risk of a profile that is so steep it creates separation bubbles in the flow. In addition to these non-uniform suction profiles, uniform suction was also investigated. Here, only one parameter was necessary,

c_q, which was held constant at all locations on the cylinder surface. In all cases, this parameter was limited such that the suction velocity at any point on the cylinder surface could be no greater than the magnitude of the free-stream velocity. This was in order to keep the problem bounded and also feasible for real implementation.

6.2.1.3 Objectives & Optimisation Methods

The objectives and optimisation methods have already been described in Chapter 3. For some of the IJAE studies, the coordinate search was used rather than the Nelder-Mead method. For the studies reported in the IJAE paper, only the separation objective was investigated, whereas the IJHFF paper looked at the separation objective, minimising total drag, and minimising pressure drag. There was also the additional objective (used in every case) to encourage the minimisation of controller effort, only after the major objectives had been achieved.

IJHFF: *In addition to these three, an additional objective was included in each of the studies. The best suction control was defined as that which would achieve the objective with least effort, therefore a secondary objective is necessary to measure the controller effort – the net suction. This objective is defined as the cost function, J_w, below. The overall cost functional for the studies investigated here, is therefore the sum of J_w and one of the main objectives (J_n) - see Equations* (3.24), (3.31) *and* (3.32) *for the main objectives. As the efficiency of control is of secondary concern to achieving the actual flow characteristic objective, a scaling factor of 0.01 was employed in the addition of J_w to the global objective as shown in Equation* (6.2)*. It was found by trial that this was sufficient to be registered in the optimisation process, but only once the primary objective is achieved over the investigated Re range.*

$$J_w = C_q = \frac{1}{2\pi} \oint c_q(\theta) d\theta \tag{6.1}$$

$$J_{global} = J_n + 0.01 J_w \tag{6.2}$$

Because the separation angle and pressure drag objectives, J_1 and J_3, will be optimal when reduced to zero, the scalar addition of objectives is reasonable and should converge to the same result provided the scaling parameter (here, 0.01) is not too large. However, for the case of total drag, J_2, the objective can never be reduced to zero. Consequently, the scaling parameter does have a meaningful effect here.

6.2.2 Validation

IJHFF: *The model was validated by comparing the separation angles for the uncontrolled flows to those found in experiments and other numerical studies, as reviewed by Wu*

et al. [2004]. This is shown in Figure 6.4 (a). It can be seen in this figure that the time-dependent simulations model the flow accurately, with the time-averaged separation angles matching extremely well ($R^2 = 0.9993$). The instantaneous behaviour is also accurate, although the values from the literature for these values are not shown in the plot. In this study, the aerodynamic characteristics of the cylinder are of particular interest, therefore it was necessary to validate the measurements of the drag components also. Again, this was carried out by comparing the uncontrolled flow from time-dependent simulations with historical data [Henderson 1995, Tritton 1959, Wieselsberger 1922b]. These results are shown in Figure 6.4 (b) and show a good fit. The data from Wieselsberger [1922a] and Tritton [1959] come from physical experiments, while the results from Henderson [1995] are from two-dimensional time-dependent simulations. The values from Henderson are used as the benchmark in this paper as the author provided good fits to his data. They are limited, however, in that Henderson only modelled the cylinder at $Re > 25$ so the fits may not be valid for the steady regimes.

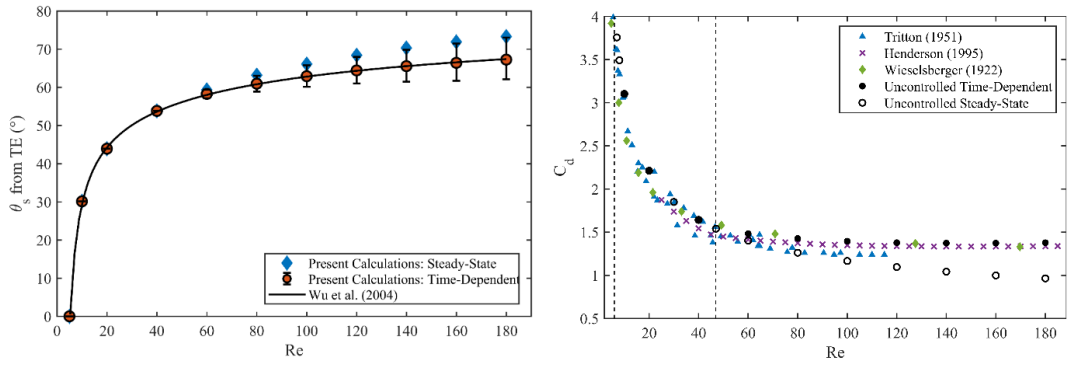

(a) (b)

Figure 6.4 Validation of model by comparison to historical data for (a) the separation angle and (b) the time-averaged total drag coefficient. Here, the error-bars indicate the span of instantaneous values, while the points are time-averaged values.

In this investigation, we made the assumption that performing optimisation using the steady-state Navier-Stokes equations would result in control that, as it should stabilise the near-wake, is also effective in the true, unsteady flow. Therefore, it was necessary to determine how the uncontrolled flow is resolved using the steady-state equations, and how this compares to the literature. As can be seen in Figure 6.4 (a), the steady-state results diverge from the expected values within the vortex shedding regime ($Re > 47$)resulting in an R^2 value of 0.9073. This is unsurprising. However, these values do follow the same trend as the actual behaviour, and they result in earlier separation angles than reality. They provide a conservative approximation of the separation angle, therefore. Similarly, for the drag coefficient, the steady-state results diverge from the actual behaviour and underestimate the total drag.

It is known that sufficient boundary layer suction can stabilise an unsteady flow, particularly near the controlled surface. We make the assumption, therefore, that control

that eliminates boundary layer separation will result in stable flows. On the other hand, it has been seen, such as in the work by Chomaz [2003], that even steady parallel wakes are not necessarily stable and can become unsteady. It is shown later in this paper, that this assumption holds true for almost the entire investigated Re range, and its effects are mostly felt in the far-wake than near the cylinder surface. The phenomena we are interested in, which arise at the cylinder surface and near wake, are therefore relatively unaffected. In fact, the maximum error in the optimised control flows was 3.29% error in the total drag at $Re = 180$*, all other characteristic features had smaller differences between the steady and time-dependent models. Further details are given at the end of the Results section.*

6.3 UNIFORM SUCTION RESULTS

IJAE: *Steady-state optimisation studies were carried out for the case of uniform suction at a variety of Reynolds Numbers (only one* c_Q *parameter for the whole cylinder). The key results are shown in Figure 6.5 below. There is a clear trend in the suction effort required to eliminate separation. At* $Re < 20$*, the suction effort is very sensitive to the Reynolds Number. This is reasonable as the separation angle for the no-suction case is very sensitive in this region as the wake develops. With increasing Re from* $Re = 20$*, the suction required decreases smoothly. A quadratic curve with equation* $C_Q = 0.0004183Re^2 - 0.2009Re + 53.74$ *has been fitted to this region as seen in Figure 6.5 (a). In addition, this figure shows that the maximum suction effort is required at* $Re = 20$*. This is unexpected as* $Re = 20$ *is in the middle of the symmetric vortex-pair regime and does not mark any significant change in the flow for the non-suction case.*

Figure 6.5 (b) provides additional information. This plot marks the separation angle before control is applied (i.e. on the cylinder with no suction) and the corresponding uniform suction required to eliminate that separation. Since Wu et al. showed that θ_s *in this Re-range could be defined solely in terms of Re, this plot is really only an alternative mapping of the one seen in Figure 6.5 (a). An uncontrolled cylinder at* $Re = 20$ *has* $\theta_s = 44.21°$*. This is very close to 45° which is an inflection point on the pressure curve for potential flow around a cylinder. The plot shows that, after the peak at 45°, the suction effort to prevent separation actually decreases despite the uncontrolled* θ_s *moving further from the trailing edge. While, the plotted curve suggests it may continue to decrease and meet the x-axis at some higher uncontrolled* θ_s*. We expect an asymptote to be reached in actuality.*

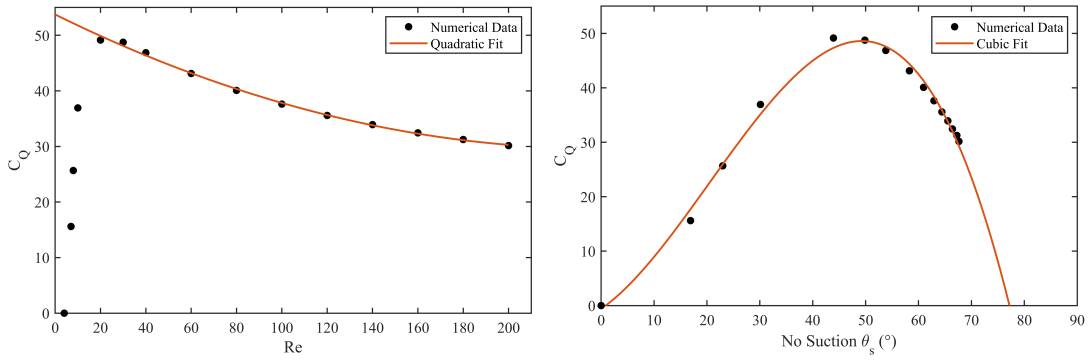

(a) (b)

Figure 6.5 Minimum suction coefficient necessary to prevent separation (a) against Reynolds Number, (b) against the separation angle without control.

The optimal parameters found by this study were confirmed by performing a variety of time-dependent simulations at $Re = 80$*. The simulations were run with a variety of suction coefficients, up to the optimal found here. This was to confirm that the above results are accurate. The results of this verification can be seen in Figure 6.6 below. This study confirmed that the optimal parameters found by the above method were correct. An apparently quadratic relationship between the suction applied and the controlled separation angle can be seen in this plot. The figure also shows that the vortex street is eliminated much sooner than boundary layer separation. Vortex shedding is eliminated between* $C_Q = 10$ *and* $C_Q = 15$*. Although the vortex shedding was eliminated at* $C_Q = 15$ *it took a much longer time than with higher suction. It is interesting to note that the angles of separation with these control parameters are 55.5° and 50.0° respectively, and vortex shedding on an uncontrolled cylinder starts at* $Re = 47$ *when the angle of separation is 55°. This and the fact that maximal suction effort is needed at* $Re = 20$ *when* θ_{s_0} $45°$ *suggest that geometric features are tightly related to the separation of the flow and its stability, and these relationships may continue to be significant even when the flow is drastically altered from the base case through control.*

Much of the motivation of this study was to investigate whether the separation angle of an uncontrolled flow is more useful in dictating the optimal control parameters than other features, such as the Reynolds Number. This would be useful for the translation of knowledge in the field of flow control. Presently, if it is desired to control the flow around a particular body – e.g. an aeroplane fuselage – it is not possible to carry much – if any – quantitative insight from control studies on a different body, e.g. the circular cylinder. Therefore, data for the optimal location of suction or the strength of suction on the cylinder at a particular Reynolds number is not transferable directly to the fuselage. Indeed, even comparing the Reynolds Number directly is not straightforward, as exhibited by the potential differences in critical Reynolds Number at which turbulence commences. This means that the engineer seeking to improve the flow around the aeroplane fuselage must define and perform their own flow control study and optimisation – a costly and

time-consuming exercise.

The present results suggest, however, that instead of comparing the Reynolds Numbers – and the control parameters for best performance at these Reynolds Numbers – comparing using the separation angle may be more appropriate. Unlike the Reynolds Number, which gives no information about the resultant flow (as seen by the same Reynolds Number describing both our uncontrolled separated flow and the controlled unseparated flow, here), the location of the separation point is both characteristic and accounts for all the static and dynamic effects in the flow. Therefore, the engineer designing control of a fuselage, need only know the conditions of the baseline uncontrolled flow in order to design a good first attempt at control using results from a flow control study on the circular cylinder. The distance of the separation point to the trailing edge may act as the 'zero-point' around which to design – regarding the location and strength of suction (or other flow control parameters). It should be stressed that the present paper does not resolutely confirm that this is, or can be, the case. However, the results do show a good dependency between the optimal control parameters and the separation angle of the uncontrolled flow.

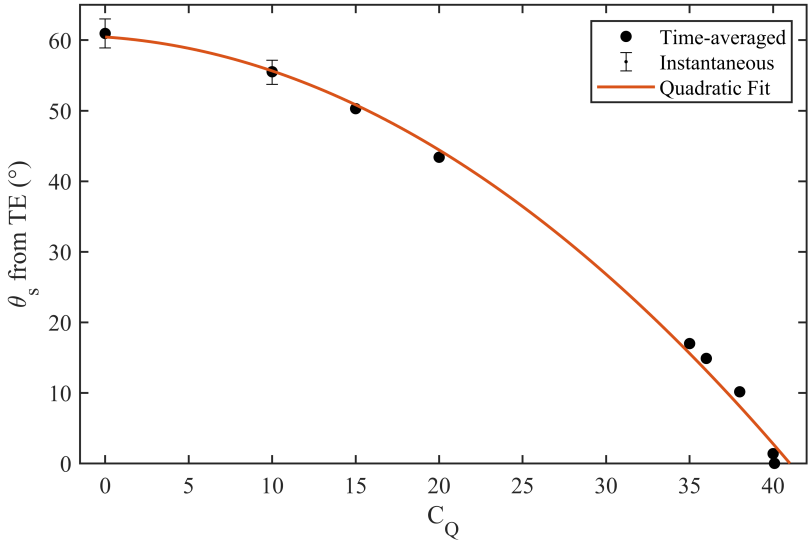

Figure 6.6 Effect of uniform suction strength on the angle of separation at $Re = 80$. Where vortex shedding occurs, the maximum and minimum θ_s is shown with error bars.

6.4 NON-UNIFORM SUCTION RESULTS

The discussion of non-uniform suction control will follow the order in which the simulations were performed and the control refined. First the segmented control (six-loci and the like) which were performed in-depth at $Re = 180$ and presented in the IJAE paper. Again, these studies only looked at the separation objective. Then the 'locus approach' of the single locus, biased locus and six-loci control as reported in the IJHFF paper. These results are lengthier and dive into greater depth on the impact of non-uniform

suction control on the flow around the cylinder. Finally, unpublished results in using the field-based approach are presented and compared to the loci-profiles and outcomes.

6.4.0.1 Segmented Control

IJAE: *Eight optimisation studies were carried out with non-uniform suction at* $Re = 180$ *using the Coordinate Search method. In each study, the number of control segments was altered to provide finer control of the suction profile. One additional study was performed using the Nelder-Mead (N-M) optimisation method to test the effectiveness of the Coordinate Search. The key results of these simulations can be seen in Figure 6.7 below.*

From the results we can conclude that non-uniform suction is more efficient than uniform suction. Additionally, the total suction required to prevent separation tends to decrease with increasing number of control segments. The decreasing trend in controller effort appears to reach a floor in effectiveness where further increasing the number of segments (and the resolution of the potential profile) is no longer effective at improving the performance or efficiency. The results from 9- and 18-control segments being almost identical. This would suggest that increasing the number of control segments further would not improve the control, despite being able to manipulate the suction profile more precisely.

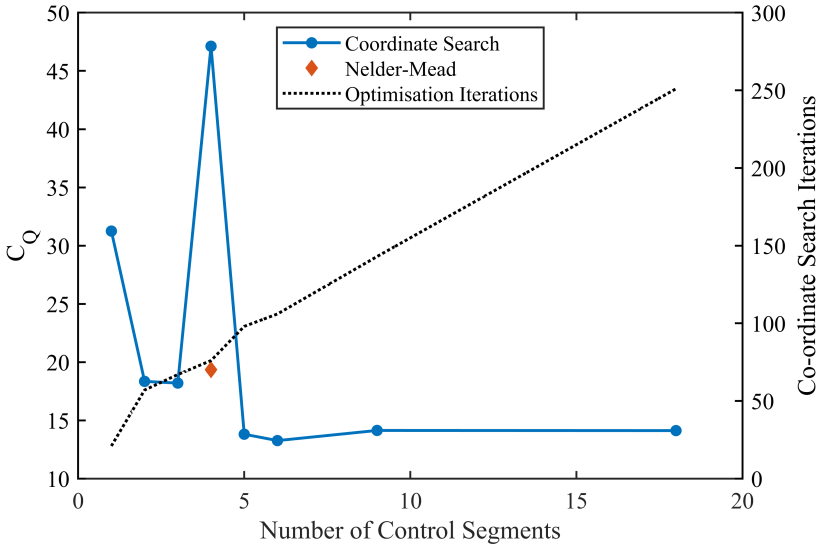

Figure 6.7 Effect of increasing number of control parameters on optimal suction.

As can be seen in Figure 6.7, the best control is achieved with six control segments, and requires an average suction coefficient of $C_Q = 13.26$. *This is less than half that required for uniform suction. The suction profile and resulting flow for this 6-segment control are shown in Figure 6.9. It is interesting that the best result is achieved with less control parameters than others investigated. One would expect the most efficient control*

would be achieved when the suction can be manipulated most precisely. In this instance, it seems reasonable to conclude that the slightly worse results with 9- and 18-segments is due to the Coordinate Search method converging to a local minimum. The Coordinate Search is a relatively simple optimisation method. As it is one-directional in each step, it is more likely to fail at finding the global optimal when the parameter space is very complex. This is illustrated by the drastic difference in optimised control when the Nelder-Mead (N-M) method was used as for the 4-segments case. This result suggests that a different optimisation algorithm may be more appropriate when the number of control parameters is large. Regardless of the optimisation approach, guaranteeing that a global minimum is reached is impossible without a thorough analytical proof that is not available for this system. The Coordinate Search is effective and quick for most situations investigated here.

Even with the improvement in controller effort when the N-M method was employed, the 4-segment case is still worse than the adjoining 3-segment case, despite the ability for the control to be more discriminate. We suggest that this discrepancy is due to the location of the control boundaries on the cylinder for 4-segment control – namely at 45° and 90° from the trailing edge. In all control cases investigated for $Re = 180$*, the optimised suction profile featured maximum suction in the region approximately 45° from the trailing edge, see Figure 6.8. The 4-segment control can only affect control at this critical angle by manipulating two control parameters in unison, due to the border of control segments being defined at 45°. It is, therefore, impossible to achieve an effective control with this setup. This implies two important conclusions: 1) the location of the suction (angle of suction) is of critical importance in the effectiveness of control, and 2) the control must be set up to account for this. Indeed, other investigations have verified the importance of the location of suction for delaying separation on the circular cylinder, including that this is dependent on the Reynolds Number. Consequently, an ideal control that will be effective over a range of Re must be able to account for the changing location of optimal suction.*

The optimal scenarios were tested with time-dependent simulations which confirmed their ability to stabilise the flow and keep it attached over the entire cylinder. For the uniform suction case, the true optimality was confirmed using parametric studies as shown in Figure 6.6 above. For the non-uniform profiles it is difficult to determine that the global optimum has been achieved without a more comprehensive search of the parameter space, but this would require very long simulation times. Comparison to similar situations in the literature can verify the results partly, however. Some of the optimal control suction profiles are shown in Figure 6.8 below. As can be seen in the figure, the best suction profiles ($N > 5$*) all featured maximum suction over the rear-half of the cylinder, particularly in the region* $30° < \theta < 90°$*. This fits well with the results seen in literature for both distributed suction [Lachmann 1961], and slot suction [Kim and Choi 2005]. Qualitatively, the optimal suction profile found with 18-segments is*

similar to that found by Li et al. [2003] using the adjoint method at $Re = 80$ *with 18 suction and blowing parameters (see Figure 5 of that paper). Unfortunately, the results cannot be compared quantitatively due to the differences in objectives and control setup.*

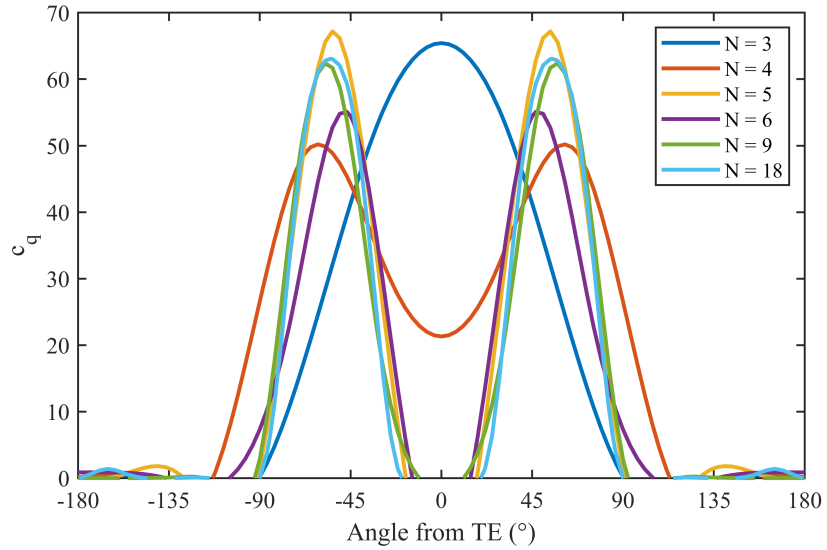

Figure 6.8 Suction profiles generated by optimisation with varying number of control segments, N. The Nelder-Mead method result for $N = 4$ is used here.

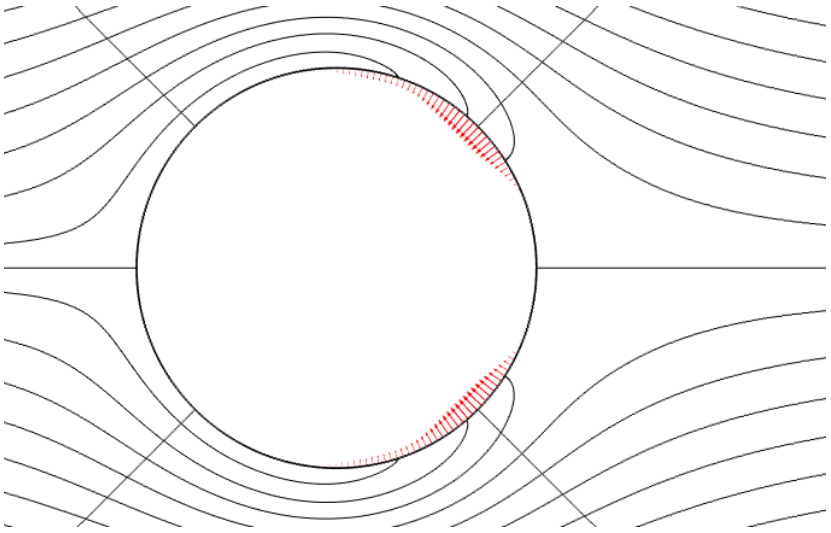

Figure 6.9 Optimised suction profile at $Re = 180$ with 6 control segments and streamlines of stabilised flow.

Verification of Optimised Results *Given the optimisation study employed steady-state simulations – which were found to be somewhat inaccurate for the uncontrolled case – it was important to verify the results with the validated time-dependent model. For each verification, the final solution for the uncontrolled time-dependent study was used as the initial conditions for the new study. In other words, the flow with the vortex shedding already fully developed was used as the starting point for these simulations. The*

fine-resolution time-stepping from that study was also used here. To maintain numerical stability the suction profile was introduced using a ramp profile increasing from 0% at $t^* = 42$ *to its full value at* $t^* = 142$*, where* t^* *is the non-dimensionalised time-value* $t^* = t\frac{U}{x_0}$ *and* x_0 *is the distance from the inlet to the centre of the cylinder (*$x_0 = 18D$*). The simulations were then run until the flow had fully developed and was steady for at least* $t^* = 20$*. The resulting flow fields for the flow with and without 18-segment control are shown in Figure 6.10. A plot of the separation angles and aerodynamic coefficients over time with the optimal uniform suction and 18-segment control is presented in Figure 6.11*

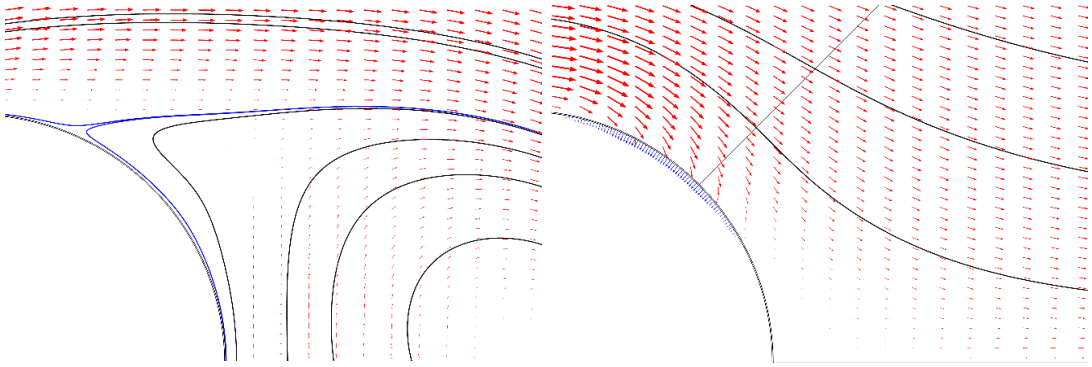

(a) (b)

Figure 6.10 Streamlines and velocity vectors for $Re = 180$ at (a) $t^* = 0$ and (b) $t^* = 180$ with the optimized 18-segment control. Blue streamlines originate from the curve used for θ_s detection.

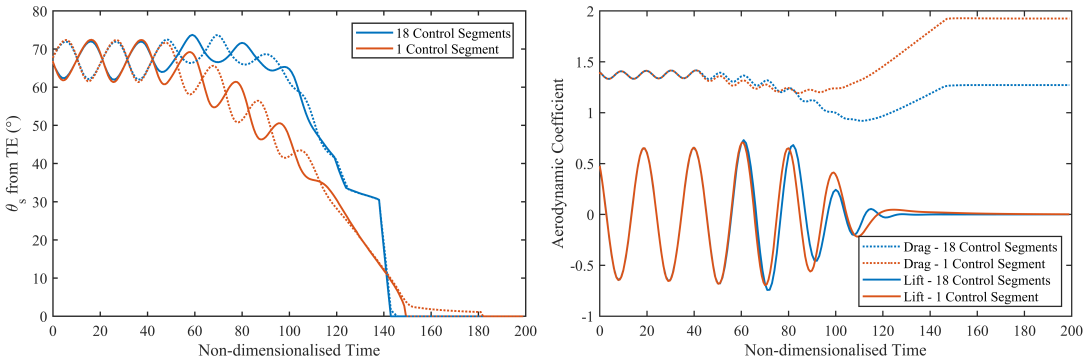

(a) (b)

Figure 6.11 Effect of the 18-segment optimised suction control on flow at $Re = 180$: (a) separation angle with dotted-line as value on upper cylinder, solid-line for lower half, (b) lift and drag coefficients (with lift plotted by the lower curves)

From the results, it is apparent that both controls eliminate separation of the flow, however the 18-segment control is slightly faster at achieving this goal. Despite reaching its full profile at $t^* = 142$*, the uniform suction control does not eliminate separation entirely until* $t^* = 182$*, whereas the segmented control does so immediately upon reaching its full profile. On the other hand, the 18-segment control is more sensitive to its*

parameters as shown by the sudden changes in the separation angle. This is likely because the control is more acutely applied, and therefore is more sensitive to flow conditions and its own parameter values. An analogy to dynamic control seems appropriate, with the uniform control similar to an overdamped system, while the 18-segment control is critically damped but potentially unstable. Another interesting feature is that the 18-segment control initially worsens the separation before improving it, despite both controls being activated at the same time-step. This is likely due to the more directional profile of the non-uniform suction, making its effect sensitive to the phase of vortex shedding when it is activated.

Despite these differences, both controls stabilise the flow (stop the vortex shedding) at the same time-step, $t^* = 130$. It should be emphasised that the suction to eliminate vortex shedding is less than that required to eliminate separation, as this example shows. The elimination of vortex shedding or the minimisation of drag has usually been the focus of research when investigating flow around cylinders, so further comparison between these two critical controls may be useful.

6.4.0.2 Locus Control

IJHFF:

Separation objective *In this section, we present results from the optimisation studies that employed objective to minimise the separation angle, J_1. We investigate the effectiveness of each suction control setup, with particular focus on the total suction coefficient, C_q, the centre of suction, θ_q, the effect on drag and its components, and the pressure profile over the cylinder with and without control.*

Comparison of control configurations *For all control configurations, the objective of eliminating boundary layer separation was successfully achieved. A sample of the resulting flows can be seen in Figure 6.12 along with the instantaneous flow field of the uncontrolled case for comparison. It can be seen in these figures that the controlled flows all have a similar structure, with a much smaller, symmetrical wake. The streamlines illustrate how the freestream fluid is entrained as it passes the cylinder to replace the fluid removed through the suctioned surface. An important feature to note is that the velocity vectors of the flow near the top and bottom of the cylinder are much larger in the controlled cases. As there is no longer stagnated or separated flow downstream, the fluid can move more quickly over the cylinder – more like potential flow.*

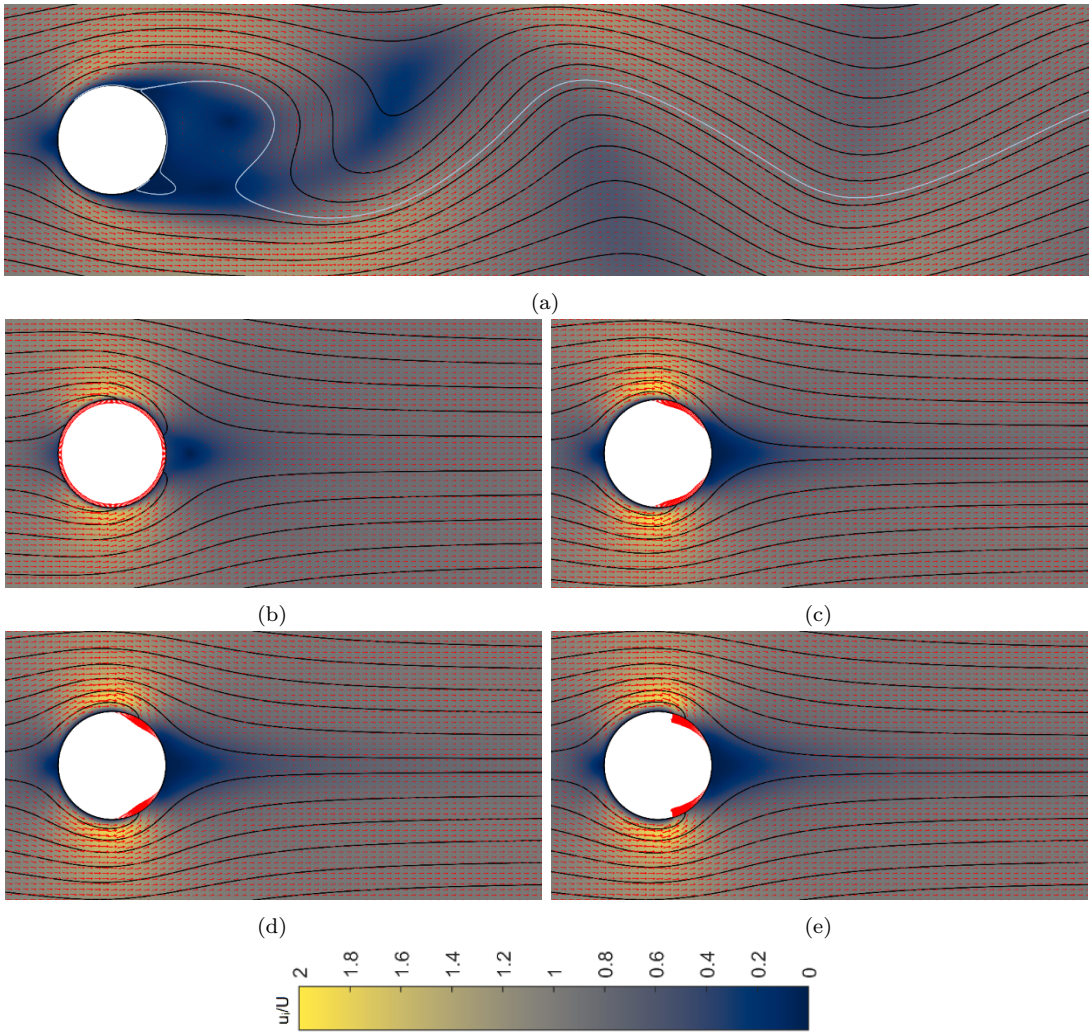

Figure 6.12 Instantaneous flow fields for controlling separation angle at $Re = 120$: (a) uncontrolled case, (b) uniform suction, (c) six-loci control, (d) single-locus, and (e) biased-locus distribution. The streamlines, non-dimensionalised velocity vectors ($\frac{u_i}{U}$) and non-dimensionalised velocity surfaces ($\frac{u_i}{U}$) are shown. The dense red arrows on the cylinders map the suction profiles.

The amount of suction required to eliminate separation is much greater for the uniform case than the non-uniform methods of control. The plots in Figure 6.13 show the suction quantity coefficient, C_q, against the Reynolds number and against the initial separation angle before control is applied, θ_{s_0}. It is clear from this figure that uniform suction requires much more control effort to eliminate separation compared to any of the other methods. In all instances (except the trivial non-separated cases), the control effort is at least twice that of non-uniform suction.

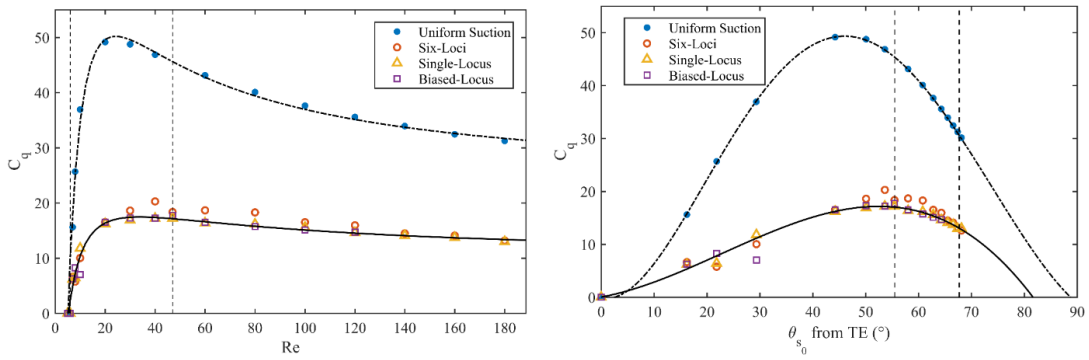

Figure 6.13 Global suction coefficient for optimised control to prevent separation plotted against (a) the Reynolds number, (b) the separation angle of the uncontrolled flow. The dashed vertical lines indicate regime changes of the uncontrolled flow.

These plots exhibit relationships between the uncontrolled flow features and the necessary control effort. For all control configurations, the amount of suction required to eliminate separation increases in the vortex-pair regime ($Re < 47$) up to a point, after which it decreases with increasing Re. Figure 6.13 (a) provides rational fits for the uniform and single-locus data each with a 2^{nd} degree numerator and denominator. For the relationships with the initial separation angle in Figure 6.13 (b), polynomial fits were more appropriate.

One of the important features shown in Figure 6.13 (a) is that decreasing suction effort is required to eliminate separation with increasing Reynolds number once the flow has become supercritical. This can be explained by the balance of inertial and viscous effects in the boundary layer before and after control. Suction through the bounding wall is an effective control because it removes low momentum particles from the boundary layer which are replaced by high momentum fluid particles from the free-stream. This delays the stagnation, separation and reversal that usually occurs. At higher Reynolds numbers, the difference in momentum between the particles in the boundary layer and the free-stream is more extreme. Consequently, given the same suction control, the stimulation of the boundary layer will be more substantial at higher Reynolds numbers. Hence, the net suction coefficient necessary to eliminate separation decreases with increasing Re. This analysis also describes why C_q decreases at different rates between the uniform and non-uniform controls. As boundary layer particles are removed from the flow at all locations on the cylinder for uniform control, the total momentum change is more significant than for the concentrated effects of the non-uniform control.

Figure 6.13 (b) shows a further interesting result. The peak control effort to eliminate separation for the uniform suction case occurs when the initial separation angle is situated at 45° from the trailing edge. On the other hand, when non-uniform suction is employed, the peak effort is aligned with the regime change at $Re = 47$ when vortex shedding commences. This suggests that optimal application of the methods of

suction control are influenced differently by the initial flow.

Extrapolating the trends shown in Figure 6.13 to higher Reynolds numbers suggests that the suction control effort would asymptote near $C_q = 23$ *and* $C_q = 10$ *for uniform and single-locus suction respectively. Pankhurst et al. [1953] found that a suction quantity of* $C_q\sqrt{Re} \geq \frac{30}{\pi}$*, was required to eliminate separation on a cylinder fitted with a splitter plate in the Re range of* $10^4 - 10^5$*. Extrapolating the present results to this regime, suggests a suction coefficient of only* $C_q\sqrt{Re} \approx \frac{14}{\pi}$ *is necessary, contrary to their experimental results.*[1] *Likewise, Pankhurst & Thwaites' relationship cannot be extended to the present regime,* $Re < 188.5$*, as it would suggest a suction coefficient of* $C_q = 150.9$ *would be required at* $Re = 40$ *to stabilise the flow, which is not the case. The Reynolds number does not contain sufficient information about the drastic changes in flow features to allow for these relationships to be extended. This is particularly the case here, given the substantial differences between laminar and turbulent boundary layers and, consequently, the effect suction has on these.*

On the other hand, the separation angle is a feature of the uncontrolled flow that itself is altered with the regime changes. Since, there is a trend between the uncontrolled separation angle, θ_{s_0}*, and the required control, it may be possible to extend the relationship with* θ_{s_0} *into higher Re ranges. After all, the mechanism by which the suction reinvigorates the boundary layer should also remain the same whenever the boundary layer and the shear layers directly adjacent to it are still laminar, in other words, almost up to the transition to turbulence at* $Re \approx 2 \times 10^5$

Optimised suction profiles *Since there seems to be little advantage in using the more complex biased-locus distribution over its symmetrical variety, the rest of the results will be concerned with the single-locus profiles only.*

An interesting result for this objective was how much the optimised profiles move and morph depending on the Reynolds number. At low Re, the suction profiles are narrowly spread and positioned near the leading edge of the cylinder. As Re increases, the profile spreads wider and moves farther leeward on the cylinder. This shift can be seen in Figure 6.14 where a sample of the results at different Re are shown for the single-locus control. In addition, lines marking the uncontrolled separation angle and the centre of suction are shown for each profile. Evidently, there is a relationship between the suction centre, θ_q*, and the Reynolds number (and by extension the uncontrolled separation angle as well). Figure 6.15 (a) and (b) plot these relationships respectively.*

From Figure 6.15, it is clear that there is a strong relationship between Re, θ_{s_0} *and* θ_q*. Similar discussion can be made about these relations as for* C_q *in the earlier section. These points will not be repeated beyond stating that the results confirm a dependence on*

[1] *Pankhurst & Thwaites defined* C_q *as the flow rate through the porous wall divided by (UD), i.e.* $C_q = v_w/U\pi$ *according to our notation, hence the introduction of the* π *term to their equation in this text.*

the Reynolds number and also on the uncontrolled separation angle for the application of suction control; that it is not constant at all Re; and that it would be of interest to see how these relationships change when extended to higher Re. There appears to be less correlation with the spread of suction, γ_q, which has an average value of 75°.

One particular feature is worth noting, however. That is the surprising result that the location of optimised suction is not centred on the uncontrolled separation point as has typically been considered the best location for this type of control [Atik et al. 2005]. In fact, θ_q moves in the opposite direction to θ_{s_0} with increasing Re. This suggests that the optimal application of boundary layer suction is not to remove the boundary layer at all locations, or even to maintain the boundary layer at the cusp of separation, but rather to manipulate the pressure profile around the body and in this way influence the separation point indirectly.

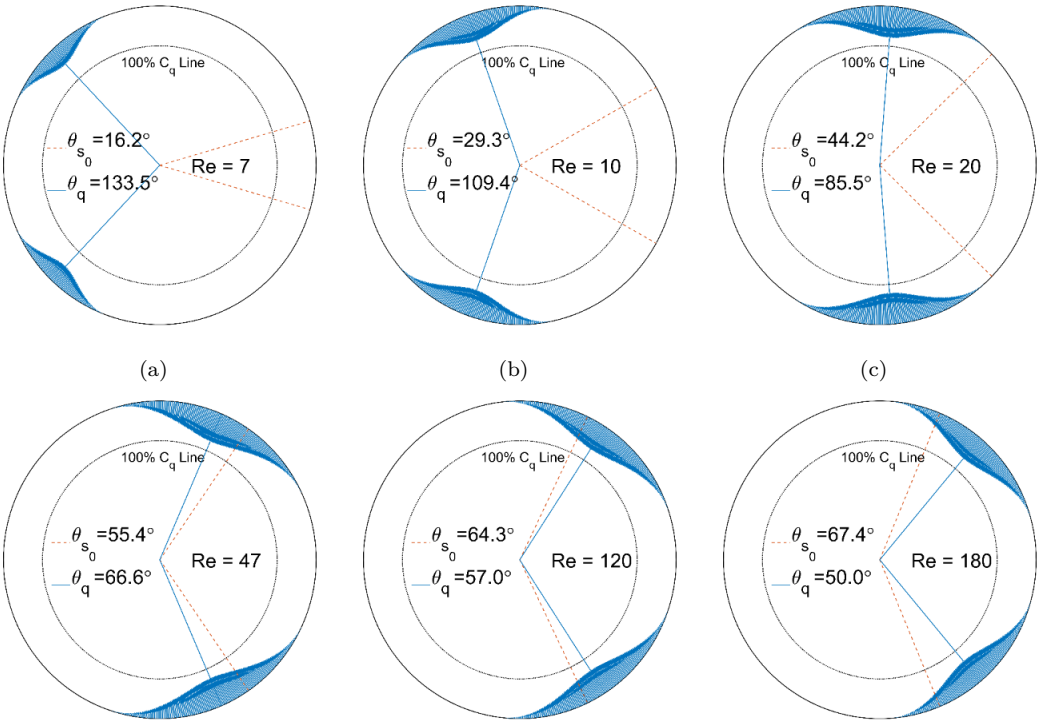

Figure 6.14 Variations in optimised suction profiles for single-locus control at various Re. The inner dotted circle marks where the local suction coefficient is 100, i.e. $v_w = U$. The uncontrolled (initial) separation angle, θ_{s_0}, and resulting centre of suction, θ_q, are also plotted as the orange and blue lines respectively. Their values area also displayed.

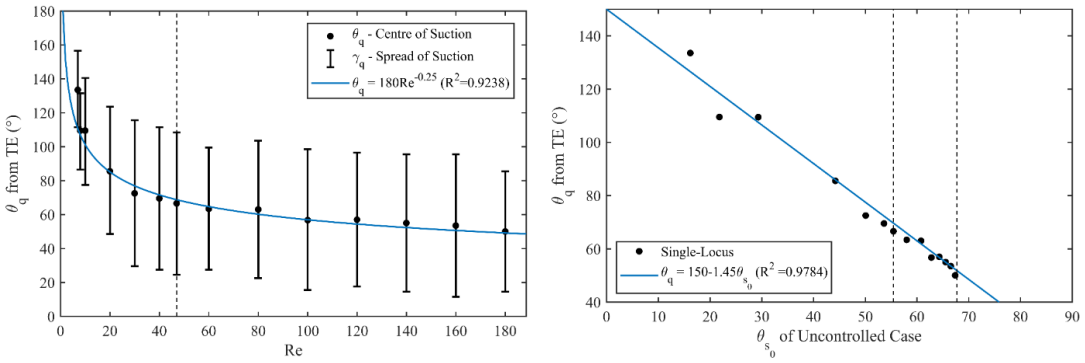

(a) (b)

Figure 6.15 How the non-uniform suction profile with single-locus control moves with (a) Reynolds number and (b) initial separation angle. The vertical lines mark the regime changes of the uncontrolled flow.

Effect on drag *The drag components for the final controlled flows were evaluated. These are plotted in Figure 6.16 alongside the values for the uncontrolled case using the relationships taken from the numerical analysis by Henderson [1995]. There are several features to note here, in particular: the general trend of the total drag, C_{d_t}, and the behaviour of its two components, C_{d_f} & C_{d_p}.*

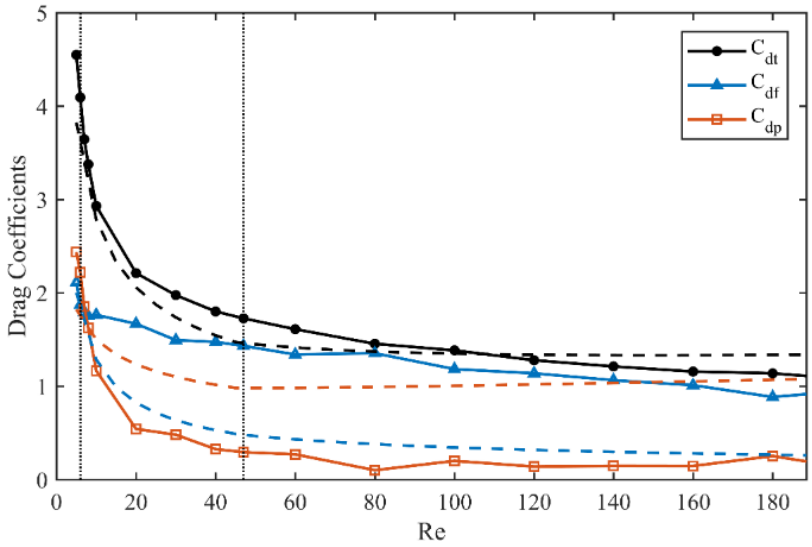

Figure 6.16 Drag components for the final controlled (solid lines) and uncontrolled (dashed lines) flows. The vertical dotted lines delineate the uncontrolled flow regime changes.

Figure 6.16 shows that all the values follow similar trends to the uncontrolled case: beginning very high and decreasing with a power-law relationship with increasing Re. However, where one might have expected the elimination of boundary layer separation to improve the drag, it is evident that this is not always the case. For all $Re < 100$, the drag is worse for the controlled case than the uncontrolled case; only above $Re = 100$ is

improvement seen. The explanation for this behaviour can be found by analysing the components of the drag, shown in the same figure.

The first thing to note is the shift in pressure drag. Since the pressure drag is predominately contributed to by the loss of momentum to the boundary layer and the vortices that form in the separated region, one might have expected the pressure drag to be eliminated entirely, along with the boundary layer separation. This is clearly not the case. The optimisation studies searched for control parameters that eliminated separation with minimal suction effort, therefore the boundary layer is not entirely removed. With this objective, despite θ_s being successfully reduced to zero, momentum from upstream is still lost to the boundary layer, so the pressure is not fully recovered over the leeward side. This can be seen visually by the slow velocity region in the wakes of the controlled flows in Figure 6.12, and is also shown in the pressure profiles given in the following section. Nevertheless, the pressure drag is substantially reduced, particularly in the vortex shedding regime.

Counteracting the improvement of this one component, is a worsening of the other: the skin friction drag. With the removal of the separated region of flow, the boundary layer has a higher velocity across the entire surface of the cylinder, as was highlighted by the increased velocity vectors in Figure 6.12. This higher boundary layer velocity results in a stronger shear force and, correspondingly, a greater skin friction drag. At low Re, where the viscous effects of the flow are more important, this increase in skin friction drag can overwhelm the improvement in pressure drag. This imbalance results in a worsening of the total drag. In this case, for the objective of eliminating separation using single-locus control, this counterproductive imbalance occurs for all $Re < 100$. Only above $Re = 100$, where the inertial effects are sufficiently dominant and the improvement in pressure drag is more substantial, does this control work in favour of reducing total drag.

Pressure profiles *To complete the analysis of the controlled flow behaviour and characteristics, the pressure coefficient profiles are provided in Figure 6.17. In the first plot, Figure 6.17 (a), the time-averaged pressure coefficients for the uncontrolled flow are compared to values from experiments in the literature. These values, labelled 'Zdravkovich', in the plot are taken from the curve fit by Zdravkovich [1997] to experimental values from Thom [1929], and Homann [1936] in the Re range $36 < Re < 107$. Hence, why at low Re values, $Re \leq 20$, the pressure coefficients are seen to differ quite substantially.*

In Figure 6.17 (b), the controlled flow is compared to the uncontrolled flow for $Re > 40$. There are several features to highlight here. Firstly, the pressure profile of the controlled flow fills out more to become similar to the profile given by potential flow theory. The minimum pressure coefficient is much lower, though, with values between -3.75 and -4.5. This is similar to what was seen in the experiments by Pankhurst et al.

[1953]. The lower pressure coefficient implies that the flow is being accelerated more than it would in the inviscid case. In addition, as the flow is no longer inhibited by the separated region, the pressure at the leading edge moves closer to $C_p = 1$. Finally, it is important to note that the plateau of C_p near the trailing edge is not eradicated – momentum is still lost to the boundary layer, hence non-zero pressure drags were observed in Figure 6.16.

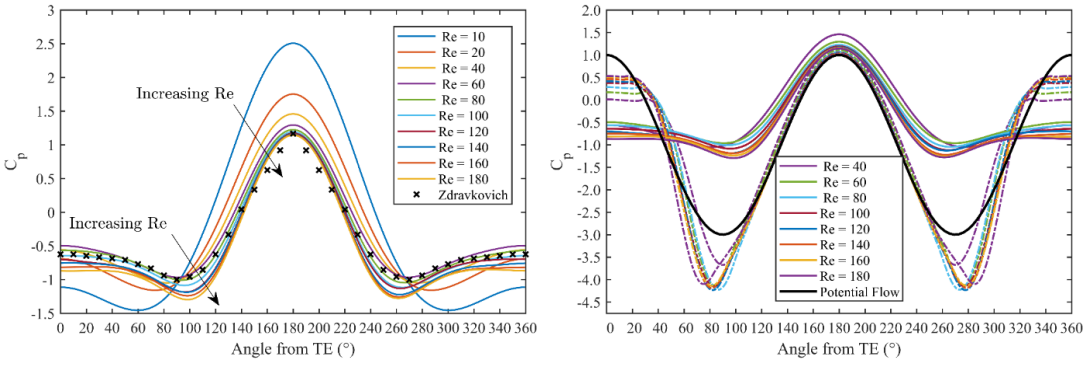

(a) (b)

Figure 6.17 Pressure coefficient profiles over surface of cylinder for (a) uncontrolled case, and (b) both uncontrolled (solid line) and controlled (dot-dashed line) cases.

C_{d_t} and C_{d_p} objectives *So far, we have discussed the results of control optimised for eliminating separation. As was described earlier, however, much of the present literature is more concerned with vortex shedding and drag coefficients than the boundary layer behaviour directly. Now, we consider the effects of changing the objective of optimisation to minimise the total drag or pressure drag using the single-locus control configuration.*

Comparison with θ_s objective *Figure 6.18 shows the resulting flow fields at $Re = 120$ for the optimised control found for each objective using the single-locus method. It is clear from this figure that the control effort required to achieve each objective differs significantly, as does the behaviour of the resulting flow. While the uncontrolled flow field was taken from a time-dependent simulation, the other figures were taken from the final stage of the optimisation process and thus with a steady-state condition. Naturally, the steady-state flows are symmetrical, therefore, and there are no lateral movements in the wake as with the uncontrolled flow.*

The first feature to note in Figure 6.18 is the difference in suction profiles for each control objective. As was shown earlier, the suction to eliminate separation at $Re = 120$ was spread wide and focussed near the trailing edge, with a relationship close to $\theta_q = 180Re^{-0.25}$. The suction profiles for the drag objectives are narrower and closer to the top and bottom of the cylinder (90° and 270°). It can be seen visually, that the amount of suction, C_q, is much smaller for these objectives also – particularly for

the total drag objective in Figure 6.18 (c). This makes sense given what the earlier results revealed about the balance of drag components: while boundary layer suction can reduce the pressure drag, it comes at the cost of increasing the skin friction drag. The separation angle objective often resulted in a net increase in drag because the suction was too strong, so it is appropriate that the suction profiles optimised to minimise total drag employ less suction.

The resulting flow fields for each objective differ significantly. The most obvious feature is the wake size – both its length and width. The wake in these figures can be considered the paler blue region centred on the trailing edge, bordered by the dark blue lines where the flow is stagnant. This delineates the two shear layers of reversed flow in the wake, and forward flow outside. With this definition, the separation objective flow in Figure 6.18 (b) has no real wake as it has no reversed flow, only stagnating fluid. On the other hand, the total drag objective has the longest wake. Both the C_{d_p} and C_{d_t} objective controls have a similar wake width, corresponding to a separation angle about 45° from the trailing edge.

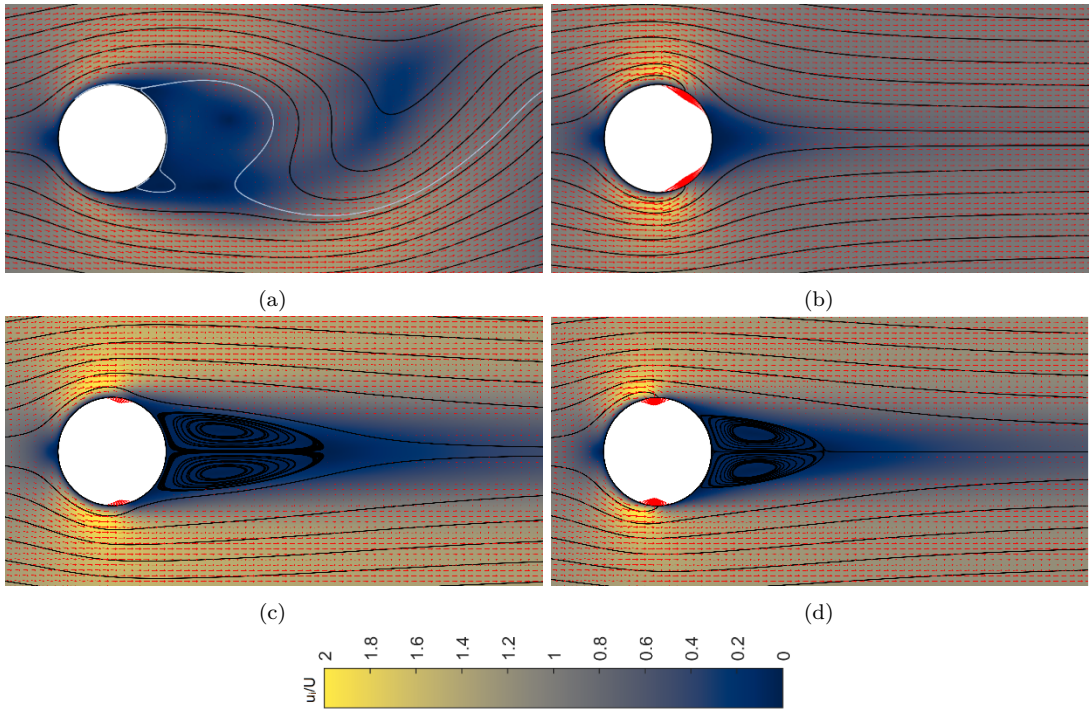

Figure 6.18 Instantaneous flow field at $Re = 120$ showing non-dimensionalised velocity vectors and surfaces $\left(\frac{u_i}{U}\right)$, as well as streamlines from the inlet for the (a) uncontrolled case, and controlled for minimising (b) separation angle, (c) total drag and (d) pressure drag objectives. Additional streamlines have been added for some of the figures to show the recirculation region.

Figure 6.19 demonstrates how the optimised control differs depending on the objective of optimisation. The amount of suction and the centre of suction are plotted against the Reynolds number, as in Figure 6.13 and Figure 6.15. As with J_1 [separation objective], *clear trends can be seen in the optimised control parameters for the other*

objectives. Contrary to the trend seen for minimising θ_s, however, Figure 6.19 (a) shows that the amount of suction required to achieve the drag objectives decreases with increasing Re in all flow regimes, not just for supercritical flows. This figure also shows a levelling off at $C_q = 5$ for the amount of suction to minimise total drag within the vortex shedding regime. It is unsurprising that more suction effort should be needed to eliminate separation than to minimise total drag or pressure drag. Substantial contributions to drag arise from the dynamic characteristics of the vortex shedding wake. It has been seen in many studies that this can be stopped without eliminating separation.

It is new and surprising however, to note how drastically the location of optimised suction differs between the drag objectives and the separation objective. Except at low Re, the centre of suction for eliminating separation is 20°-40° further aft than the drag objectives. For these drag objectives, θ_q is usually focused near the top and bottom of the cylinder, particularly in the vortex shedding regime. This would make sense if the control and dampening of the vortex shedding is the most critical aspect to reducing drag for the cylinder. As vortex shedding results in substantial lateral movements, applying suction at the top and bottom of the cylinder allows the suction to have the most impact, not just on the boundary layer, but on the free-stream pressure profile too.

Figure 6.19 (b) shows that the centre of suction, when optimised for the drag objectives, follows a similar trend to that for J_1. A power law is seen for each, and approximate fits are given in the legend of that figure. These fits have been rounded, so are not necessarily the best fits for the data, but help to make comparisons easier. It can be seen that the drag objectives result in suction profiles located closer to the leading edge, and begins to level off near 90°. This fits with what Kim and Choi [2005] found for $Re = 100$, with the drag on a cylinder improving most by slot-suction and blowing when the slots were located between 80° and 100°. These results suggest that earlier studies focused on eliminating vortex shedding may provide the best, or near-optimal, improvement in drag also. In contrast, eliminating separation marks the extreme case. It is seen here, that control to best prevent separation is positioned on the leeward half of the body instead of acting near the separation point or constantly removing the boundary layer as was formerly thought to be most effective. The results suggest that it may be better to consider the impact of boundary layer suction as a tool for manipulating the pressure profile to achieve desired momentum and flow characteristics, rather than as a simple removal of the boundary layer.

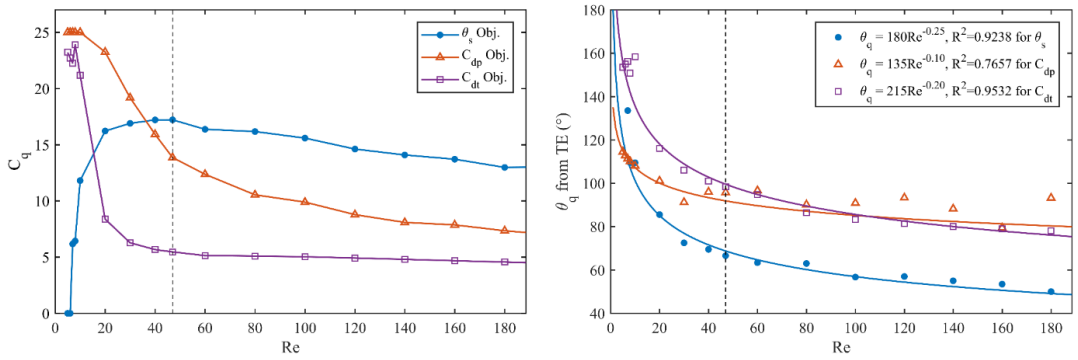

(a) (b)

Figure 6.19 Effect of objective on optimised suction characteristics: (a) the amount of suction, and (b) the location of suction.

Since the drag objectives result in controlled flows that still have boundary layer separation, Figure 6.20 shows the separation angle for each controlled case in comparison to the time-averaged value for the uncontrolled case. Again, we see a levelling off of the data for the total drag objective. Here the separation angle plateaus near the 45° mark, thus the difference in separation angle before and after control is applied increases through the vortex shedding regime.

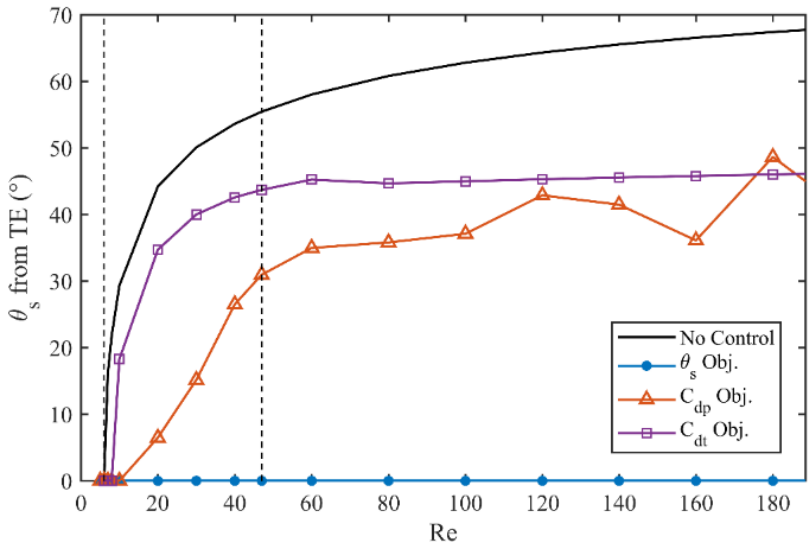

Figure 6.20 Separation angle for the resulting controlled flow for each objective. Uncontrolled values taken from Wu et al. [2004].

Resulting drag characteristics *The effect of control on the components of drag is of great interest for these objectives, particularly how the skin friction and pressure drag changes are balanced to achieve the minimum total drag. The total drag of the flows with optimised single-locus control are displayed in Figure 6.21. Here, the relationships from Henderson [1995] are also plotted for comparison to the uncontrolled case.*

From this figure, it can be seen that the improvement to drag is much more substantial for these objectives than when eliminating separation – particularly in the vortex shedding regime. Before the von Karman street begins forming at $Re = 47$*, there is little improvement in the total drag from either the* C_{d_t} *or* C_{d_p} *objectives. Although, whereas the separation objective in many instances resulted in a worsened total drag coefficient, the* C_{d_t} *objective resulted in controlled flows that were never worse than the uncontrolled flow. On the surface this is unsurprising, as the optimisation algorithm would return zeroed control parameters if no suction configuration could improve upon the uncontrolled flow – thus the total drag should never be higher than the uncontrolled case for this objective – however, as can be seen in Figure 6.19 and Figure 6.20, significant control effort was applied in every instance. This shows that the drag can always be improved, or at least matched, by the application of non-uniform suction control in the entire investigated Reynolds range. It also suggests that very different control parameters can result in flows with near-identical macroscale features. The* C_{d_p} *objective had slightly worse drag characteristics in the unseparated and vortex pair regimes, but large improvements in the vortex shedding regime. This fits with the observations from the separation objective results.*

The particularly important result shown in Figure 6.21 is the vast improvement in drag that occurs in the vortex shedding regime. The maximum decrease in drag was achieved at $Re = 180$ *for the total drag objective, with a reduction of 0.578 (43.3%). This is in comparison to the modest 0.198 (14.8%) reduction seen for the separation angle objective for the same conditions. Here, while the uncontrolled drag curve begins to level off before increasing again, the drag on the optimised cylinder continues to decrease at the same rate as at lower Re. This means that, once vortex shedding has begun, as Re continues to increase, the maximum improvement in drag also increases.*

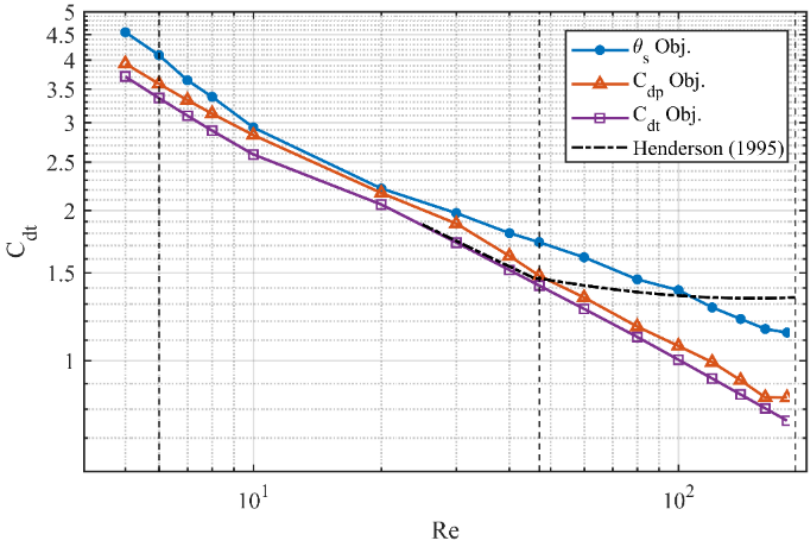

Figure 6.21 Total drag of the optimised, controlled cases compared with the time-averaged value for the uncontrolled flow.

This result was also seen with the implementation of suction/blowing as in Min and Choi [1999]. At $Re = 100$ and $Re = 160$ the authors achieved a reduction of 39% and 50%, whereas the present drag-optimised control results in a 25% and 40% reduction respectively. This difference can be explained by the implementation of blowing as well as suction. This implies that boundary layer suction has a stronger impact on drag-reduction than blowing, but that better results can be achieved in combination than individually.

It is interesting that the characteristics for the total drag objective continue along the same trend as the 'subcritical' uncontrolled flow (subcritical here meaning before the onset of vortex shedding, $Re < 47$). The transition from steady separated flow to transient vortex shedding has a big impact on the aerodynamic characteristics of the uncontrolled cylinder: the pressure drag stops decreasing with Re and begins to increase, while the skin friction drag coefficient continues to decrease at near its prior rate. The fact that the drag-optimised cylinder is unaffected by this transition, with the total drag continuing to decrease at its prior rate, suggests that the significant change imposed by the control is the counteracting of the pressure drag contribution attributable to the dynamic wake. It will be shown in the following sections that this improvement is not due to the use of steady-state equations to resolve these flows. Time-dependent simulations with the same control as used in the steady-state simulations result in nearly the same value (a maximum error of 3.29%).

Verification by time-dependent studies *One of the potential limiting factors of the optimisation procedure in this study was the use of steady-state solvers for flows that, when not appropriately controlled, are unsteady ($Re > 47$. To test the validity of the assumptions in the optimisation process, time-dependent studies were performed with the optimised control found for each objective at $Re = 60$ and $Re = 180$. This tests the two extremes of the 2D vortex shedding regime. In each case, the vortex shedding was allowed to fully develop on the uncontrolled cylinder, before the control was ramped up linearly from 0% to 100% over the course of $t = 5T$, where T is the period of vortex shedding given by Roshko's equation $St = \frac{D}{TU} = 0.212 - \frac{4.5}{Re}$ [Wieselsberger 1922a]. The controlled flow was then allowed to fully develop. The time was non-dimensionalised according to $t^* = t\frac{U}{D}$.*

Figure 6.22 shows the results of these verification studies, with the steady-state results shown as markers on the right vertical axis. As can be seen in Figure 6.22, the results fit well between the time-dependent and steady-state controlled results. In Figure 6.22 (b) it can be seen by the small oscillation of the separation angles on the upper and lower surfaces that the flow is not entirely steady at $Re = 180$ with the drag-optimised controls. For these controls, the wake became unsteady at some distance from the cylinder surface. Despite this, the major features of the cylinder flow were accurately evaluated by the steady-state studies, particularly the drag components and

separation angles. The maximum error in these values was for the pressure drag objective at $Re = 180$*. Here the maximum error was for the total drag, being lower by 0.106 (3.29%) in the steady-state simulations than the time-dependent models.*

In addition to some of the transient details being missed in the steady-state simulations, another feature was absent for the flow at $Re = 60$ *with the* C_{d_t} *objective control applied. That feature is a small separation bubble which formed where the suction was applied in the time-dependent study. The impact of this can be seen in Figure 6.22 (a) where the separation angle was detected first at 93.39° where the separation bubble formed. This bubble was very small, as shown by the inset of this figure, and had no significant impact on the flow or the later major separation point (which is also plotted on this figure).* For animations of the resulting time-dependent flows, the reader is directed to the Gallery of Fluid Motion video submission by the our group [Ramsay et al. 2019].

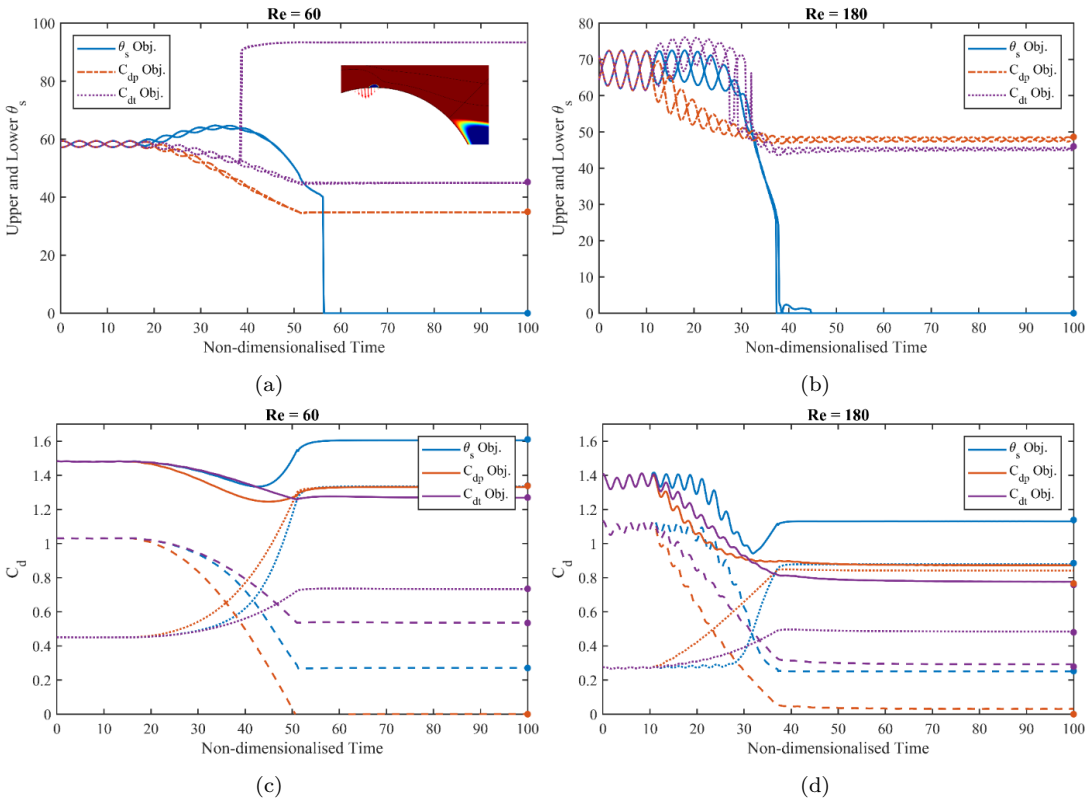

Figure 6.22 Results from time-dependent studies of the optimum single-locus control for each objective, showing (a-b) the instantaneous separation angles, and (c-d) the drag components. In (c-d) the dotted lines mark the skin friction drag, and the dashed lines mark the pressure drag. Inset on (a) is a tangential velocity surface for the C_{d_t} objective at $Re = 60$ showing the separation bubble and main separation, that give rise to two sets of measurement for θ_s.

The aim of quickly designing effective boundary layer control using optimisation with steady-state assumptions was achieved, and the results proved reliable. These time-dependent models took 11× and 43× longer to solve than the steady-state simulations

at $Re = 60$ & 180 respectively. They also required a solution for the fully-developed uncontrolled flow for their initial conditions, and must be run until fully developed – which for less effective control may take even longer. Furthermore, each optimisation process took between 100-300 iterations, therefore substantial savings in time were made by applying the steady-state assumption for the optimisation. With this approach, the major characteristics of the flow were accurately modelled and the transient studies verified that the optimised control parameters found by steady-state simulations are effective for the real flows. It is not sure that this approach can be extended to substantially different systems however – such as for higher Reynolds numbers or where the control is not expected to completely stabilise the flow.

In addition to these time-dependent studies, the effectiveness of the optimisation was tested by performing a full parametric study for the single-locus configuration at $Re = 180$. With steps of 20° for the centre of suction and spread of suction, as well as steps of 5 for the suction strength, it was found that all objectives successfully converged to the appropriate minimum – the point where the primary objective was at its lowest in this parameter space with the least controller effort, C_q. These results are summarised in Table 6.2 below.

Table 6.2 Comparison of optimised results and parametric study global minima for $Re = 180$

Objective	**Optimisation Result**				**Parametric Minimum**			
	$c_{q_{max}}$	θ_q	γ_q	J_{global}	$c_{q_{max}}$	θ_q	γ_q	J_{global}
J_1 – separation angle	66.29	50.02	70.48	**0.1298**	65	60	100	**0.1806**
J_2 – total drag	40.98	78.03	40.04	**0.8039**	35	80	40	**0.8081**
J_3 – pressure drag	98.02	93.23	26.98	**0.0734**	65	80	40	**0.0789**

6.4.0.3 Field-Based Control

The results to this point employed mostly pre-defined non-uniform suction profiles. While the results have been excellent, it would do well to confirm that other non-uniform suction profiles – which cannot be achieved by the pre-specified functions – are not capable of providing better control. Therefore, the field-based approach was employed for the total drag objective at $Re = 120$. The key results for the optimised flow for field-based control is compared to the single locus and biased locus results in Table 6.3 below. The field-based control was able to improve upon the single locus results. Only by about 1.2% and by even less (0.2%) against the biased locus control, though. On the other hand, it uses 18.8% more suction than the single locus to achieve this modest improvement. The control profiles are compared in Figure 6.23 and their key parameters are given in Table 6.4 while the resulting flow fields are shown in Figure 6.24. As can be seen, the controlled flows are nearly identical.

Overall, the single locus and biased locus control have been very effective at producing near-optimal control (if the field-based control is assumed to be the benchmark). The simplification of the control to a simple 3- or 4-parameter profile makes it easy to manipulate and apply the control. The difference in the key results are small so both approaches can be used with confidence in future studies.

Table 6.3 Comparison of key results for optimised control at $Re = 120$ using field-based control, single locus control, and biased locus control.

Parameter	Field-based	Single Locus	Difference (%)	Biased Locus	Difference (%)
C_{d_t}	0.9106	0.9212	1.1652	0.9132	0.2844
C_{d_p}	0.2597	0.3617	39.2780	0.2678	3.1384
C_{d_f}	0.6509	0.5595	-14.0426	0.6457	-0.8020
C_q	0.0606	0.0492	-18.8117	0.0602	-0.6519
θ_s	40.9413°	45.2861°	10.6122	41.0230°	0.1996

Table 6.4 Parameters for the optimised control. Note the values for the field-based control are inferred from the resulting profile.

Parameter	Single Locus	Biased Locus	Field-Based
θ_q	81.4993°	92.0873°	90°
γ_q	37.1946°	42.2850°	40.5°
λ_q	0.5	0.5943	-
$c_{q_{max}}$	0.4762	0.5065	0.5777

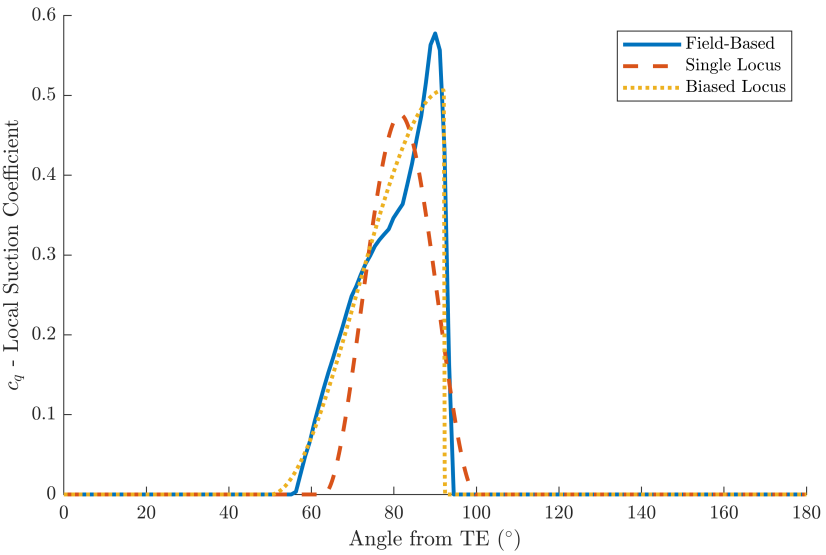

Figure 6.23 Comparison of suction profiles for the field-based, single and biased locus controls.

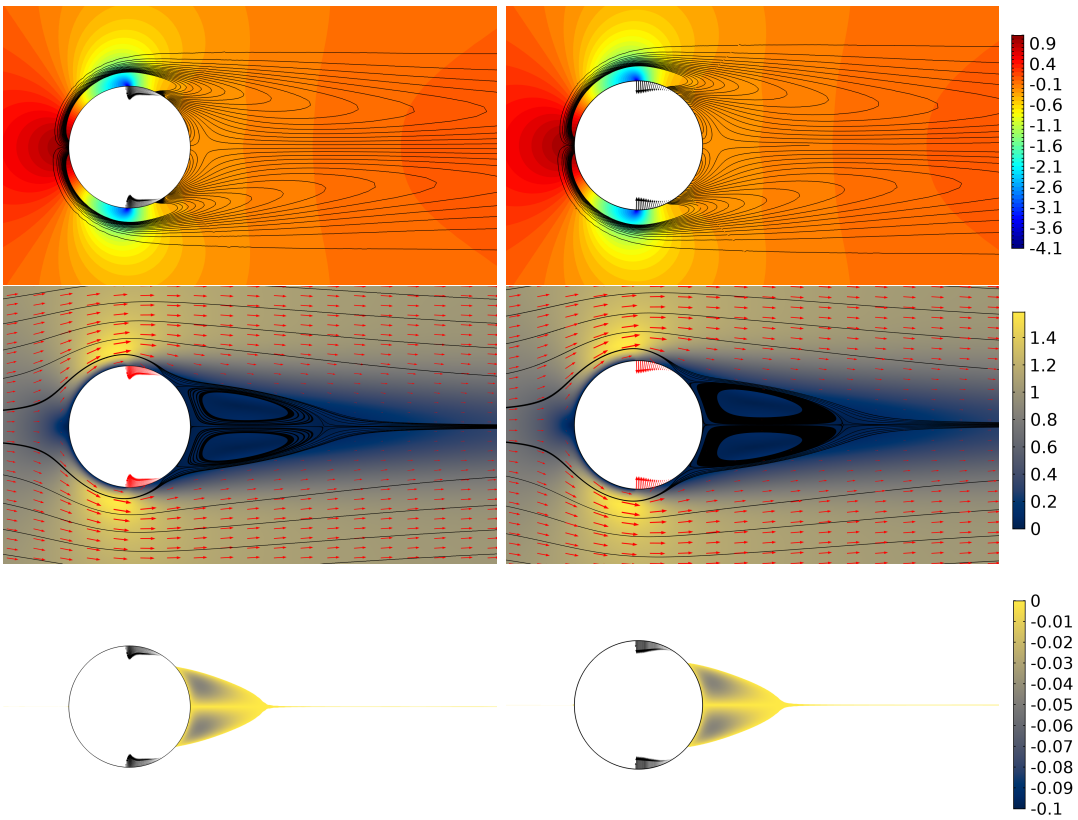

Figure 6.24 Comparison of resulting flow from field-based (left) and biased locus (right) optimisation to minimize drag at $Re = 120$. Pressure contours (with vorticity lines) (a), velocity surface (b), and reversed flow (c).

6.5 SUMMARY AND NEXT STEPS

Summary of Results Overall, BL suction (and non-uniform suction especially) was found to be extremely effective at controlling the separation or aerodynamic characteristics of a bluff body, even at relatively low Reynolds numbers. At $Re = 180$, the total drag coefficient was almost halved for the flow (C_{d_t} reduced by 43%). The improvement in drag arises from a balancing of the pressure profile over the front and rear halves of the cylinder (sometimes referred to as base pressure). Suction control can greatly affect the pressure profile over the body, but at the cost of increasing skin friction as the boundary layer has higher momentum when the free-stream is entrained to replace the removed fluid particles. Interestingly, the suction flow rates generated by the optimised flow control were much higher than are typically quoted for BL suction in textbooks [Schlichting 1987]. Schlichting states that $C_q = 0.0001 - 0.001$ is appropriate for strong effect. However, this difference is partly because the calculations demonstrating the effect of suction at that time relied on the boundary layer equations which would break down at higher suction flow rates, and because the effectiveness of suction control increases with Re.

Strong trends between the uncontrolled separation characteristics of the flow and the parameters for optimal control were uncovered. Whether these exact relationships will apply at higher Re is questionable due to the changing regimes. For more streamlined bodies though, where there are much fewer distinct flow regimes, these trends may be particularly useful. Similar dependencies were found for the diffuser, however, in this case there are fewer geometric parameters that can be changed to alter the relationships. This makes their usefulness more apparent. If a bluff body flow is desired to be controlled, and the uncontrolled flow is known, many simulations may be avoided if optimisation is not needed and these relationships can be employed instead.

The single locus control approach is simple to apply and greatly reduced the number of parameters to optimise. Fortunately, it was found to also be extremely effective and very near-optimal. The unrestricted field-based approach with adjoint-optimisation resulted in much the same profile, despite having no control as its initial starting point. For the design of autogenous suction control, where any suction must be balanced by an equivalent blowing (in terms of flow-rate and some pressure matching) the use of this simplified profile is invaluable.

Moving Towards Autogenous Control With a firm understanding of the flow around the circular cylinder – both with and without suction control – the development of autogenous control can be pursued. The effectiveness of non-uniform suction has been showed to be strong, which suggests that if autogenous control can be generated – even if it is quite far from the optimal parameters – it is likely to have a good impact on the flow.

The next stages were to employ the dual locus approach with coupled flow-rates. Then optimisation simulations can be performed to balance the average pressures of these loci to simulate the necessary conditions to drive autogenous control – upwind or otherwise. However, implementing this control by imposed boundary conditions – even if they are designed to be as realistic as possible (by balancing pressures etc.) – is a far-cry from a physical design with all the corresponding difficulties that arise. So following preliminary simulations of autogenous control by boundary condition, efforts were then made to design and model physical systems that might operate, using porous surfaces and internal ducting to drive the controlling flow. These efforts are described in the next chapters, Chapters 7 and 8.

Chapter 7

AUTOGENOUS CONTROL BY IMPOSED BOUNDARY CONDITIONS

7.1 SUMMARY

A methodical approach was taken to develop potentially autogenous suction/blowing control to minimise drag on the circular cylinder at $Re = 40$ and $Re = 120$. The dual-loci control scheme was developed which uses two single locus control areas – one for blowing and one for suction. Three investigations were carried out using this control. The first treated each locus as independent and determined the optimal improvement in drag possible from combined suction/blowing with this approach ('unbalanced dual-loci'). Then the constraint that the suction and blowing must have balanced flow rates so that the net mass injection/removal is zero. Parametric and optimisation studies were carried out for this 'Q-balanced dual-loci control' using the steady state model and some control arrangements were verified using full time-dependent simulations. Finally, the full autogenous requirements were imposed on the control design by performing optimisation of dual-loci control with the constraints that the flow rates must be balanced and the average pressure drop from suction to blowing locus is greater than zero. Again, time-dependent verification studies were also performed.

These investigations found that the dual-loci control could be extremely effective at reducing drag – especially when no constraint on the net flow is imposed, with the optimised unbalanced dual-loci controls producing reductions in total drag of over 20% However, the control pressure gradients for this were highly unfavourable and would require significant power to drive the control. The methodical investigation of the Q-balanced dual-loci control uncovered general trends that are useful for the design of potentially autogenous control. Suction produces a local pressure decrease, but a net increase in the pressure downstream, while blowing does the opposite. The best control arrangement features suction just upstream of the 90° mark and blowing near the trailing edge. This reduces the drag by as much as 13% and 21% for $Re = 40$ and $Re = 120$ respectively when optimised. The parametric study also showed that very few arrangements of the dual-loci control produced improvement while maintaining a

positive pressure drop, $dP > 0$, however it was possible.

The P-Q-balanced dual-loci control found that the total drag could be reduced on the cylinder while maintaining a positive pressure drop. When optimised on the steady-state model, the drag was only reduced by up to 5.5% and 3.7% and the result of the optimisation was quite dependent on the initial values. The veracity of this control and the conclusions of the optimisation studies at $Re = 120$ (where the uncontrolled flow is unsteady) were confirmed by time-dependent simulations. It was found that all the optimised P-Q-balanced dual-loci controls were effective in the full unsteady case, and maintained their autogenous pressure gradient. Surprisingly, the control that performed worse in the steady-state case actually performed better in the time-dependent model. The drag improvement was 4.3% for the best case in the time-dependent simulations and the fluctuations of the drag components were reduced by almost half.

Based on these simulations where the control was imposed by boundary conditions, the outlook is positive that autogenous control is feasible for the flow around the cylinder. In fact, substantial improvements in drag could be achieved. The major concern is whether the pressure drop consideration is sufficient (that $dP > 0$ is enough to drive the control flows), and this must be confirmed by simulations of practical implementations, which will be described in Chapter 8.

7.2 INTRODUCTION

In theory, autogenous suction control consists of suction and blowing with equal flow rates and arranged such that a pressure gradient drives the control flow naturally. To satisfy the "control" aspect of its name, it should provide some improvement to the flow also. It is not possible to look at a flow field and determine immediately whether autogenous suction control will be beneficial for the flow, nor how it should be applied. For one, the application of the suction and blowing affects the pressure profile over the body – which is needed to drive the control flow. For another, the velocity profile of each control region is customisable, and this too affects the resulting pressure field. Therefore, the placement and design of the suction and blowing loci must be an iterative process.

It is not clear either what the required pressure drop between the suction and blowing regions must be. This loss factor is a function of the control flow rate, the internal ducting, the external flow and the materials used. It is possible to approximate these losses by making assumptions about the nature of each of these contributions – and one approach is described in this chapter – however there will naturally be much uncertainty in this. Only a full simulation or experiment of the chosen design will reveal the true pressure loss. The external pressure field, control pressure drop and the control flow rate are all naturally interlinked.

To make matters worse, for most Reynolds numbers, the flow around the circular cylinder and other bluff bodies is unsteady. This means that the pressure field fluctuates, which impacts what autogenous control arrangements are possible at any given moment. This can be addressed by considering time-varying control, but it makes it hard to design the control system. This is further compounded if one considers how the controlled flow might be developed from the uncontrolled case. It was seen in the suction control simulations that the pressure profile around the cylinder is drastically different when optimally controlled than its uncontrolled state. Therefore the arrangement of autogenous control in the initial state may be quite different to the final state (assuming the optimal suction profile could be produced using autogenous control).

It was usually attempted to go from a starting point of desired *suction* control – in terms of profile, location and flow rate – and determine how it can be applied to an existing flow by placing a balancing *blowing* profile. This proved to be a very difficult approach and likely to produce unsatisfactory results. An alternative is to optimise the full autogenous system constraining the control to satisfy the autogenous requirements by adjusting both the blowing and the suction, and then optimising for the main objective, e.g. minimise drag. This approach is better, and gives a clearer answer of whether autogenous control will be beneficial for a flow, but it also relies on assumptions of the pressure drop needed through the control ducts. A more holistic approach is to develop a practical design which includes the porous surfaces and internal ducting, and produce it in a parameterised way that can be modified and optimised. This does away with the BC approach and the uncertainty in pressure drop assumptions. As this approach has by far the most variables, it also makes it harder to produce generalizable results. The first two approaches will be discussed in this chapter, while the final approach in the following chapter.

The aim of the studies discussed in this chapter was to ascertain whether autogenous suction control is feasible for bluff bodies, how it is best arranged at different Re, and what factors are important in its design. These lessons can then be applied to design a practical system that achieves this, or an experimental approach for this design and testing at high Re.

The first two approaches – attempting to achieve a desired suction control by matching it with autogenous blowing, and optimising a full autogenous BC system – were tested on the flow around the circular cylinder. Due to the complexity and uncertainties in these tests, the flow was investigated at fewer Reynolds numbers, typically at $Re = 120$. There is a major drawback here that suction control becomes more efficient at higher Re where the momentum difference between the free-stream and boundary layer (BL) is very large. In contrast, high suction flows were needed to optimally control the flow at low Re, and these will be very hard to achieve using the natural pressure gradients in the flow. Low Re simulations were favoured for several reasons: 1) we know the optimal non-uniform suction profiles for minimising drag, 2)

the simulations are faster therefore the iterative convergence on autogenous control setups was feasible, 3) for testing the final designs with practical designs, flow through porous media can be coupled with free-stream flow easily for laminar flow.

Therefore, three sets of investigations were performed to develop autogenous suction control by imposed boundary conditions on the flow around the circular cylinder. Firstly, simulations were performed with both suction and blowing control around the cylinder with independent parameters and without constraints on the flow-rate and pressure of each control region. This was to develop a base-line of the possible improvement when autogenous design is not cared for, and machinery can be used to drive the control flows. Secondly, a constraint on the flow-rates was applied to the system, specifically that $Q_s = Q_b$. This was simple for the case of the cylinder as the geometry is continuous and uniform, unlike for the diffuser. This represents a closed system where no fluid is removed from the overall domain, but power likely needs to be applied to drive the control flow. Finally, a further constraint was added, that the average pressure of the suction region must match the average pressure of the blowing region, with some pressure drop, dP:

$$P_s - P_b - dP = 0, \tag{7.1}$$

where P represents the averaged pressure and its subscript denote describes the region over which it is averaged (this notation is used throughout this chapter). Several values of dP were investigated. In the following chapter, the design of practical systems – where the internal ducts and porous surfaces are included in the model – will be described, following on from the present discussion.

7.3 MODELS

7.3.1 CFD Model

The CFD model was identical in terms of geometry, mesh and boundary conditions as for the non-uniform suction investigations of the flow around the cylinder, and the reader is directed to these details Chapter 6. The 'Velocity Outlet' Dirichlet BC applied to the cylinder wall is able to produce inflow and outflow, so this did not have to be changed. Though, functions for describing the combined suction and blowing control applied to the cylinder surface had to be developed.

Many of the simulations were performed using the steady-state (SS) Navier-Stokes (N-S) equations even though the uncontrolled flow is unsteady/time-dependent (TD). This is in-line with the approach taken for the suction control simulations. The justification in that case was that effective suction control would stabilise the flow. However, in this case it is unclear whether the blowing locus will produce instability and

maintain the unsteady flow. Therefore, the results from SS simulations are never taken as definitive, as the dynamic effects of the real flow have a serious effect. It is much faster to undertake an optimisation using steady-state simulations than time-dependent ones. Therefore, it made this part of the investigation more agile before applying them to the real time-dependent conditions. Unsurprisingly, it was found in many cases that what was effective for a steady flow, is not so for an unsteady one. On the other hand, often controls that were optimal in the steady-state cases were highly effective in the unsteady cases too. Where results are presented, the type of simulation that was performed will be specified.

7.3.2 Suction/Blowing Combinations

To simplify the approach taken in these investigations, it was decided to use the single locus profile for the suction and blowing regions. While this may not be the optimal profile, it was found to be nearly as effective for the case of suction only. This also simplifies the mathematics also; the same function that defines the suction profile can be re-purposed for the blowing. The location, spread and strength of the blowing are defined by $\theta_{q_b}, \gamma_{q_b}$, & $c_{q_{max_b}}$. Provided $c_{q_{max_b}}$ is negative the function will impose a blowing profile. This control is described as 'dual-loci' suction/blowing control. More details are given in Chapter 3. Combined suction and blowing can be defined simply by superimposing the suction and blowing functions:

$$c_q(\theta) = c_{q_s}(\theta) + c_{q_b}(\theta). \tag{7.2}$$

7.3.2.1 Model I – No Relationship Restrictions

In the first case, no constraints were placed on the balance between suction and blowing. Each had constraints on their profile though: $0 \leq c_{q_{max}} \leq 1$ and $0.5° \leq \gamma_q \leq 90°$ so that the local suction velocity never exceeds the free-stream velocity and so that the suction and blowing loci could take up at most half of the cylinder (to allow room for the other). The lower bound on γ_q is simply to ensure stability for the functions defining the profiles.

In some cases, an additional constraint was placed such that the suction and blowing loci cannot overlap. It is not an issue if the loci overlap, as superimposed profiles are simply produced, however it became important later on when the pressure-balance objective was considered. Fully overlapped suction and blowing would annihilate each other resulting in no control (but perfectly balanced average pressures). This constraint was imposed using a Boolean operator which checks if

$$(ub_s \geq lb_b \;\&\; ub_s \leq ub_b) \; or \; (ub_b \geq lb_s \;\&\; ub_b \leq ub_s), \tag{7.3}$$

where, *lb* and *ub* are the lower and upper bounds respectively of the control regions. If this condition is satisfied, it means there is some overlap of the control loci. Using this approach allows the order of the suction and blowing to freely swap, i.e. it does not insist that suction must be upwind of the blowing.

Other than these simple constraints, the dual-loci profile could take any form it liked. The optimisation adjusts the location, spread and strength of the suction and blowing independently, producing six control parameters.

7.3.2.2 Model II – Flow-Rate Balanced (Q-Balanced)

For the flow-rate balanced studies, an additional constraint was imposed that $C_{q_s} = C_{q_b}$. As these are imposed a priori by the control parameters, this was simple to do. We have that

$$C_q = \frac{\gamma_q c_{q_{max}}}{360}, \tag{7.4}$$

where the equation is written for the general control case and γ_q is in degrees. Therefore,

$$\gamma_q c_{q_{max}} = \gamma_{q_b} c_{q_{max_b}}.$$

The number of control parameters can be reduced by one as a consequence of this coupling. To enforce the flow rate, one arrives at

$$c_{q_{max_b}} = \frac{\gamma_{q_s}}{\gamma_{q_b}} c_{q_{max_s}}. \tag{7.5}$$

7.3.2.3 Model III – Pressure and Flow-Rate Balanced (P-Q-Balanced)

To achieve a control that could feasibly be driven passively, the suction and blowing flow rates must be balanced in terms of flow rate and pressure drop. The pressure constraint is the most difficult to achieve because it is not known a priori, and it is a function of the natural flow-field and the control parameters. Therefore, rather than just being imposed as a constraint, this requirement was satisfied by optimising the blowing parameters with the objective of finding a satisfactory pressure location as a minor optimisation. The total objective of the minor optimisation is to both minimise drag and maintain a positive pressure gradient. The major optimisation has just the drag objective but keeps the *dP* condition as a constraint. Using this approach of major and minor optimisation was more effective and reliable than using just a constraint and optimising both the suction and blowing parameters simultaneously. A flow-chart of

the optimisation process is shown in Figure 7.1. To reiterate from Chapter 3, the minor pressure-balance objective is

$$J_{auto} = P_s - P_b - dP \geq 0. \tag{7.6}$$

The choice of dP is particularly important as this is the pressure drop needed to drive the control flow. In this chapter, it is assumed that any positive dP would be sufficient.

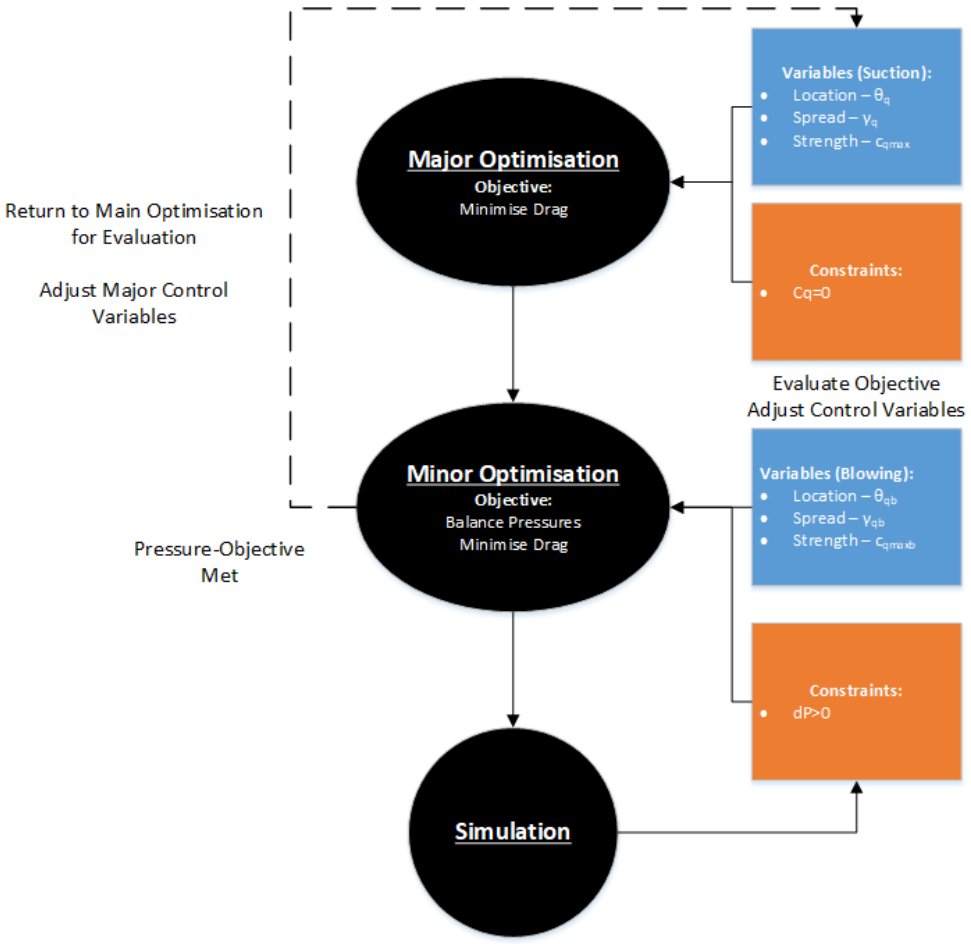

Figure 7.1 Flow-chart of P-Q-Balanced Dual-Loci optimisation.

7.3.3 Investigations

The following studies were carried out to investigate BC-imposed autogenous suction control on the cylinder:

7.3.3.1 Model I – Independent Suction and Blowing

In the first investigation, the dual-loci control was implemented but without the flow-rate constraint. The suction and blowing loci could have independent flow rates resulting in

a net suction or net blowing if this was optimal. An optimisation study was performed at $Re = 40$ and $Re = 120$ with the objective of minimising total drag. The simulations at $Re = 120$ were steady-state, despite the uncontrolled flow being unsteady.

7.3.3.2 Model II – Q-Balanced

Three sets of studies were performed on the Q-balanced dual-loci model. These were:

1. Parametric study of control (SS)
2. Optimisation to minimise drag (SS)
3. Verification time-dependent studies (TD)

For the parametric study the sweeps on each control parameters described in Table 7.1 were used.

Table 7.1 Parametric sweep for Q-balanced dual-loci control of cylinder.

Parameter	**Symbol**	**Range**
Suction Location	θ_q	30°:30°:150°
Suction Spread	γ_q	15°:15°:75°
Suction Peak Strength	$c_{q_{max}}$	0.1
Blowing Location	θ_{q_b}	30°:30°:150°
Blowing Spread	γ_{q_b}	15°:15°:75°
Blowing Peak Strength	$c_{q_{max_b}}$	0.1
Reynolds Number	Re	$40, 120$

All combinations of parameters were investigated, resulting in 750 total simulations for each Reynolds number. In some cases the suction and blowing overlap completely resulting in no control. In this investigation the maximum strength of the control was the dependent variable while the spread was pre-defined as a control parameter. A major limitation of these parametric studies is that the peak strength of the control was not altered. This may have an important effect on the conclusions reached from the results.

The purpose of this investigation was to determine the relative sensitivity to each parameter, get some idea of the most effective arrangements, and to determine in how many cases the pressure profile was favourable for an autogenous control flow. The parametric study was performed at $Re = 40$ where the uncontrolled flow is known to be steady, but it was also repeated at $Re = 120$ to get some idea of the control for a simplified version of the real flow. It was expected that for some combinations of control parameters at $Re = 120$ the flow would not be resolved when the flow is too

unsteady. Additionally, the results for the $Re = 120$ case are less conclusive than those for $Re = 40$.

The parametric study is limited due to its finite values, and in particular with only one value of the suction strength being investigated. An optimisation study can alter all parameters and determine the best improvement possible. It was found that the steady-state results at $Re = 120$ were quite different to unsteady simulations for the autogenous control arrangements especially – not entirely surprising. Therefore, a time-dependent optimisation of the dual-loci control at $Re = 120$ was implemented despite its long runtime.

In some cases, control configurations were tested in the full unsteady model. Here, the control was ramped up over $1T$ on a fully-developed solution of the uncontrolled flow. The simulation was run until the flow was fully-developed again (usually $10T$).

7.3.3.3 Model III – P-Q-Balanced

Optimisation studies were performed to determine the best improvement in total drag possible by autogenous suction control where the necessary control pressure gradient was assumed to be any pressure gradient greater than zero, $dP \geq 0$ (SS). In post-processing the results, we also consider the approximation given by the analytical expression above to check whether this minimum estimate is satisfied too. Optimisation studies were performed directly because the primary objective was to determine whether any substantial improvement in drag could be achieved by autogenous control. Searching for the best-case scenario reveals this.

One further constraint was also employed in this model to produce more realistic results. If the blowing locus was allowed to be any size (within the bounded values of γ_{q_b}) then under some arrangements the blowing strength could be tremendous (many multiples of the free-stream velocity). This is both unrealistic and problematic for the numerical resolution of the domain. Therefore, the peak blowing strength was limited as $c_{q_{max_b}} \leq 1$.

The initial values are particularly important for this optimisation. Initial values must be contained within the feasible set. In this case, since there is a constraint for a particular pressure drop between the suction and blowing loci, this should be reflected for the first values evaluated. Any further issues where the output does not satisfy the constraint are dealt with by a penalty constraint-handling method. The initial values for the P-Q-balanced dual-loci optimisation are given in Table 7.2.

Table 7.2 Initial values of control parameters for P-Q-balanced dual-loci optimisation.

Control parameter	Initial Values (IV1)	Alternative Initial Values (IV2)
θ_q	150°	120°
γ_q	20°	40°
$c_{q_{max}}$	0.1	0.1
θ_{q_b}	90°	80°
γ_{q_b}	10°	10°
$c_{q_{max_b}}$	-0.2	-0.4

7.4 RESULTS

7.4.1 Model I – Independent Suction and Blowing

The results for Model I will be discussed by first describing the optimised control and its effect on the drag components, then analysing the resulting flow, and finally restating the key conclusion.

7.4.1.1 Optimised Control and Effects on Drag

The control parameters for the optimised control at $Re = 40$ & 120 (SS) are given in Table 7.3 while the key results are compared to the uncontrolled cases in Table 7.4. The unbalanced suction and blowing control was able to drastically improve the total drag coefficient. At both $Re = 40$ & 120, over 10% reductions in total drag were achieved. In the case of $Re = 120$, the total drag coefficient was reduced by a quarter. It is apparent that these improvements are due entirely to the reduction in pressure drag by producing a more balanced pressure distribution over the cylinder surface. A major contribution to this is the delay in separation angle which was pushed much further aft, especially at $Re = 120$. On the other hand, the skin friction drag increases substantially due to the increased interactions at the wall-boundary. Higher velocities at the bounding wall result in stronger gradients and greater viscous losses. In both cases, the skin friction drag increased by over 100%. This is less important at higher Re where skin friction is a much smaller contributor to the total drag, but at the slow $Re = 40$ flow this is a substantial change influencing the total drag. In fact this results in a reversal of the contributions of skin friction and pressure drag at $Re = 40$. For the uncontrolled flow, C_{d_p} is twice as large as C_{d_f}, but for the controlled flow, C_{d_f} is four times larger than C_{d_p} (and larger than the pressure drag component of the uncontrolled flow). This result reflects the conclusions of the suction-only investigations, as reported in [Ramsay et al. 2020d].

Table 7.3 Control parameters and key results for optimised control for both unbalanced dual-loci control and single locus suction at $Re = 40$ & 120.

Parameter	Re=40		Re=120	
	Dual-Loci	Single Locus	Dual-Loci	Single Locus
θ_q	97.116°	100.931°	76.542°	81.499°
γ_q	39.016°	20.404°	55.774°	37.195°
$c_{q_{max}}$	1	1	0.506	0.476
θ_{q_b}	22.003°	-	17.521°	-
γ_{q_b}	90°	-	81.701°	-
$c_{q_{max_b}}$	-0.4977	-	-0.4529	-
C_q	-0.00369	0.05667	-0.01073	0.04920

Table 7.4 Key results for optimised unbalanced dual-loci control with comparison to no control and optimised single locus suction at $Re = 40$ & 120

Parame-ter	Re=40			Re=120		
	Dual-Loci	No Control	Single Locus	Dual-Loci	No Control (SS)	Single Locus
C_{d_t}	**1.3718**	-16%	-10%	**0.8196**	-25%	-11%
C_{d_p}	**0.2578**	-76%	-60%	**0.1265**	-85%	-65%
C_{d_f}	**0.1141**	100%	28%	**0.6931**	158%	24%
θ_s	**34.834°**	-36%	-18%	**29.392°**	-57%	-35%

The parameters for the suction portion of the dual-loci control are very similar to the values produced by the single locus optimisation studies. The location, spread and peak strength of the suction locus are very similar at both Re, with the biggest changes occurring for the suction spread, γ_q, which is larger for the dual-loci control. The dual-loci control is able to achieve a further improvement on suction-only control, reducing the total drag by a further 10% at both Reynolds numbers. Again, this is due to the improvement in pressure profile, as the skin friction is worse in the dual-loci control. This comparison helps elucidate the relative contributions of the suction and blowing portions. While single locus suction control reduced the uncontrolled total drag coefficient by 0.1131 at $Re = 40$, the addition of the blowing locus (and the changes to the overall arrangement) brought a further reduction of 0.1472 – a greater impact. At $Re = 120$, single locus suction reduced C_{d_t} by 0.165 and the modification to unbalanced dual-loci control reduced this by a further 0.102 – in this case, less of an impact than at the lower Re. Therefore, we can state that at low Re normal blowing can have as much or more of an impact on the total drag than suction, but at higher Re this is lessened and suction has the stronger effect. To some extent this improvement comes

from reducing the 'sink drag' which is the drag force felt by a body which absorbs some of its surrounding fluid. This effect is realised in the pressure profile around the body, and can be quite substantial with strong suction.

While the blowing parameters are very similar between the two Re for the dual-loci control, the suction profile is drastically different. At $Re = 40$, the suction is 'maxed-out' with a peak suction coefficient of 1 (the upper bound). The suction spread is also much tighter. At $Re = 40$, the optimised control also converged on the upper bound of the blowing spread. Blowing at the hindmost point is beneficial for several reasons, but this result may actually speak more about the constraints on the control implementation than the flow. Blowing at the trailing edge (TE) reduces drag by: 1) raising the base-pressure of the cylinder, 2) providing (very modest) thrust force (which is reflected in the pressure profile), 3) does not blow the boundary layer away which would usually be undesirable upstream. From these results, one can infer that blowing control is best situated at the rear of the cylinder, and presumably the best location for blowing is right at the TE. Though the control arrangement of Model I makes it possible to have the blowing control situated at the TE, symmetry of control is enforced which may affect results. For example, a blowing locus situated at $\theta_{q_b} = 0°$ and a maximum spread of $\gamma_{q_b} = 90°$ would have only 45° of spread in the upper half in actuality. So perhaps the optimised blowing control is situated slightly upstream of the TE with a large spread so as to get the best of both. Allowing a wider spread for the blowing locus, or adjusting the symmetry condition may reveal a different result for the blowing.

7.4.1.2 Resulting Flow

Figure 7.2 shows that the controlled flows around the cylinder. The wake is very narrow as the flow is nearly unseparated in both cases. Interestingly, for both Reynolds numbers there is a small net mass injection ($C_q = -0.00369$ & -0.011 for $Re = 40$ & 120 respectively). Overall, this is quite a small imbalance between the suction and blowing control. The pressure contours are slightly different, with the minimum pressure at $Re = 40$ further forwards than is optimal (situated at 90°), and this is likely due to any further control (or changes to the existing control) to improve the pressure profile further would worsen the skin friction drag component which is substantial at low Re. Suction at 90° helps the flow to 'hug' the wall as it traverses the apex of the cylinder, improving the pressure recovery on the leeward half, but this also increases the interaction between the wall and the flow when it is at its fastest. This can be seen in the skin friction plots in Figure 7.3 with the spike at 90°.

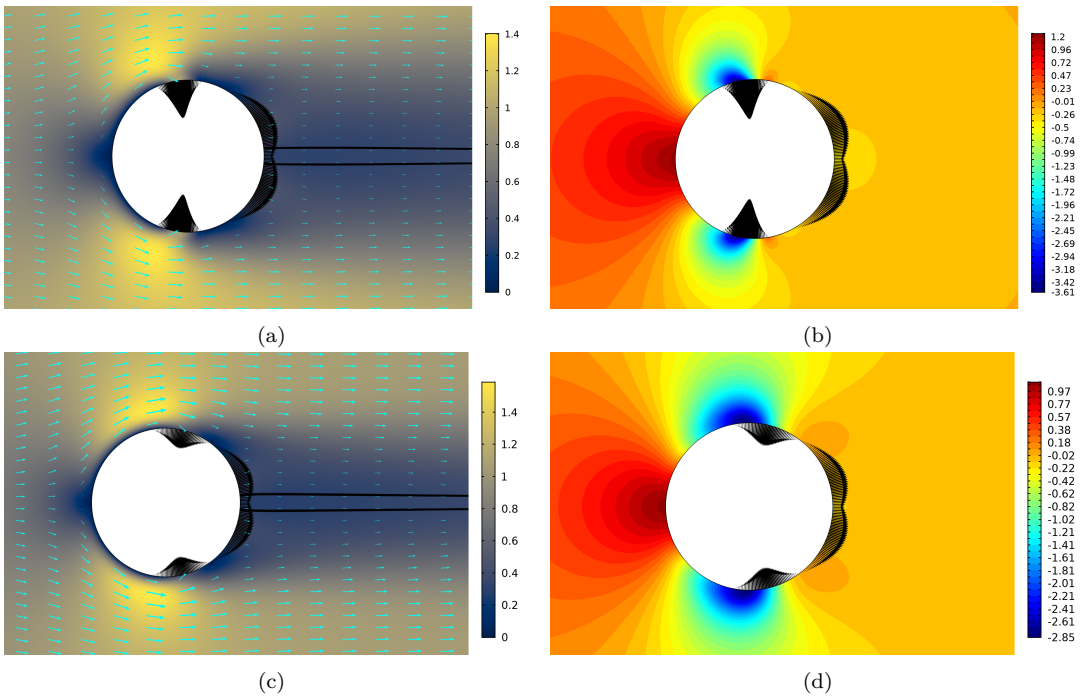

Figure 7.2 Velocity surface (a,c) and pressure contours (b,d) for optimised unbalanced dual-loci controlled flow round cylinder at $Re = 40$ (a,b) and $Re = 120$ (c,d). The velocity is non-dimensionalised by the free-stream velocity, U, and the pressure by the inlet dynamic pressure, h_0

The pressure, skin friction, and control profiles are plotted in Figure 7.3. These reveal that the major improvement in drag arises from a reduction in C_{d_p} by improving the pressure distribution over the cylinder. The suction at the top and bottom lowers the frontal pressure significantly, while the suction/blowing combination at the rear raises the base pressure. These two effects produce a much smaller pressure deficit on the leeward half. On the other hand, the skin friction is increased over almost all of the cylinder due to the thinner boundary layer, causing C_{d_f} to also increase substantially, but the improvement in pressure drag outweighs these effects. Unfortunately this C_{d_t}-optimised arrangement is the opposite of an ideal autogenous configuration. The blowing region is at a much higher average pressure than the suction regions – both before and after the control is applied.

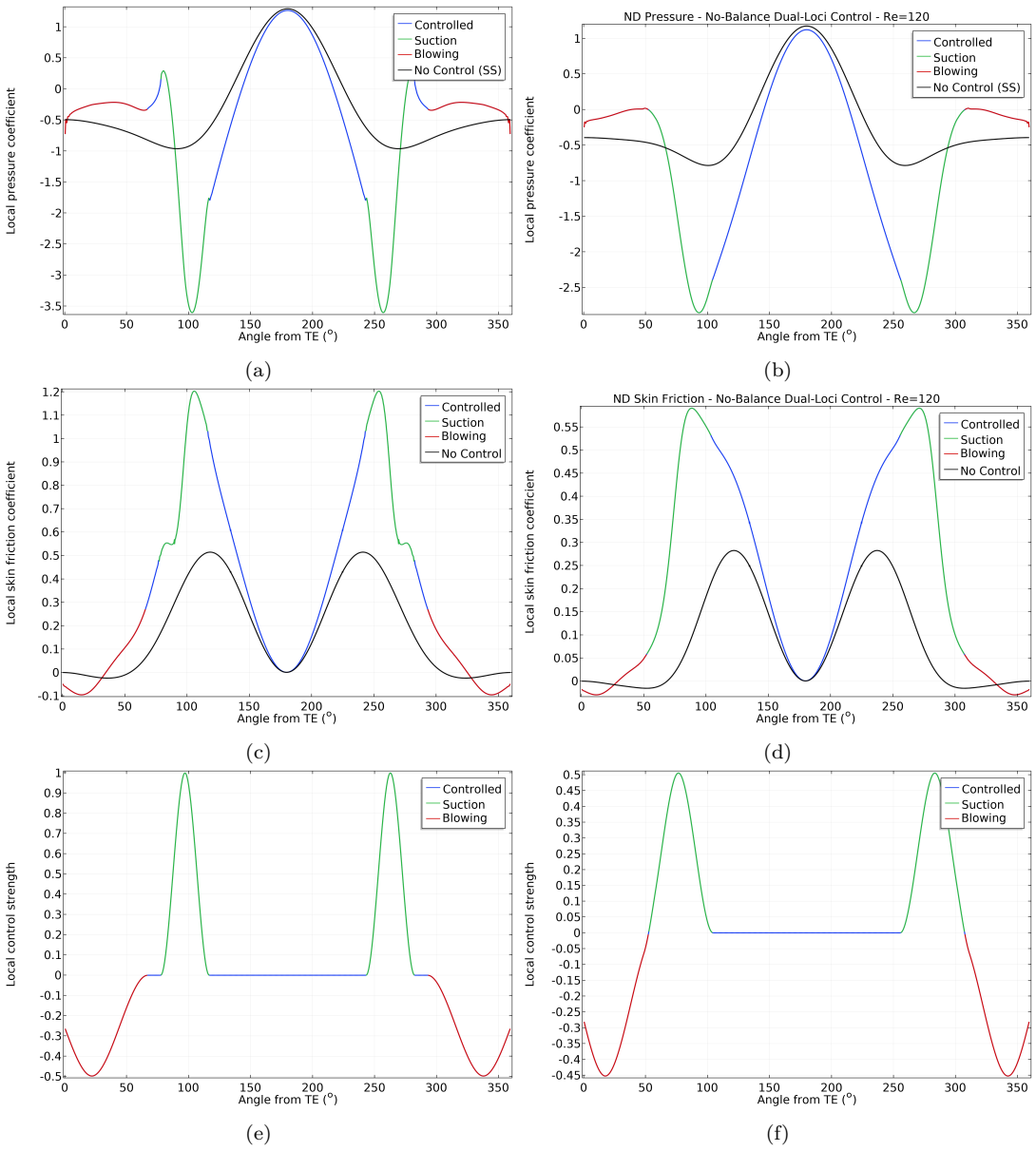

Figure 7.3 Pressure (a), skin friction (b), and control strength (c) coefficient plots for optimised unbalanced dual-loci control at $Re = 40$ (left) and steady-state $Re = 120$ (right).

7.4.1.3 Conclusions from Model I

Suction/blowing control with the dual-loci arrangement is even more effective than suction control on its own. This control is effective by the same mechanisms as suction control on its own – improving the pressure distribution over the cylinder by lowering the front pressure and raising the base pressure. The addition of blowing, particularly when located at the rear of the cylinder, aids greatly in the latter process. However, the optimised control is not favourable for autogenous control. With sufficient leeway in between the uncontrolled values and the optimal values, there may be one or many autogenous arrangements that can still provide substantial improvement in total drag.

The next step is to determine what effect dual-loci control with imposed flow-rate balance (Q-balanced dual-loci) has on the overall control, and to investigate what suction/blowing arrangements can potentially be produced autogenously while providing some benefit to the total drag value.

7.4.2 Model II – Q-Balanced Suction and Blowing

7.4.2.1 Parametric Study

The pressure profiles for all simulations in the parametric study for $Re = 40$ and $Re = 120$ are shown in Figure 7.4 to convey the overall range of Q-balanced dual-loci control at these Reynolds numbers. While all parameter values produced a converged result at $Re = 40$, this was not the case at $Re = 120$ where 37 of the 750 simulations failed to converge, presumably because the real flow is too unsteady to be solved with steady-state equations. The plots are very similar both for the uncontrolled values and the resulting control profiles. Details to note are narrower skin friction envelope at $Re = 120$ where inertia begins to dominate, and the contraction of the minimum pressure at the higher Re as the flow becomes less sensitive to the geometric effects of the cylinder due to faster convection. The range of effects from the control are comparable. Large spikes are seen for both profiles at the locations where suction and blowing are applied in the parametric sweep.

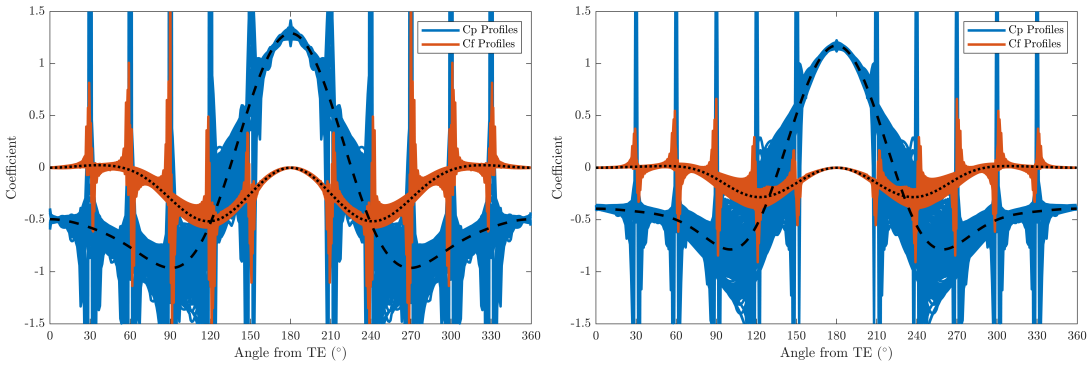

(a) $Re = 40$ (b) $Re = 120$

Figure 7.4 All pressure and skin friction profiles resulting from the parametric simulations at $Re = 40$ (left) and $Re = 120$ (right). The uncontrolled profiles are given by the dashed and dotted black lines.

The benefit of a parametric study is that the effect of each parameter on the results can be considered individually. One of the most important parameters is the location of each locus, θ_q & θ_{q_b}, and whether suction upstream of blowing or vice versa is best. The balance of improvement to the total drag (predominantly by influencing the pressure profile) and the potential for autogenous control (based on the average pressures of each locus) is the primary focus of this investigation. First let us consider the general impact of suction and blowing, then consider the effect of their location/order.

General Effect of Suction/Blowing The impact of suction and blowing and their relative location over the cylinder is demonstrated by the pressure plots in Figure 7.5 below. Here, two representative cases are shown where the same suction/blowing loci (spread and strength) are implemented alternately with suction upstream ($\theta_q = 150°$) and downstream ($\theta_q = 30°$ and with the blowing locus occupying the converse location.

At the Control Surface Suction causes the pressure to drop where it is applied but produces a net increase after the control region. The lower pressure in the region is needed to produce the suction (or rather a consequence of imposing the suction). This is because a pressure gradient from the free-stream to the boundary wall (control surface) is produced drive the flow into the suction locus. Conversely, blowing results in an increase in pressure where it is applied for the same reasons as the suction produces lower pressures.

Downstream of the Control Surface After each control region, the opposite effect is seen on the flow, however. After the suction region the pressure usually recovers above its uncontrolled profile, while after the blowing it is reduced below the uncontrolled profile. Presumably this is because the BL is reinvigorated by the free-stream after the suction region and the free-stream pressure has been less affected by the effect of the geometry and so still has a higher pressure. Suction alleviates the pressure in the near-stagnant fluid in the boundary layer. Meanwhile, on the rear-half, the suction usually produces a local decrease in pressure (again due to alleviating the fluid interactions in the stagnant BL) but can produce an increase in pressure on the base-pressure as it pulls the free-stream fluid around the body more closely. The fluid particles bully up against each other and provide a cushion of support for the cylinder, whereas without the suction/blowing they separate from the cylinder and leave a low pressure vacuum in the wake.

Impact of Reynolds number The effects of suction/blowing are generally the same at $Re = 120$ as at $Re = 40$, however the strength of the effect is subdued at the higher Reynolds number. In particular the effect of control on the leeward half is significantly damped. This is because the greater inertia of the free-stream flow means that the control is most effective by acting on the BL, and this is already separated over the rear of the cylinder. Overall it appears that the sensitivity to control upstream is relatively unaffected.

Skin Friction The x-component of the skin friction profiles are shown in Figure 7.6 also. The opposite trends are seen for C_f as for C_p with suction causing a net *decrease* in skin friction, and blowing causing the reverse. The influence of Re on these profiles is weaker, and it remains relatively consistent. Overall though, given the greater magnitude of the pressure to the skin friction effects (as shown in Figure 7.4) the influence of control on the pressure profile is the dominant concern.

Generally The parametric study showed that the application of suction usually

results in a drop in pressure where it is applied, but a commensurate or greater increase in pressure downstream of it. Its net effect is usually to raise the pressure downstream. On the other hand, blowing results in an increase in pressure followed by a reduction. To decrease the pressure drag, it is desirable to raise the base pressure (the pressure on the leeward half of the cylinder) or lower it on the upwind half, therefore it seems most appropriate for blowing to be applied upstream and suction downstream. This is only from a pressure perspective however, and the impact on skin friction drag is actually the reverse.

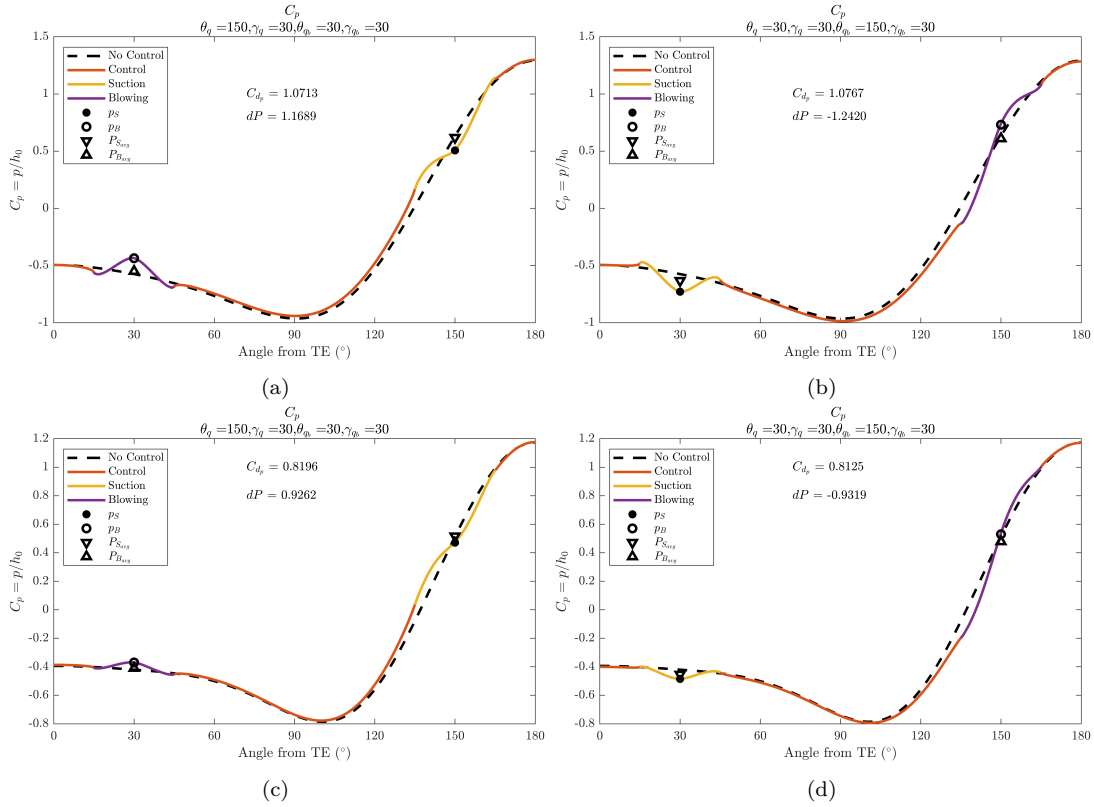

Figure 7.5 Comparison of effect of control at $Re = 40$ (a,b) and $Re = 120$ (c,d) on the pressure profiles with different suction/blowing locations. Plots on the left, the suction is upstream, while on the right suction is downstream.

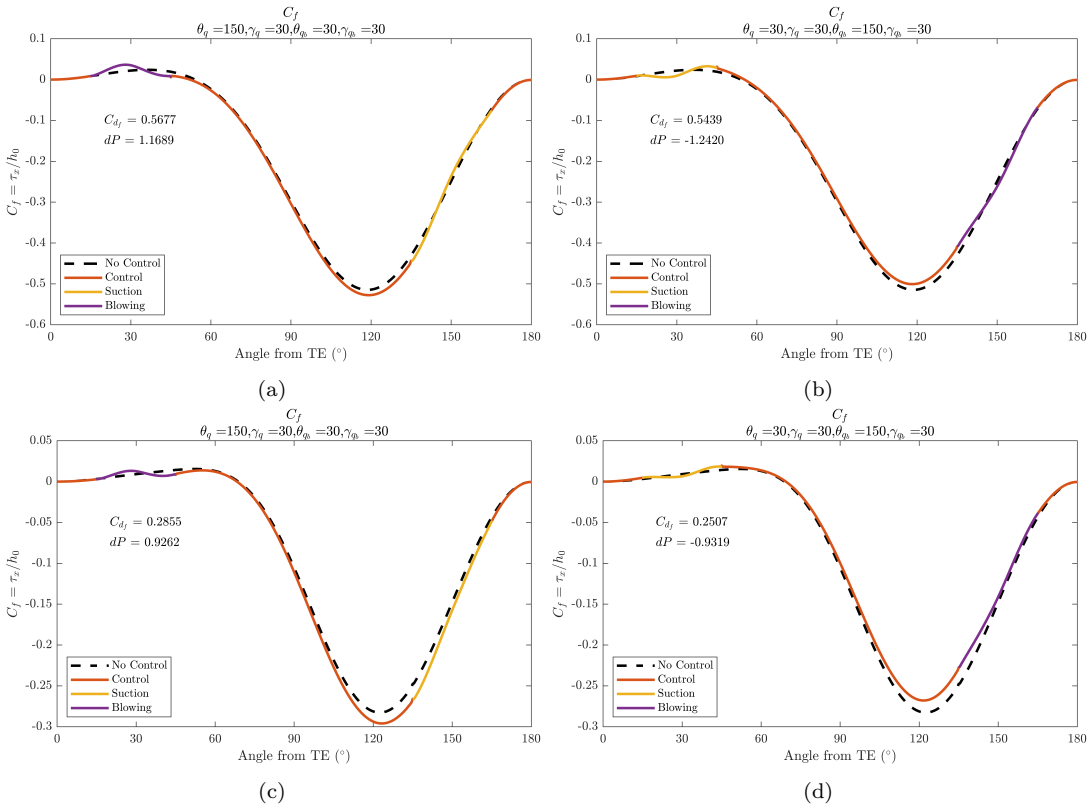

Figure 7.6 Comparison of effect of control at $Re = 40$ (a,b) and $Re = 120$ (c,d) on the skin friction profiles with different suction/blowing locations. Plots on the left, the suction is upstream, while on the right suction is downstream.

Statistical Effect on Pressure While the representative cases above are a useful tool for understanding the general effect of suction and blowing, a more holistic analysis is necessary to consider the effects of each parameter (location, spread, strength) and specifically their integrated effect – pressure and skin friction drag. The average change in pressure from the uncontrolled case is determined for each solution, and then this is plotted against each control parameter. The plots shown in Figure 7.7 are produced. While much of the information is obscured (and is difficult to show given the 5-dimensional nature of the data), there are some clear trends here. Most notably, the spread of the suction, γ_q, has a tremendous effect on the change in pressure profile. The wider the suction, the stronger the impact on the pressure profile (in either direction). The spread of the blowing, γ_{q_b}, does not have much of an effect, on the other hand.

As expected, the location of the suction and blowing has a strong impact also, and are negatively correlated (due to their opposite effects on the flow). Suction applied on the front half ($\theta > 90°$) increases the base pressure (the pressure on the leeward half), while it can have a positive or negative effect on the front pressure depending on the overall arrangement. In most cases blowing on the rear is best for raising base pressure, though it can decrease it with some arrangements. Regardless, it has a better effect than blowing placed on the front half.

The best results for improving drag are achieved when the base pressure is raised and the front half decreased. It can be seen, therefore, that wide-spread suction over the front-half of the cylinder (blue dots) results in the best base pressure improvements. In order for the blowing to improve the base-pressure, it must be situated on the leeward half. For reducing the front-pressure, there is clearly an optimal location for both the suction and the blowing, with the suction situated at roughly 90° with strong suction, and for the blowing, located as close to the leading edge as possible with a small spread. Though this blowing arrangement has a large power cost as will be discussed shortly.

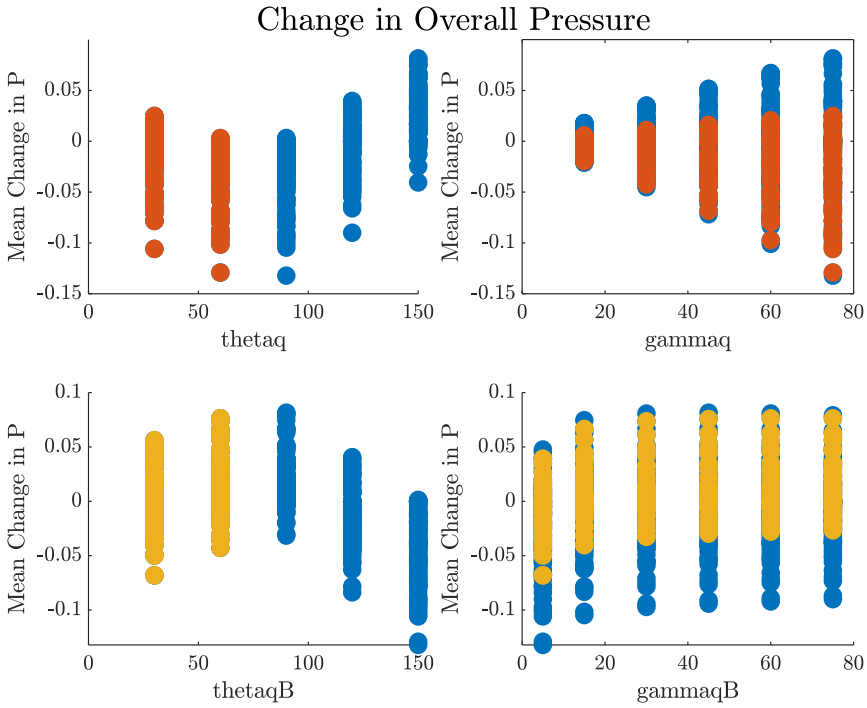
Change in Overall Pressure
Mean Change in P
thetaq
gammaq
thetaqB
gammaqB

(a)

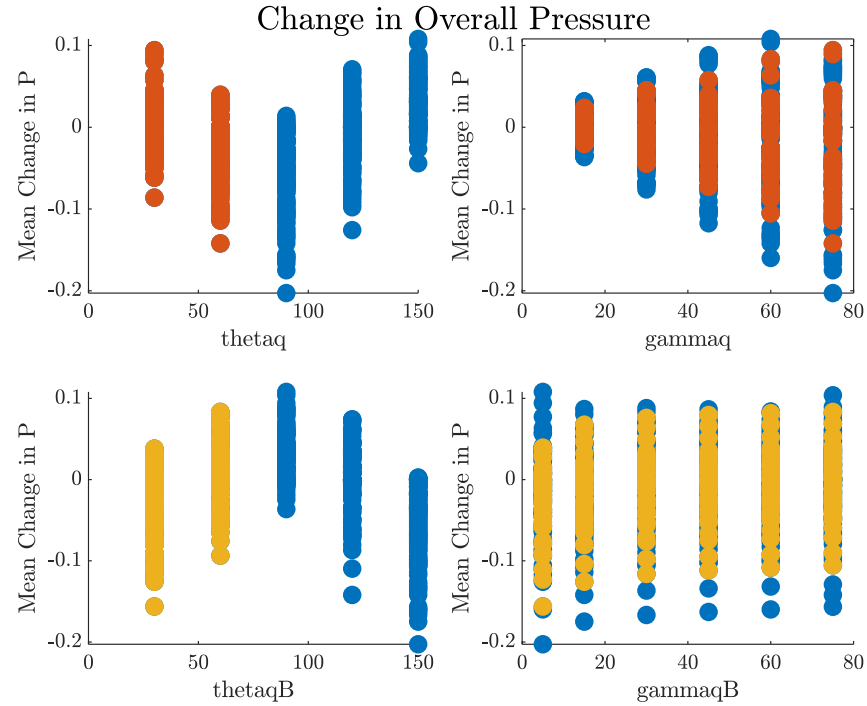
Change in Overall Pressure
Mean Change in P
thetaq
gammaq
thetaqB
gammaqB

(b)

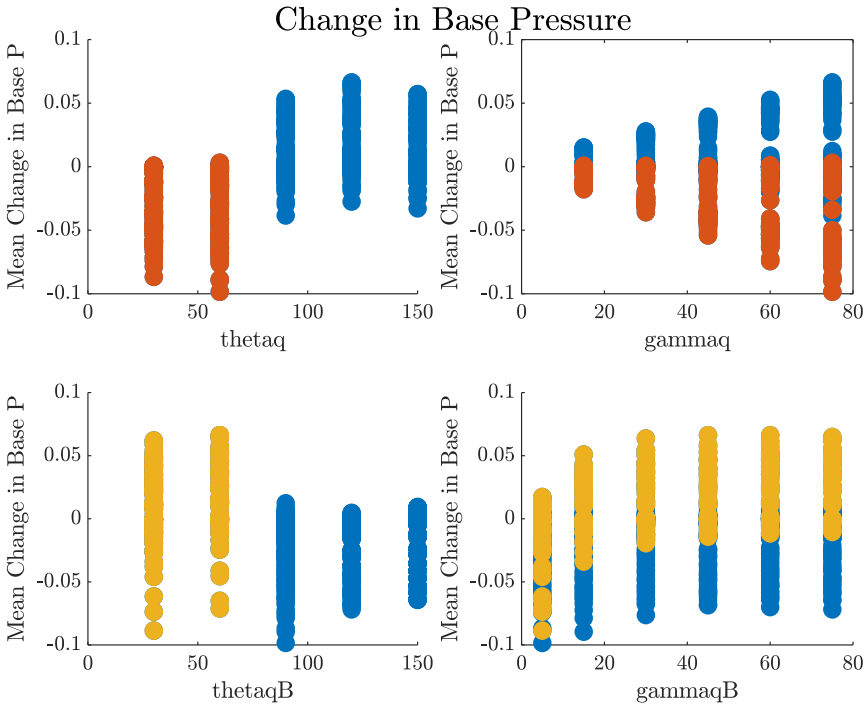

(c)

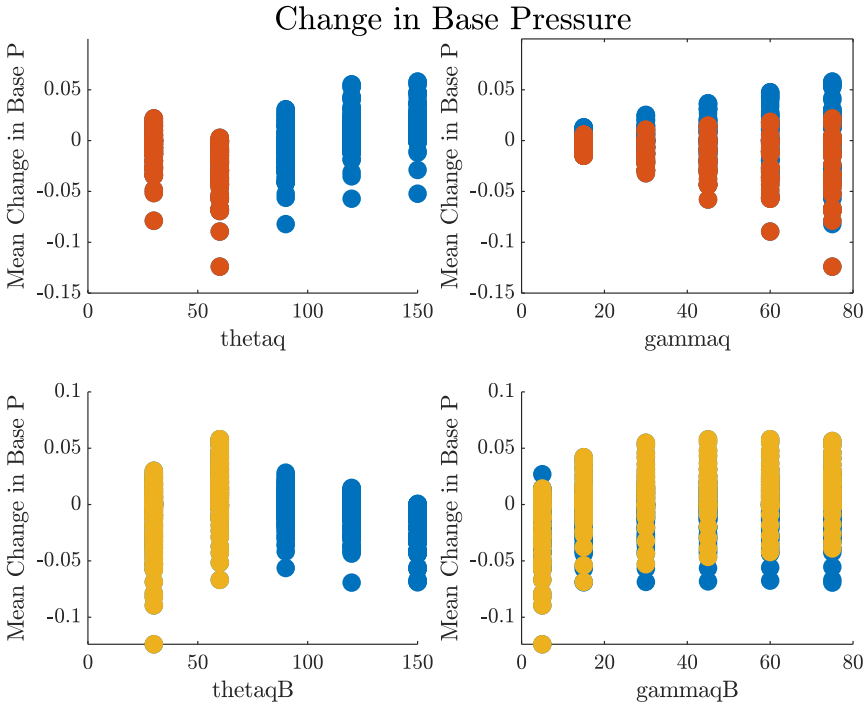

(d)

Figure 7.7 Effect of control parameters on the (a) total pressure, (b) base pressure and (c) front pressure on the cylinder at $Re = 40$ (a,c) and $Re = 120$ (b,d). The change in pressures from the uncontrolled case are shown plotted against each control parameter. Where the control is applied in the rear-half, an orange or yellow colour is used.

Feasibility of Effective Autogenous Suction Control Now let us look at what these results say about the feasibility of employing autogenous suction control to reduce drag, beginning with the case at $Re = 40$ followed by the $Re = 120$ implementation. At the minimum the following requirements are needed for effective autogenous suction control:

1. A positive pressure gradient from the suction control region to the blowing control region: $dP = P_s - P_b \geq 0$
2. An improvement in drag coefficient.

The data-points where these conditions are satisfied are extracted from the overall set and shown in in Figure 7.8 for $Re = 40$ and Figure 7.11 for $Re = 120$. First, we plot the pressure drag and the control pressure gradient for each simulation performed. Then the control arrangements where the pressure gradient is positive are extracted. Finally, this subset is thinned further by taking only the iterations where the pressure gradient is positive and an improvement in pressure drag resulted. The pressure drag was used as the criteria first as it is the dominant contributor to total drag, but later the process is repeated for C_{d_f} and C_{d_t}.

The most interesting and important thing to note is for how few of the arrangements a positive control pressure gradient is achieved, as shown by the first two sub-plots. Only 287 of the 750 simulations resulted in a positive dP value, and in many cases this was near zero. Furthermore, the arrangements where the best improvement in pressure drag are seen, are usually when the control pressure gradient is negative. The first 300 iterations (where most of the candidates are situated) are the simulations where the suction is located in the front-half of the cylinder, $\theta_q = 150°, 120°$ (to be expected as the overall analysis above showed this to produce the best base and front pressure changes).

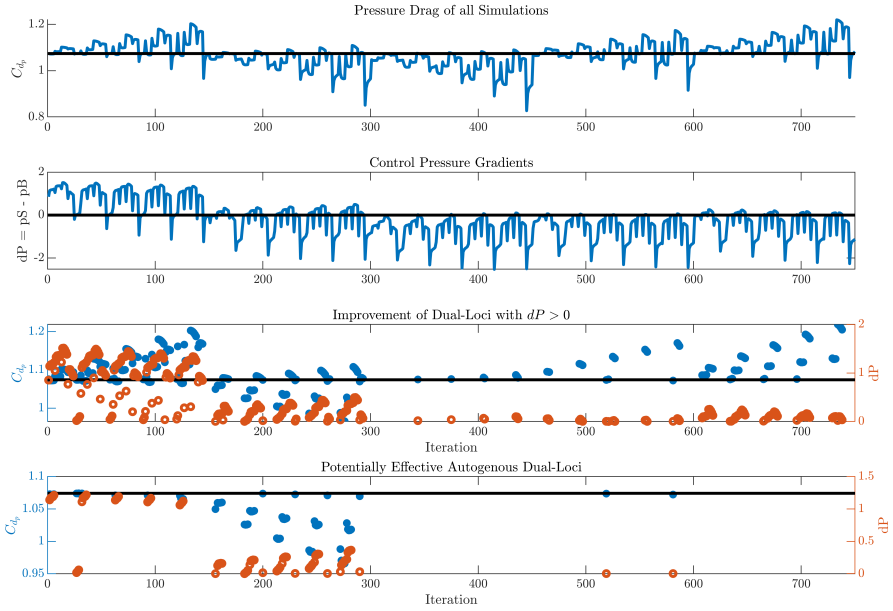

Figure 7.8 Break down of each control's effectiveness at $Re = 40$. Firstly, the pressure drag of each control arrangement, then the pressure gradient between suction and blowing loci, both data-points shown only for the potentially autogenous arrangements, and finally only the potentially autogenous control that improves the pressure drag. The black lines indicate the values for the uncontrolled flow.

The last two sub-plots show the cases where $dP > 0$ and where C_{d_p} is improved under such conditions. In this last sub-plot we see that only 74 of the 750 arrangements investigated ($\sim$ 10%) resulted in an improved pressure profile and are – at least hypothetically – possible to achieve by autogenous control. In many cases, the pressure improvement is very small. The best improvement in pressure drag was 10.14%, with a $C_{d_p} = 0.9653$ and $dP = 0.1757$. However, the total drag is 1.5983, an improvement of only 1.9598% (compared to $C_{d_{t_0}} = 1.6303$). The resulting pressure and skin friction profiles from this control are shown below in Figure 7.9. It can be seen by the change to the uncontrolled pressure profile that the control is effective because it lowers the pressure profile over the forward-half while increasing it over the leeward half. There is relatively little change to the skin friction, though it is worsened slightly. It is important to note that the skin-friction component shown here, C_f, is only the x-component, whereas the pressure curve must be resolved into its x-component before considering its net influence on the drag.

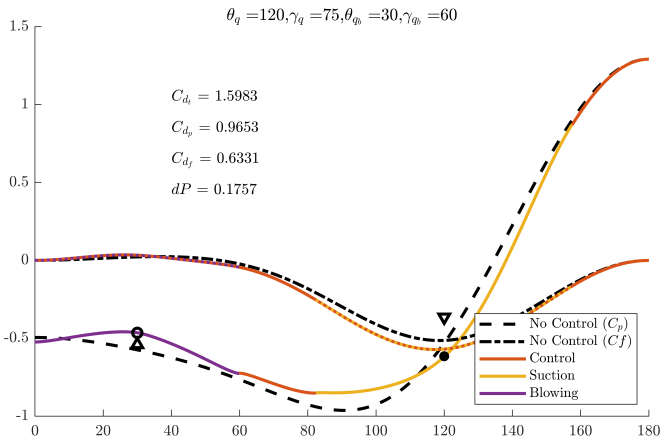

Figure 7.9 Pressure and skin friction profiles for control which gives the best improvement in pressure drag with potentially autogenous control.

The above is the best improvement in pressure drag (with potentially autogenous control), but when accounting for the skin friction drag contribution also, the best total drag case is not quite the same. However, it is a very similar control, with just a slightly wider blowing locus ($\gamma_{q_b} = 75°$) which produces a slightly smaller total drag of $C_{d_t} = 1.5981$ (compared to 1.5983) with $dP = 0.2005$. This is a negligible difference. It is clear that the pressure drag is the more dominant contributor, even at the lower Reynolds numbers, and this trend increases with Re also. The profiles for this case are very similar and so will not be shown.

Compare these autogenously-generated results with the best case regardless of if $dP > 0$ or not, which is shown in Figure 7.10 below. Here, very strong blowing is applied upstream, causing a dramatic reduction in pressure over the front half (despite the sudden spike). The suction on the leeward half then brings the pressure up slightly here. Overall, in this instance, the heavy-lifting is being done by the strong blowing force. This is quite a different arrangement to the optimised unbalanced dual-loci control found with Model I, and achieves improvement in pressure drag in a totally different way. This is likely due to the limited combination of parameters investigated. A full optimisation study may produce a different optimal result. Here, $C_{d_t} = 1.4162$, and $C_{d_p} = 0.8275$, which is quite a bit worse than the total drag coefficient achieved by the unbalanced dual-loci control (1.3718). This control arrangement has a pressure gradient value of $dP = -2.5015$ meaning the control would require a lot of effort to drive the flow from the suction to blowing location.

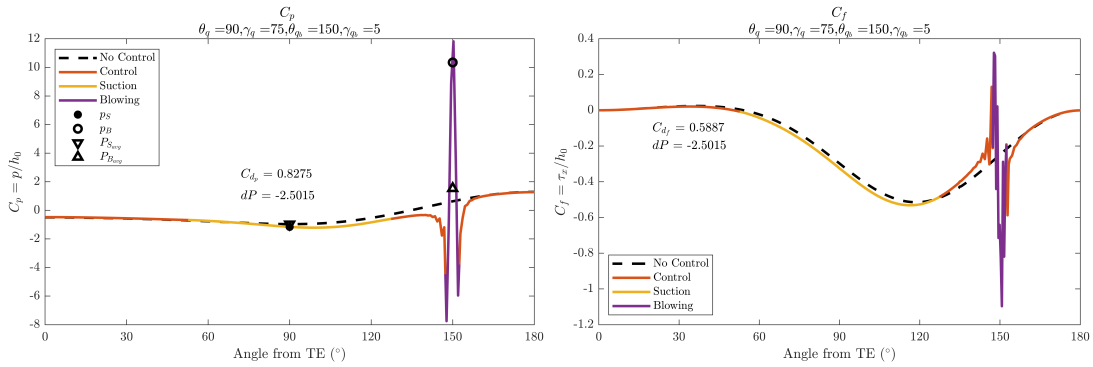

Figure 7.10 Pressure (a) and skin friction (b) profiles for the case which most improves total drag regardless of dP. Shown on separate plots for clarity.

At $Re = 120$ there are roughly the same number of potential candidates for effective autogenous control as at $Re = 40$ (277 at $Re = 120$ vs 287 at $Re = 40$). However for autogenous control cases that also improve pressure drag, there are much fewer candidates – only 25 compared with 74 at $Re = 40$ (see Table 7.5 for further details). These are grouped around the same iteration range as for $Re = 40$, from 150-300, where the suction locus is located at $\theta_q = 120°$. This appears to be the most important factor. These data are shown in Figure 7.11.

It is important to highlight here, before discussing the impact of the pressure drag results, that the drag on the steady cylinder at $Re = 120$ is significantly lower than its unsteady variety. Therefore the values here are only indicative. This will be discussed further after all results have been presented.

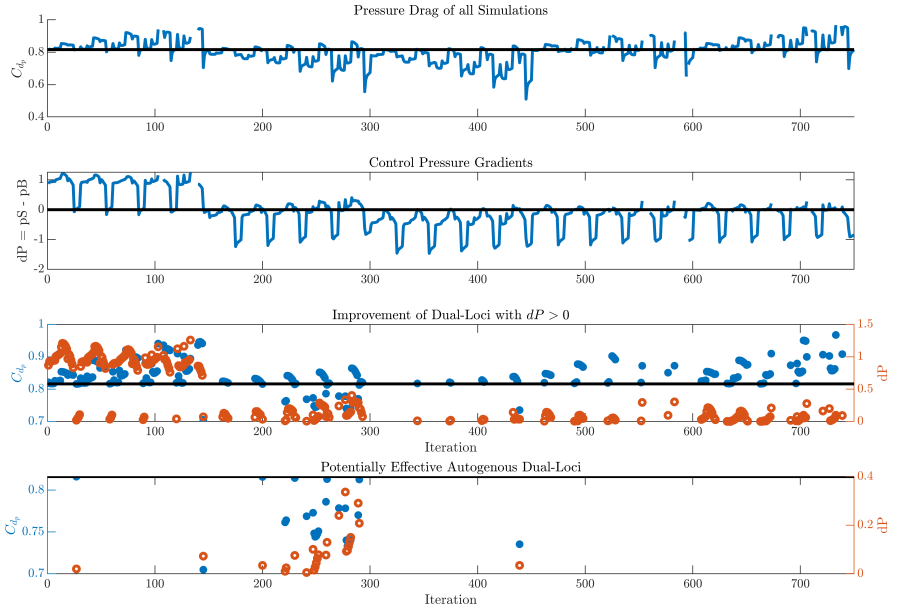

Figure 7.11 Break-down of data-points at $Re = 120$ which reduce the pressure drag and could be autogenously generated. Note missing data-points in the first two plots from unconverted solutions. Black line gives the values for the uncontrolled flow.

Table 7.5 Number of data-points (out of 750) that had a positive pressure gradient ($dP > 0$) and produced improvement in a characteristic

	$Re = 40$		$Re = 120$	
Result	Number	% of Sweep	Number	% of Sweep
Improved C_{d_t}	51	7%	25	3%
Improved C_{d_p}	74	10%	22	3%
Improved C_{d_f}	51	7%	166	22%
Improved C_{d_p}& C_{d_f}	7	1%	9	1%

The best improvement in pressure drag is slightly higher than for $Re = 40$, with an improvement of 13.64% ($C_{d_p} = 0.7049$) when $dP = 0.0727$. This pressure gradient, dP, is quite a bit weaker though and may cause issues in practice. Looking at the pressure profile for this control (Figure 7.12), it is seen that this control is overlapping (the blowing locus contained within the suction locus) and so is not a good candidate. Let us look instead at the potentially autogenous control which minimises total drag, as shown in Figure 7.12 (c). This reduces total drag coefficient by 11.34% but again, this is overlapping. For the case where the control is not overlapping, the best improvement in total drag is only 0.74%. The pressure and skin friction profiles for this control is shown in Figure 7.12 (d). The result for the best (non-overlapping) autogenous control at $Re = 120$ is quite different to its counterpart at $Re = 40$, as demonstrated by the

key data in Table 7.6. The suction and blowing locations are reversed and the method by which the total drag is reduced is also reversed. For this control the pressure drag *increases* whereas the skin friction is decreased which is unusual for this type of control. It must be remembered that these results are for a simple arbitrary set of parameters, optimised dual-loci autogenous control may produce a much larger benefit.

In these results, several things are made clear:

1. The optimal autogenous control for total drag is different to that for pressure drag.
2. The reduction in pressure drag is not a good indicator for the reduction in total drag in terms of magnitude, as the skin friction usually rises by a large fraction of this saving, but often the best control for the total drag and pressure drag objective are the same or very alike.
3. Overlapping suction/blowing loci appears to produce favourable results, but may be hard to implement in practice.

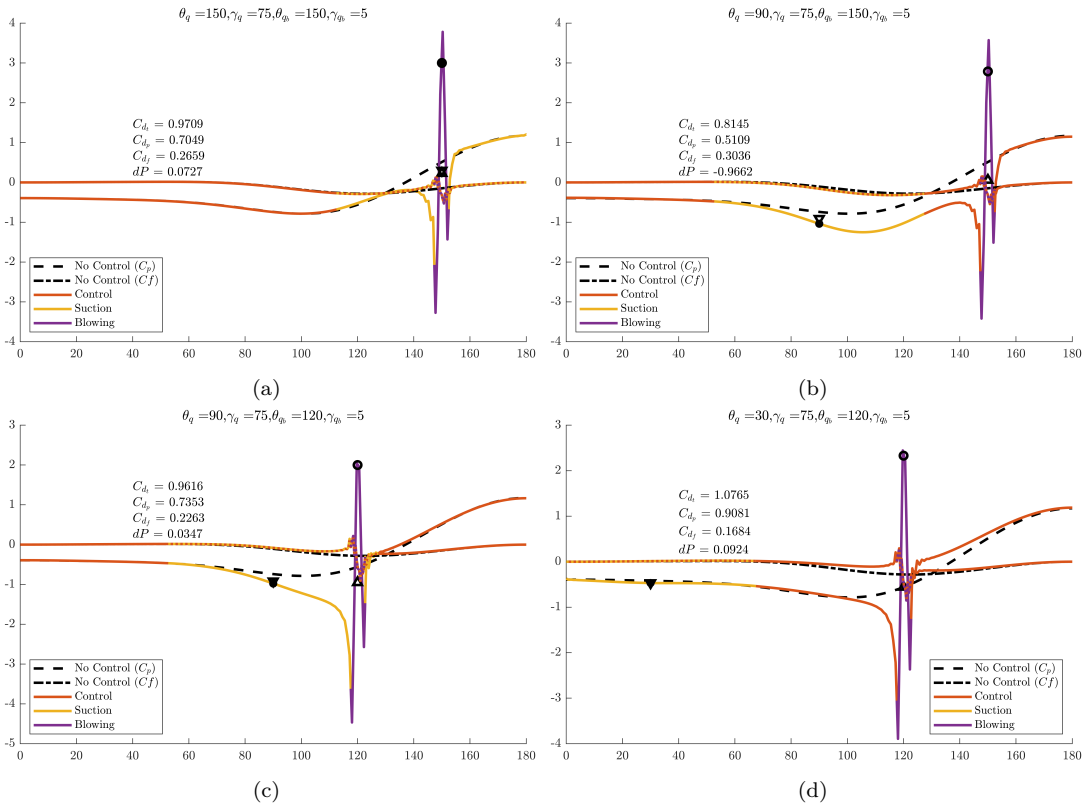

Figure 7.12 Control candidates with best improvement in pressure or total drag. (a) best autogenous C_{d_t} candidate, (b) best general C_{d_p} candidate, (c) best C_{d_t} candidate, (d) best autogenous C_{d_t} with no overlap.

Table 7.6 Q-balanced dual-loci control that produces the best total drag reduction with an autogenous-capable arrangement.

Parameter	$Re = 40$	Change (%)	$Re = 120$	Change (%)
θ_q	120°	-	30°	-
γ_q	75°	-	75°	-
θ_{q_b}	30°	-	120°	-
γ_{q_b}	75°	-	5°	-
C_{d_t}	1.5981	-2.08%	1.0765	-0.88%
C_{d_p}	0.966	-10.22%	0.9081	11.06%
C_{d_f}	0.6322	13.69%	0.1684	-37.24%
dP	0.2005		0.0924	

Application to Real Time-Dependent Flow It is worth considering the potential application of this control to the real time-dependent flow at $Re = 120$. Figure 7.13 shows the pressure profile of the unsteady flow, as solved using our COMSOL model. The time-averaged and five instantaneous plots are shown to demonstrate the range and fluctuations of the pressure profile in the periodic vortex shedding flow. The pressure profile from the uncontrolled steady-state simulation is also shown. The base-pressure profile especially is quite different from the steady-state version. The dynamic wake causes oscillations in the pressure profile, and the shedding vortices cause less pressure to be recovered over the leeward half, instead losing the energy to the eddies.

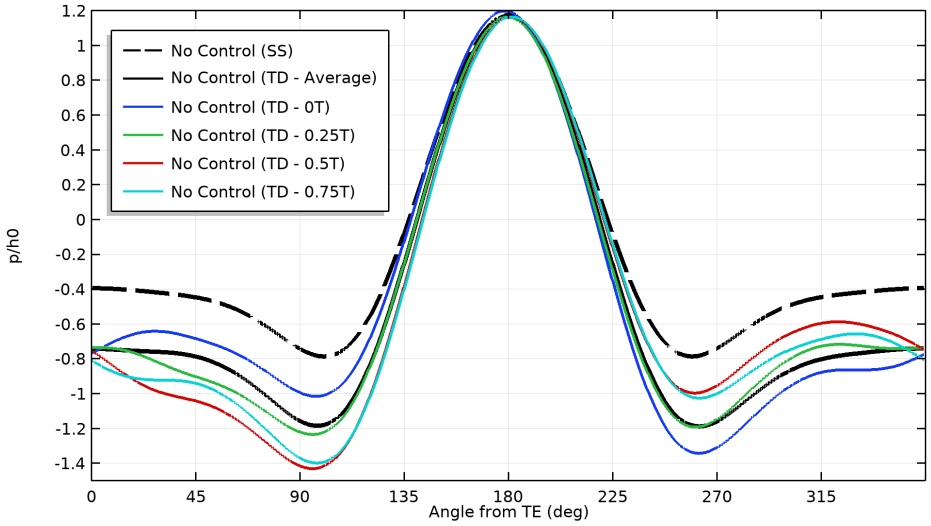

Figure 7.13 Instantaneous and time-averaged pressure profile on uncontrolled cylinder at $Re = 120$.

Now let us consider applying the best non-overlapping autogenous control to this pressure profile. The suction is centred on $\theta = 120°$ with a spread of $\gamma_q = 75°$. The steady and unsteady pressure profiles begin substantially diverging at about $\theta = 140°$

which means that the average pressure of the suction control region will actually be quite a bit lower than in the steady-state simulations. On the other hand, the regions where blowing pressure is applied are also reduced, so the effect on dP may be negated. Though it seems reasonable to expect a drop in dP which may jeopardise the real application of autogenous control as a larger dP than even the 0.09 available from the steady-state case may be needed to overcome friction and porous losses.

Overall, it is feasible that this control may be applied to the unsteady flow and the condition of $dP > 0$ still be satisfied always. What remains to be seen is if the impact felt in the flow by the control also carries through. Time-dependent simulations are needed in order to test this either way.

7.4.2.2 Optimisation Study

Performing a derivative-free optimisation on the Q-balanced dual-loci control produced control arrangements that greatly improved on the indications provided by the parametric study. The control parameters and key results are shown in Table 7.7 and Table 7.8 compared to the unbalanced case. At both Re, much larger suction strengths are employed for the optimised control than the 0.1 value used in the parametric study. The unusual behaviour for the best total drag control from the parametric study at $Re = 120$ is not reflected in the optimised result. Here, the usual trend of upstream suction and leeward blowing was again produced. Unlike for the unbalanced case, the spread of the blowing locus was much narrower. This may be partly due to the constraint imposed that neither locus should spread over their half of the cylinder (i.e. the lower bound for the spread of either locus was 0° and the upper bound 180° from the TE).

Unsurprisingly, the improvement in total drag is not as substantial as for the case with unbalanced control, given that this Q-balanced arrangement is a subset of the unbalanced dual-loci arrangement. Despite the slightly worse result, the improvement in drag is still strong at both Re, again producing over 20% reduction at $Re = 120$. However, when the pressure differential between the suction and blowing loci are considered, it can be seen that this control would require substantial power to run due to the strong APG between suction and blowing loci. For completeness, the pressure and skin friction profiles are shown alongside their unbalanced variety in Figure 7.14.

Table 7.7 Key control parameters for drag-optimised Q-balanced dual-loci control compared to its unbalanced variety.

	$Re = 40$		$Re = 120$	
Parameter	Q-Balanced	Unbalanced	Q-Balanced	Unbalanced
θ_q	97.898°	97.116°	78.897°	76.542°
γ_q	31.676°	39.016°	43.607°	55.774°
$c_{q_{max}}$	0.987	1	0.569	0.506
θ_{q_b}	31.501°	22.003°	27.835°	17.521°
γ_{q_b}	63.001°	90°	55.669°	81.701°
$c_{q_{max_b}}$	-0.496	-0.498	-0.446	-0.453
C_q	0	-0.004	0	-0.011

Table 7.8 Key results for optimised dual-loci control with unbalanced control, and Q-balanced control compared to uncontrolled case.

	$Re = 40$			$Re = 120$		
Parame-ter	No Control	Unbal-anced	Q-Balanced	No Control	Unbal-anced	Q-Balanced
C_{d_t}	1.6321	1.3718	1.4158	1.086	0.8196	0.8486
C_{d_p}	1.076	0.2578	0.4365	0.8177	0.1265	0.1998
C_{d_f}	0.5561	1.1141	0.9793	0.2683	0.6931	0.6487
θ_s	54.107°	34.834°	37.809°	68.826°	29.392°	32.612°
dP	-	-1.6333	-1.5387	-	-1.5388	-1.4143

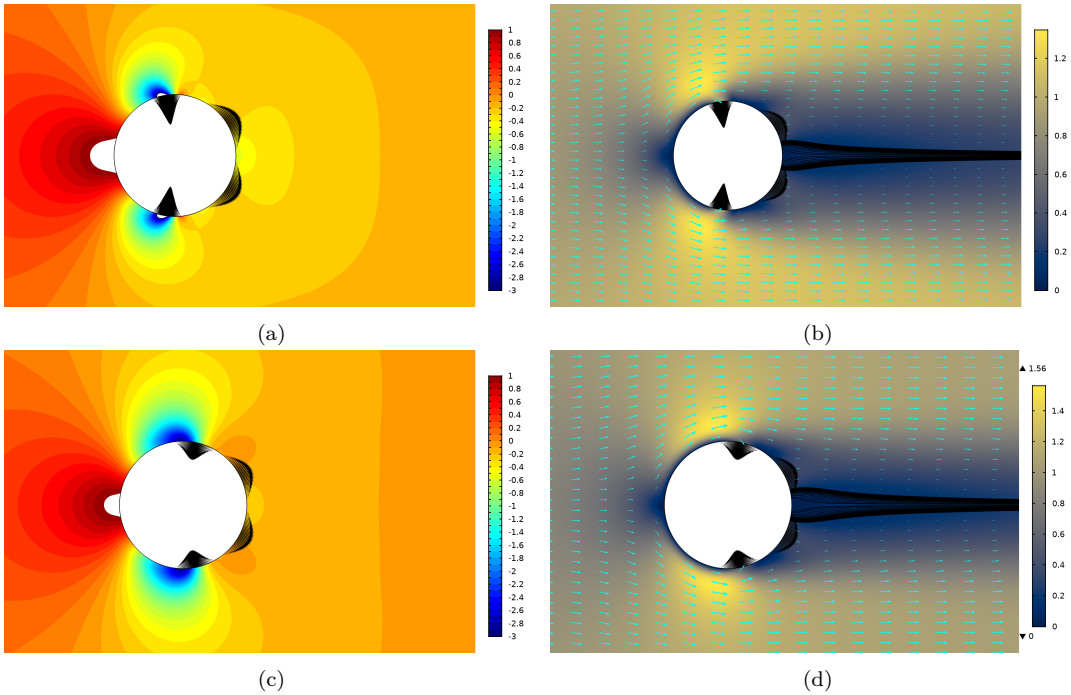

Figure 7.14 Velocity surface (a,c) and pressure contours (b,d) for optimised Q-balanced dual-loci controlled flow at $Re = 40$ (a,b) and $Re = 120$ (c,d).

7.4.2.3 Time-Dependent Simulation Verification

To understand the impact of the time-dependent effects, a few control arrangements were tested on the unsteady model. These were: a) the representative case where suction is upstream and blowing downstream, as well as its converse arrangement, and b) the best non-autogenous control. The results for the suction upstream/downstream comparison are shown in Figure 7.15. The general response of the flow to suction and blowing is effectively the same as in the steady-state simulations. However, the accumulative effect of blowing upstream (suction downwind) is a lot stronger. The pressure drop after blowing at $\theta_{q_b} = 150°$ is large and persists even after the suction downstream. This is quite different to the result from the steady-state simulation where the pressure profile returned to its uncontrolled state at the trailing edge. Also, the effect on skin friction is worsened; the magnitude of the shear stress is much greater, particularly at its zenith.

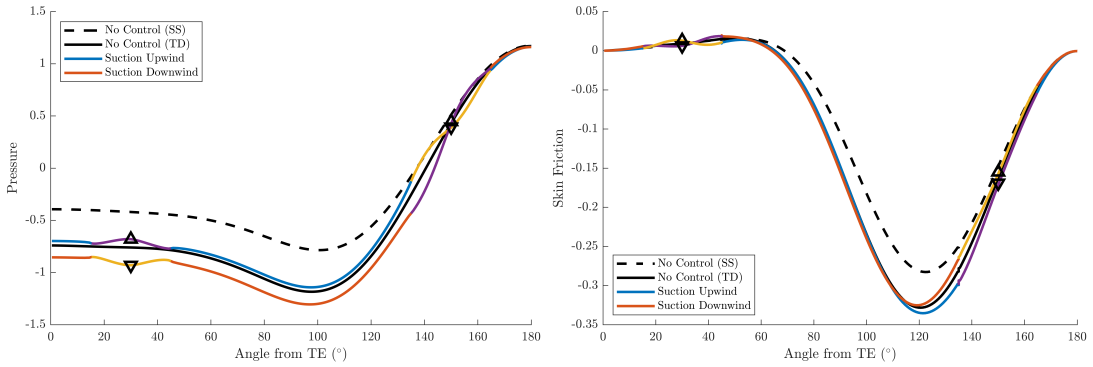

(a) (b)

Figure 7.15 Time-averaged plots of pressure and skin friction plots with dual-loci control arranged with either suction upstream or downstream. The yellow regions represent where suction is applied and purple where blowing is.

The key results for best non-autogenous control from the optimisation study at $Re = 120$ are shown in Table 7.9. It turns out that this control is strong enough to fully stabilise the flow. Therefore, the results from the steady-state simulations match perfectly with the time-dependent simulations. However, since this control should be compared against the drag for the time-dependent case, the improvement is now seen to be 38.7%. The data in Table 7.10 clearly indicates that this massive improvement comes from the large reduction in pressure drag, while the skin friction drag has almost doubled. The control arrangement is still highly unfavourable for autogenous control, and its actual efficiency would be low given the large APG that the control flow has to overcome. However, it is encouraging to see that the dual-loci control can be extremely effective on unsteady flows. The pressure and velocity contours are not shown for this simulation as they match in practically every aspect, those in Figure 7.14.

Table 7.9 Key results for optimised Q-balanced dual-loci control verified on time-dependent simulations at $Re = 120$.

Parameter	No Control (SS)	No Control (TD)	Q-Opti (SS)	Change from No Control SS (%)	Q-Opti TD	Change from No Control TD (%)
C_{d_t}	1.086	1.3851	0.8486	-21.90%	0.8486	-38.70%
C_{d_p}	0.8177	1.0585	0.1998	-75.60%	0.1997	-81.10%
C_{d_f}	0.2683	0.3266	0.6487	141.80%	0.6489	98.70%
dP	-	-	-1.414	-	-1.415	-

7.4.3 Model III – P- Q-Balanced

7.4.3.1 Steady-State Optimisation

Using the two-optimisation process, the dual-loci control was successfully optimised to minimise drag while maintaining a specified pressure drop between the suction and blowing loci. Firstly, the results where the condition $dP > 0$ was enforced which is the most liberal allowance for control. The major optimisation has the total drag of the cylinder as its objective and it controls the suction loci parameters, while the minor optimisation has the same objective but the additional constraint of $dP > 0$, and it controls the blowing loci parameters. The optimised control parameters and key results are shown in Tables 7.10 to 7.12

As was expected, based on the results of the parametric study, the improvement in drag is much weaker when the autogenous constraint is imposed. Nevertheless, the drag on the cylinder was successfully reduced while maintaining a positive pressure gradient from the suction to blowing loci. For IV1, at $Re = 40$ the drag was reduced by 5.45% while at $Re = 120$ a more modest 3.68% improvement was achieved while the improvements from the IV2 case were even lower. In both cases, the drag improvement was through a combination of the pressure drag and skin friction drag. Unlike for the case of suction only, where the pressure drag is substantially improved but the skin friction worsened to produce a net benefit, here both components are slightly reduced. While the angle of separation is reported as very far forward on the cylinder, this is not quite accurate. Indeed there is a small separation here, but this is mostly due to the control and is quickly stamped out. At both Reynolds numbers, a quite different control flow was utilised to achieve the drag objective. This was to produce a suction and blowing very close to each other on the front half. This is effective at manipulating the C_f and C_p profiles over the front half, reducing the pressure and skin friction, rather than delaying separation or improving the base pressure.

This dramatically different control arrangement appears to be a factor of the initial values provided for the control. When alternative initial values are provided (as described in the Models section Section 7.3.3.3), the resulting control was quite different. The final optimised controls were very similar to their initial conditions which suggests that there are other local optima that are yet to be determined.

Table 7.10 Optimised control values for different dual-loci settings.

Parameters	$Re = 40$			$Re = 120$		
	P-Q-Balanced	Q-Balanced	Unbalanced	P-Q-Balanced	Q-Balanced	Unbalanced
θ_q	165.520°	97.898°	97.116°	165.260°	78.897°	76.542°
γ_q	26.015°	31.676°	39.016°	27.158°	43.607°	55.774°
$c_{q_{max}}$	0.381	0.987	1	0.162	0.569	0.506
θ_{q_b}	144°	31.501°	22.003°	146°	27.835°	17.521°
γ_{q_b}	10°	63.001°	90°	4.410°	55.669°	81.701°
$c_{q_{max_b}}$	-0.99	-0.496	-0.498	-1	-0.446	-0.453
C_q	0	0	-0.004	0	0	-0.011

Table 7.11 Optimised control values for different dual-loci settings.

Parameter	$Re = 40$				$Re = 120$			
	No Control	Unbalanced	Q-Balanced	P-Q-Balanced	No Control	Unbalanced	Q-Balanced	P-Q-Balanced
C_{d_t}	1.6321	1.3718	1.4158	1.5432	1.086	0.8196	0.8486	1.046
C_{d_p}	1.076	0.2578	0.4365	1.03	0.8177	0.1265	0.1998	0.8013
C_{d_f}	0.5561	1.1141	0.9793	0.51316	0.2683	0.6931	0.6487	0.2447
θ_s	54.107°	34.834°	37.809°	176.08	68.826°	29.392°	32.612°	147.74
dP	-	-1.6333	-1.5387	0.3403	-	-1.5388	-1.4143	0.4928

Table 7.12 Change in optimised result depending on initial values for control at $Re = 40$ and $Re = 120$.

Parameters	IV1	Re=40 Opti	Re=120 Opti	IV2	$Re = 40$ Opti	$Re = 120$ Opti
θ_q	150°	165.52°	165.26°	120°	119.96°	121.91°
γ_q	20°	26.015°	27.158°	40°	42.566°	51.7°
$c_{q_{max}}$	0.1	0.3807	0.16239	0.1	0.111	0.053
θ_{q_b}	90°	144°	146°	80°	24.313°	39.5°
γ_{q_b}	10°	10°	4.4102°	10°	47.125°	23.5°
$c_{q_{max_b}}$	-0.2	-0.9904	-1	-0.4	-0.1002	-0.1176
dP	-	0.3403	1.046	-	0.0277	1.077
C_{d_t}	-	1.5432	0.8013	-	1.6083	0.7716

The pressure contour and velocity surfaces are shown for the best optimised P-Q-Balanced dual-loci control (IV1 case) below at $Re = 40$ & 120 in Figure 7.16, the profiles over the surface are shown in Figure 7.17. The control is concentrated on the front-half and improves both the skin friction and pressure drag modestly. This control arrangement is highly dependent on the initial values used for the optimisation study.

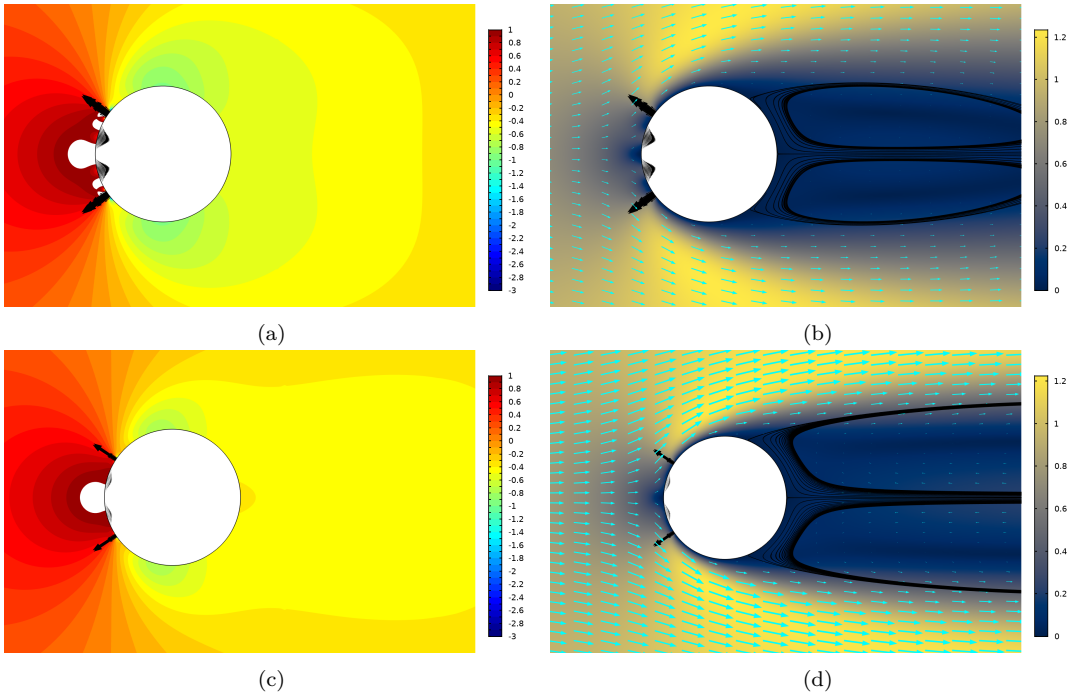

Figure 7.16 Velocity surface (a,c) and pressure contours (b,d) for optimised P-Q-balanced dual-loci controlled flow round cylinder at $Re = 40$ (a,b) and $Re = 120$ (c,d).

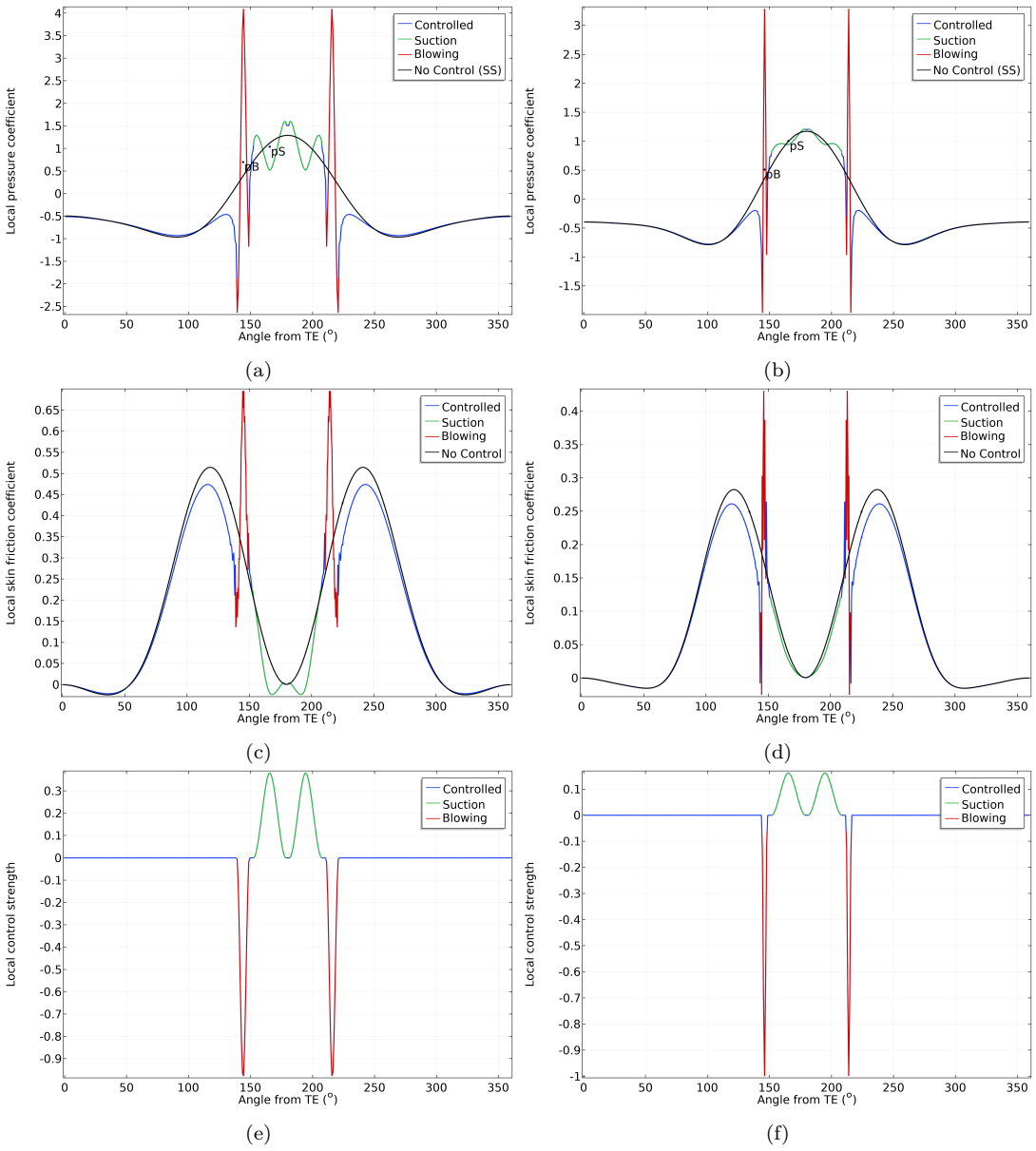

Figure 7.17 Pressure (a), skin friction (b), and control strength (c) coefficient plots for optimised P-Q-balanced dual-loci control with IV1 at $Re = 40$ (left) and steady-state $Re = 120$ (right).

Overall, the major research question of "can autogenous suction control theoretically be used to reduce drag for bluff body flows?" appears to be true. Certainly for $Re = 40$, whereas the flow at $Re = 120$ should be resolved with an unsteady simulation to confirm. However, there are other caveats also. With the present arrangement, in a real system the fluid removed by the autogenous control has to perform a near-180° rotation within the control duct. The momentum of this change must be transferred as a force to the body – in just the same way that a Pelton wheel is rotated. This factor is not encompassed by the pressure and skin friction profiles. Furthermore, there is still the open question of whether the dP value in these optimised controls are truly sufficient to drive the controlling flow imposed here. This question will be addressed in the following

section.

7.4.3.2 Time-Dependent Verification

To verify whether these results are feasible for the true unsteady flow at $Re = 120$, time-dependent simulations were carried out with the optimised control parameters applied – for both sets of optimised results (one for each initial value set used). Though this study cannot confirm whether the pressure drop is sufficient to drive the imposed control, it verifies that the control does reduce drag while maintaining a positive dP value. Indeed the optimised control did satisfy the requirements in both full time-dependent cases. The time-averaged values (over one vortex-shedding period), and their fluctuation are given for the key parameters of the first P-Q-balanced design compared to the steady-state values in Table 7.13. The key parameters for both P-Q-balanced designs are provided in Table 7.14 Additionally, the plots of the drag coefficients over non-dimensionalised time ($t^* = tU/D$) are shown in Figure 7.18.

As expected, the drag coefficient values are quite different from the steady-state values, but the reaction to the control is consistent in the TD simulations. For the first optimised arrangement (with the suction and blowing situated at the front of the cylinder), the improvement in drag is dulled. An average 2.5% improvement was produced compared to the 3.7% predicted by the steady-state study. Importantly, the positive pressure gradient between the suction and blowing loci remains, and in fact is greater for the TD case (0.5764 vs. 0.4928). This makes sense as the pressure profile is steeper and has a larger fluctuation for the unsteady case, even for the uncontrolled flow, which is beneficial for the autogenous constraint.

The most interesting result is the dramatic change in performance for the second P-Q-balanced design (produced using the second set of initial values in the optimisation). Where the steady-state result suggested a reduction in drag of only 0.83%, the actual result when applied to the unsteady cylinder flow was actually 4.3%. This is not just better than the SS estimate, but it is a greater improvement than the first P-Q-balanced design. Figure 7.18 shows the development of the drag coefficients for both controls over time which clearly illustrates the different methods for improving the total drag. While the first design reduces both skin friction and pressure drag modestly, the second design uses the same mechanisms as suction-only control to minimise total drag by greatly reducing the pressure drag at the cost of slightly increasing the skin friction drag. The design of this control fits better with the findings from the studies of Models I and II – that suction near the 90° mark with blowing situated near the rear produces the best drag-reduction but is difficult to achieve with autogenous pressure gradients.

Table 7.13 Key results for SS-optimised P-Q-balanced dual-loci control applied to time-dependent simulation compared to the steady result and uncontrolled values. SS= steady-state, TD= time-dependent.

Parameter	SS No Control	SS P-Q Opti	TD No Control Average	TD P-Q Average	TD P-Q Fluctuation (±)	% Change
C_{d_t}	1.086	1.046	1.3851	1.3517	0.0169	−2.50%
C_{d_p}	0.8177	0.8013	1.0585	1.0485	0.0155	−1.00%
C_{d_f}	0.2683	0.2447	0.3266	0.3032	0.0017	−7.70%
dP	-	0.4928	-	0.5764	0	-

Table 7.14 Comparison of the two optimised P-Q-Balanced dual-loci control in full time-dependent simulation.

Parameter	TD No Control Average	TD Fluctuation (±)	IV1 TD P-Q Average	IV1 TD P-Q Fluctuation (±)	IV2 TD P-Q Average	IV2 TD P-Q Fluctuation (±)
C_{d_t}	1.3851	0.0171	1.3517	0.0169	1.3274	0.0096
C_{d_p}	1.0585	0.0156	1.0485	0.0155	0.9715	0.0088
C_{d_f}	0.3266	0.0017	0.3032	0.0017	0.356	0.0008
dP	-	-	0.5764	0	0.0747	0.0027

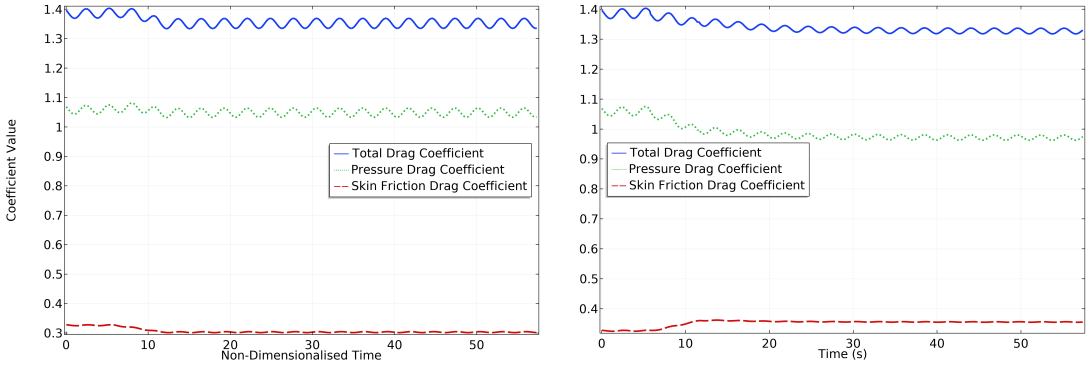

(a) (b)

Figure 7.18 Evolution of drag coefficients as P-Q-balanced control is ramped up on the fully-developed cylinder at $Re = 120$, for the first, front-loaded P-Q-balanced control (a), and the second, improved version (b).

This second arrangement of the P-Q-balanced control is particularly promising for a variety of reasons. Firstly, the control flow rates are much lower. While we have basically ignored the relationship between the control flow rate and the necessary

pressure to drive it, it is likely that large control flows will require larger pressure drops. The peak suction strength is only $c_{q_{max}} = 0.053$ which is more like the level of suction seen for early boundary layer studies [Schlichting 1987, p. 383]. Secondly, the flow-path for the control is better. While the optimisation procedure accounts for the effects of blowing control on the boundary layer and the second-order impact on the pressure profile, it seems logical to have the flow exhausted out the rear of the cylinder. This prevents the boundary layer from being blown away, and does not have to produce a dramatic change in the momentum direction of the control flow. Finally, the second control arrangement appears to dampen the dynamics of the flow. The fluctuations of the drag coefficients are all reduced from the uncontrolled case. The time-averaged and instantaneous flow fields are shown for the two controlled and uncontrolled cases in Figure 7.19 and Figure 7.20. The changes to the flow are subtle so there is little to remark on except the small morphing of the reversed flow region in the wake from the blowing in the second case.

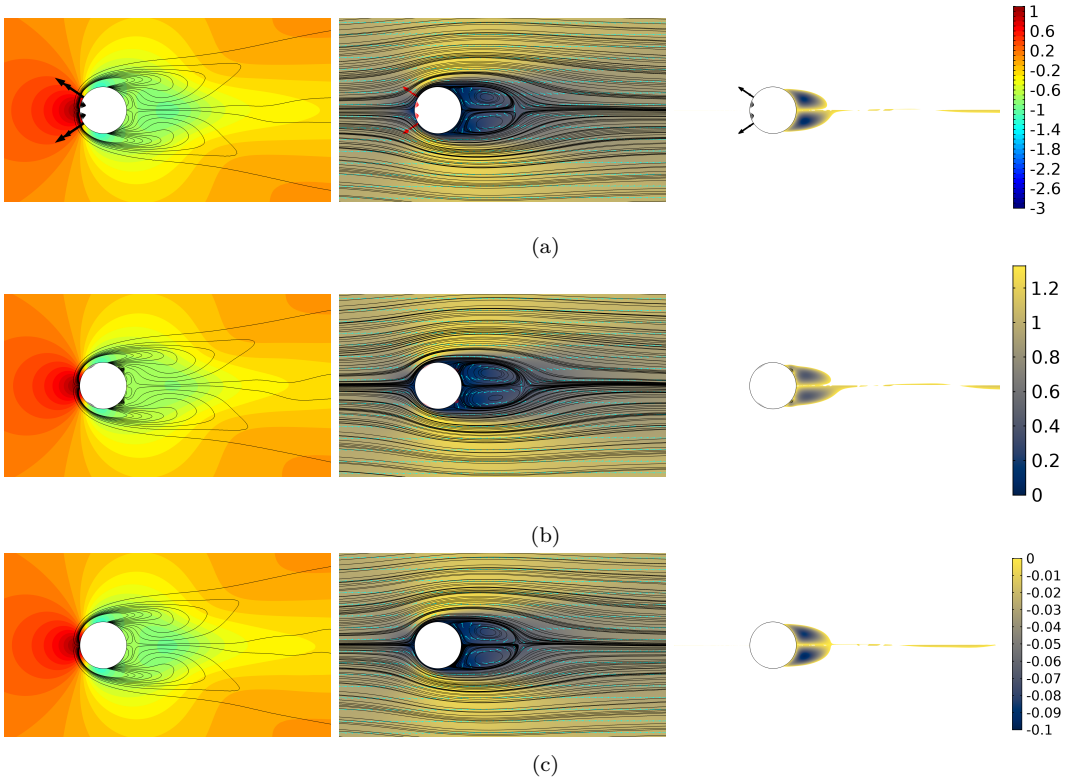

Figure 7.19 Pressure contours with vorticity streamlines (left), velocity surface with streamlines (middle) and reversed flow surfaces for the time-averaged flow round the cylinder for the IV1 optimised control (a), IV2 optimised control (b) and no control (c). Flow field is averaged over 1 vortex shedding period of the uncontrolled flow. The colour bars for the pressure, velocity and reversed flow surfaces are shown in the final column (in descending order).

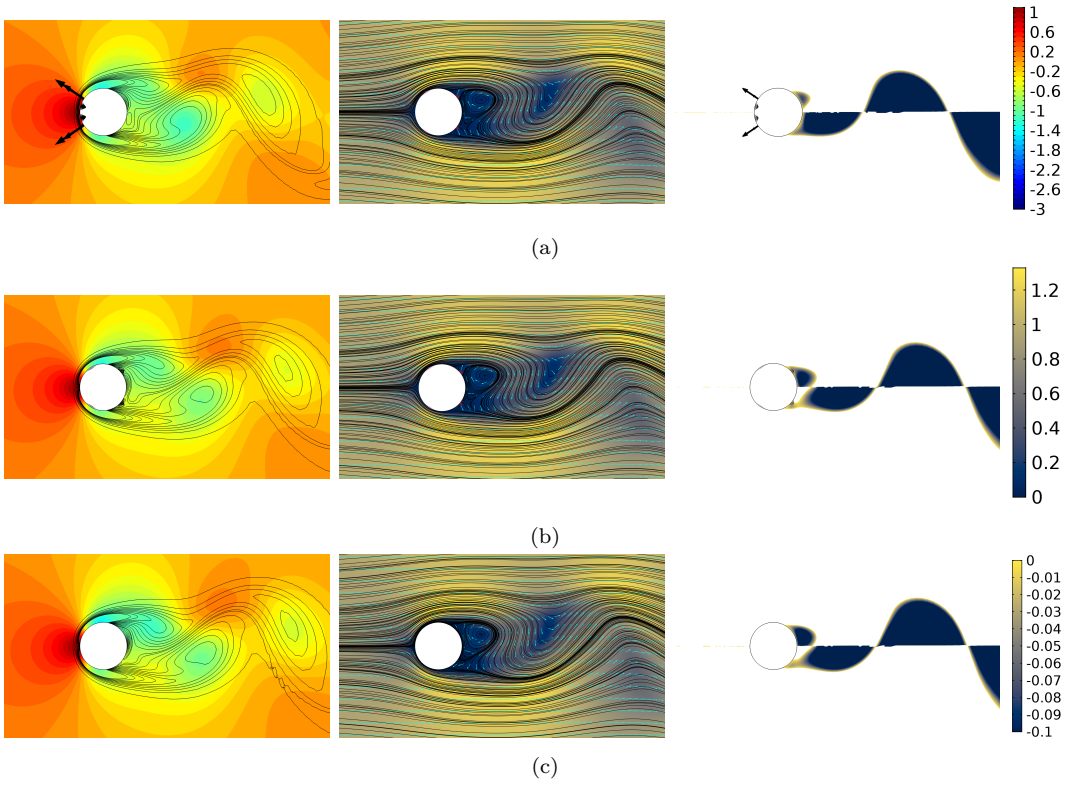

Figure 7.20 Pressure contours with vorticity streamlines (left), velocity surface with streamlines (middle) and reversed flow surfaces for the instantaneous flow round the cylinder for the IV1 P-Q optimised control (a), IV2 P-Q optimised control (b) and no control (c). Flow field is from the final time-step. The colour bars for the pressure, velocity and reversed flow surfaces are shown in the final column (in descending order).

7.5 CONCLUSIONS & NEXT STEPS

7.5.1 Conclusions

The development of an autogenous dual-loci suction/blowing control arrangement was developed for the circular cylinder at $Re = 40$ & $Re = 120$. The dual-loci control consists of a suction and blowing locus, each with a symmetric cubic distribution about their centre. The dual-loci control was gradually refined and constrained from a fully unbalanced dual-loci arrangement – where the suction and blowing could be adjusted completely independently – to a control that enforces a positive pressure drop from suction to blowing loci, and flow-rate balanced suction/blowing. These studies – both parametric and optimisation – were performed on steady-state models, and the best results verified by full time-dependent simulations (for the case where unsteady flow was expected at $Re = 120$).

While the best improvement in total drag was achieved with the unbalanced dual-loci, with an improvement in total drag of 16% & 25% for $Re = 40$ & 120 respectively, the pressure drop, dP, was highly unfavourable for an autogenous control

($dP = -1.633$ & -1.538). Next, the flow-rate constraint was imposed so that the same amount of fluid removed by the suction is injected by the blowing. Parametric and optimisation studies were performed for this arrangement, and it was found that only a small subset of control arrangements could produce potentially autogenous control ($dP > 0$) while also improving the total drag (7% & 3% of the investigated arrangements). Typically this consisted of suction on the front half, particularly near the 90° mark (top and bottom of cylinder) and blowing on the leeward half. Improvement in total drag could be achieved by raising the base pressure and lowering the front pressure, but the skin friction also plays a role. The optimisation of the Q-balanced dual-loci control produced a milder improvement of 13% & 22% to the total drag, again with the control situated in an arrangement that is not conducive for autogenous control ($dP = -1.539$ & -1.4143). The best control situated suction near the 90° mark with a wide spread and blowing concentrated at the rear of the cylinder at both Re. The control was also very strong at $Re = 40$, with the suction strength nearly the same as the free-stream velocity ($c_{q_{max}} = 0.987$).

Finally, optimisation studies were performed with the condition for autogenous control $dP > 0$ imposed as a constraint. The iterative optimisation procedure – where a minor optimisation (for the blowing parameters) is performed inside the major one (for the suction parameters) – and was successful. While the drag improvement was very small when compared to the unbalanced control, an improvement was still achieved. At $Re = 40$ this was a 5.5% improvement from one optimisation, and 1.5% from another with different initial values. At $Re = 120$, a reduction of only 3.7% and 0.8% were produced by optimised P-Q balanced dual-loci when compared to the uncontrolled steady solution.

These optimised controls for $Re = 120$ were applied to a full time-dependent simulation and ramped up on a fully-developed uncontrolled flow. Here, the conclusions of the steady-state study were broadly confirmed: an improvement in drag was achieved for the full unsteady flow while maintaining a positive dP value. Interestingly, the control which performed worse in the steady-state simulation actually produced the best improvement in the full TD case: an improvement of 4.3% including the fluctuation of the drag values almost halving also. For the first case, suction and blowing were situated on the front of the cylinder producing a slight improvement in both C_{d_f} and C_{d_p}. For the second case, a wide weak suction was applied near the top/bottom of the cylinder and the fluid ejected near the rear in a narrow slot.

It is interesting that for the P-Q-balanced control, the skin friction drag is often just as important as the pressure drag. For the case of suction only, the improvement in the pressure drag component is by far the dominant factor for improved drag characteristics. In fact the skin friction often increases when non-uniform suction is applied due to the higher velocity gradients on the cylinder walls. Here, where balanced suction and blowing are applied, the skin friction can be reduced when the control loci are applied

appropriately.

One potential issue was accounting for the momentum change of the fluid removed and injected by the control loci. Some of the optimised P-Q-balanced dual-loci control arrangements featured suction and blowing both situated on the front of the cylinder. Theoretically, the forces on the cylinder are accounted for entirely by the skin friction and pressure values, however in these simulations they do not account for loads inside the cylinder. In a real system, the fluid removed by the suction would have to reverse direction to be ejected out the blowing locus. This is almost a 100% change in momentum for the fluid, which would impart a substantial force on the cylinder.

While optimisation studies were performed for all models, the results suggest that there are several local minima in the objective space for this type of control. Trialling other initial values may produce other control arrangements that are also effective. Additionally, these results have given enough information about the design and effects of potentially autogenous control that optimisation of dual-loci control applied to time-dependent simulations is reasonable. Each P-Q-balanced SS optimisation study used about 1000 iterations of the forward problem, while the unsteady verification simulations described above took about 45 minutes on a desktop computer. Without any changes to the model and using the same hardware, a comparable optimisation study would take 750 hours.

7.5.2 From Imposed Control to Practical Design

Two major questions remain after these investigations into potential autogenous suction/blowing control: 1) Is the assumption that any $dP > 0$ is sufficient to ensure the imposed control will be produced in a real physical system correct? 2) What would a physical implementation of the optimised P-Q-balanced control look like? 3) Can useful suction be induced in low pressure regions by careful internal ducting design? These will now be addressed in Chapter 8 by performing simulations of full physical systems.

Chapter 8

PRACTICAL AUTOGENOUS CONTROL

8.1 SUMMARY

Three physical designs were generated with the objective to produce the optimised suction/blowing profiles from Chapter 7 (in particular the IV2 P-Q dual-loci profiles outlined in Table 7.12). These designs were described as: 'Straight-Ducted', 'Centre-Ducted' and 'Ring-Ducted'. Each consisted of duct geometries connecting the suction and blowing loci; the cylinder wall was replaced with thin porous material at the loci. The flow for each model was simulated and the results analysed with particular attention to the resulting suction/blowing profiles and the drag characteristics. Various permeabilities were employed for the porous material to test its influence. For the $Re = 120$ case, both steady-state and unsteady simulations were performed.

It was found that though a net suction/blowing was achieved in the desired direction, the overall control profile was not achieved satisfactorily. While the velocity profile of the blowing portion could be achieved quite well, a recirculating flow was always produced at the suction locus (the entry to the duct) due to the strong tangential pressure gradient over the front half of the cylinder. As a consequence of this, the drag was actually worsened at $Re = 120$, although at $Re = 40$ a modest improvement was achieved (1.55% for the Straight-Ducted geometry).

In all cases, the Straight-Ducted geometry achieved the best drag results, however the differences were very small. Overall, regardless of internal duct geometry, the resulting suction/blowing profiles were very similar between the designs. The permeability had a strong effect on these, but mostly by affecting the magnitude rather than the shape of the profiles. A Darcy number of $Da = 10^{-2}$ gave the best results at $Re = 40$ while $Da = 10^{-4}$ was best at $Re = 120$.

To improve upon these rather cursory results, some avenues for further research were described. In particular, the use of anisotropic and spatially-varying porous materials may be an effective approach. Additionally, the Venturi effect might be exploited to produce a plenum of much lower pressure inside the cylinder, overwhelming the pressure gradient at the suction locus, preventing the recirculation. The results of the study in Chapter 3 are encouraging to this end.

8.2 METHODOLOGY

Three designs for practically producing the optimised suction/blowing profiles at $Re = 40$ and $Re = 120$ from Chapter 7 were produced and the resulting flows resolved. The 'Free and Porous Media Flow' module of COMSOL was used, as described in Chapter 3. The objectives of this investigation were to

1. determine whether the BC-imposed profiles would be achieved naturally if the suction/blowing loci were connected by appropriate ducting,
2. measure the effect of the physical system on the drag, and
3. ascertain what physical parameters need to be improved to produce a physically autogenous beneficial flow control.

At $Re = 120$, since the uncontrolled and controlled flow are unsteady, time-dependent simulations were performed in addition to simplifying steady-state ones. The unsteady simulations commence with the cylinder wall being fully impermeable and resolving the uncontrolled, vortex-shedding flow for several periods. Then the permeability of the porous regions were ramped up to the desired permeability over a period of $2T$, allowing the flow to move through the internal geometries. The flow was then allowed to fully develop. Since the numerical domain is different for each geometry modelled, and also different from the domain used for the original simulations, the uncontrolled flow had to be developed first for the new domain before it could be used as the initial condition for the ramp up control cases. This was achieved for each model in the same way as in Chapter 6.

In all cases, the drag can no longer be determined simply by integrating the pressure and shear stresses over the surface because there are now internal surfaces also. Hence, the momentum integral approach was used to determine the total drag. Unfortunately this does mean that the relative contributions of each drag component were not resolved. Additionally, for the uncontrolled case, the momentum approach resulted in values slightly above those from the surface stress integrations (1.669 vs 1.632 at $Re = 40$ and 1.390 vs. 1.385 for $Re = 120$). This is due to numerical effects as the mesh is coarser further away from the cylinder where the momentum values are evaluated. The result is consistent though so this small difference can, overall, be ignored.

8.2.1 Designs for Practical Control

All the following designs were produced for generating the IV2 P-Q-balanced dual-loci control described in Chapter 7. The desired control consists of two control loci - one suction (upstream), and one blowing (downstream). To achieve this, the solid cylinder wall was replaced with a thin porous material at the loci, which were connected by internal ducting (hollow cross-section). The way that these porous loci are connected

that were the subject of the three present concepts. These are demonstrated in Figure 8.1 and will now be described in greater depth.

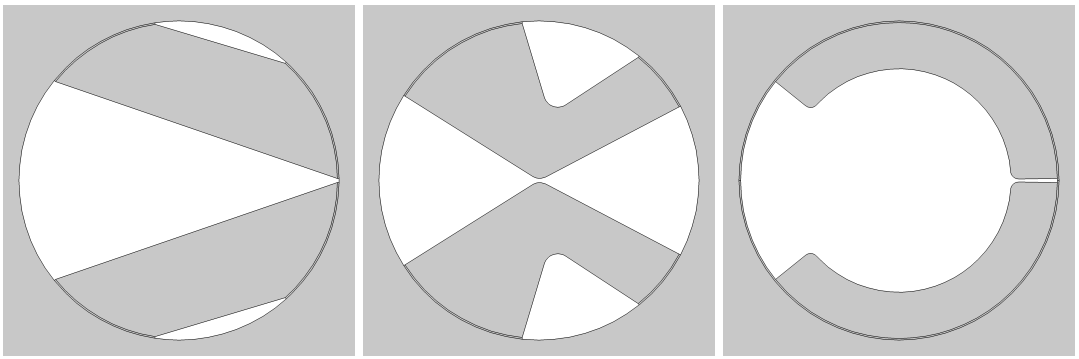

(a) (b) (c)

Figure 8.1 Designs for achieving the IV2 P-Q-balanced Dual-Loci control at $Re = 40$: (a) straight-ducted, (b) centre-ducted, (c) ring-ducted. The white areas are solid, while the grey areas are fluid. The rim of the cylinder consists of a porous material.

8.2.1.1 Straight-Ducted

Perhaps the simplest design is to just connect the two loci with a straight channel. This produces a nice geometry for the IV2 dual-loci cases at both Reynolds numbers, but for an arrangement such as that given by the IV1 solution – where the two loci are close together – the straight duct would be ungainly. Typical aerodynamic design would seek to gradually redirect the fluid flow using smoothly curving geometries.

8.2.1.2 Centre-Ducted

The centre-ducted approach seeks to guide the direction of the flow. The desired suction/blowing velocities are normal to the cylinder wall, therefore having each duct wall intersect the cylinder wall at a normal angle is sensible. To keep the design generalisable, we decided to have the duct route towards the centre of the cylinder. Two points are defined along the vertical-plane in the centre of the cylinder. The first is situated at the centre, and the second situated $1/2(\gamma_q + \gamma_{q_b})$ away (the average locus width, since the suction and blowing loci have different spreads). The first point connects the innermost duct wall, and the second the outermost duct wall. To produce a smooth geometry for the flow, the corners produced at these points were filleted with a radius of the distance between the loci centres multiplied by 10^{-4}. For the $Re = 120$ case this is 4.5 mm. Again, this was to make the geometry generalisable, however larger fillets could be used in the present case to make an even smoother duct geometry.

8.2.1.3 Ring-Ducted

The final approach was to attempt to keep the internal volume relatively intact. This was achieved by having the ducting follow the cylinder wall, rather than routing inwards. As a consequence though, this design is likely to cause issues generating a normal suction/blowing control. The main parameter for this design is the duct width (or ring width). after experimentation it was found that a duct width of $0.3R$ worked well for achieving the desired control velocity profiles. However, this large duct width does undermine the benefit of suction control to preserve internal space. The internal corners of this design were filleted with a radius of $0.05R$. The objective of this fillet was not to create a smooth profile catered for the flow – as for the Centre-Ducted approach – merely to reduce sharp edges which can lead to numerical issues.

8.2.2 Porous Material

The geometry of the porous material was kept consistent for the geometries with a thickness of $0.01R$ (1% of the cylinder radius) and a constant porosity of 0.8. The permeability, on the other hand, was varied from effectively impermeable ($\kappa = 10^{-32}\ m^2$) to effectively completely permeable ($\kappa = 100\ m^2$). No fillets or smoothing of the geometry where the porous material meets the cylinder or ducting walls was applied. The permeability can be made dimensionless by dividing the dimensional value by the square of the cylinder diameter – this is referred to as the Darcy number, Da, which is calculated as follows:

$$Da = \frac{\kappa}{D^2}. \tag{8.1}$$

In our case, this simply increases the value of the dimensional permeability, κ, by 100 since $D = 0.1\ m$. From now the Darcy numbers will be quoted in keeping with the dimensionless presentation.

For each steady-state model, a parametric sweep of the permeability was performed to ascertain which value produces suction/blowing velocities closest to the desired profiles. Darcy number values of 10^{-30} (effectively impermeable), 10^{-10}, $10^{-6}, 10^{-4}, 10^{-2}$ and 1 (effectively no solid material) were used. It was found that values on the order of 10^{-6} to 10^{-2} produced suction/blowing profiles close to those desired, so it is these values that are described in the Results section.

8.2.3 Mesh

Three geometric designs, and several variations of each design, were modelled. Therefore, it was decided to use an unstructured mesh approach. Hence, for each of these simulations an unstructured triangular-dominant mesh was generated. Five inflation layers were used on every no-slip wall, and the maximum element size was limited to 0.3 (scaled by D). COMSOL's 'Free Triangular' method was used to produce the mesh outside of the

boundary layers which naturally produces a coarser mesh in areas of unconfined flow, and gradual refinement as the cylinder is approached. Examples of the resulting meshes are shown in Figure 8.2. The final meshes are unlikely to produce mesh independent results, particularly for the resulting values near corners. However, trial-and-error found that the results from these meshes were of acceptable quality for the purposes of the present investigation.

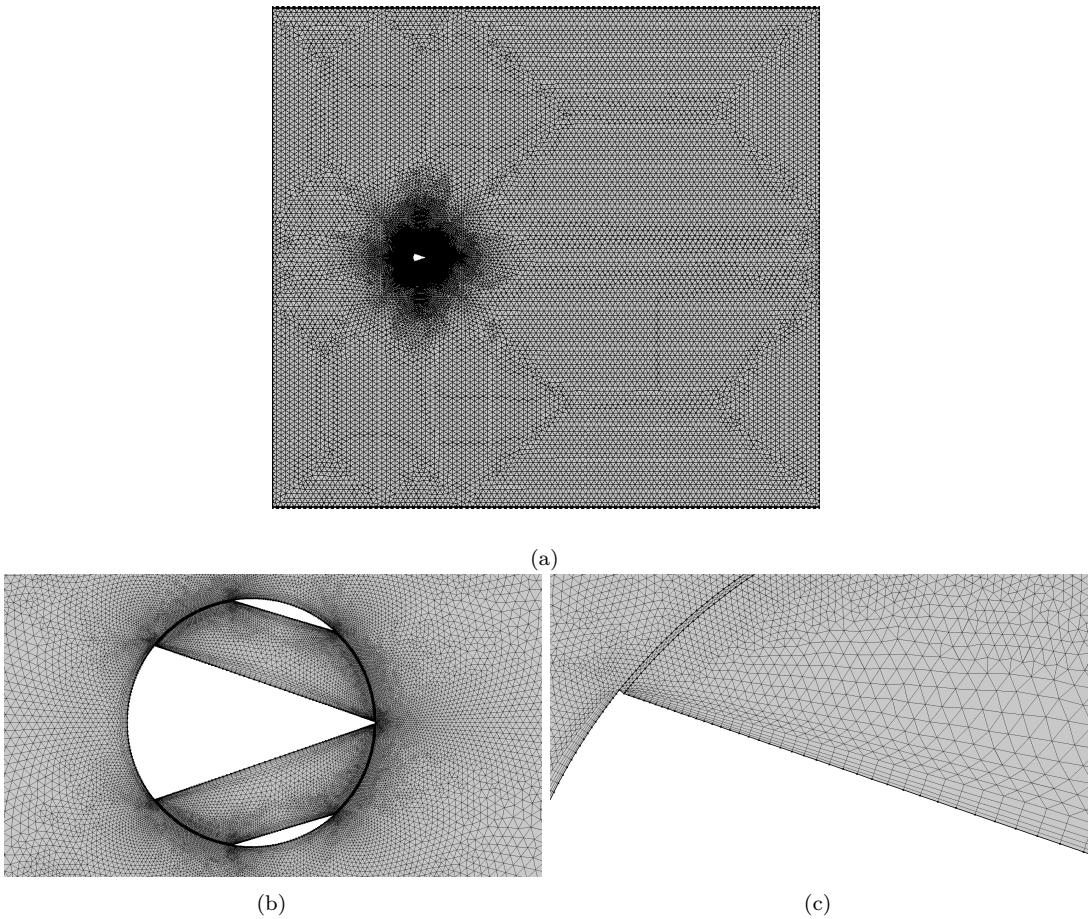

Figure 8.2 Example mesh for straight-ducted design. Full domain (a), mesh round the cylinder (b), and close-up of internal duct/boundary layer. Meshes for the other designs are similar.

8.3 RESULTS

8.3.1 Steady Results

8.3.1.1 Flow Field

The resulting pressure, velocity and reversed flow fields are shown in Figure 8.3 for steady-state simulations at $Re = 40$ and Figure 8.4 for $Re = 120$ with the best performing Da for each flow. Here, and throughout the results analysis, 'best' means 'produces the

closest suction/blowing profiles to the target values' as interpreted qualitatively from the plots presented later in Figure 8.5.

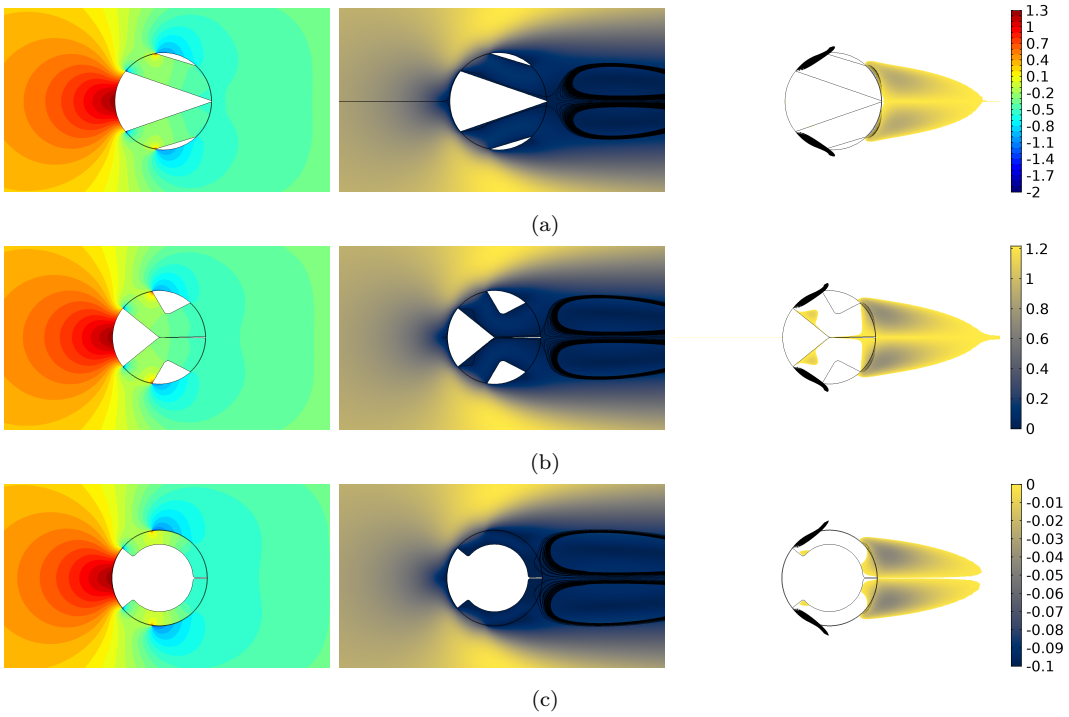

Figure 8.3 The pressure (left), velocity magnitude (middle), and reversed flow (right) fields for the Straight Ducted (a), Centre-Ducted (b) and Ring-Ducted (c) designs at $Re = 40$. For clarity, vectors for the suction/blowing velocities are shown in the reversed flow figures only. In all cases the permeability of the porous loci was given by $Da = 10^{-2}$. The colourbars for the each field are given on the far right in order of appearance (pressure, velocity magnitude, reversed flow velocity).

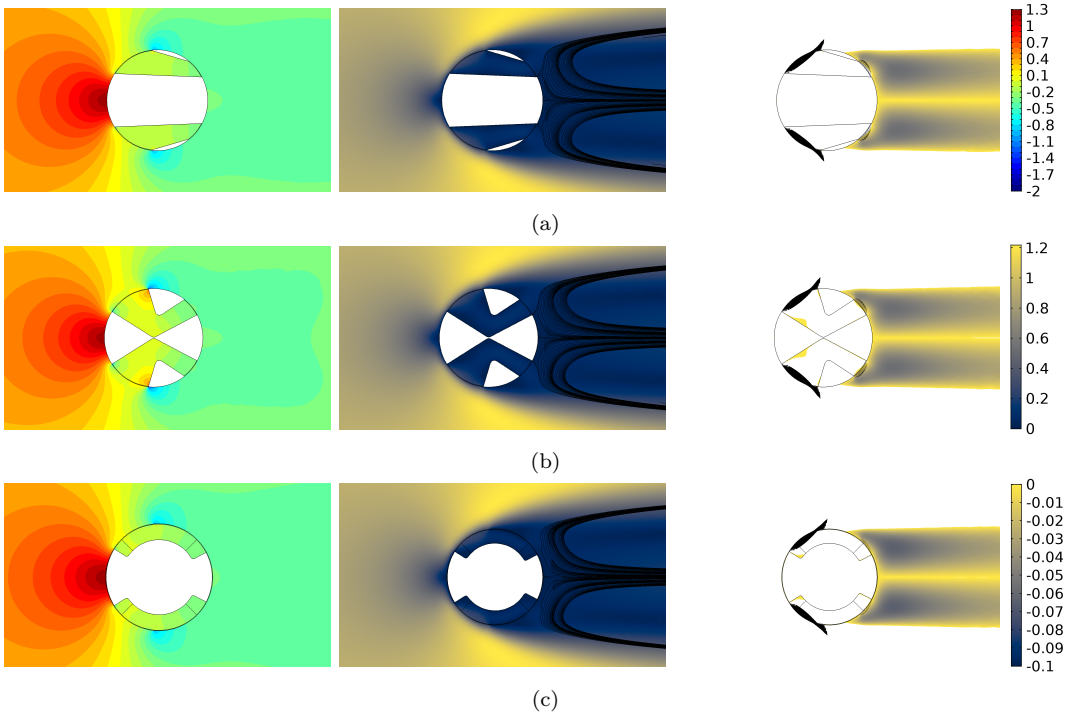

Figure 8.4 The pressure (left), velocity magnitude (middle), and reversed flow and suction/blowing vectors (right) fields for the Straight Ducted (a), Centre-Ducted (b) and Ring-Ducted (c) designs at $Re = 120$. In all cases the permeability of the porous loci was given by $Da = 10^{-4}$. The colourbars are the same as for Figure 8.3

Overall, at each Re the resulting flows are all very similar. At $Re = 40$, the external pressure contours are virtually identical between the designs, as shown in Figure 8.3. Internally, though, they all show pressure concentrations round the corners of the geometry. Looking at the velocity surface, the flow-field is similar with some higher velocity encroaching at the suction entry to the ducts, but with mostly stagnant flow within it. The reversed flow shows the areas where the velocity tangential to the cylinder wall is negative. It is interesting to see that the Centre Ducted and Ring Ducted designs produce a wake that encroaches somewhat into the ducting. These designs also had regions of reversed flow in the early stages of the ducting around corners.

The features of the flows at $Re = 120$ show similar trends to those at $Re = 40$, except for the features of the wake. Looking at the pressure contours in Figure 8.4. The Centre Ducted design has some large pressure concentrations encroaching into the duct as the flow moving from left-to-right moves through the porous material and hits the outermost duct wall. This is a further indication that the 'suction' flow is not normal to the cylinder surface here. Because of the now porous region on the front half of the cylinder, the fluid is not fully arrested and redirected to follow the surface tangentially. Instead part of the free-stream which intersects the cylinder at the suction location moves straight through. The wake behind the cylinder is virtually identical between all the designs, but the actual unsteady wake may be different.

8.3.1.2 Achieving Desired Suction/Blowing Profiles

The resulting suction/blowing profiles for each design with varying wall permeabilities are shown in Figure 8.5, and are separated to show the effect of each design in Figure 8.6 and the effect of permeability in Figure 8.7. As can be seen in Figure 8.6, the practical designs are quite capable of achieving the magnitude of suction and blowing. In particular, at $Da = 10^{-2}$ for the $Re = 40$ case and $Da = 10^{-4}$ for the $Re = 120$ case. The natural profiles produced by the ducting in all cases is effectively the same as the biased locus shape. However, though the magnitudes are achieved adequately, the ability to reproduce the suction component of the profile is poor.

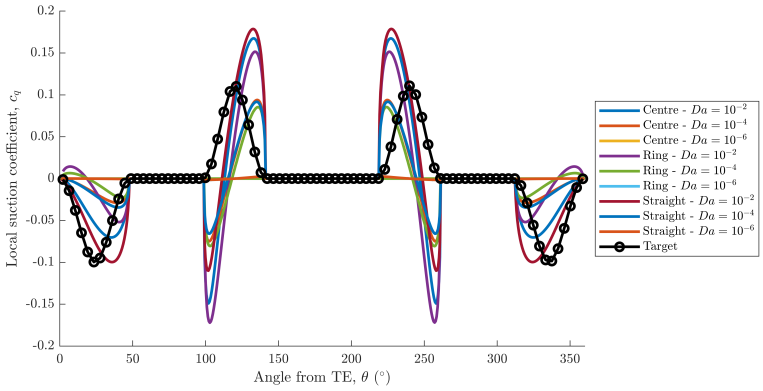

(a)

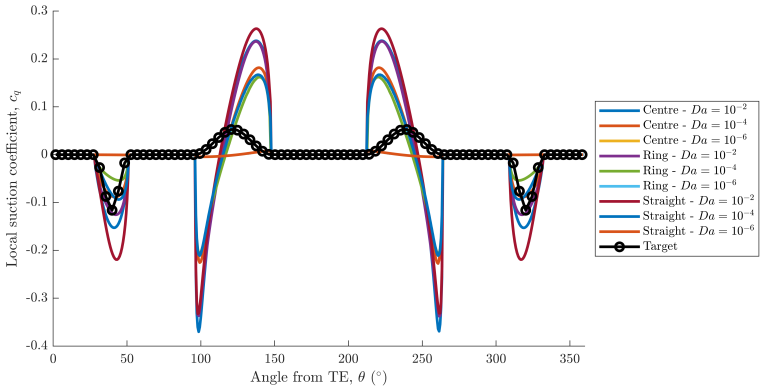

(b)

Figure 8.5 All suction/blowing profiles for the different designs at $10^{-2} \leq Da \leq 10^{-6}$ at (a) $Re = 40$ and (b) $Re = 120$.

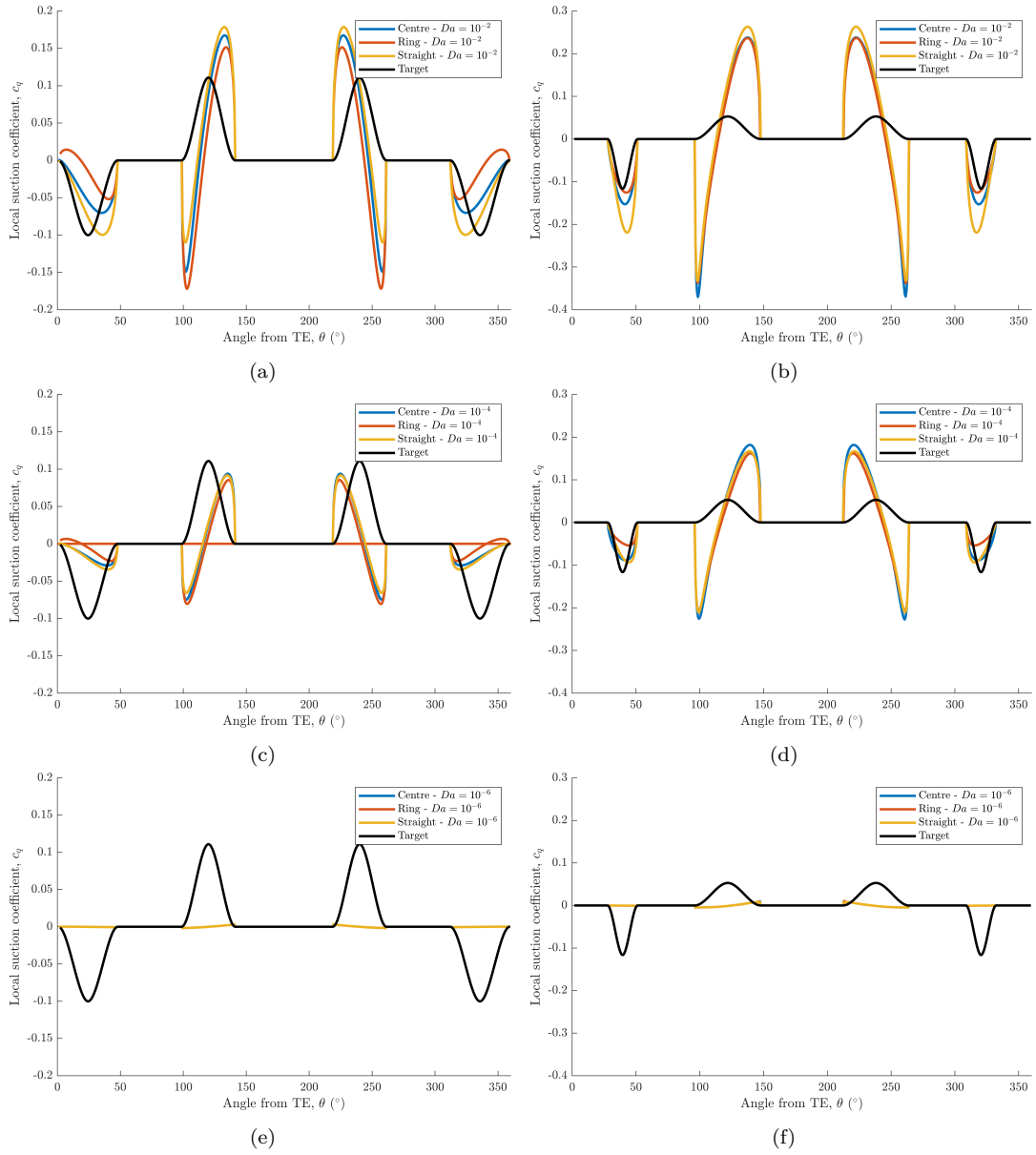

Figure 8.6 Resulting suction/blowing profiles over the cylinder grouped by permeability. $Da = 10^{-2}$ (a,b), $Da = 10^{-4}$ (c,d), and $Da = 10^{-6}$ (e,f). Left is $Re = 40$ and right is $Re = 120$ (evaluated with steady-state assumptions). c_q is positive for suction and negative for blowing.

As can be seen in Figure 8.6, there is little variation between the system designs. All of them have the same profiles, with small discrepancies in magnitude between them. The permeability has a substantial influence, but apparently only on the magnitude of the control velocity. None of the designs quite match the target profiles, particularly for the suction regions. For these cases, the peak suction velocity is much higher than its target, but this is to compensate for the fluid which recirculates and exits back out the same locus.

The 'suction' locus never consists of only suction, but rather has a region of suction and blowing – the result of a recirculating flow at the entrance to the ducts. Presumably

this is due to the strong pressure gradient in the tangential direction along the cylinder surface. There is a strong favourable pressure gradient (FPG) over the front half of the cylinder, so the path of least resistance for the control flow is to enter through the first half of the suction locus and exit out the second half. Even with a low pressure region at the other end of the duct, it is not strong enough to counteract the FPG immediately at hand at the suction locus. Only a small portion of the flow continues down the duct to be exhausted at the blowing locus – as will be shown later, only about 1/3 of the flow that enters at first. This has a major effect on the flow and, as will be discussed shortly, is the likely cause for why drag is not reduced for these control systems.

This is a real issue for generating the suction-blowing control. Varying the permeability of the porous wall over its length may help to reduce the amount of flow recirculating, however it cannot change the FPG which generates it (except by altering the flow upstream). Using something like the approach in Chapter 5 to exploit other flow phenomena, such as the Venturi effect, would reveal how much the geometry design could improve this result. On the other hand, the strong FPG which produces the recirculation might be avoided by more careful placement of the suction locus. If the pressure drop from the suction to blowing loci were very strong, the effect of the FPG would likely be inconsequential preventing the recirculation. Or alternatively, if the FPG were weaker. Therefore, if the duct entry cannot be designed so as to prevent the recirculation, a further constraint on the design of autogenous control should be considered: maximum FPG in the suction region.

8.3.1.3 Effect of Permeability

As can be seen in Figure 8.7, the permeability of the porous wall (at the entrance and exit of the ducting) has a strong influence on the resulting suction/blowing profiles. The effect of Da is mostly on the magnitude of the c_q profiles, however the locations of key points do move a little, e.g. the location of peak suction and location of suction-blowing transition in the suction locus. This is consistent with expectations as in the governing equations for the porous media flow used in this model, the flow through it is dominated by the pressure gradient with non-linear velocity effects much smaller. However, since the effectiveness of the control influences the external pressure profile also, there are coupled effects. The results are effectively the same for all the geometries and at both Re.

Overall, these results suggest that manipulating the characteristics of the porous material may help to reduce the recirculation at the suction locus, however their influence will be weaker than changing the location/shape of the loci in the first place. The permeability can be adjusted to effectively control the strength of the suction/blowing, but even a varying porous material may be unable to achieve the desired suction profile. The external pressure field is the most important factor.

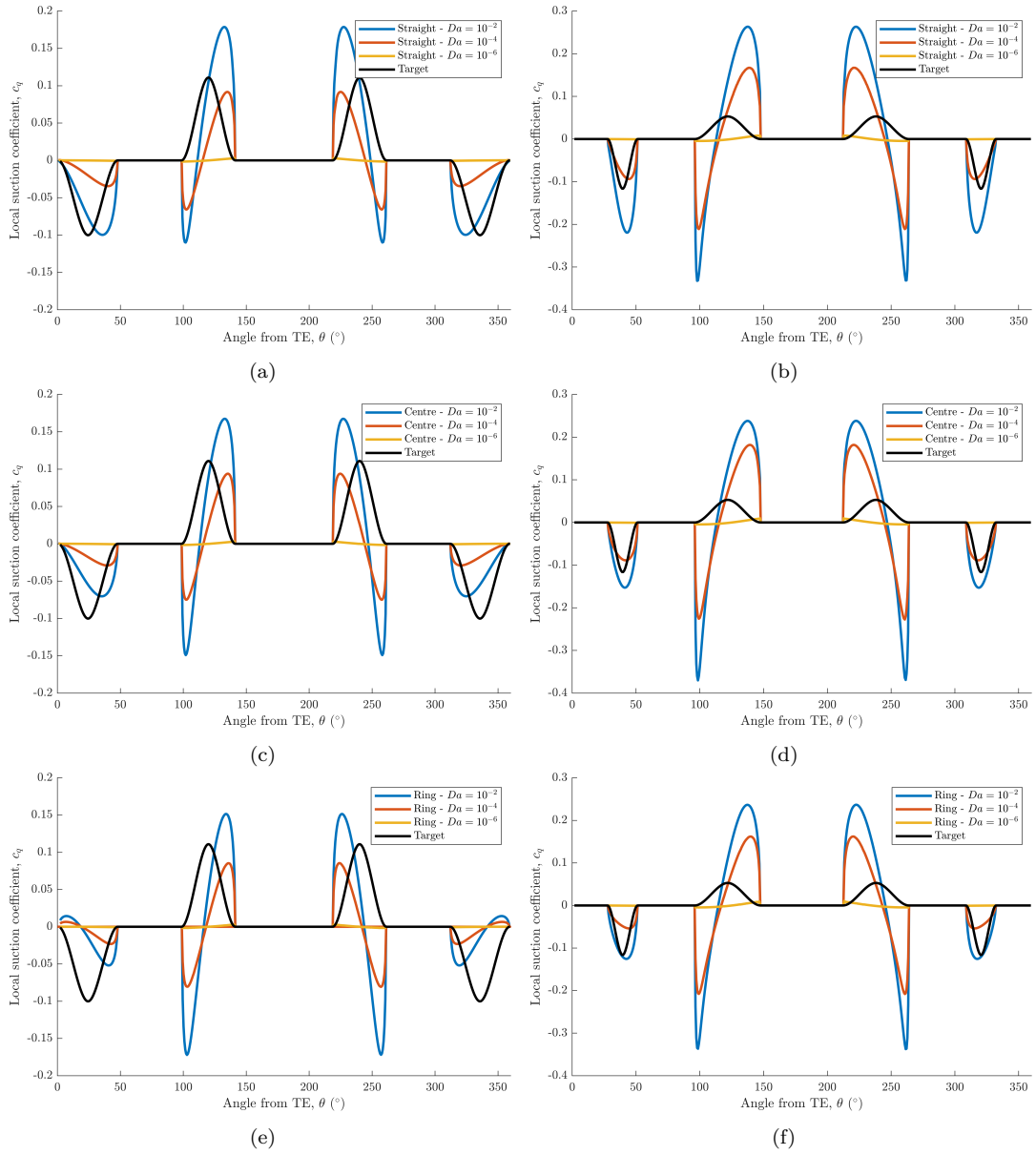

Figure 8.7 Resulting suction/blowing profiles over the cylinder grouped by design. Straight Ducted (a,b), Centre Ducted (c,d), and Ring Ducted (e,f) with varying permeabilities for the porous region.Left is $Re = 40$ and right is $Re = 120$ (evaluated with steady-state assumptions). c_q is positive for suction and negative for blowing.

8.3.2 Unsteady Results

For the $Re = 120$ case, each design (with the best permeability, $Da = 10^{-4}$) was solved in the unsteady model. The results were very similar to the steady-state ones, but with some oscillation in the strength of the control flow as the wake fluctuates. This is very similar to the BC-induced simulations at the end of Chapter 7 – that the steady-state models offer a good approximation for design and preliminary testing. The pressure contours at the start and middle of each vortex shedding period, T are shown

in Figure 8.8 with the velocity vectors of the suction/blowing also shown. The effect on the control profiles are shown in Figure 8.9, further showing the minor fluctuations in values.

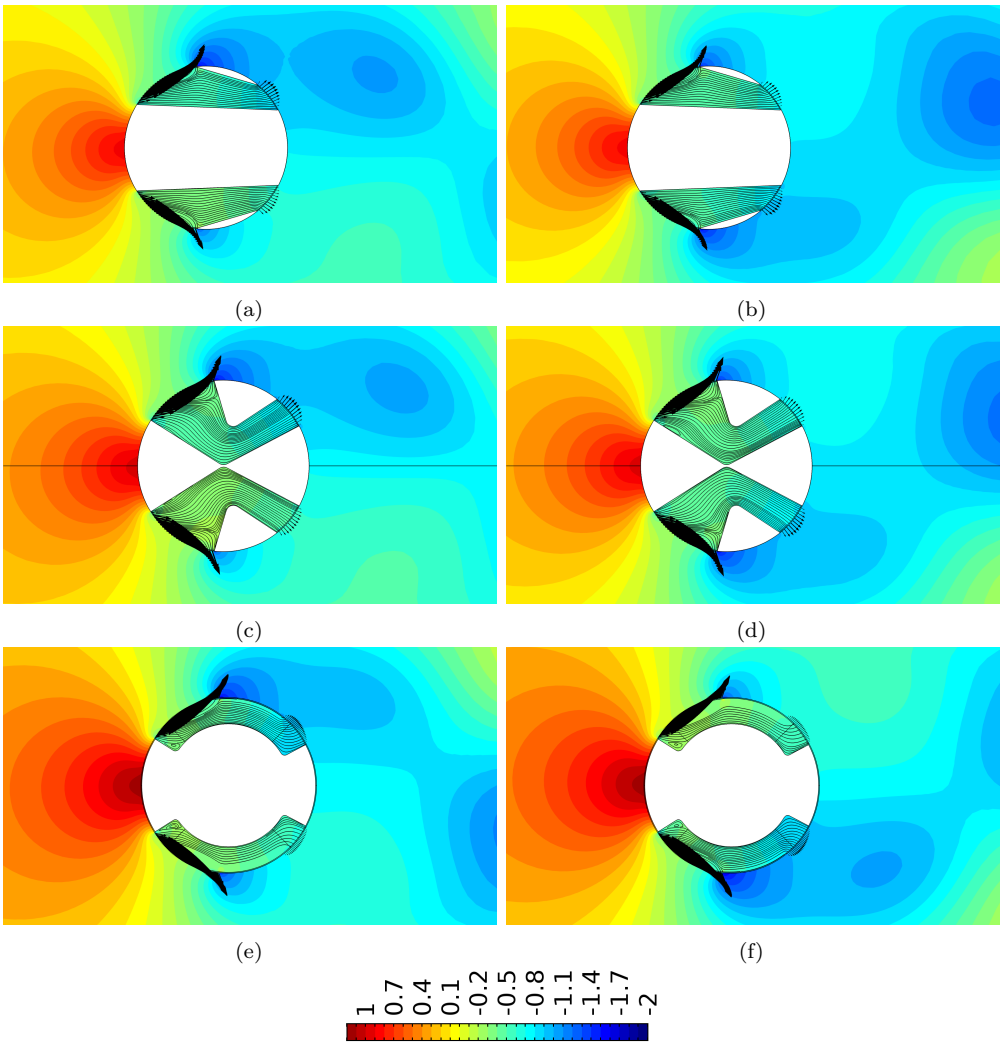

Figure 8.8 Pressure contours at start of shedding period (left) and end (right) with the colorbar shown at the bottom. Streamlines are plotted within the ducts with a density of 0.009.

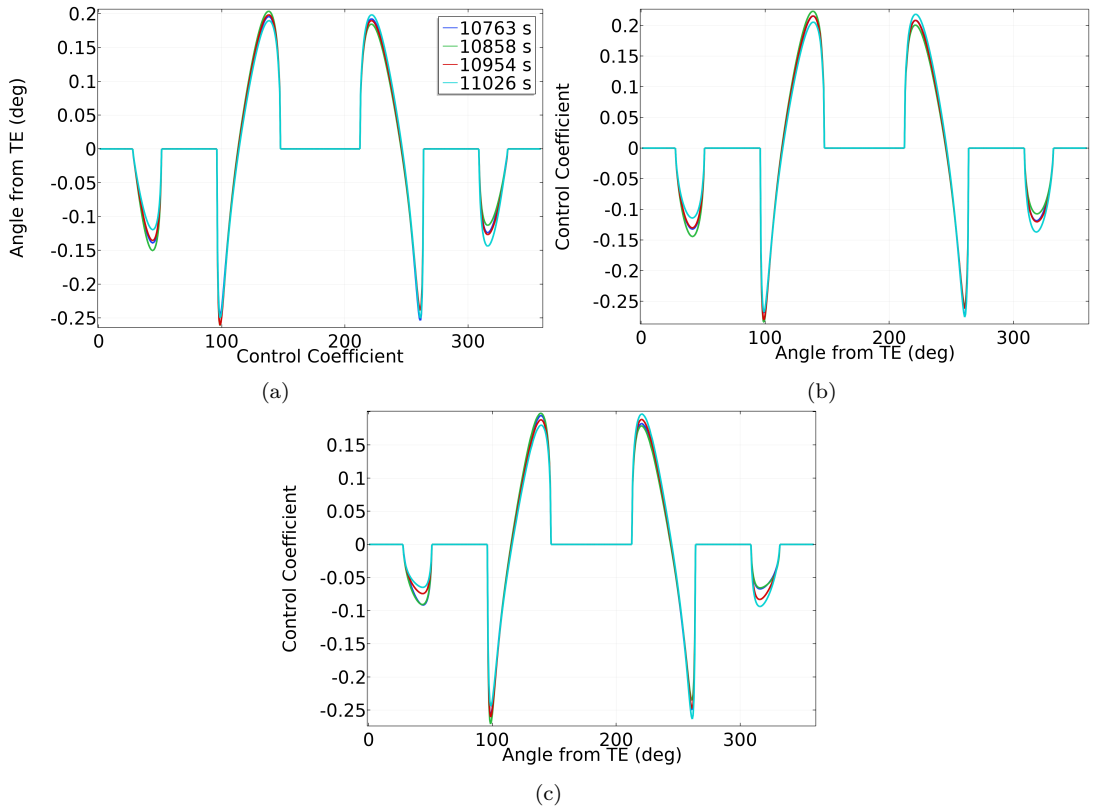

Figure 8.9 Variation of suction/blowing profiles over a vortex shedding period at $Re = 120$: (a) Straight-Duct, (b) Centre-Ducted, (c) Ring-Ducted.

8.3.3 Drag of Physical System

The total drag on each cylinder was measured by the momentum integral approach for each model. Figure 8.10 shows how the drag varies over time at $Re = 120$ as the control ducts are 'opened' (by increasing the permeability to the set value). The figures clearly show that the autogenous control ducts actually make the drag worse. There are a few reasons for this. Firstly, the internal ducts and porous walls do produce slight additions to the viscous drag felt by the system. Secondly, the arrangement of each duct system can also generate some pressure drag, particularly for the case of the centre-ducted arrangement where a duct wall is nearly normal to the free-stream direction. Thirdly, and probably most importantly, because the suction profile is not being achieved by any of these designs. As a consequence the flow of the front-half of the cylinder does not match that from the simulations in Chapter 7 and the external pressure profile is not improved. We think the main objective in developing autogenous suction control further should be to try and induce the appropriate suction here, preventing the recirculation that has been described above.

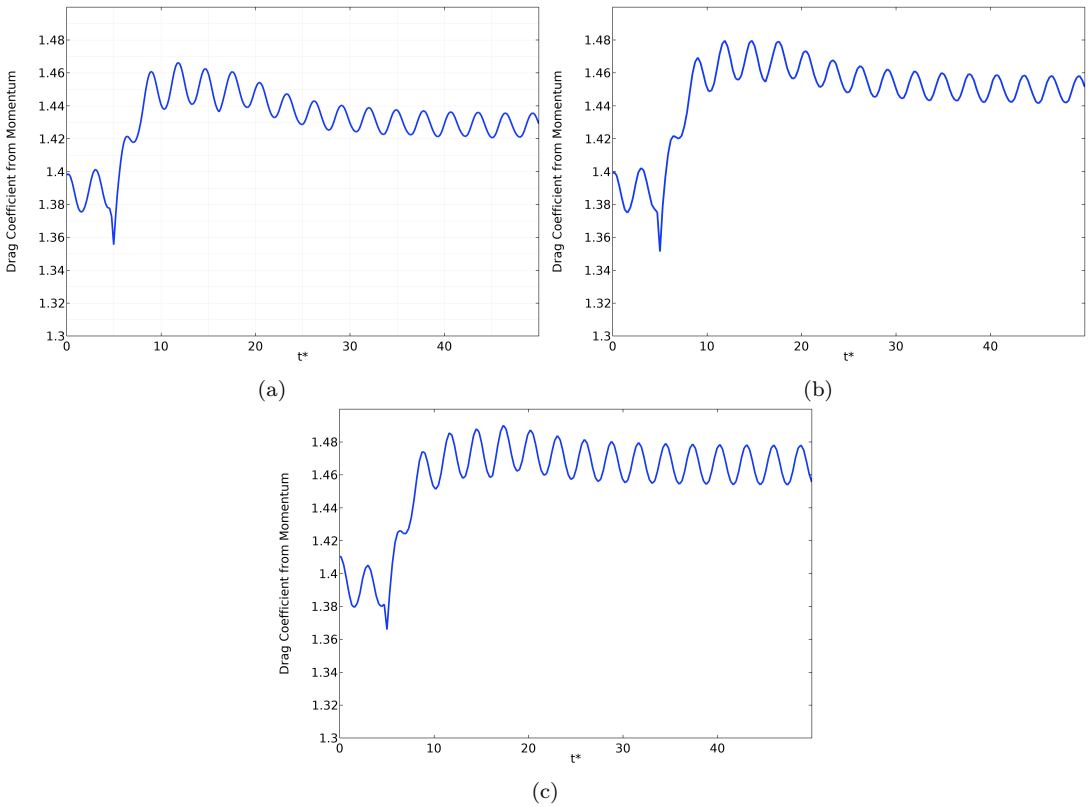

Figure 8.10 Drag coefficient as permeability is ramped up to its final value (allowing fluid to flow through the control ducts) for the (a) Straight Duct, (b) Centre-Ducted and (c) Ring-Ducted concepts. This coefficient is the total drag as measured by momentum analysis, $C_{d_{t_u}}$.

The worsening of the drag characteristics from the uncontrolled flow was found only for the case of $Re = 120$, whereas at $Re = 40$ a modest improvement in drag was found. These values are summarised in Table 8.1, and details of the control flow at the suction and blowing loci are given in Table 8.2 and Table 8.3 for each Re. In these tables, the suction locus coefficient is symbolised by C_{q_1} since it also exhibits blowing. For consistency, the blowing locus coefficient was also replaced by C_{q_b}. It is interesting that the $Re = 40$ case produced an improvement in drag, though a very modest one (1.5%). This could be due to the different locations of the duct entry/exits at the two Re, or due to the lesser influence of pressure effects at $Re = 40$ with the drag dominated by viscous effects instead.

In almost every case, the Straight-Ducted design had the best drag out of the studied designs. Only for $Re = 120$ (SS) is it beaten out by the Ring-Ducted design (see Table 8.1). Presumably it impedes the control flow the least, and does not act as an obstacle to the free-stream. However, the differences in drag coefficient are small and improvements to the other designs (blunting corners, improving the geometric curves) would likely result in similar values. The dominating factor is the pressure at entry and exit.

The breakdown of C_{q_1} (the control coefficient at the desired suction locus) into its

components, as shown in Table 8.2 and Table 8.3, demonstrates that there is a lot of recirculated flow at the duct entry. In all cases, the amount of recirculated flow at the suction locus is over twice the amount ejected at the blowing locus ($C_{q_{1_b}}$ compared to C_{q_2}). Preventing this recirculation will be key in implementing practical autogenous control designs.

Table 8.1 Total drag coefficients (as measured by momentum integral) for the different designs at. For $Re = 120$ both the steady-state (SS) results and time-dependent (TD) results are shown. The values in bold improved upon the uncontrolled value.

Design	$Re = 40$	$Re = 120$ (SS)	$Re = 120$ (TD)
None	1.6698	1.1143	1.3900
Straight-Ducted	**1.6440**	1.1710	1.4280
Centre-Ducted	**1.6451**	1.1728	1.4498
Ring-Ducted	**1.6531**	1.1678	1.4658

Table 8.2 Key parameters of the resulting control flow for each design at $Re = 40$. Since the 'suction locus' actually has suction and blowing, the flow rate coefficient here has been renamed C_{q_1} and it is broken into its components $C_{q_{1_b}}$ and $C_{q_{1_s}}$ to better describe the control flow. $Da = 10^{-2}$.

Parameter	Uncontrolled	Straight	Centre	Ring
$C_{d_{t_u}}$	1.6698	1.6440	1.6451	1.6531
C_{q_1}	-	0.0155	0.0109	0.0042
C_{q_2}	-	-0.0155	-0.0109	-0.0042
$C_{q_{1_b}}$	-	0.0034	0.0033	0.0031
$C_{q_{1_s}}$	-	0.0121	0.0076	0.0011

Table 8.3 Key parameters of the resulting control flow for each design from the unsteady models at $Re = 120$ (TD). Since the 'suction locus' actually has suction and blowing, the flow rate coefficient here has been renamed C_{q_1} and it is broken into its components $C_{q_{1_b}}$ and $C_{q_{1_s}}$ to better describe the control flow. $Da = 10^{-4}$.

Parameter	Uncontrolled	Straight	Centre	Ring
$C_{d_{t_u}}$	1.3901	1.4280	1.4498	1.4658
C_{q_1}	-	0.0118	0.0124	0.0078
C_{q_2}	-	-0.0118	-0.0124	-0.0077
$C_{q_{1_b}}$	-	-0.0129	-0.0144	-0.0142
$C_{q_{1_s}}$	-	0.0247	0.0268	0.0220

8.4 CONCLUSIONS AND FUTURE WORK

Overall the results of the practical design simulations satisfy the open questions from the earlier studies. The locations for placing suction and blowing loci to produce autogenous control flows were appropriate. However, the suction profile was difficult to achieve due to the strong tangential pressure gradient over the front-half of the surface and the incidence of the free-stream at a non-normal angle. This caused some of the 'sucked' fluid to recirculate back out the entry, counteracting any improvements that the suction locus might have produced. The designs tested in this study were very simple and also had features that are likely to increase drag (e.g. sharp corners). As a consequence of these factors, the drag was actually worsened at $Re = 120$, though at $Re = 40$ a very small improvement was achieved (1.55% with the Straight-Ducted design).

Based on the results in Chapter 7, if the optimised P-Q dual-loci control profiles can be achieved, reasonable improvements in drag can be expected. The major factor is the suction profile, which was drastically different in the physical implementations. Dealing with this should be the major objective of implementing practical designs. Overall, several possible solutions have been suggested in this chapter, and a few more are offered here:

1. Anisotropic permeability
2. Venturi-based suction-inducing designs
3. Variable characteristics of the porous material (in the tangential direction)
4. Complex geometry design of ducts
5. Adjust BC-autogenous model (Chapter 7) to reflect the natural profiles
6. Optimise the physical model directly

Of these, the first three have the most potential.

Looking at the velocity vectors in the rightmost images of Figures 8.3, 8.4 and 8.8 shows that the blowing produced by the recirculation at the duct entry is highly non-normal. Whereas, the suction/blowing profiles imposed in the BC studies had suction/blowing only normal to the surface. Therefore, using customised porous materials which have anisotropic permeability may help to trap the flow within the ducts. For example, using a material that is permeable in the radial direction only, or – even better – one that allows fluid through but not back out. The second option – variable porosity in the tangential direction – is similar. However, the flow through the porous medium is pressure-dominated and the porosity itself cannot reverse the direction of the pressure gradient (to turn the blowing to suction).

We have seen from the results in the present investigation that the design of the internal duct actually has a relatively negligible effect on the resulting control flow – and therefore on the overall flow. Therefore there is not much hope for the fourth option, however if a third suction locus is introduced further upstream, the Venturi-induced

suction approach might be implemented successfully. This would involve more complex duct design by necessity – as was illustrated in Chapter 5 – so this would be the suggested approach if further geometric options were pursued (rather than material choices).

A schematic of potential duct concepts that employ the Venturi effect to produce better suction profiles (or produce suction in regions of low pressure) is shown in Figure 8.11. This approach utilises a higher pressure and flow rate flow at the first suction locus where the flow is incident (1) to induce a compelling suction in the second locus (S) where the main benefit is achieved. The static pressure of the duct flow must be lowered from the high value at (1) using the Venturi effect before it interacts with (S), and the joined flow must then have enough momentum to overcome any APG (if present) to exhaust at (2). Testing and developing this design may be useful foil to the problem of recirculating flow at the suction locus.

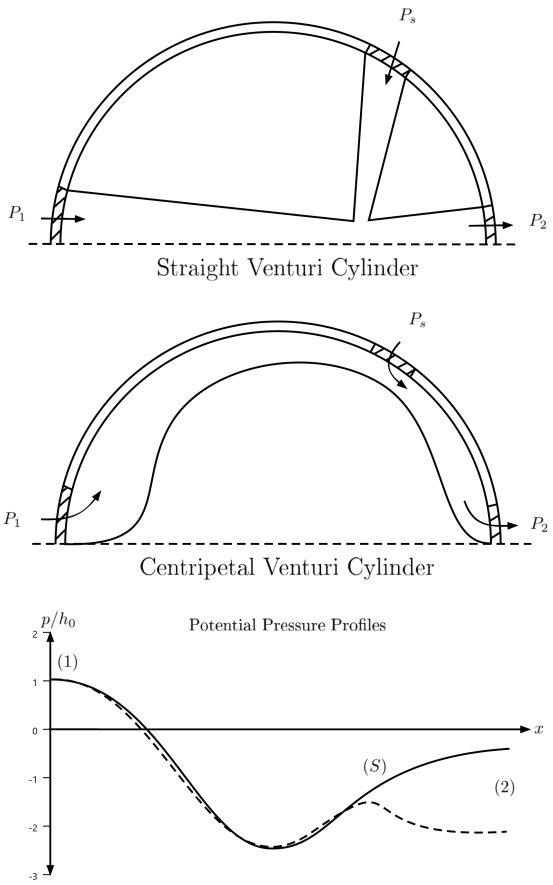

Figure 8.11 Potential suction-inducing duct geometries to produce stronger pressure gradients for the suction locus. The pressure profiles are hypothetical with the solid-line for the case of an APG from suction locus (S) to blowing locus (2), and the dashed line for an FPG.

Finally, the original model where the autogenous control was developed by imposing profiles by the boundary conditions might be adjusted to better reflect the profiles achieved by simple ducting. Altering the upstream locus to have the half-suction

half-blowing that was seen here, then optimising that system, may uncover positive arrangements for these practical designs. Alternatively, one could optimise the practical designs directly. Some brief attempts were made at this towards the end of the present PhD research. Careful constraints have to be imposed so that the optimisation does not seek just to make the cylinder a streamlined shape. Using a low enough permeability may be sufficient.

Chapter 9

CONCLUSIONS AND FUTURE WORK

9.1 CONCLUSIONS

In this work, the use of suction/blowing flow control has been thoroughly investigated by numerical simulations combined with optimisation processes. What follows in this chapter are a summary of each of the key studies, before we return to the original research questions and assess how well they have been answered.

It was shown that non-uniform suction of the boundary layer was always more efficient, and sometimes more effective, than uniform suction in our representative cases – the flow around the circular cylinder, and the flow through a conical diffuser. We showed that separation could be entirely eliminated around the cylinder when sufficient suction control is applied, and that there is a compelling relationship between the optimal control parameters and the uncontrolled separation values. Combining suction with blowing control using the dual-loci control produced even better performance under some circumstances, especially if a non-zero mass flux was permitted (net suction or net blowing). Constraining the control so that the flow-rates were balanced (Q-balanced) and that a positive pressure gradient from suction-to-blowing loci is present (P-balanced) allowed for the design and testing of potentially autogenous suction control. For the 5° diffuser, this control arrangement was unable to improve performance, but for the cylinder at $Re = 40$ and $Re = 120$ it was capable of reducing the drag from the uncontrolled case, and in unsteady simulations also reduced fluctuations in the flow. Overall, autogenous suction control was shown to be a feasible option for improving the aerodynamics of bluff bodies. When considering a practical implementation, with ducting and porous materials to produce the connection between suction/blowing loci, additional losses are present that are not accounted for by assuming that $dP > 0$ is sufficient for autogenous control. Some numerical tests of promising dual-loci control were performed with geometric changes to the cylinder. It was found that at $Re = 40$ the practical concepts still reduced the drag slightly, but not at $Re = 120$. This was predominantly because the suction locus does not match the single locus profile as the strong tangential pressure gradient causes a recirculation at the duct entry (suction

locus). Remedying this, using porous materials with anisotropic permeability or more complex geometries, will likely produce a flow that better resembles those induced by BC-imposed suction/blowing.

9.1.1 Controlling Internal Flows – Diffuser

In Chapter 4, the use of suction control was investigated to improve the performance of a conical diffuser with a validated axisymmetric simulation. A strong foundation understanding of the uncontrolled flow was developed using the numerical simulations. Uniform suction control was optimised for the diffuser at a variety of semi-divergence angles, $5° \leq \alpha \leq 85°$, Reynolds numbers, $Re \leq 1400$, and with a flat inlet profile, $n = 1000$. The performance of the diffuser for the case where suction is applied was measured using η_{out} which is evaluated by taking the pressure power of the flow at the exit of the diffuser as a ratio of the total power on entry and the power needed to produce the suction (see Equation (2.14)). This accounts for the energy needed to run produce the control.

For diffusers with $\alpha \leq 45°$, uniform suction control was able to improve upon the uncontrolled performance, sometimes quite significantly. For example at $\alpha = 5°, Re = 1000$ the performance was improved from $\eta_{out} = 0.4335$ to $\eta_{out} = 0.4720$ (a 9% improvement). Hysteresis of the fully-developed flow was observed in the range of $25° \leq \alpha \leq 35°$ for certain suction flow rates, C_q, and Re. Where hysteresis occurs, control that is ramped down from a higher suction flow rate produces the best flow. For example, at $\alpha = 35°, Re = 1400$ the optimised ramped down control improved upon the uncontrolled case by 789% ($\eta_{out} = 0.3492$ vs. $\eta_{out} = 0.0393$) while the ramped up control only achieved a 118% improvement ($\eta_{out} = 0.0855$).

Suction control improves the diffuser performance by promoting the flow to follow the geometry walls, delaying separation, and thereby causing the pressure to rise higher than it would in the uncontrolled case (though still less than ideal potential flow would suggest). If too much suction is applied, however, the energy needed to produce the control outweighs the benefits, reducing η_{out}. Also, since the supply of flow is limited within the diffuser (i.e. there is no free-stream accessible above/below as in an external flow, only from upstream) too much suction. or suction at low Re can be detrimental as the momentum removed by the suction is needed to keep the flow moving and the boundary layer attached.

Non-uniform suction was able to improve even further on the uniform control result. At $\alpha = 5°, Re = 1000$, the single locus profile improved the performance further to $\eta_{out} = 0.665$ and the field-based approach produced a similar result, $\eta_{out} = 0.6758$, with a biased locus-type profile. The significant improvements over the uniform case ($\eta_{out} = 0.4720$ is due to less suction being needed due to more targeted placement of the control, and thereby achieving a similar pressure rise with less energy input.

Dual-loci control was implemented on this model and optimised for performance. Unfortunately, BL suction is most effective when placed near the entry of the diffuser, and blowing in the first half is more likely to be detrimental than beneficial. This is an issue as the pressure profile in the diffuser is only really appropriate for suction downstream and blowing upstream. If the pressure requirement is ignored, the unbalanced dual-loci control could achieve a performance of $\eta_{out} = 0.8283$ with strong net blowing, while the flow-rate balanced variety (Q-balanced dual-loci) produced a performance of $\eta_{out} = 0.5820$. That the Q-balanced dual-loci control could improve the performance of the diffuser so significantly is quite promising. This control does not remove or add any fluid, it only adds energy by removing and replacing some of the flow in critical areas. While it would still require energy to be operated it is a useful result. Furthermore, this study was only for the $\alpha = 5°, Re = 1000$ diffuser, and better results/improvements may be seen up to the $\alpha = 45°$ diffuser as was seen for the uniform suction. On the other hand, the P-Q-balanced dual-loci control – in other words, the autogenous control arrangement – was unable to produce an improvement in performance. By situating the suction downstream in the region of higher pressure, and the blowing upstream, the control is unable to have much of an effect. The upstream blowing separates the boundary layer (which then resets), and the suction is unable to produce enough 'pull' on the bulk flow later in the diffuser to produce a benefit.

The key results for the best control on the $\alpha = 5°, Re = 1000, n = 1000$ diffuser flow are repeated here in Table 9.1. Overall, non-uniform suction or non-uniform suction/blowing control offers great promise for the improvement of diffuser performance. Especially exciting, is that steeper diffusers, such as those in the range of $5° \leq \alpha \leq 35°$ – which have typically been relegated due to poor performance – can produce a good pressure rise when uniform suction is applied. Non-uniform suction is likely to improve this even further, making their use much more viable in a wide range of applications where short diffusers are necessary. Unfortunately, upwind autogenous suction control does not appear viable for the case of the diffuser. There remains a possibility that downwind autogenous control could be generated for this case, however, by means of inducing suction via the Venturi effect.

Table 9.1 Copy of Table 4.8: Comparison of $\alpha = 5°, Re = 1000, n = 1000$ diffuser with different optimised controls. Note the P-Q-balanced control was unable to improve the performance.

Control	η_{out}	% Change	C_q
Uncontrolled	0.4335	-	-
Uniform	0.4720	9%	0.159
Field	0.6758	56%	0.220
Single-Locus	0.6650	53%	0.145
Unbalanced Dual	0.8283	91%	-0.761
Q-Balanced	0.5820	34%	0
P-Q-Balanced	-	-	-

9.1.1.1 Inducing Non-Uniform Suction Profiles by Venturi Effect

In some cases, such as for the diffuser, the optimal location for non-uniform suction to be applied is in a region of low pressure – relative to the rest of the flow. This makes the prospect of autogenous control unlikely. Therefore, an investigation of whether non-uniform suction profiles could be induced using flow sourced from upstream was investigated using a toy parallel-channel problem in Chapter 5. It was found that non-uniform suction profiles through a porous divider could be induced by appropriate geometric design of the control duct/channel. A test 'spike' suction profile was adequately induced by appropriate upper wall modifications, while the single locus profile was even better. Artificial neural networks (ANN) were trained to design these geometries using randomised CFD results, and this procedure was also effective. While direct optimisation provided the best geometry to produce a desired suction profile, the ANNs produced good first-approximations and were versatile. Generally, it was shown that arbitrary non-uniform suction profiles could be induced by exploiting the Venturi effect, but the geometries are more complex than for a simple Venturi tube. This was shown to be effective in a toy problem where the pressures in the main and control channels were initially equal. Extending the model to the case where the control channel is initially at a *higher* pressure would be beneficial for the development of downwind autogenous control.

9.1.2 Controlling Bluff Bodies by Suction – Cylinder

Next, the flow around the circular cylinder was controlled by uniform and non-uniform suction as described in Chapter 6. Optimising the non-uniform suction profiles to minimise the separation angle, θ_s, minimise the total drag, C_{d_t}, or minimise the pressure drag C_{d_p}. Interesting relationships were found between the separation characteristics of the uncontrolled flow and the optimal control parameters for both the uniform and non-uniform suction control. Overall BL suction was found to be extremely effective at

achieving all these objectives in the Re range of $20 \leq Re \leq 180$, and was particularly useful in reducing drag in the unsteady flow regime $Re \geq 48$. At $Re = 180$ the total drag coefficient was reduced by 43% with optimised single locus control. The optimised control typically required quite large suction volumes, in the area of $C_q \sim 0.05$ for minimising drag in the unsteady regime. However, the necessary suction volumes decreases with Re as its benefits continue to grow due to the increasing difference in free-stream momentum and BL momentum. The field-based approach produced similar results to the biased locus profile, which is useful in the design and implementation of optimal non-uniform suction control. The results for different non-uniform suction profiles are compared to the uncontrolled characteristics at $Re = 120$ in Table 9.2.

Table 9.2 Optimised control parameters and resulting characteristic for different non-uniform suction profiles at $Re = 120$. The uncontrolled data is for the unsteady flow as taken from Henderson [1995].

Parameter	Uncontrolled	Single Locus	Biased Locus	Field-based
θ_q	-	81.4993°	92.0873°	90°
γ_q	-	37.1946°	42.2850°	40.5°
λ_q	-	0.5	0.5943	-
$c_{q_{max}}$	-	0.4762	0.5065	0.5777
C_q	-	0.0492	0.0602	0.0606
C_{d_t}	1.3385	0.9212	0.9132	0.9106
C_{d_p}	0.3188	0.3617	0.2678	0.2597
C_{d_f}	1.0197	0.5595	0.6457	0.6509
θ_s	64.3163°	45.2861°	41.0230°	40.9413°

9.1.3 Autogenous Control Development

In Chapter 7, the results of systematic development and testing of theoretical autogenous dual-loci control on the cylinder were presented. Dual-loci control with unbalanced suction/blowing, balanced flow-rates (Q-balanced), and balanced pressures and flow rates (P-Q-balanced) were tested and optimised on the cylinder at $Re = 40$ and $Re = 120$. It was found that theoretically autogenous suction control could be produced using the P-Q-balanced dual-loci control, and that it could improve the drag characteristics of the cylinder. This conclusions was reached by performing parametric and optimisation studies of the flow with both steady and unsteady conditions, and developing the dual-loci control from unbalanced flow-rates and pressures, to the Q-balanced control with a positive control gradient, $dP = P_s - P_b > 0$.

The unbalanced dual-loci control always produced the best results – improving even on the optimal non-uniform suction control – at $Re = 40$ the unbalanced dual-loci control reduced the total drag by 16% from the uncontrolled case, while at $Re - 120$ it

improved upon the stead-state value by 25% (and even more for the actual unsteady value). These results are shown in Table 7.3 and Table 7.4. These controls had net blowing, but only to a small degree ($|C_q| \leq 0.011$. When the Q-balanced dual-loci control was implemented, the optimised control was not quite as good as the single locus control, but still was a significant improvement on the uncontrolled flow. The optimised Q-balanced control was verified by unsteady simulation and was found to stabilise the flow, resulting in the same outcome as the steady-state simulation. This suggests that a net-zero mass flux control system can be very effective at reducing drag, though energy would need to be supplied to the system to overcome pressure differences.

The pressure constraint was applied to the Q-balanced dual-loci control and the steady flow optimised to minimise drag using the major-minor-optimisation procedure (where the blowing parameters are optimised as a nested optimisation for each suction parameter iteration). The resulting optimised control was quite sensitive to the initial values for this model. The optimised controls were verified by applying them to the unsteady model for the $Re = 120$ case. There was some variation between the steady-state results and the unsteady ones, however the drag was still improved upon and the control maintained a positive pressure gradient.The results suggest that upwind autogenous control is feasible for bluff bodies to reduce drag. The drag-reduction is significant, with a 4.3% drop in drag from the uncontrolled case, and the fluctuations in the flow being reduced by about half. However, these simulations imposed the suction/blowing control by boundary conditions rather than using physical implementations.

Optimised P-Q-balanced control were applied with physical designs for the circular cylinder at $Re = 40$ & $Re = 120$. The suction and blowing loci were connected by internal ducting – Straight-, Centre-, and Ring-Ducted – and a thin porous material was placed at the entrance/exit of this ducting. Each of the design concepts performed very similarly, producing nearly identical suction/blowing profiles over the cylinder surface. At both Re, while the blowing profile could be achieved quite well, the suction locus was not. This was because the strong tangential pressure gradient on the front half of the cylinder caused the control flow to recirculate at the suction locus. This may be remediable using porous materials with anisotropic permeability or more complex duct geometries (possibly even a Venturi approach as in Chapter 5). The permeability of the porous wall had a strong impact on the suction/blowing flow, but predominantly on its magnitude rather than its profile. At $Re = 40$ a Darcy number of $Da = 10^{-2}$ performed best while at $Re = 120$ a slightly less permeable material $Da = 10^{-4}$ was better at qualitatively achieving the desired profiles.

9.1.4 Returning to the Research Questions

Here we restate the original research questions which dictated the direction of this PhD research then describe how they have been answered:

1. If any **suction/blowing control** can be applied to the flow around a circular cylinder or through a conical diffuser, what is their **optimal application** to a) prevent separation, and b) reduce drag?
2. What **relationships** can be uncovered between the optimal control and the characteristics of the uncontrolled flows?
3. **Is autogenous suction control possible** for these flows? And in what arrangement?
4. What is the **optimal autogenous suction control** for one of these flows, and how much better is it?
5. What would a **practical implementation** of this control look like? Can we design a physical system to achieve autogenous suction control that improves drag for the circular cylinder?

1. Suction and blowing can effectively be used to control the flow around bluff bodies and through internal systems with adverse pressure gradients. In all investigated cases, non-uniform control was much more efficient than uniform control and almost always could produce the same *or better* effect on the flow. The 'biased locus' cubic suction/blowing profile was the most effective of those profiles tested, and the unconstrained field-based control usually converged to this approximate profile also – usually arranged to give a sudden peak and long tail.

2. For the bluff body flows, tight relationships were found between the separation characteristics of the uncontrolled flow and the optimal suction control parameters. However, in many instances, these relationships are better described as a relationship to the Reynolds number directly – which the separation point is also related to. It was interesting to find that the location of optimal non-uniform suction was not always at the separation point, as is typically assumed in the literature. At low Re, the optimal suction location, θ_q, begins upstream of the separation point, and moved contrary to the separation point (which marches upstream) as the Reynolds number is increased. In all cases, less and less suction control is needed at higher Re to achieve the same improvement, and the maximum improvement in performance also increases with Re. In most cases, drag reductions or pressure improvements by suction control were not solely due to delayed separation. In other words, the control that optimally eliminates separation entirely is almost never the same as the control that minimises drag. The major influence of suction control is on the pressure contours of the flow, but optimal suction control often has an impact beyond the boundary layer to the whole flow.

3. Upwind autogenous control is possible for the flow around the circular cylinder, however – though a secondary flow can be produced easily in the diffuser – it appears unlikely that upwind autogenous control is beneficial for the flow through

the diffuser. However, only a finite range of parameters has been investigated for the diffuser case, and at steeper divergence angles or other Reynolds numbers the conclusion may be different. The monotonically increasing pressure profile of the diffuser flow is detrimental for the development of beneficial autogenous suction control. Almost always, the best arrangement for minimising drag or maximising performance is to have suction upstream of the minimum pressure point, and blowing downstream; this was the case for both flows. However, if the pressure profile only increases in the streamwise direction, this arrangement will not operate if two control points are simply connected. More complex suction-inducing geometries would be needed, such as those described in Chapter 5. This does mean that for most external flows autogenous suction control is a viable flow control method.

4. Parametric and optimisation studies were used to determine the best arrangements of flow-rate balanced suction and blowing control loci, while constraining the pressure drop from suction to blowing to be positive (P-Q-balanced dual-loci control). This determined that – for the flow around the cylinder – only particular arrangements satisfied the constraints and produced a tangible benefit to the flow (reduced drag). While there was some variety to the profiles, the best usually consisted of suction upstream in the leading half, and blowing downstream in the trailing half. Though blowing right at the trailing edge appears to be the best for minimising drag, it is usually not possible by simple autogenous control due to the small pressure rise from its minimum to the TE that naturally occurs. These studies were performed with symmetrical loci for the suction and blowing loci, but we would anticipate biased loci to produce even better results in the same way that the biased locus was more effective than the single locus profile in Chapter 6. With this arrangement, a drag reduction of 4.3% was achieved at $Re = 120$ and 5.5% at $Re = 40$. It is interesting to note that this arrangement is quite different to that generated in the paper by Atik and van Dommelen [2008] to eliminate BL separation. We think this is a positive result as it gives the aerodynamic engineer two alternative approaches to utilising autogenous control.

5. A variety of potential implementations were designed and tested using steady and unsteady numerical simulations. Using a porous wall where the suction/blowing is desired, and internal ducting with varying shapes/geometries, suction/blowing was achieved. As expected, the characteristics of the porous material were important – particularly the permeability, which tended to work best at $Da = 10^{-4}$ to $Da = 10^{-2}$. Ducts that ran straight from one locus to the other (Straight-Ducted), that routed through the centre of the cylinder (Centre-Ducted), and that followed the edge of the cylinder (Ring-Ducted) were tested. All designs had similar success at achieving the desired suction/blowing profiles. While the blowing control is

quite effectively achieved, the suction is heavily affected by the tangential pressure gradients, causing a mixture of suction and blowing rather than the full-normal suction desired at the suction locus (duct entry). Using a porous material with varying or anisotropic permeability or further geometric changes may prevent this. As a consequence of the mixed suction, coupled with the losses in the control ducts, the total drag was actually increased except for the $Re = 40$ case. Nevertheless, there are many avenues to progress the design and achieve the desired and expected drag reductions. If the suction profile can be appropriately reproduced, one would expect a similar drag coefficient to the BC-imposed results.

Overall the research questions of what optimal suction/blowing control looks like and its relationship to the separation parameters have been answered in great depth for the cylinder and diffuser by systematic CFD investigations, parametric and optimisation studies. We showed that autogenous suction control is possible for these flows, but is sometimes completely ineffectual at improving performance in the upwind arrangement. Since more complex arrangements appeared necessary for some flows – such as inducing suction in low pressure regions – a method for designing suction-inducing geometries was produced, coupling artificial neural networks with CFD. The P-Q-balanced dual-loci control improved upon the uncontrolled flow around the cylinder, but the arrangements where it was effective were limited so require careful design. Hence, optimisation of the control was an essential component. We also investigated a few practical designs for this control, and provided some preliminary results of how capable these were of achieving the desired, optimal control. In summary, the research questions have all been answered in-depth, though there are several avenues of further research that could improve the results and applicability.

9.2 FUTURE WORK

The aim of flow control is to improve the characteristics of a given flow. The motivation of this thesis was to improve the efficiency of internal and external flows in response to the increasing impetus to reduce carbon emissions. The studies described in this thesis have demonstrated that non-uniform suction/blowing control is highly effective at reducing drag and improving performance, and that autogenous suction control is feasible. However, to take these simulated results to real-world flow requires further work. The major steps needed are the following:

1. Apply methodology to other geometries (e.g. streamlined bodies)
2. Refine design of physical systems
3. Determine capability of Venturi-induced autogenous suction systems
4. Extend the studies to turbulent flows
5. Develop and test porous materials with varying permeabilities over their length

6. Validate and iterate by experimentation

Some steps have been taken to extend the present results to turbulent flows (by 3D LES simulations), and the Product Design department at the University of Canterbury has developed porous materials with customisable properties. The results from Chapter 5 suggested that Venturi suction-inducing geometries are a promising avenue for generating non-uniform suction profiles, in addition to the varying-porous materials. It seems reasonable that the qualitative results of this research can be extended to other flows and geometries. Autogenous suction control appears to be possible wherever a varying pressure profile is present (all bodies in external flows). It is anticipated that at higher Re, this control will be more efficient as suction becomes more and more effective due to the increasing momentum difference between the BL and the free-stream. Therefore, of the outlined areas for future research, the most important is the physical implementation and the design of custom anisotropic porous materials. The method and approach for designing autogenous suction control is robust and can be extended to 3D turbulent and unsteady flows, but being able to replicate the optimised dual-loci (or biased dual-loci) control with practical designs is the greater task ahead.

In addition to these steps to develop practical autogenous control, the present studies uncovered various findings that would benefit from further study. These include

1. The negative correlation of the motion of the separation point and location of optimal suction
2. The hysteresis that develops in some suction-controlled diffusers and how this can be exploited
3. Extending the biased-locus and dual-loci optimisation studies to more Re, α, β for the diffuser, and more Re for the cylinder
4. Improving the coupling of artificial neural networks with CFD and optimisation studies, e.g. using the interim results during an optimisation study to train a neural network at the same time

While these are not necessary for developing autogenous suction control further and applying it to real-world applications, they are of scientific interest. All these extensions would provide valuable data to aid the improvement and understanding of flow control and optimisation. Future work can now be undertaken with confidence that non-uniform suction/blowing control and autogenous suction control can effectively improve performance the characteristics separated flows.

Appendix A

Q-BALANCED DUAL-LOCI PARAMETRIC RESULTS – ADDITIONAL FIGURES

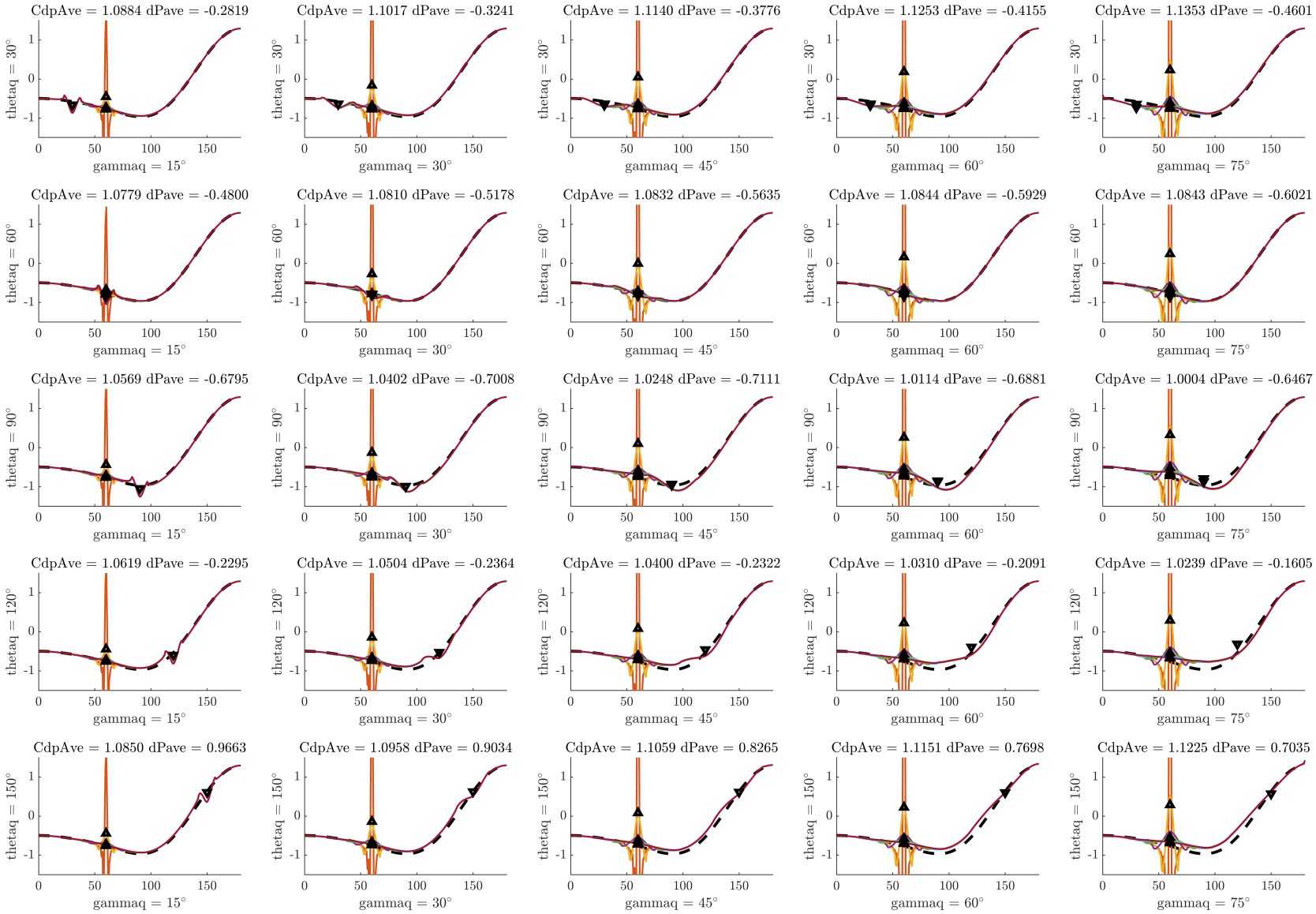

Figure A.1 Pressure profiles at $Re = 40$ grouped by suction parameters. Increasing γ_q from left to right, and increasing θ_q (measured from the trailing edge) from top to bottom. The average pressure drag and pressure gradient values are also given.

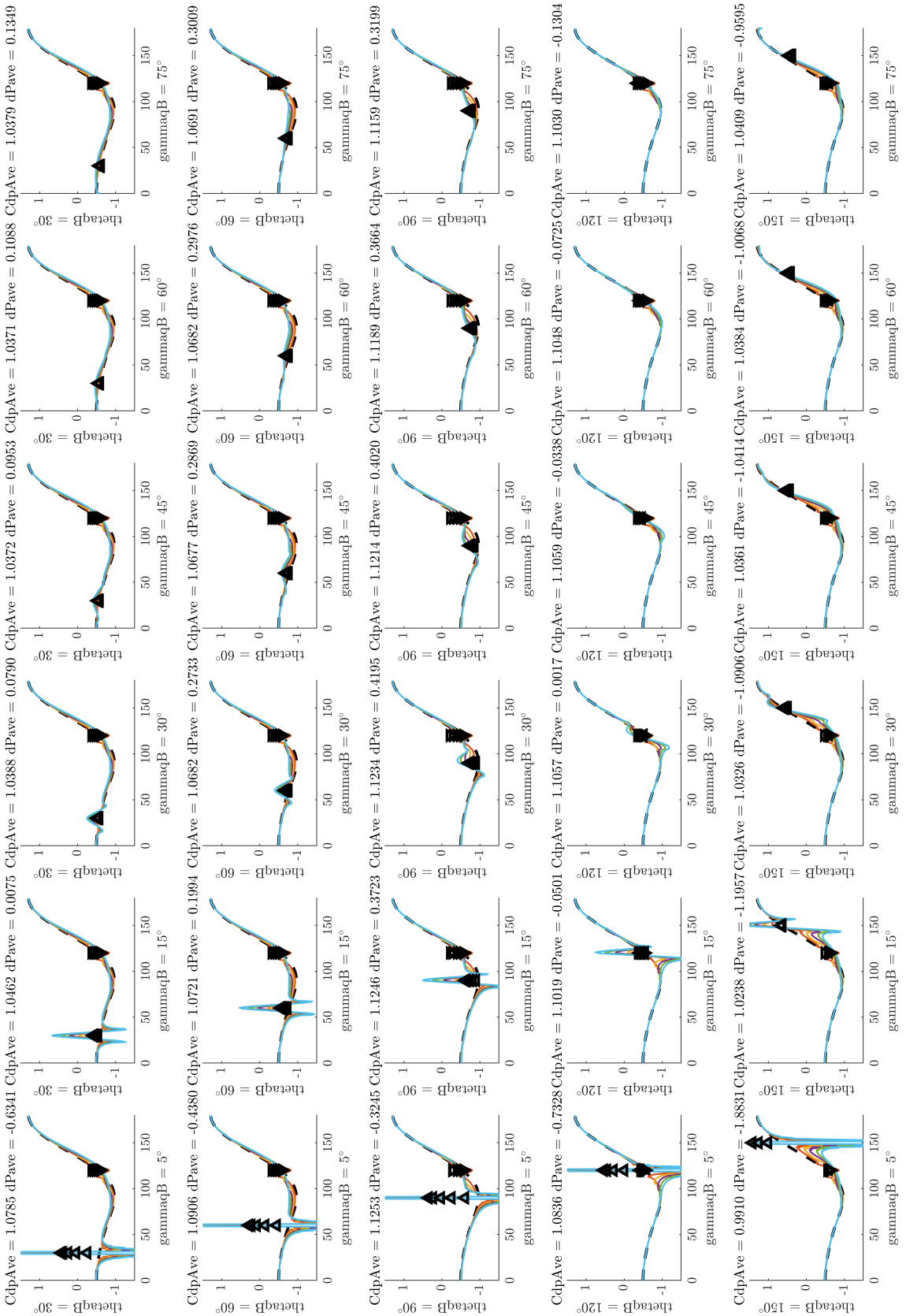

Figure A.2 Pressure profiles at $Re = 40$ grouped by blowing parameters. Increasing γ_{q_b} from left to right, and increasing θ_{q_b} (measured from the trailing edge) from top to bottom. The average pressure drag and pressure gradient values are also given.

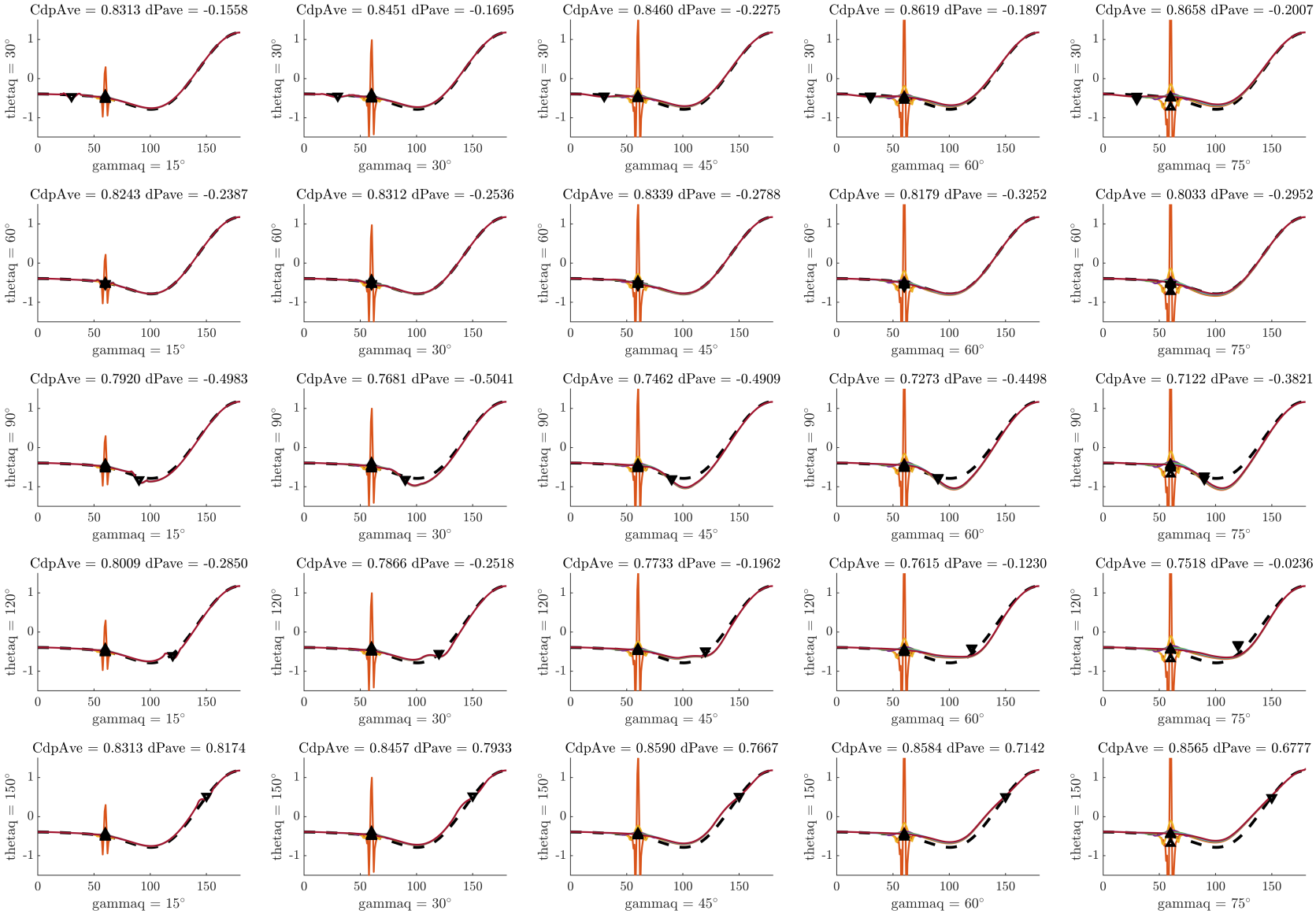

Figure A.3 Pressure profiles at $Re = 120$ grouped by suction parameters. Increasing γ_q from left to right, and increasing θ_q (measured from the trailing edge) from top to bottom. The average pressure drag and pressure gradient values are also given.

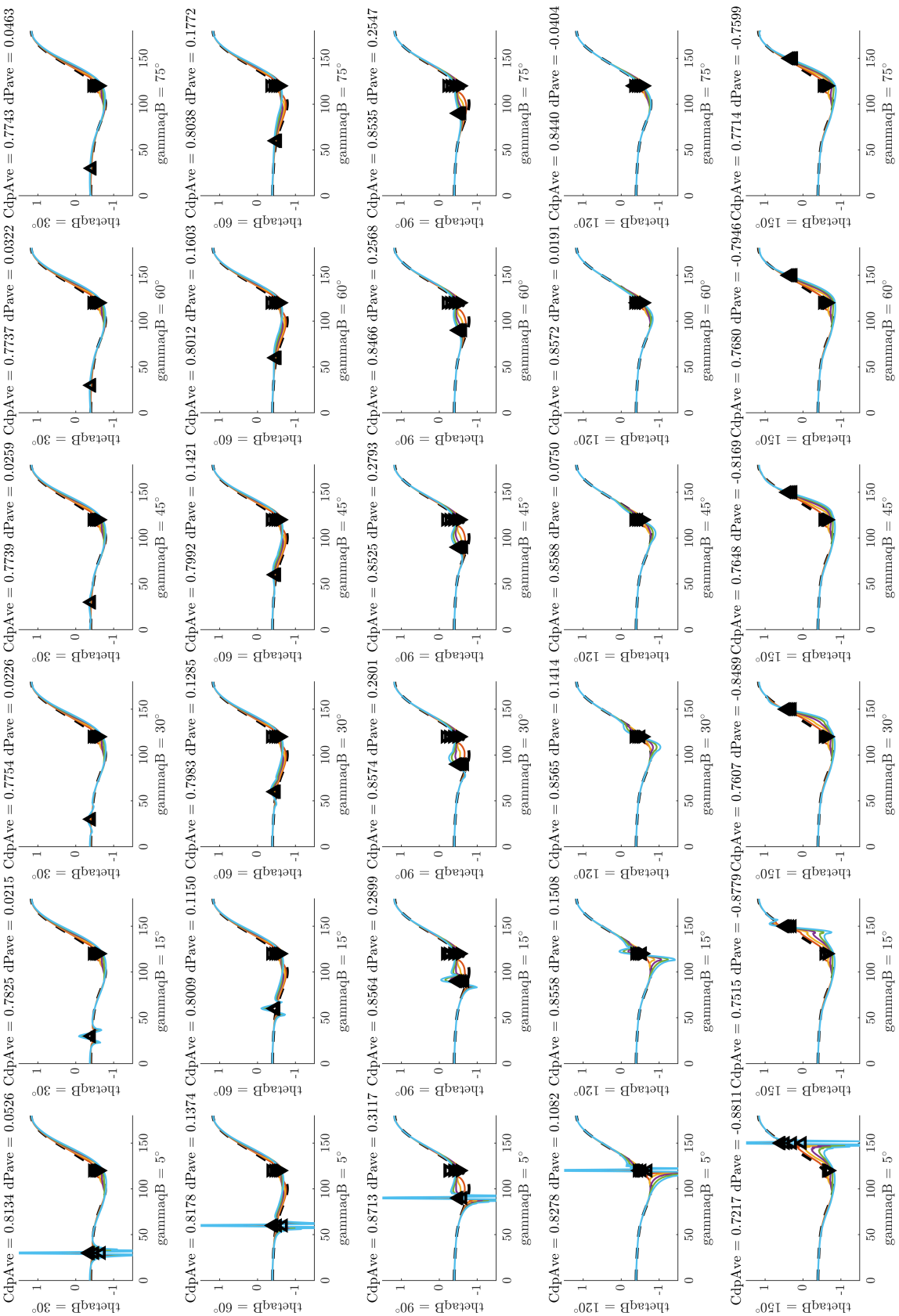

Figure A.4 Pressure profiles at $Re = 120$ grouped by blowing parameters. Increasing γ_{q_b} from left to right, and increasing θ_{q_b} (measured from the trailing edge) from top to bottom. The average pressure drag and pressure gradient values are also given.

REFERENCES

Achenbach, E. (1968), 'Distribution of local pressure and skin friction around a circular cylinder in cross-flow up to Re = 5x10ˆ6', *Journal of Fluid Mechanics*, Vol. 34, No. 4, pp. 625–639.

Achenbach, E. (1972), 'Experiments on the flow past spheres at very high Reynolds numbers', *Journal of Fluid Mechanics*, Vol. 54, No. 3, pp. 565–575.

Ackeret, J. (1926), 'Grenzschichtabsaugung', *Zeitschrift des VDI*, Vol. 70, No. 35, pp. 1153–1158.

Afroz, F., Lang, A., Habegger, M.L., Motta, P. and Hueter, R. (2016), 'Experimental study of laminar and turbulent boundary layer separation control of shark skin', *Bioinspiration & Biomimetics*, Vol. 12, No. 1, p. 016009.

Alton, M.J.S.B. (1997), 'Ship wake signature suppression, U.S. Patent 5787048', 5.

Argyropoulos, C.D. and Markatos, N.C. (2015), 'Recent advances on the numerical modelling of turbulent flows', *Applied Mathematical Modelling*, Vol. 39, No. 2, pp. 693–732.

Armstrong, J., Butcher, K. and Rowe, J. (2003), *CIBSE concise handbook*, Chartered Institution of Building Services Engineers.

Atik, H., Kim, C.Y., van Dommelen, L. and Walker, J. (2005), 'Boundary-layer separation control on a thin airfoil using local suction', *Journal of Fluid Mechanics*, Vol. 535, pp. 415–443.

Atik, H. and van Dommelen, L. (2008), 'Autogenous Suction to Prevent Laminar Boundary-Layer Separation', *Journal of Fluids Engineering*, Vol. 130, No. 1, pp. 011201–1.

Ayton, L.J., Colbrook, M.J., Geyer, T.F., Chaitanya, P. and Sarradj, E. (2021), 'Reducing aerofoil–turbulence interaction noise through chordwise-varying porosity', *Journal of Fluid Mechanics*, Vol. 906.

Back, L.H. and Roschke, E.J. (1972), 'Shear-Layer Flow Regimes and Wave Instabilities and Reattachment Lengths Downstream of an Abrupt Circular Channel Expansion', *Journal of Applied Mechanics*, Vol. 39, No. 3, pp. 677–681.

Ballengee, D.W. and Chen, C.F. (1974), 'Experimental determination of the separation point of flow around a circular cylinder', *Flow: Its measurement and control in science and industry.*, Vol. 1, pp. 419–427.

Barkley, D. (2016), 'Theoretical perspective on the route to turbulence in a pipe', *Journal of Fluid Mechanics*, Vol. 803, pp. 1–80.

Baskharone, E.A. (1991), 'Finite-element analysis of turbulent flow in annular exhaust diffusers of gas turbine engines', *Journal of Fluids Engineering*, Vol. 113, No. 1, pp. 104–110.

Baya, A., Muntean, S., Câmpian, V.C., Cuzmoş, A., Diaconescu, M. and Bălan, G. (2010), 'Experimental investigations of the unsteady flow in a Francis turbine draft tube cone', *IOP Conference Series: Earth and Environmental Science*, Vol. 12, p. 12007.

Beck, N., Landa, T., Seitz, A., Boermans, L., Liu, Y. and Radespiel, R. (2018), 'Drag Reduction by Laminar Flow Control', *Energies*, Vol. 11, No. 1, p. 252.

Bellhouse, B.J. and Schultz, D.L. (1966), 'Determination of mean and dynamic skin friction, separation and transition in low-speed flow with a thin-film heated element', *Journal of Fluid Mechanics*, Vol. 24, No. 2, pp. 379–400.

Boujo, E., Fani, A. and Gallaire, F. (2019), 'Second-order sensitivity in the cylinder wake: Optimal spanwise-periodic wall actuation and wall deformation', *Physical Review Fluids*, Vol. 4, No. 5, p. 053901.

Braslow, A.L. (1999), 'A History of Suction-Type Laminar-Flow Control with Emphasis on Flight Research', In *Monographs in Aerospace History #13*, NASA History Division, Washington DC.

Brayton, R.K., Gustavson, F.G. and Hachtel, G.D. (1972), 'A new efficient algorithm for solving differential-algebraic systems using implicit backward differentiation formulas', *Proceedings of the IEEE*, Vol. 60, No. 1, pp. 98–108.

Brinkman, H.C. (1949), 'A calculation of the viscous force exerted by a flowing fluid on a dense swarm of particles', *Flow, Turbulence and Combustion*, Vol. 1, No. 1, pp. 27–34.

Burkardt, J. (2011), 'Finite Elements for the (Navier) Stokes Equations', In *ISC 5939: Advanced Graduate Seminar*, Florida State University, pp. 1–69.

Cantwell, C.D., Barkley, D. and Blackburn, H.M. (2010), 'Transient growth analysis of flow through a sudden expansion in a circular pipe', *Physics of Fluids*, Vol. 22, No. 3, p. 34101.

Carroll, J., Varcoe, R.L., Barber, T. and Simmons, A. (2019), 'Reduction in anastomotic flow disturbance within a modified end-to-side arteriovenous fistula configuration: Results of a computational flow dynamic model', *Nephrology*, Vol. 24, No. 2, pp. 245–251.

Cattafesta, L.N. and Sheplak, M. (2011), 'Actuators for Active Flow Control', *Annual Review of Fluid Mechanics*, Vol. 43, No. 1, pp. 247–272.

Chan, W.H.R., Mirjalili, S., Jain, S.S., Urzay, J., Mani, A. and Moin, P. (2019), 'Birth of microbubbles in turbulent breaking waves', *Physical Review Fluids*, Vol. 4, No. 10, p. 100508.

Chen, W.L., Xin, D.B., Xu, F., Li, H., Ou, J.P. and Hu, H. (2013), 'Suppression of vortex-induced vibration of a circular cylinder using suction-based flow control', *Journal of Fluids and Structures*, Vol. 42, pp. 25–39.

Chen, W.L., Cao, Y., Li, H. and Hu, H. (2015), 'Numerical investigation of steady suction control of flow around a circular cylinder', *Journal of Fluids and Structures*, Vol. 59, pp. 22–36.

Choi, H., Jeon, W.P. and Kim, J. (2008), 'Control of Flow Over a Bluff Body', *Annual Review of Fluid Mechanics*, Vol. 40, No. 1, pp. 113–139.

Chomaz, J.M. (2003), 'Fully nonlinear dynamics of parallel wakes', *Journal of Fluid Mechanics*, Vol. 495, pp. 57–75.

Christchurch City Council (2019), 'Christchurch sets 2045 carbon neutral target : Newsline', 9.

Cochran, D.L. and Kline, S. (1958), 'Use of Short Flat Vanes for Producing Efficient Wide-Angle Two-Dimensional Subsonic Diffusers', Tech. rep., National Advisory Committee for Aeronautics, Washington.

COMSOL Multiphysics® (2020a), 'CFD Module User's Guide', .

COMSOL Multiphysics® (2020b), 'Optimization User's Guide', .

Darcy, H. (1856), *Les fontaines publiques de la ville de Dijon: exposition et application...*, Victor Dalmont.

Debuysschère, R., Siconolfi, L., Rimez, B., Gallaire, F. and Scheid, B. (2020), 'Influence of the inlet velocity profile on the flow stability in a symmetric channel expansion', *Journal of Fluid Mechanics*, Vol. 909, pp. 13–14.

Delany, N.K. and Sorensen, N.E. (1958), 'Low-speed drag of cylinders of various shapes', Tech. rep., National Advisory Committee for Aeronautics.

Delaunay, Y. and Kaiktsis, L. (2001), 'Control of circular cylinder wakes using base mass transpiration', *Physics of Fluids*, Vol. 13, No. 11, pp. 3285–3302.

Dimopoulos, H.G. and Hanratty, T.J. (1968), 'Velocity gradients at the wall for flow around a cylinder for Reynolds numbers between 60 and 360', *Journal of Fluid Mechanics*, Vol. 33, No. 2, pp. 303–319.

Egashira, R., Fujikawa, T., Yaguchi, H. and Fujikawa, S. (2018), 'Microscopic and low Reynolds number flows between two intersecting permeable walls', *Fluid Dynamics Research*, Vol. 50, No. 3, pp. 35502–1.

Egashira, R., Fujikawa, T., Yaguchi, H. and Fujikawa, S. (2019), 'Low Reynolds number flows in a microscopic and tapered tube with a permeability', *Fluid Dynamics Research*, Vol. 51, No. 2.

Eiffel, G. (1912), 'Sur la résistance des sphères dans l'air en mouvement', *Comptes rendus de l'Académie des Sciences*, Vol. 155, p. 1597.

Elsevier (2021), 'Copyright Policies, https://www.elsevier.com/about/policies/copyright', .

Fage, A. and Falkner, V.M. (1931), 'Further Experiments on the Flow Around a Circular Cylinder', Tech. rep., Aeronautical Research Committee.

Fiedler, R.A. and Gessner, F.B. (1972), 'Influence of Tangential Fluid Injection on the Performance of Two-Dimensional Diffusers', *Journal of Basic Engineering*, Vol. 94, No. 3, pp. 666–674.

Fiedler, R.A. (1970), *Influence of Wall Jets on Compact Diffuser Performance*, PhD thesis, University of Washington.

Flinois, T.L. and Colonius, T. (2015), 'Optimal control of circular cylinder wakes using long control horizons', *Physics of Fluids*, Vol. 27, No. 8.

Fox, R.W. and Kline, S.J. (1962), 'Flow regimes in curved subsonic diffusers', *Journal of Basic Engineering*, Vol. 84, No. 3, pp. 303–312.

Fransson, J.H.M., Konieczny, P. and Alfredsson, P.H. (2004), 'Flow around a porous cylinder subject to continuous suction or blowing', *Journal of Fluids and Structures*, Vol. 19, No. 8, pp. 1031–1048.

Fried, E. and Idelchik, I.E. (1989), *Flow resistance : a design guide for engineers*, Taylor & Francis, Boca Raton.

Fujikawa, T., Egashira, R., Fujikawa, S., Takeda, K. and Kodama, T. (2016), 'Extended Bernoulli equation, friction loss, and friction coefficient for microscopic Jeffery-Hamel flow with small Reynolds number up to O(1)', *Journal of Fluid Science and Technology*, Vol. 11, No. 3.

Fulker, D., Kang, M., Simmons, A. and Barber, T. (2013), 'The flow field near a venous needle in hemodialysis: A computational study', *Hemodialysis International*, Vol. 17, No. 4, pp. 602–611.

Furuya, Y., Sato, T. and Kushida, T. (1966), 'Loss of Flow in the Conical Diffusers with Suction at the Entrance', *Bulletin of JSME*, Vol. 9, No. 33, pp. 131–137.

Furuya, Y., Fujimoto, T., Yamazato, E., Tsuzuki, I. and Nishiura, I. (1970), 'Performance of the Two-Dimensional Diffusers with Suction at the Entrance', *Bulletin of JSME*, Vol. 13, No. 56, pp. 264–271.

Gibson, A.H. (1912), 'V.—On the Resistance to Flow of Water through Pipes or Passages having Divergent Boundaries', *Transactions of the Royal Society of Edinburgh*, Vol. 48, No. 1, pp. 97–116.

Gibson, A.H. and Petavel, J.E. (1910), 'On the flow of water through pipes and passages having converging or diverging boundaries', *Proceedings of the Royal Society of London. Series A, Containing Papers of a Mathematical and Physical Character*, Vol. 83, No. 563, pp. 366–378.

Gill, P.E., Murray, W. and Saunders, M.A. (2005), 'SNOPT: An SQP algorithm for large-scale constrained optimization', *SIAM Review*, Vol. 47, No. 1, pp. 99–131.

Goldstein, S. (1948), 'On a solution of the laminar boundary-layer equation near a position of separation', *Quarterly Journal of Mechanics and Applied Mathematics*, Vol. 1, No. 1, pp. 385–407.

Hammad, K.J., Ötügen, M.V. and Arik, E.B. (1999), 'A PIV study of the laminar axisymmetric sudden expansion flow', *Experiments in fluids*, Vol. 26, No. 3, pp. 266–272.

Henderson, R.D. (1995), 'Details of the drag curve near the onset of vortex shedding', *Physics of Fluids*, Vol. 7, No. 9, pp. 2102–2104.

Hindawi (2021), 'Copyright, https://www.hindawi.com/copyright/', .

Holzhauser, C.A. and Hall, L.P. (1956), 'Exploratory investigation of the use of area suction to eliminate air-flow separation in diffusers having large expansion angles', Tech. rep., National Advisory Committee for Aeronautics, Washington.

Homann, F. (1936), 'Influence of higher viscosity on flow around cylinder', *Forschung aus dem Gebiete das Ingenieurwesen*, Vol. 17, pp. 1–10.

Hsu, S.H., Hsin, W.B. and Hung, P.F. (2015), 'A 3-D numerical simulation of the flow field around a porous cylinder', *Journal of Chinese Soil and Water Conservation*, Vol. 46, No. 4, pp. 239–251.

Huang, L., Huang, P.G., LeBeau, R.P. and Hauser, T. (2004a), 'Numerical Study of Blowing and Suction Control Mechanism on NACA0012 Airfoil', *Journal of Aircraft*, Vol. 41, No. 5, pp. 1005–1013.

Huang, L., LeBeau, R., Huang, P. and Hauser, T. (2004b), 'Optimization of blowing and suction control on NACA 0012 airfoil using genetic algorithm', *AIAA Paper*, pp. 2314–2326.

Hurley, D.G. and Thwaites, B. (1951), 'An experimental investigation of the boundary layer on a porous circular cylinder', Tech. rep., Aeronautical Research Council.

Iribarne, A., Frantisak, F., Hummel, R.L. and Smith, J.W. (1972), 'An experimental study of instabilities and other flow properties of a laminar pipe jet', *AIChE Journal*, Vol. 18, No. 4, pp. 689–698.

Jotkar, M. and Govindarajan, R. (2019), 'Two-dimensional modal and non-modal instabilities in straight-diverging-straight channel flow', *Physics of Fluids*, Vol. 31, No. 1, p. 14102.

Jotkar, M.R. and Govindarajan, R. (2017), 'Non-modal stability of Jeffery-Hamel flow', *Physics of Fluids*, Vol. 29, No. 6, p. 64107.

Kim, J. and Choi, H. (2005), 'Distributed forcing of flow over a circular cylinder', *Physics of Fluids*, Vol. 17, No. 3, pp. 33103–33116.

Kim, J. and Bewley, T.R. (2007), 'A linear systems approach to flow control', *Annual Review of Fluid Mechanics*, Vol. 39, pp. 383–417.

Kline, S.J., Abbott, D.E. and Fox, R.W. (1959), 'Optimum Design of Straight-Walled Diffusers', *Journal of Basic Engineering*, Vol. 81, No. 3, pp. 321–329.

Kline, S.J. (1959), 'On the Nature of Stall', *Journal of Basic Engineering*, Vol. 81, No. 3, pp. 305–319.

Klyuev, N., Kryukov, Y. and Gimadiev, A. (2017), 'Reducing Friction Drag on Flat Plates', *Procedia Engineering*, Vol. 176, pp. 661–668.

Kornilov, V.I. (2015), 'Current state and prospects of researches on the control of turbulent boundary layer by air blowing', *Progress in Aerospace Sciences*, Vol. 76, pp. 1–23.

Kumar, R.A., Sohn, C.H. and Gowda, B.H. (2010), 'Passive Control of Vortex-Induced Vibrations: An Overview', *Recent Patents on Mechanical Engineering*, Vol. 1, No. 1, pp. 1–11.

Kwon, K. and Choi, H. (1996), 'Control of laminar vortex shedding behind a circular cylinder using splitter plates', *Physics of Fluids*, Vol. 8, No. 2, pp. 479–486.

Lachmann, G.V. (editor) (1961), *Boundary layer and flow control: its principles and application*, Boundary Layer and Flow Control: Its Principles and Application, Pergamon Press, 1st ed.

Lamb, H. (1911), 'XV. On the uniform motion of a sphere through a viscous fluid', *The London, Edinburgh, and Dublin Philosophical Magazine and Journal of Science*, Vol. 21, No. 121, pp. 112–121.

Langtangen, H.P. and Logg, A. (2016), *Solving PDEs in Python*, Springer International Publishing.

Latornell, D.J. and Pollard, A. (1986), 'Some observations on the evolution of shear layer instabilities in laminar flow through axisymmetric sudden expansions', *Physics of Fluids*, Vol. 29, No. 9, pp. 2828–2835.

Le Bars, M. and Worster, M.G. (2006), 'Interfacial conditions between a pure fluid and a porous medium: Implications for binary alloy solidification', *Journal of Fluid Mechanics*, Vol. 550, No. -1, pp. 149–173.

Leal, L.G. (1989), 'Vorticity transport and wake structure for bluff bodies at finite Reynolds number', *Physics of Fluids A: Fluid Dynamics*, Vol. 1, No. 1, pp. 124–131.

Lebon, B., Nguyen, M.Q., Peixinho, J., Shadloo, M.S. and Hadjadj, A. (2018a), 'A new mechanism for periodic bursting of the recirculation region in the flow through a sudden expansion in a circular pipe', *Physics of Fluids*, Vol. 30, No. 3, p. 31701.

Lebon, B., Peixinho, J., Ishizaka, S. and Tasaka, Y. (2018b), 'Subcritical transition to turbulence in a sudden circular pipe expansion', *Journal of Fluid Mechanics*, Vol. 849, pp. 340–354.

Li, Z., Navon, I.M., Hussaini, M.Y. and Le Dimet, F.X. (2003), 'Optimal control of cylinder wakes via suction and blowing', *Computers & Fluids*, Vol. 32, No. 2, pp. 149–171.

Ligrani, P., Potts, G. and Fatemi, A. (2017), 'Endwall aerodynamic losses from turbine components within gas turbine engines', *Propulsion and Power Research*, Vol. 6, No. 1, pp. 1–14.

Linke, W. (1931), 'New measurements on aerodynamics of cylinders particularly their friction resistance', *Phys. Z*, Vol. 32, p. 900.

Lozano, P. (2008), '"Momentum Integral Applications" - Lecture 10 Fluid Mechanics and Aerodynamics', .

Macagno, E.O. and Hung, T.K. (1967), 'Computational and experimental study of a captive annular eddy', *Journal of Fluid Mechanics*, Vol. 28, No. 1, pp. 43–64.

Madhavan, S. and Kemmerling, E.M. (2018), 'The effect of inlet and outlet boundary conditions in image-based CFD modeling of aortic flow', *BioMedical Engineering Online*, Vol. 17, No. 1, p. 66.

Marsan, A., Trébinjac, I., Coste, S. and Leroy, G. (2012), 'Study and Control of a Radial Vaned Diffuser Stall', *International Journal of Rotating Machinery*, Vol. 2012, pp. 1–12.

McDonald, A.T. and Fox, R.W. (1966), 'An experimental investigation of incompressible flow in conical diffusers', *International Journal of Mechanical Sciences*, Vol. 8, No. 2, pp. 125–139.

Min, C. and Choi, H. (1999), 'Suboptimal feedback control of vortex shedding at low Reynolds numbers', *Journal of Fluid Mechanics*, Vol. 401, pp. 123–156.

Ministry for the Environment (2016), 'New Zealand's Greenhouse Gas Inventory 1990-2014', Tech. rep., Ministry for the Environment.

Ministry of Transport (2017), 'Environmental impact of transport: Climate change', Tech. rep., Ministry of Transport, Wellington, New Zealand.

Moore Jr, C.A. and Kline, S.J. (1958), 'Some effects of vanes and of turbulence in two-dimensional wide-angle subsonic diffusers', Tech. rep., NACA TN4080, Washington DC.

Müller, W. and Patone, G. (1998), 'Air transmissivity of feathers', *Journal of Experimental Biology*, Vol. 201, No. 18, pp. 2591–2599.

Nagamatsu, H., Trilling, T. and Bossard, J. (1987), 'Passive drag reduction on a complete NACA 0012 airfoil at transonic Mach numbers', In *19th AIAA, Fluid Dynamics, Plasma Dynamics, and Lasers Conference*, p. 1263.

Nelder, J.A. and Mead, R. (1965), 'A Simplex Method for Function Minimization', *The Computer Journal*, Vol. 7, No. 4, pp. 308–313.

New Zealand Parliament (2019), 'Climate Change Response (Zero Carbon) Amendment Act', .

New Zealand Parliament (2020), 'Motions — Climate Change—Declaration of Emergency - New Zealand Parliament', .

Newton, I.S. (1687), *Philosophiae Naturalis Principia Mathematica*, Royal Society, London.

Nicoll, W.B. and Ramaprian, B.R. (1970), 'Performance of Conical Diffusers With Annular Injection at Inlet', *Journal of Basic Engineering*, Vol. 92, No. 4, pp. 827–835.

Nield, D.A. and Bejan, A. (2013), *Convection in porous media*, Springer, New York, 3rd ed.

Nilakantan, P. (1945), 'On diffuser efficiency in compressible flow', In *Proceedings of the Indian Academy of Sciences-Section A*, Vol. 22, Springer, pp. 67–74.

Nishimura, H. and Taniike, Y. (2001), 'Aerodynamic characteristics of fluctuating forces on a circular cylinder', *Journal of Wind Engineering and Industrial Aerodynamics*, Vol. 89, No. 7, pp. 713–723.

Pankhurst, R.C., Thwaites, B. and Walker, W.S. (1953), 'Experiments on the Flow Past a Porous Circular Cylinder Fitted with a Thwaites Flap', Tech. rep., British Aeronautical Research Council, London.

Parikh, P.G. (2011), 'Passive removal of suction air for laminar flow control, and associated systems and methods, U.S. Patent 7866609', .

Peixinho, J. and Besnard, H. (2013), 'Transition to turbulence in slowly divergent pipe flow', *Physics of Fluids*, Vol. 25, No. 11, p. 111702.

Pelacci, M. (2019), *Drag reduction on a circular cylinder through the use of architectured woven coatings*, PhD thesis, University of Surrey.

Polanczyk, A., Podgorski, M., Wozniak, T., Stefanczyk, L. and Strzelecki, M. (2018), 'Computational fluid dynamics as an engineering tool for the reconstruction of hemodynamics after carotid artery stenosis operation: a case study', *Medicina*, Vol. 54, No. 3, p. 42.

Pollard, A. (1981), 'A contribution on the effects of inlet conditions when modelling stenoses using sudden expansions', *Journal of biomechanics*, Vol. 14, No. 5, pp. 349–355.

Prandtl, L. (1904), 'Über Flüssigkeitsbewegung bei sehr kleiner Reibung', In *Verhandlungen des dritten internationalen MathematikerKongresses*, Vol. Heidelberg, pp. 484–491.

Ramsay, J., Sellier, M. and Ho, W.H. (2019), 'V0025: Dynamics and Control of Flow around Circular Cylinder', In *APS Gallery of Fluid Motion*, American Physical Society, Seattle, Washington.

Ramsay, J., Sellier, M. and Ho, W.H. (2020a), 'Designing Suction-Inducing Geometries for Flow Control using CFD-Coupled Artificial Neural Networks', In *22nd Australasian Fluid Mechanics Conference AFMC2020*, University of Queensland Library.

Ramsay, J., Sellier, M. and Ho, W.H. (2020b), 'Effects of boundary layer suction control on flow through an axisymmetric diverging channel', *Journal of the Royal Society of New Zealand*, pp. 1–20.

Ramsay, J., Sellier, M. and Ho, W.H. (2020c), 'Eliminating Boundary Layer Separation on a Cylinder with Nonuniform Suction', *International Journal of Aerospace Engineering*, Vol. 2020, p. 9137369.

Ramsay, J.R., Sellier, M. and Ho, W.H. (2020d), 'Non-uniform suction control of flow around a circular cylinder', *International Journal of Heat and Fluid Flow*, Vol. 82, p. 108559.

Rashidi, S., Dehghan, M., Ellahi, R., Riaz, M. and Jamal-Abad, M.T. (2015), 'Study of stream wise transverse magnetic fluid flow with heat transfer around an obstacle embedded in a porous medium', *Journal of Magnetism and Magnetic Materials*, Vol. 378, pp. 128–137.

Rashidi, S., Hayatdavoodi, M. and Esfahani, J.A. (2016), 'Vortex shedding suppression and wake control: A review', *Ocean Engineering*, Vol. 126, pp. 57–80.

Reid, E.G. (1953), 'Performance characteristics of plane-wall two-dimensional diffusers', Tech. Rep. 2888, Stanford University, Washington.

Relf, E.F. (1914), 'Discussion of the results of measurements of the resistance of wires with some additional tests on the resistance of wires of small diameter', Tech. rep., Aeronautical Research Council.

Reynolds, O. (1883), 'XXIX. An experimental investigation of the circumstances which determine whether the motion of water shall be direct or sinuous, and of the law of resistance in parallel channels', *Philosophical Transactions of the Royal society of London*, Vol. 174, pp. 935–982.

Roshko, A. (1961), 'Experiments on the flow past a circular cylinder at very high Reynolds number', *Journal of Fluid Mechanics*, Vol. 10, No. 3, pp. 345–356.

Rouse, H. (1983), 'Highlights in the History of Hydraulics', *Books at Iowa*, Vol. 38, No. 1, pp. 3–17.

Rouse, H. and Ince, S. (1963), *History of Hydraulics*, Springer, New York, 1st ed.

Runstadler, P.W., Dean, R.C. and Dolan, F.X. (1975), *Diffuser data book*, Creare.

Schenk, O. and Gärtner, K. (2004), 'Solving unsymmetric sparse systems of linear equations with PARDISO', *Future Generation Computer Systems*, Vol. 20, No. 3, pp. 475–487.

Schlichting, H. and Gersten, K. (1961), 'Berechnung der Strömung in rotationssymmetrischen Diffusoren mit Hilfe der Grenzschichttheorie', *Z. Flugwiss*, Vol. 9, No. 4/5, pp. 136–140.

Schlichting, H. (1987), *Boundary-Layer Theory*, McGraw-Hill, New York, 7th ed.

Schumm, M., Berger, E. and Monkewitz, P.A. (1994), 'Self-excited oscillations in the wake of two-dimensional bluff bodies and their control', *Journal of Fluid Mechanics*, Vol. 271, pp. 17–53.

Scruton, C. and Walshe, D.E.J. (1957), 'A means for avoiding wind-excited oscillations of structures with circular or nearly circular cross section', Tech. rep., National Physics Lab.

Sedghi, M., Saboonchi, A. and Ghane, M. (2018), 'An experimental study on the permeability of flying and flightless birds' contour feathers', *Journal of Porous Media*, Vol. 21, No. 13, pp. 1347–1357.

Selvam, K., Peixinho, J. and Willis, A.P. (2015), 'Localised turbulence in a circular pipe flow with gradual expansion', *Journal of Fluid Mechanics*, Vol. 771, pp. R21–R213.

Selvam, K., Peixinho, J. and Willis, A.P. (2016), 'Flow in a circular expansion pipe flow: Effect of a vortex perturbation on localised turbulence', *Fluid Dynamics Research*, Vol. 48, No. 6, p. 61418.

Shenoy, D.V., Shadloo, M.S., Peixinho, J. and Hadjadj, A. (2019), 'Direct numerical simulations of laminar and transitional flows in diverging pipes', *International Journal of Numerical Methods for Heat and Fluid Flow*, Vol. 30, No. 1, pp. 75–92.

Shtendel, T. and Seifert, A. (2014), 'Three-dimensional aspects of cylinder drag reduction by suction and oscillatory blowing', *International Journal of Heat and Fluid Flow*, Vol. 45, pp. 109–127.

Sohankar, A., Khodadadi, M. and Rangraz, E. (2015), 'Control of fluid flow and heat transfer around a square cylinder by uniform suction and blowing at low Reynolds numbers', *Computers and Fluids*, Vol. 109, pp. 155–167.

Son, J.S. and Hanratty, T.J. (1969), 'Velocity gradients at the wall for flow around a cylinder at Reynolds numbers from 5 × 103 to 105', *Journal of Fluid Mechanics*, Vol. 35, No. 2, pp. 353–368.

Sparrow, E., Abraham, J. and Minkowycz, W. (2009), 'Flow separation in a diverging conical duct: Effect of Reynolds number and divergence angle', *International Journal of Heat and Mass Transfer*, Vol. 52, No. 13-14, pp. 3079–3083.

Stewart, M.B. and Miner, E.W. (1987), 'Bubble Dynamics in a Turbulent Ship Wake', Tech. rep., Naval Research Laboratory, Washington DC.

Stroman, J.C. (1997), *Aerodynamic drag coefficients of a variety of electrical conductors*, PhD thesis, Texas Tech University.

Strouhal, V. (1878), 'Über eine besondere Art der Tonerregung', *Annalen der Physik*, Vol. 241, No. 10, pp. 216–251.

Su, W.Y., Chen, Y., Zhang, F.R. and Tang, P.P. (2018), 'Control of pseudo-shock oscillation in scramjet inlet-isolator using periodical excitation', *Acta Astronautica*, Vol. 143, pp. 147–154.

Sung, Y., Kim, W., Mungal, M.G. and Cappelli, M.A. (2006), 'Aerodynamic modification of flow over bluff objects by plasma actuation', *Experiments in Fluids*, Vol. 41, No. 3, pp. 479–486.

Tani, I. (1964), 'Low-speed flows involving bubble separations', *Progress in Aerospace Sciences*, Vol. 5, pp. 70–103.

Taylor & Francis (2021), 'Understanding Copyright for Journal Authors, https://authorservices.taylorandfrancis.com/publishing-your-research/moving-through-production/copyright-for-journal-authors/', .

Thom, A. and Ingram, T.G. (1933), 'The flow past circular cylinders at low speeds', *Proceedings of the Royal Society of London. Series A, Containing Papers of a Mathematical and Physical Character*, Vol. 141, No. 845, pp. 651–669.

Thom, A. (1929), 'An investigation of fluid flow in two dimensions', *Reports and Memoranda of Great Britain Aeronautical Research Committee*, Vol. 1194.

Thompson, M.C. and Hourigan, K. (2005), 'The shear-layer instability of a circular cylinder wake', *Physics of Fluids*, Vol. 17, No. 2, p. 21702.

Tiainen, J., Grönman, A., Jaatinen-Värri, A. and Backman, J. (2017), 'Flow Control Methods and Their Applicability in Low-Reynolds-Number Centrifugal Compressors—A Review', *International Journal of Turbomachinery, Propulsion and Power*, Vol. 3, No. 1, p. 2.

Tietjens, O.K.G. and Prandtl, L. (1957), *Applied hydro-and aeromechanics: based on lectures of L. Prandtl*, Vol. 2, Courier Corporation.

Trevorrow, M.V., Vagle, S. and Farmer, D.M. (1994), 'Acoustical measurements of microbubbles within ship wakes', *The Journal of the Acoustical Society of America*, Vol. 95, No. 4, pp. 1922–1930.

Tritton, D.J. (1959), 'Experiments on the flow past a circular cylinder at low Reynolds numbers', *Journal of Fluid Mechanics*, Vol. 6, No. 4, pp. 547–567.

UNFCCC (2015), 'Paris Agreement to the United Nations Framework Convention on Climate Change', .

UQ (2020), 'AFMC Proceedings Copyright Policy, https://espace.library.uq.edu.au/view/UQ:4ec3ee5', In *22nd Australasian Fluid Mechanics Conference AFMC2020*, University of Queensland Library, https://espace.library.uq.edu.au/view/UQ:4ec3ee5.

Veldman, A.E.P. (2009), 'A simple interaction law for viscous–inviscid interaction', *J Eng Math*, Vol. 65, pp. 367–383.

Veldman, A.E.P. (2017), 'Entrainment and boundary-layer separation: a modeling history', *Journal of Engineering Mathematics*, Vol. 107, No. 1, pp. 5–17.

Von Karman, T. (1911), 'Über den Mechanismus des Widerstandes, den ein bewegter Körper in einer Flüssigkeit erfährt', *Nachrichten von der Gesellschaft der Wissenschaften zu Göttingen, Mathematisch-Physikalische Klasse*, Vol. 1911, pp. 509–517.

Wang, A.B. and Lin, C.C. (1997), 'Flow visualization of the buoyancy effects on the flow in horizontal pipe with axisymmetric sudden expansion', In *1st Pacific Symposium on Flow Visualization and Image Processing*, Honolulu, Hawaii.

Weidman, P.D. (1968), *Wake transition and blockage effects on cylinder base pressures*, PhD thesis, California Institute of Technology.

White, F.M. (2017), *Fluid Mechanics*, McGraw Hill, 8th ed.

Wieselsberger, C. (1922a), 'Further Information on the Laws of Fluid Resistance', *Physikalische Zeitschrift*, Vol. 23, No. 1, pp. 1–12.

Wieselsberger, C. (1922b), 'New data on the laws of fluid resistance', *Physikalische Zeitschrift*, Vol. 22, No. 1, pp. 21–46.

Williamson, C.H.K. (1996), 'Vortex Dynamics in the Cylinder Wake', *Annual Review of Fluid Mechanics*, Vol. 28, No. 1, pp. 477–539.

Williamson, P., Docherty, P.D., Yazdi, S.G., Jermy, M., Khanafer, A., Kabaliuk, N. and Geoghegan, P.H. (2019), 'PIV Analysis of Stented Haemodynamics in the Descending Aorta', In *2019 41st Annual International Conference of the IEEE Engineering in Medicine and Biology Society (EMBC)*, IEEE, pp. 4737–4740.

Wood, R.M. (2002), 'A discussion of aerodynamic control effectors (ACEs) for unmanned air vehicles (UAVs)', *1st UAV Conference*.

Wood, R.M. (2004), 'Impact of Advanced Aerodynamic Technology on Transportation Energy Consumption', In *SAE Technical Papers*, SAE International, p. 1306.

Wu, M.H., Wen, C.Y., Yen, R.H., Weng, M.C. and Wang, A.B. (2004), 'Experimental and numerical study of the separation angle for flow around a circular cylinder at low Reynolds number', *Journal of Fluid Mechanics*, Vol. 515, pp. 233–260.

Yamazato, E. (1969), 'Performance of Wide-Angle Two-Dimensional Diffusers with Area Sction (1st Report)', Tech. rep., University of the Ryukyus.

Yamazato, E. (1970), 'Performance of Wide-Angle Two-Dimensional Diffusers with Area Sction (2nd Report)', Tech. rep., University of the Ryukyus.

Yu, P., Zeng, Y., Lee, T.S., Chen, X.B. and Low, H.T. (2011), 'Steady flow around and through a permeable circular cylinder', *Computers and Fluids*, Vol. 42, No. 1, pp. 1–12.

Zdravkovich, M.M. (1997), *Flow Around Circular Cylinders*, Oxford University Press Inc., Oxford, 1st ed.

Zuo, D., Jones, N.P. and Main, J.A. (2008), 'Field observation of vortex- and rain-wind-induced stay-cable vibrations in a three-dimensional environment', *Journal of Wind Engineering and Industrial Aerodynamics*, Vol. 96, No. 6-7, pp. 1124–1133.